BLEND OF 1-BUTYL-3-METHYLIMIDAZOLIUM BIS(TRIFLUOROMETHYLSULFONYL)IMIDE−MONOETHANOLAMINE-SULFOLANE AS A NOVEL NON-AQUEOUS SOLVENT FOR CARBON DIOXIDE ABSORPTION AND ITS THERMOPHYSICAL PROPERTIES

MOHD AZLAN BIN KASSIM

DEPARTMENT OF CHEMISTRY
FACULTY OF SCIENCE
UNIVERSITY OF MALAYA
KUALA LUMPUR

2018

BLEND OF 1-BUTYL-3-METHYLIMIDAZOLIUM BIS(TRIFLUOROMETHYLSULFONYL)IMIDE−MONOETHANOL AMINE-SULFOLANE AS A NOVEL NON-AQUEOUS SOLVENT FOR CARBON DIOXIDE ABSORPTION AND ITS THERMOPHYSICAL PROPERTIES

MOHD AZLAN BIN KASSIM

THESIS SUBMITTED IN FULFILMENT OF THE REQUIREMENTS FOR THE DEGREE OF DOCTOR OF PHILOSOPHY

DEPARTMENT OF CHEMISTRY
FACULTY OF SCIENCE
UNIVERSITY OF MALAYA
KUALA LUMPUR

2018

UNIVERSITI MALAYA

ORIGINAL LITERARY WORK DECLARATION

Name of Candidate: **MOHD AZLAN BIN KASSIM**

Registration/Matric No: **SHC 120106**

Name of Degree: **DOCTOR OF PHILOSOPHY (EXCEPT MATHEMATIC AND SCIENCE PHILOSOPHY)**

Thesis: **BLEND OF 1-BUTYL-3-METHYLIMIDAZOLIUM BIS(TRIFLUOROMETHYLSULFONYL)IMIDE-MONOETHANOLAMINE-SULFOLANE AS A NOVEL NON-AQUEOUS SOLVENT FOR CARBON DIOXIDE ABSORPTION AND ITS THERMOPHYSICAL PROPERTIES**.

Field of Study: **PHYSICAL CHEMISTRY**

I do solemnly and sincerely declare that:

(1) I am the sole author / write of this Work;
(2) This Work is original;
(3) Any use of any work in which copyright exist was done by way of fair dealing and for permitted purposes and any excerpt or extract from, or reference to or reproduction of any copyright work has been disclosed expressly and sufficiently and the title of the Work and its authorship have been acknowledged in this Work;
(4) I do not have any actual knowledge nor do I ought reasonably to know that the making of this work constitutes an infringement of any copyright work;
(5) I hereby assign all and every rights in the copyright to this Work to the University of Malaya ("UM"), who henceforth shall be owner of all the copyright in this Work and that any reproduction or use in any form or by any means whatsoever is prohibited without the written consent of UM having been first had and obtained;
(6) I am fully aware that if in the course of making this Work I have infringed any copyright whether intentionally or otherwise, I may be subject to legal action or any other action as may be determined by UM.

Candidate's Signature Date

Subscribed and solemnly declared before,

Witness's signature Date
Name:
Designation:

BLEND OF 1-BUTYL-3-METHYLIMIDAZOLIUM BIS(TRIFLUOROMETHYLSULFONYL)IMIDE−MONOETHANOLAMINE-SULFOLANE AS A NOVEL NON-AQUEOUS SOLVENT FOR CARBON DIOXIDE ABSORPTION AND ITS THERMOPHYSICAL PROPERTIES

ABSTRACT

In this work, carbon dioxide (CO_2) solubility studies and thermophysical properties were conducted on non-aqueous ternary mixtures of 1-butyl-3-methylimidazolium bis(trifluoromethylsulfonyl)imide ([BMIM][NTf_2]), monoethanolamine (MEA) and sulfolane carried out at various compositions and temperatures. CO_2 solubility study conducted in this study was focused on the evaluation of [BMIM][NTf_2] + MEA + sulfolane non-aqueous binary and ternary mixtures in absorbing CO_2 at high pressure. The CO_2 absorption experiment was conducted at pressure from 500 to 2000 kPa and temperatures ranging from 303.15 to 333.15 K. Highest CO_2 loading was obtained by using 0B-30M (30 wt% MEA + 70 wt% sulfolane) binary mixture (2.224 – 2.861 mol CO_2/ kg absorbent) and 5B-25M (5 wt% [BMIM][NTf_2] + 25 wt% MEA + 70 wt% sulfolane) ternary mixture (1.882 – 2.705 mol CO_2/ kg absorbent), at pressure range from 500 to 2000 kPa. Biphasic layer formation was observed in all mixtures containing MEA due to the formation of polar MEA-carbamate salt, which is insoluble in hydrophobic [BMIM][NTf_2] and dipolar sulfolane. Compositions of the CO_2-rich and CO_2-lean layers were identified by ^{13}C NMR. The CO_2-rich layer can be easily separated and transported to the stripper to be regenerated. Thermophysical properties studies; density, viscosity and refractive index were conducted for [BMIM][NTf_2] + sulfolane, MEA + sulfolane, [BMIM][NTf_2] + MEA binary mixtures and [BMIM][NTf_2] + MEA + sulfolane ternary mixtures over whole compositions at

temperatures ranging from 303.15 to 343.15 K and at atmospheric pressure. Results show that the thermophysical properties of both binary and ternary mixtures demonstrate a composition and temperature-dependent behaviour. Thermophysical excess properties; excess molar volume, viscosity deviation and refractive index deviation were determined using experimental data to elucidate molecular interaction between molecules in both binary and ternary mixtures. Subsequently, the calculated excess properties were regressed to a Redlich-Kister equation. Molecular model using a conductor-like screening model for realistic solvation (COSMO-RS) computational method was conducted to determine the molecular interaction between components of binary and ternary over the whole range of composition. σ-profile, σ-potential, activity coefficient and excess enthalpies of each component of the composition described the polarity and H-bonding tendency of the molecules. Strong interaction between [BMIM][NTf_2] and sulfolane was deduced while weaker interaction between MEA and both [BMIM][NTf_2] and sulfolane in the binary mixtures. For [BMIM][NTf_2]-MEA-sulfolane ternary mixtures, the predominant molecular interaction in the ternary mixtures would likely depend on the major binary mixtures present in the composition in the ternary mixtures.

Keywords: non-aqueous CO_2 absorption, ionic liquids, alkanolamine, sulfolane, excess properties, COSMO-RS

GABUNGAN 1-BUTIL-3-METILIMIDAZOLIUM BIS(TRIFLOROMETILSULFONIL)IMIDA - MONOETHANOLAMINA - SULFOLAN SEBAGAI PELARUT BUKAN AKUES BARU BAGI PENYERAPAN KARBON DIOKSIDA SERTA PENCIRIAN TERMAFIZIKAL

ABSTRAK

Kajian mengenai keterlarutan karbon dioksida (CO_2) dan ciri-ciri terma fizikal bagi campuran pertigaan tanpa akueus 1-butil-3-metilimidazolium bis(triflorometilsulfonil)imida ([BMIM][NTf_2]), monoethanolamina (MEA) dan sulfolan telah dijalankan pada pelbagai suhu dan komposisi. Keterlarutan CO_2 telah dijalankan dalam kajian ini berfokuskan pada penilaian campuran deduan dan pertigaan tanpa akueus [BMIM][NTf_2] + MEA + sulfolan untuk menyerap CO_2 pada tekanan tinggi. Ujikaji penyerapan CO_2 telah dijalankan pada tekanan 500 hingga 2000 kPa dan suhu pada julat 303.15 sehingga 333.15 K. Serapan CO_2 paling tinggi ditunjukkan oleh campuran dedua 0B-30M (30 wt% MEA + 70 wt% sulfolan) (2.224 – 2.861 mol CO_2/ kg penyerap) dan campuran pertigaan 5B-25M (5 wt% [BMIM][NTf_2] + 25 wt% MEA + 70 wt% sulfolan) (1.882 – 2.705 mol CO_2/ kg penyerap) pada tekanan 500 hingga 2000 kPa. Lapisan dwifasa telah diperhati pada campuran yang mengandungi MEA yang mana terhasil dari pembentukan garam karbamat MEA terkutub yang tidak larut di dalam larutan [BMIM][NTf_2] (hidrofobik) dan sulfolan (dwikutub). Komposisi lapisan tepu CO_2 dan lapisan tanpa CO_2 telah dikenalpasti menggunakan ^{13}C NMR. Lapisan tepu CO_2 tersebut dapat dipisahkan dengan mudah dari campuran dan dipindahkan ke dalam pemisah untuk dijana semula. Kajian ciri-ciri terma fizikal; ketumpatan, kelikatan dan indek biasan telah dijalankan bagi campuran dedua [BMIM][NTf_2] + sulfolan, sulfolan + MEA, dan [BMIM][NTf_2] + MEA serta campuran pertigaan [BMIM][NTf_2] + MEA + sulfolan pada seluruh julat komposisi dan suhu dari 303.15 sehingga 343.15 K pada tekanan atmosfera. Hasil menunjukkan bahawa ciri-ciri

terma fizikal campuran dedua dan pertigaan bergantung pada komposisi dan suhu. Ciri-ciri terma fizikal lebihan; lebihan isipadu molekul, sisihan kelikatan dan sisihan indek biasan telah dikenalpasti berdasarkan data ujikaji bagi mentafsir interaksi molekul di dalam campuran dedua dan pertigaan. Seterusnya, nilai ciri-ciri lebihan diregresi pada persamaan Redlich-Kister. Model molekular menggunakan kaedah pengkomputeran model penyaringan seperti konduktor bagi pensolvatan realistik (COSMO-RS) telah dijalankan bagi menentukan interaksi molekular antara setiap komponen dalam campuran dedua dan pertigaan di dalam seluruh julat komposisi. Profil σ, keupayaan σ, pemalar aktiviti dan lebihan entalpi bagi setiap komponen komposisi akan menggambarkan kekutuban dan kecenderungan menghasilan ikatan hidrogen di dalam molekul. Interaksi yang kuat antara [BMIM][NTf_2] dan sulfolan telah dikenalpasti manakala interaksi yang lemah ditunjukkan antara MEA dan [BMIM][NTf_2] serta sulfolan di dalam campuran dedua. Bagi campuran pertigaan [BMIM][NTf_2] + MEA + sulfolan, interaksi molekul pradominan di dalam campuran bergantung kepada campuran dedua utama yang hadir di dalam campuran pertigaan.

Kata kunci: penyerapan CO_2 bukan akues, cecair ionik, alkanolamina, sulfolan, ciri-ciri lebihan, COSMO-RS

ACKNOWLEDGEMENTS

First and above all, alhamdulillah to Almighty Allah S.W.T. for giving me the strength to complete my doctoral thesis. I would like to express my deepest appreciation to my supervisor, Dr. Nor Asrina Sairi for her invaluable guidance, consistent support and encouragement throughout the course of this research. My appreciation also goes to Prof. Madya Ir. Dr. Rozita Yusoff for her strong support, constructive comments and guidance. Special mention to my supporting research supervisors Prof. Dr. Mohamed Kheireddine Aroua and Prof. Dr. Yatimah Alias for their guidance and moral supports.

A special thanks to my University Malaya Center for Ionic Liquids (UMCiL) laboratory members in Faculty of Science, University of Malaya: Zati Ismah Ishak, Dazylah Darji, Nor Rahimah Said, Wan Melissa Wan Mazlan, Maizathul Akmam, Siti Mastura Mohd Zakaria, Kumuthini Chandrasekaram and other labmates for their continuous support, encouragement and sharing. Also, Nurul Ain Ramli, Nurul Fatin Nabilah Abdul Samat and friends from Thermodynamics Laboratory, Faculty of Chemical Engineering, University of Malaya for their warm welcome and assistance during my research. Special appreciation to my *Gelep* buddies, Asrul Farrish OKR Udaiyappan, Mohd Rizal Chumati, Nur Fariza Abdul Rahman, Siti Efliza Ashari, Nur Faizlin Md Jadi and Intan Diana Mat Azmi for their support and friendship. Special gratitude to my personal mentor, Khairulazhar Jumbri for his consistent support and encouragement throughout the course of this research.

I would also like to acknowledge the Ministry of Education (MOE) for their generous financial support in the form of MyPhD, under MyBRAIN 15 and the research grant allocation which aided me in the completion of my study. Thank you to the administrative staff in the Department of Chemistry, Faculty of Science and Department of Chemical

Engineering, Faculty of Engineering, University of Malaya for their assistance during my research work.

Last but not least, my heartfelt appreciation extends to my beloved parents, Kassim Yaakob and Rodziah Zainuddin and my siblings, Nur Azleen Kassim, Muhammad Azhar Kassim and Muhammad Azham Kassim, for their unceasing love, patience, support, encouragement and understanding. Words cannot express how grateful I am for their care and concern for me.

TABLE OF CONTENTS

LIST OF FIGURES

LIST OF TABLES

LIST OF ABBREVIATIONS AND SYMBOLS

[BMIM][BF_4]	:	1-butyl-3-imidazolium tetrafluoroborate
[BMIM][DCA]	:	1-butyl-3-imidazolium dicyanamide
[BMIM][FAP]	:	1-butyl-3-methylimidazolium tris(pentafluoroethyl)trifluorophosphate
[BMIM][OAc]	:	1-butyl-3-imidazolium acetate
[BMIM][PF_6]	:	1-butyl-3-methylimidazolium hexafluorophosphate
[BMIM][Tf_2N]	:	1-butyl-3-methylimidazolium bis(trifluoromethylsulfonyl)imide
[C_2mim][$AlCl_4$]	:	1-ethyl-3methylimidazolium tetrachloroaluminate
[C_2mim][Cl]	:	1-ethyl-3-methyimidazolium chloride
[C_2MIM][$EtSO_4$]	:	1-ethyl-3-methylimidazolium ethylsulfate
[C_2mim][Tf_2N]	:	1-ethyl-3-methylimidazolium bis(trifluoromethylsulfonyl)imide
[C_4MIM][NO_3]	:	1-n-butyl-3-methylimidazolium nitrate
[C_4MIM][PF_6]	:	1-butyl-3-methylimidazolium hexafluorophosphate
[$C_6H_4F_9$MIM][Tf_2N]:		1-methyl-3-(nonafluorohexyl)imidazolium bis(trifluoromethylsulfonyl)imide

$[C_6MIM][Tf_2N]$	:	1-hexyl-3-methylimidazolium bis(trifluoromethylsulfonyl)imide
$[C_8MIM][BF_4]$	:	1-n-octyl-3- ethylimidazolium tetrafluoroborate
$[C_8MIM][PF_6]$	:	1-n-octyl-3-methylimidazolium hexafluorophosphate
$[EMIM][OcSO_4]$	:	1-ethyl-3-methylimidazolium octyl sulfate
$[EtNH_3][NO_3]$	:	ethylammonium nitrate
$[N_{1111}][Gly]$	:	tetramethylammonium glycinate
$[N_{1111}][Lys]$	:	tetramethylammonium lysinate
$[N_{2222}][Gly]$	:	tetraethylammonium glycinate
$[N_{2222}][Lys]$	:	tetraethylammonium lysinate
[*N*-bupy][BF_4]	:	*N*-butylpyridinium tetrafluoroborate
AMP	:	aminomethylpropanol
AR	:	analytical reagents
bheaa	:	bis(2-hydroxyethyl) ammonium acetate
CASRN	:	chemical abstracts service registry number
CCS	:	carbon capture and storage
CO_2BOL	:	CO_2 binding organic liquids
COSMO-RS	:	Conductor-like Screening Model for Real Solvents

DEA	:	diethanolamine
DGA	:	diethylene glycolamine
DIPA	:	diisopropanolamine
DMPEG	:	dimethyl ether of polyethylene glycol
DMX	:	1,3-dipropil-methyl-xanthine
GC	:	gas chromatography
HFCs	:	hydrofluorocarbons
HPLC	:	high-performance liquid chromatography
IEA	:	International Energy Agency
IGCC	:	Integrated Gasification Coal Cycle
IPCC	:	Intergovernmental Panel on Climate Change
IUPAC	:	International Union of Pure and Applied Chemistry
MDEA	:	methyldiethanolamine
MEA	:	monoethanolamine
MMEA	:	methylethanolamine
MPE	:	methyl isopropyl ether of polyethylene glycol
n_D	:	refractive index
NMP	:	*N*-methyl-2-pyrrolidone

NMR	:	nuclear magnetic resonance
NOA	:	National Oceanic and Atmospheric
PC	:	propylene carbonate
PFCs	:	perfluorocarbons
PSA	:	pressure swings adsorption
PZ	:	piperazine
QM	:	quantum mechanic
TEA	:	triethanoleamine
TETA	:	triethylenetetramine
TMGL	:	1,1,3,3-tetramethylguanidium lactate
TSA	:	temperature swing adsorption
TSIL	:	task specific ionic liquid
V^E	:	excess molar volume
α_{CO2}	:	CO_2 loading capacity (mol CO_2 / kg absorbent)
Δn_D	:	refractive index deviation
$\Delta\eta$	:	viscosity deviation
η	:	viscosity
ρ	:	density

χ_{CO2}	:	CO_2 loading capacity (mol CO_2 / mol absorbent)

CHAPTER 1: INTRODUCTION

1.1 Background study

Global warming due to increase emission greenhouse gasses has become a major issue faced by the current human population. Over 195 countries agreed on the plan to minimize the emissions of carbon dioxide (CO_2) and other greenhouse gasses during the United Nation Climate Change Conference. Their aim is to limit the increase of global temperature below 2 °C in relative to the pre-industrial climate. Ever since the industrial revolution in the year 1750, an increase in global CO_2 concentrations has been observed due to the rapid growth in industrialization and human population within the past century. Over the recent past five years, we have been experiencing a consistent increase in global atmospheric CO_2 concentration as shown in Figure 1.1.

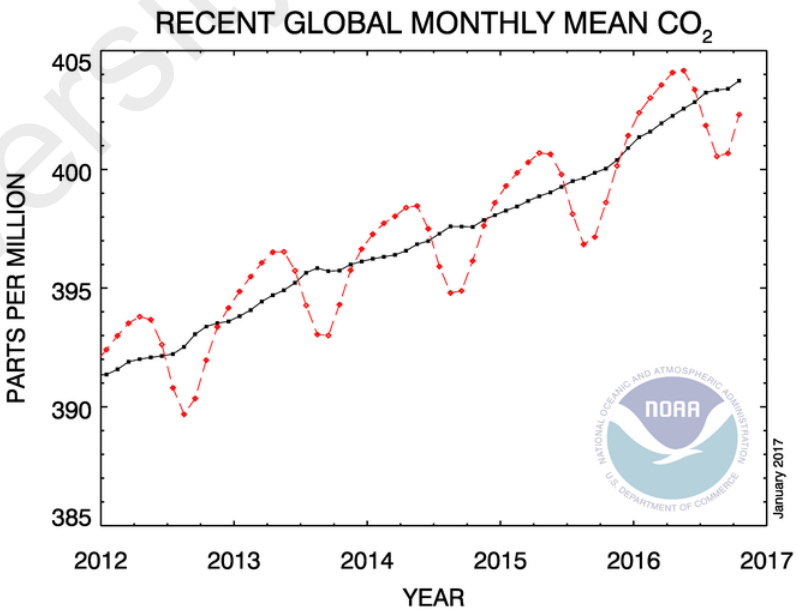

Figure 1.1: Recent monthly mean carbon dioxide globally averaged over marine surface sites. (-♦-: monthly mean values, -■-: after correction for the average seasonal cycle) (Dlugokencky & Tans, 2017)

Figure 1.1 shows the monthly mean of global CO_2 concentration over the marine surface site as reported by the Global Monitory Division of National Oceanic and Atmospheric (NOA) / Earth System Research Laboratory. The 2016's data is a preliminary data that is subject to recalibration to standard emission gas and quality control (Dlugokencky & Tans, 2017). Regardless, the trends still reflect on the severity in the increased of CO_2 global concentration. As reported by the International Energy Agency, a steady rise of CO_2 emission was recorded in the past ten years that the concentration of CO_2 in the atmosphere is about 400 ppm, a significant increase in comparison to the pre-industrial period, which is less than 300 ppm (Oh, 2010). A significant increase of global CO_2 emission was reported in 2013, an increase of 2.2% over the previous year with 68% of total global emission originates from the energy sector. CO_2 is the main gas that contributes to global warming contributing more than 60% in greenhouse gas composition (Albo et al., 2010). Major source of CO_2 is from the industrial sector, for instance, fossil−fuel power plants and natural gas treatments as well as hydrocarbon processing. The most pressing issue with high CO_2 concentration in the atmosphere is that it leads to major environmental issues, primarily the increase in global temperature which commonly referred as global warming. This will cause drastic changes in the natural environment such as melting of the polar ice caps, rising of sea levels and severe weather patterns (IPCC, 2013). It was predicted by the Intergovernmental Panel on Climate Change (IPCC) that by the year 2100, the global atmospheric temperature will increase by 1.9 °C (Wang et al., 2013). Therefore, it is necessary to capture CO_2 to cope with the worsening scenario of global warming.

The need for a reduction of CO_2 concentration in the atmosphere has catalyzed research for CO_2 capture technologies to counter the global CO_2 emission predicament. The primary solution to reduce the CO_2 emission is using non-carbon energy sources (renewable energy and hydrogen) as an alternative to fossil fuel. However, due to the high cost of renewable energies and hindrance in adopting into industrial application, it will take longer time to make renewable energies a viable option.

Another option to remedy the increment of CO_2 emission is by improving the current fossil fuel energy efficiency by reducing the CO_2 emission per energy consumption. The current implemented solution is the carbon capture and storage (CCS) which focused upon the development of CO_2 capture method and sequestration technologies. There are three main steps in the CCS approach. The first step is capturing of CO_2 from various gas sources, for example, natural gas streams, industrial flue gas or synthetic gas from power plants. The second step is transporting purified CO_2 gas to storage location. The final step is storing compressed CO_2 gas in a geological formation, such as depleted oil and gas reservoir or underground aquifer (Fahrenkamp-Uppenbrink, 2015).

CO_2 removal could be done in three basic approaches which are, (1) pre-combustion: CO_2 was removed from the reformed synthetic of gas in the upstream; (2) post-combustion: CO_2 gas was removed from the flue gas after the combustion and (3) oxy-fuel combustion: fuel was combusted in oxygen diluted in recycling flue gas which resulted in a final flue gas mainly consist of CO_2 and H_2O (Tan et al., 2012). Post-combustion process is much more mature technology in comparison to pre-combustion and oxy-fuel process. Post-combustion

process is much simpler to be applied, whereby the process can be retrofitted into the current combustion technology without any major modification to the system. In the post-combustion process, several technologies can be applied for the CO_2 removal which includes (1) absorption via chemical or physical solvent, (2) adsorption, (3) membrane separation and (4) cryogenic separation (Shafeeyan et al., 2014; Wang et al., 2011).

Over the years, ionic liquids have demonstrated potentials as solvents used for various applications and were reported to be a potential alternative solvent for CO_2 removal. This is due to their almost negligible volatility, thermal stability, and low heat capacity (Hasib-ur-Rahman et al., 2010; Sairi et al., 2015). Ionic liquid seems to be suitable alternative solvents for energy efficient gas separations (Sánchez et al., 2007). Furthermore, ionic liquid can be tailored to specific requirements by varying the combinations of constituent ionic counterparts. Investigation on the possible application of ionic liquids either in the pure form (Jing et al., 2012; Sharma et al., 2012) or in combination with alkanolamines (Camper et al., 2008; Iliuta et al., 2014) for physical/chemical absorption processes were reported in the literature. Ionic liquid−alkanolamine combination was reported to offer reductions in energy by forming a carbamate precipitate and also prevents corrosion to the system.

1.2 Problem statement

Chemical absorption using aqueous alkanolamine has been a common practice for the CO_2 removal process as it is more developed and mature system. The foremost aqueous alkanolamine solutions applied to industrial processes are monoethanolamine (MEA),

diethanolamine (DEA), methylethanolamine (MMEA), methyldiethanolamine (MDEA), aminomethylpropanol (AMP), diethylene glycolamine (DGA), diisopropanolamine (DIPA), piperazine (PZ), triethanoleamine (TEA) and were used either as a single or blended aqueous solution (Gouedard et al., 2012; Shakerian et al., 2015). Although this process removes CO_2 efficiently, it does pose severe economic and environmental drawbacks: (1) corrosion to the equipment, (2) solvent loss via evaporation, (3) thermal and oxidative degradation during absorption-desorption cycle and (4) high energy cost of solvent regeneration (Gao et al., 2013).

In short, rapid equipment corrosion and alkanolamine degradation at high temperatures were due to the presence of water in the system. Furthermore, due to the high heat capacity of water in the aqueous solution, large amount of heat was utilized during the regeneration process to increase the temperature of the solution to the stripping temperature. This later leads to around 50-80% of total energy consumption. Therefore, by substituting water with other high-boiling point organic solvents, a considerable amount of thermal energy can be saved during the solvent heating cycle, and the corrosion will also be prevented.

1.3 Scope and research objectives

In view of the current approach of reducing the total operational cost of CO_2 capture using conventional aqueous based CO_2 capture process, in which the majority of the consumed energy was utilized by the reboiler heat duty, the development of a novel non-

aqueous solvent poses the highest potential of reducing the cost of CO_2 capture. Therefore, the aim of this work was to evaluate the solubility of CO_2 in the new potential non-aqueous blends of 1-butyl-3-methylimidazolium bis(trifluoromethylsulfonyl)imide ([BMIM][NTf_2]), MEA and sulfolane, whereby MEA was chosen as the chemical solvent and [BMIM][NTf_2] and sulfolane as physical solvent. Sulfolane also acts as an aqueous substitute in the solvent mixture due to its high thermal and hydrolytic stability with high density and boiling point.

In light of the novel non-aqueous blends, essential thermophysical properties were measured to provide engineering data and evaluate the molecular interaction between each of the components within the mixture system. Then the absorption experiment was conducted at high pressure from 500 to 2000 kPa at temperature ranging from 303.15 to 333.15 K to evaluate the performance of the solvent mixture in capturing CO_2.

Hence, the objectives of this work are as follows:

i) To investigate the CO_2 absorption potential of the novel non-aqueous mixture of [BMIM] [NTf_2]-MEA-sulfolane system at high pressure system (500 to 2000 kPa) with temperature ranges between 303.15 to 333.15 K.

ii) To determine the thermophysical properties of [BMIM][NTf_2]-sulfolane, [BMIM][NTf_2]-MEA and sulfolane-MEA binary mixtures and [BMIM][NTf_2]-MEA-sulfolane ternary mixtures over an entire range of composition at different temperatures and excess properties.

iii) To evaluate the molecular interaction of binary and ternary mixtures using COSMO-RS modeling.

1.4 Outline of the thesis

In order to accomplish the objectives, a number of detailed studies were conducted, which are presented in the following chapters:

Chapter 1. Introduction

In this chapter, the research background, problem statements, objectives, scope of work and layout of the thesis are described.

Chapter 2. Literature review

A detailed literature review has been conducted on the theoretical background to CO_2 absorption process. Thorough literature reviews on the alkanolamines, ionic liquids and non-aqueous solvent application were detailed throughout this chapter. The thermophysical properties such as density, viscosity and refractive index and their thermodynamic excess properties were also reviewed. Literature backgrounds on COSMO-RS modeling are also explained.

Chapter 3. Materials and methods

This chapter provides detailed information on the materials, experimental and analytical apparatus and methods used in the experiments.

Chapter 4. Results and discussions

Results and discussions were embedded into five sub-chapters in Chapter 4 as follows:

1. **4.1 CO_2 absorption at high pressure**
    - This chapter reports on the experimental data of CO_2 absorption using non-aqueous [BMIM][NTf_2]-MEA-sulfolane ternary mixtures at high pressure. The experiments were conducted at pressures ranges of 500 to 2000 kPa over temperature ranges of 303.15 to 333.15 K.

2. **4.2 Thermophysical properties**
    - **4.2.1. Density**

      This chapter reports on the density of [BMIM][NTf_2]-sulfolane, [BMIM][NTf_2]-MEA, sulfolane-MEA binary and [BMIM][NTf_2]-MEA-sulfolane ternary mixtures system at different temperatures at a constant atmospheric pressure. Extended data on thermal expansion and the correlation of density as a function of temperature were presented. Excess properties of binary and ternary mixtures were also calculated and presented.

- **4.2.2 Viscosity**

  This chapter reports on the viscosity of [BMIM][NTf_2]-sulfolane, [BMIM][NTf_2]-MEA, sulfolane-MEA binary mixtures and [BMIM][NTf_2]-MEA-sulfolane ternary mixtures system at different temperatures at a constant atmospheric pressure. Correlations of viscosity as a function of temperature were presented. Excess properties of binary and ternary mixtures were also calculated and presented.

- **4.2.3 Refractive index**

  This chapter reports on the refractive index of [BMIM][NTf_2]-sulfolane, [BMIM][NTf_2]-MEA, sulfolane-MEA binary mixtures and [BMIM][NTf_2]-MEA-sulfolane ternary mixtures at different temperatures at a constant atmospheric pressure. Correlations of the refractive index as a function of temperature were presented. Excess properties of binary and ternary mixtures were also calculated and presented.

3. **4.3 COSMO-RS model**

   This chapter reports on the activity coefficient of each component in [BMIM][NTf_2]-sulfolane, [BMIM][NTf_2]-MEA, sulfolane-MEA binary mixtures and [BMIM][NTf_2]-MEA-sulfolane ternary mixtures at different temperatures at a constant atmospheric pressure. Molecular interactions between each component were deduced based on the σ-profile and activity coefficient generated by the model.

Chapter 5. Conclusions and recommendations

Summaries of the findings in each objective are provided under this chapter. Furthermore, recommendations for future work were also provided.

CHAPTER 2 : LITERATURE REVIEW

2.1 Global warming

Climate change has become one of the major risks faced by the current human population. Over 195 countries agreed to the plan to minimize the emissions of CO_2 and other greenhouse gasses in the United Nation Climate Change Conference. Their aim is to limit the increase of global temperature below 2 °C in relative to the pre-industrial climate. Association of CO_2 with the increase of global temperature or known as "greenhouse effect" has caught the attention of researchers, politicians and the general public. CO_2 is considered to be the major greenhouse gas contributing to global warming. Figure 2.1 illustrates the general mechanism of global warming attributed by the greenhouse effect. Earth received energy from the sun via solar radiation in the form of ultraviolet, visible and near-infrared radiation. This solar radiation passed largely unimpeded through the atmosphere and absorbed by the Earth's surface, thereby warming it. In-turn, energy was emitted back to atmosphere in the form of infrared radiation that was absorbed by CO_2 and water vapor, forming a blanket surrounding earth. The strength of the greenhouse effect will depend on the atmosphere's temperature, and on the amount of greenhouse gases that the atmosphere contains. Hence, high concentration of greenhouse gases in the atmosphere will lead to a more prominent greenhouse effect triggering a higher increment of global temperature. This will cause drastic changes in the natural environment such as melting of the polar ice caps, rising of sea levels and severe weather patterns (Stocker et al., 2014).

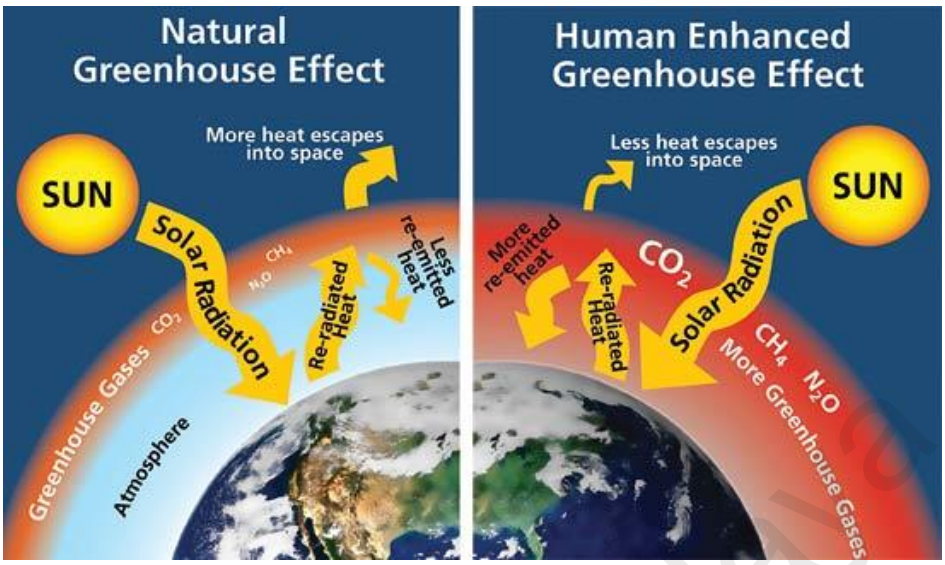

Figure 2.1: The ‘‘greenhouse effect.’’ Left - Naturally occurring greenhouse gases—carbon dioxide (CO_2), methane (CH_4), and nitrous oxide (N_2O)—normally trap some of the sun’s heat, keeping the planet from freezing. Right - Human activities, such as the burning of fossil fuels, are increasing greenhouse gas levels, leading to an enhanced greenhouse effect. The result is global warming and unprecedented rates of climate change (Dlugokencky & Tans, 2017)

CO_2, methane (CH_4), nitrous oxide (N_2O), hydrofluorocarbons (HFCs), perfluorocarbons (PFCs) and sulfur hexafluoride (SF_6) have been identified as the primary greenhouse gases responsible for human-induced climate change (Javid et al., 2014) with CO_2 is the main gas that contributes to the global warming; more than 60% in greenhouse gas composition (Albo et al., 2010; Metz et al., 2005). Major source of CO_2 is from the industrial sector, for instance, fossil−fuel power plants and natural gas treatments as well as hydrocarbon processing. Figure 2.2 shows the reported atmospheric CO_2 concentration as recorded by the Global Monitory Division of National Oceanic and Atmospheric Administration / Earth System Research Laboratory with the current atmospheric CO_2 concentration is at 407.69 ppm. However, the current and 2016’s data are the preliminary data that is subject to recalibration to standard emission gas and quality control, but any revisions are expected to be small (Dlugokencky & Tans, 2017). Regardless, this report is in

line with previous studies reported by the International Energy Agency that shows a steady rise of CO_2 emission been recorded in the past ten years with the concentration of CO_2 in the atmosphere is about 400 ppm, a significant increase in comparison to the pre-industrial period, less than 300 ppm (Oh, 2010). It was predicted by the IPCC that by the year 2100, the atmosphere may contain up to 570 ppm CO_2 causing the global atmospheric temperature to increase by 1.9 °C (Wang et al., 2013). The International Energy Agency (IEA) suggests that by 2050 the global emissions of CO_2 from all energy-related technologies need to be reduced to half of their 2007 levels (29 Gt CO_2 per annum) to stabilize global warming (Zhao et al., 2013).

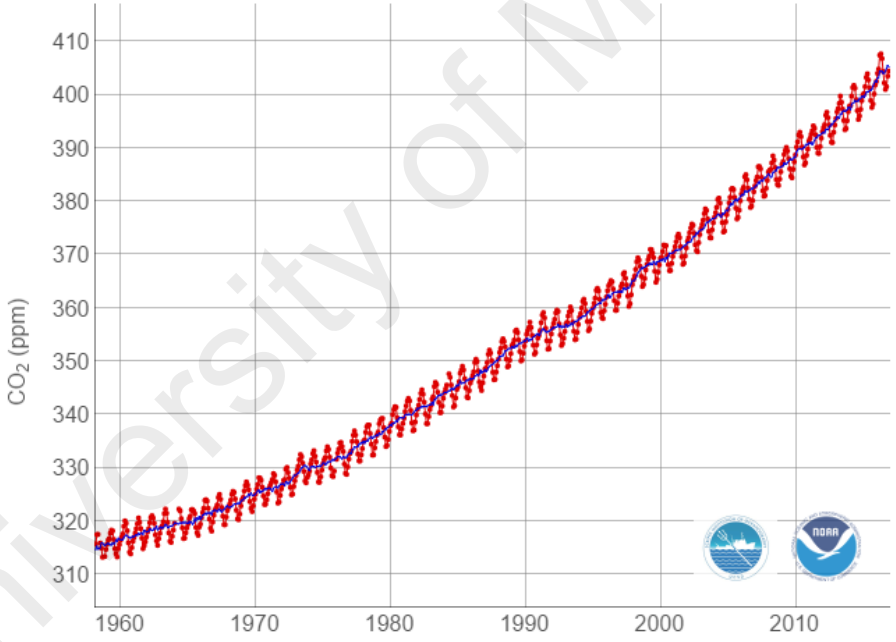

Figure 2.2: Recorded mean carbon dioxide globally averaged over marine surface sites. (-♦-: monthly mean values, -■-: after correction for the average seasonal cycle) (Dlugokencky & Tans, 2017)

2.2 Carbon capture technologies

2.2.1 CO_2 mitigation

There are multiple approaches that were suggested and adopted in many countries to reduce their CO_2 emissions. One of the direct approaches to implement a cleaner fuel in energy generation is by substituting coal to natural gas. Natural gas has a higher combustion efficiency and 50% less CO_2 emission. Natural gas also produces cleaner exhaust flue gas with fewer particulate and sulfur dioxide (SO_2). The drawback of this approach is the conventional natural gas price is higher than coal. Another alternative is to utilize a clean coal technology by replacing the common coal combustion system with Integrated Gasification Coal Cycle (IGCC) or pressurized fluidized bed combustor which permit usage of coal as fuel with less emission of air pollutants. However, this approach requires a high investment cost to implement the system widely (Leung et al., 2014).

Usage of a renewable energy sources such as solar, hydro, wind energy and biofuel or nuclear energy is a promising approach in producing cleaner energy. Renewable energy source utilized local natural resources which produce zero greenhouse gases and any toxic gases, therefore it can be adopted by any countries. However, the technology utilizing renewable resources are still not matured to make a viable alternative and much more expensive than conventional combustion energy. On the other hand, nuclear technology gives rise to much controversy due to recent Fukushima accident in 2011(Leung et al., 2014).

2.2.2 Carbon capture and storage (CCS)

Carbon capture and sequestration (CCS) in the process whereby the waste CO_2 from the source such as a fossil fuel power plant was captured via various methods. The captured CO_2 was later transported and deposited at the depositing site, normally this site is an underground geological formation like an emptied aquifer or emptied natural gas or oil fields. Hence the CO_2 will not enter back into the atmosphere. Based on the configuration of the source plant, there are a number of technologies, which are being evaluated for the capture of industrial CO_2 emissions. These include pre-combustion, post-combustion or oxy-combustion. Table 2.1 summarizes the advantages and disadvantages of different CO_2 capture technologies (Leung et al., 2014).

Table 2.1: Advantages and disadvantages of different CO_2 capture technologies

Capture Process	Utilization Area	Advantages	Disadvantages
Pre-combustion	• coal-gasification plant	• high CO_2 concentration • fully develop technology • deployed commercially in some industries • possibility to be retrofitted to existing plants	• high power requirement for sorbent regeneration. • less mature technology due to low number of operating plant. • high operating cost.
Post-combustion	• coal-fired plant • gas-fired plant	• most mature technology than other alternatives • easily retrofit into existing plants	• low CO_2 concentration affects the capture efficiency
Oxyfuel combustion	• coal-fired plant • gas-fired plant	• high CO_2 concentration, improve absorption efficiency	• high cost of cryogenic O_2 production • corrosion

Figure 2.3 illustrates the general schematic of a pre-combustion CO_2 capture process. In the pre - combustion process, the carbon content of the fuel (coal or natural gas) is reduced prior to combustion, which leads to a stream of pure CO_2 after combustion. If coal were used as fuel, pre-combustion processes usually include partial oxidation forming synthesis gas (syngas) composed primarily of carbon monoxide (CO) and hydrogen (H_2) (Equation 2.1), and mainly free of other pollutants (Figueroa et al., 2008). Syngas produced in the initial stage of the pre-combustion partial oxidation stage is then subjected to the water gas shift reaction forming CO_2 and H_2 (Equation 2.2). The CO_2 and H_2 were then separated using pressure swing adsorption or physical adsorption. The pure CO_2 was later compressed and stored. The hydrogen stream can either be used as a feedstock for chemical process or used as fuel to generate electricity. If natural gas, which is composed mainly of CH_4, was used as fuel, it can be reformed into syngas (Equation 2.3) and the subsequent process is similar to that observed coal as fuel.

$$Coal \xrightarrow{partial\ oxidation} CO + H_2 \tag{2.1}$$

$$CO + H_2O \xrightarrow{water-gas\ shift} H_2 + CO_2 \tag{2.2}$$

$$CH_4 + H_2O \xrightarrow{reform} CO + H_2 \tag{2.3}$$

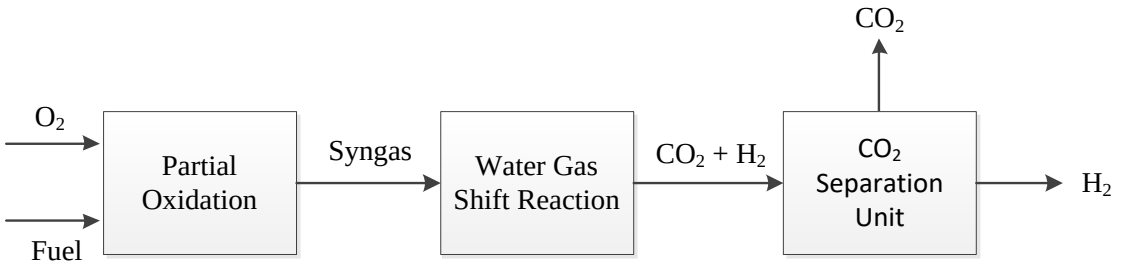

Figure 2.3: General flow of pre-combustion CO_2 capture (Mondal et al., 2012)

In the post-combustion process, CO_2 from the flue gas stream was removed after the combustion stage as represented in Figure 2.4. Existing power plant utilize air for combustion, generating a flue gas stream at an atmospheric pressure with typical CO_2 concentration less than 15%. Such diluted concentration of CO_2 in the flue gas stream requires the gas to be handled in large volume, resulting in large equipment volume and high capital cost. Post-combustion technology is more feasible as its offers some advantages over the existing combustion technologies whereby this approach can be easily retrofitted into the existing system without major modification as compared to the other two technologies. Even with such advantage, post-combustion application requires high power consumption. The separation stage during the CO_2 capture process is an energy intensive, which contributes to about 80% of the total operating cost of the CCS process (Davison, 2007).

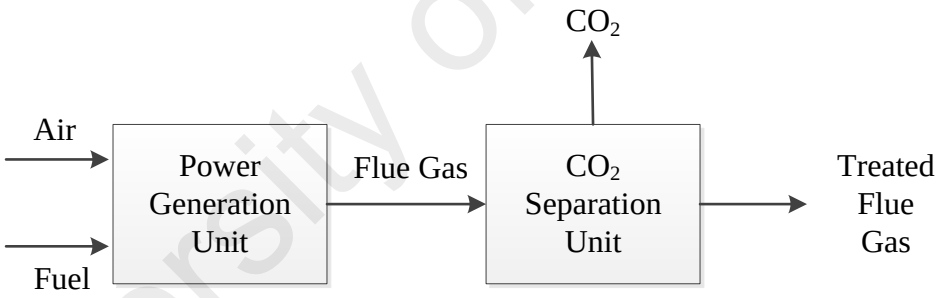

Figure 2.4: General flow of post-combustion CO_2 capture (Mondal et al., 2012)

Figure 2.5 illustrates the general schematic of an oxy-fuel combustion CO_2 capture process. In oxy-fuel combustion, fuel is consumed in oxygen rich environments (>95%) resulting in extreme high temperature, up to 3500 °C. Combustion in O_2 reduces the amount of nitrogen present in the exhaust gas, which will affect the subsequent separation process. By recycling fractions of the exhaust flue gases into the combustion mixtures, the temperature can be moderated down to levels that the equipment material can withstand.

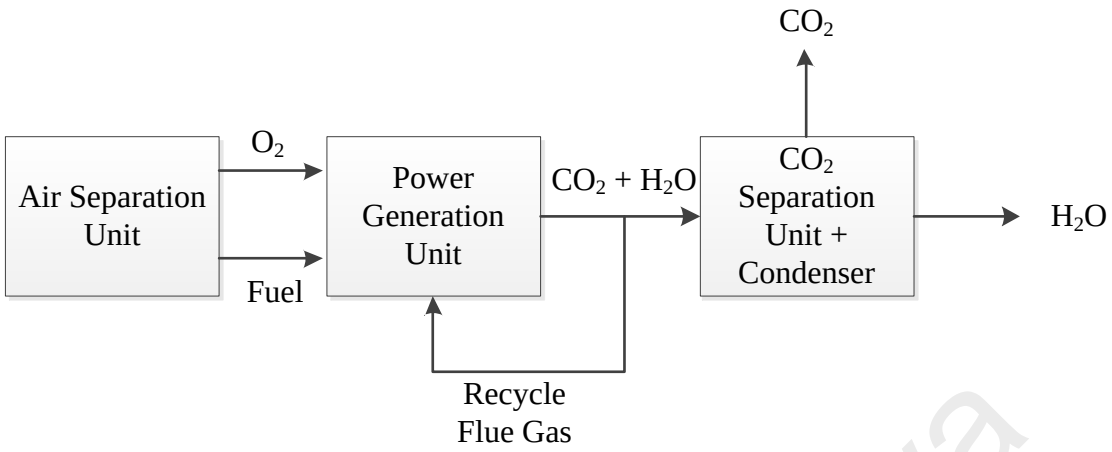

Figure 2.5: General flow of oxy-fuel combustion CO_2 capture (Mondal et al., 2012)

The flue gas stream produced from the oxy-fuel combustion consist of mainly CO_2, water vapor particulate and SO_2. Particulates are removed by a conventional electrostatic precipitator, while SO_2 is removed via flue gas desulphurization methods. Water vapor can be separated by condensation process and the remaining CO_2 can be further purified and compressed for storage. Technically, this is a feasible process, but consumes a large amount of energy for producing large amounts of oxygen from the air separating unit (Pfaff & Kather, 2009), resulting in high cost and energy consumption up to 7% in comparison with plant without CCS implemented (Burdyny & Struchtrup, 2010).

2.2.3 CO_2 separation techniques

There are numbers of CO_2 separation processes that can be utilized along with post-combustion CO_2 capture, which includes absorption via physical or chemical solvent,

adsorption, cryogenic separation, membrane separation and also biological fixation as illustrated in Figure 2.6.

In the adsorption process, the CO_2 adsorbs to the solid surface of the adsorbent. The process is based on the interaction force between gases or liquids on the surface of the adsorbent materials. This interaction can be either chemical (covalent bonding) or physical (van der Waals) interaction. Usually, adsorbents are solid materials with large surface area, high selectivity and regeneration. Typical sorbents consist of zeolite, calcium oxide, molecular sieve, activated carbon, hydrotalcite and lithium zirconate. CO_2 was separated from the flue gas stream by flowing the flue gas into contact with the absorbent. Once the bed is saturated, the flue gas flow is redirected to another lean adsorbent bed while the saturated adsorbent bed is regenerated. The adsorbent bed can be regenerated by either swinging the pressure or temperature throughout the system containing the CO_2-saturated adsorbent. Pressure swing adsorption (PSA) is a commercially available process for CO_2 separation in a power plant with an efficiency higher than 85% (Takamura et al., 2001). CO_2 is adsorbed onto the adsorbent surface at high pressure and later swings to atmospheric pressure to desorb the adsorbent bed and release the CO_2. For temperature swing adsorption (TSA), the CO_2 saturated adsorbent bed is desorbed by increasing the temperature throughout the system using hot air or steam. TSA process has a long regeneration interval than PSA but produces higher CO_2 purity (95%) (Clausse et al., 2011).

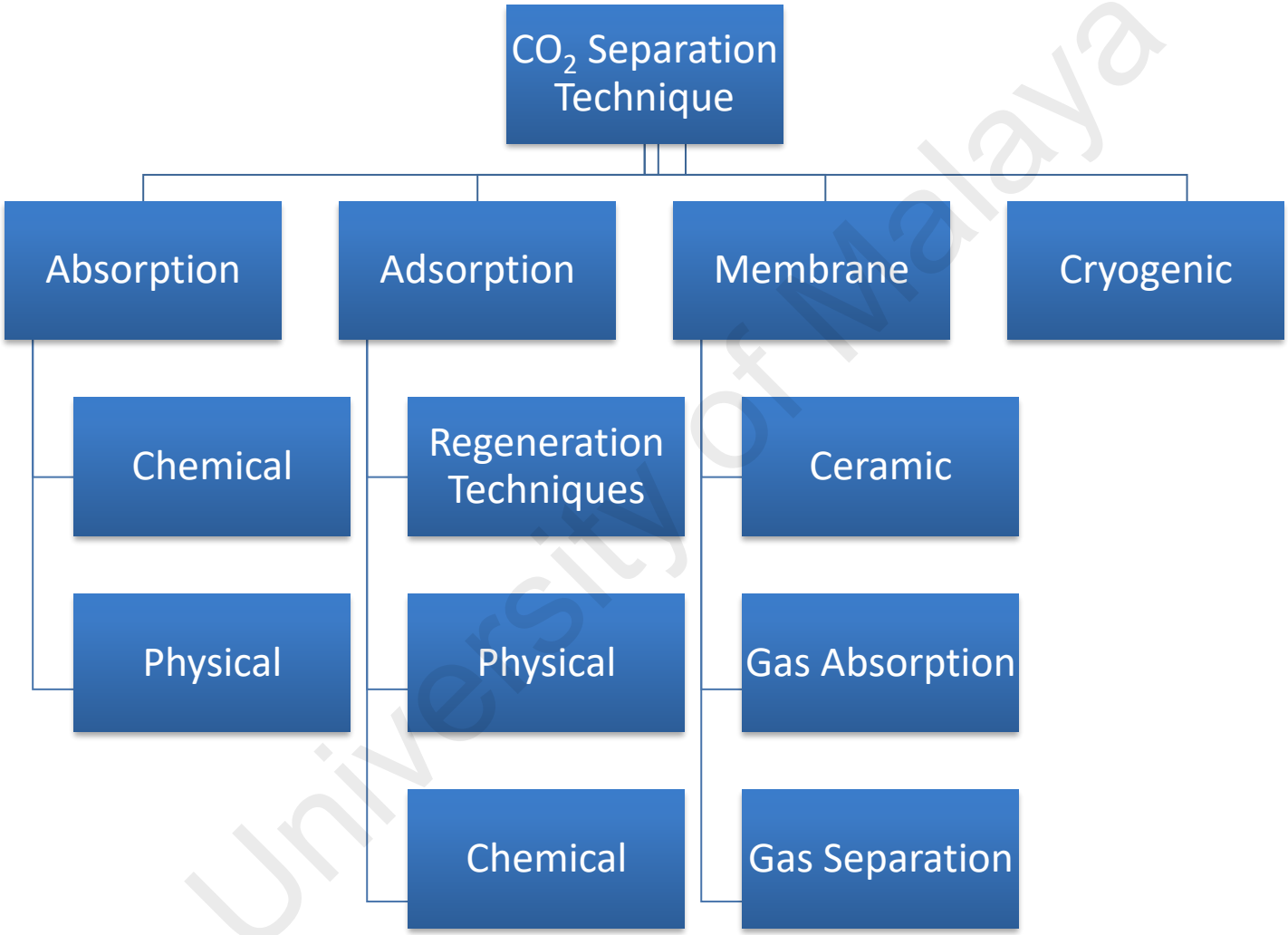

Figure 2.6: CO_2 separation technique

In membrane separation, the contacts between the flue gases and liquid solvents are mediated through the membrane. Separation is based on the interaction between gases with the membrane material by physical or chemical interaction. For CO_2 transport through the membrane, the pressure on the liquid and gas side is similar. Other than the separation of CO_2 from the flue gas stream, this method is also suitable for other gas separation such as O_2 from N_2 or CO_2 from natural gas. There are varieties of membrane suitable for gas separation such as zeolite, polymeric membrane and porous inorganic membrane. High CO_2 separation up to 88% were achieved by the development of highly efficient membrane (Leung et al., 2014). Achieving high CO_2 separation using membrane in one stage has been a hurdle, hence this process usually conducted in multiple stages. Due to this, it leads to an increase of total cost and energy consumption. Furthermore, the performance of the membrane separating system is significantly affected by the condition of the flue gas stream, such as temperature, pressure and CO_2 concentration (Brunetti et al., 2010).

The cryogenic separation technique is based on distillation phenomena. In principle, the separation was conducted at a very low temperature and high pressure, unlike the conventional distillation process with different gas mixture separation (instead of liquid mixture). In CO_2 separation, the temperature of the flue gas stream is cooled down to desublimation temperature (-135 °C) causing CO_2 to solidified. The solidified CO_2 is later separated from the flue gas and compressed to high pressure (100 – 200 atm). As an advantage, pure liquid CO_2 is directly produced, thus, profiting transportation options. On the downside, cryogenic process requires high energy consumption for the cooling process, especially for low CO_2 concentration gas stream. Hence, this technique is more suitable for

gas stream with high CO_2 concentration, such as in pre-combustion or oxyfuel combustion (Göttlicher & Pruschek, 1997).

As to date, CO_2 separation via an absorption process has been widely utilized, especially in oil and gas industries, coal fire plant and also in chemical industries. A liquid solvent is used to separate the CO_2 from the flue gas stream. CO_2-saturated solvent is subsequently regenerated through the stripping process by heating or/and depressurization. Figure 2.7 illustrates the general schematic for absorption/stripping process for CO_2 capture. The absorption process can be either by chemical or physical absorption. In physical adsorption, the solubility of CO_2 into the solution depends on the temperature and pressure of the system. An example of the physical absorption solvents is Rectisol, Selexol, fluorinated solvent, sulfolane and even ionic liquid. On the other hand, chemical absorption of CO_2 is through the acid-base neutralization reaction between CO_2 and solvent such as an aqueous solution of ammonia or alkanolamine. Details of absorption process will be discussed in detail in later sub-chapter.

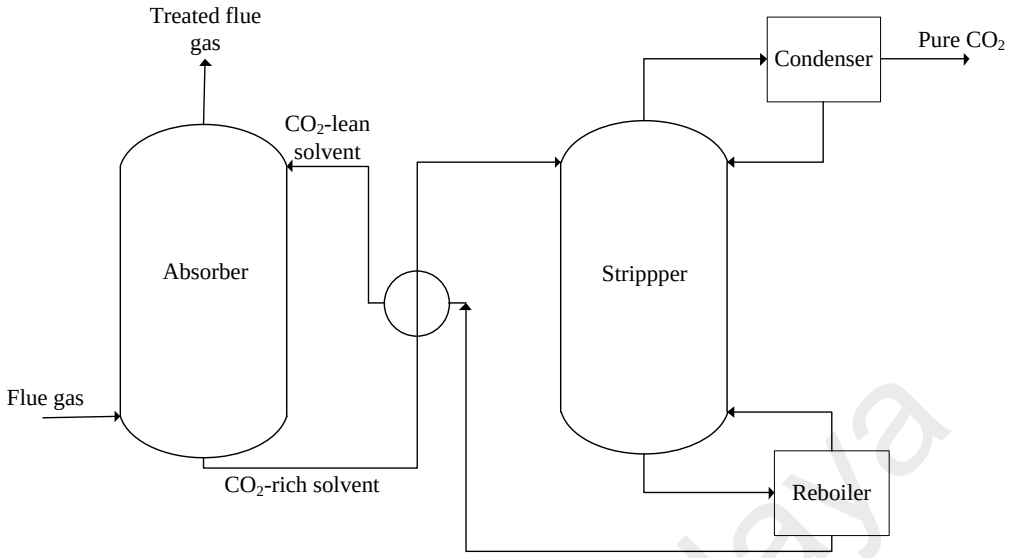

Figure 2.7: Schematic of basic absorption/stripping process for CO_2 capture

2.3 Solvents for CO_2 absorption

As mention earlier, there are numbers of technique for the separation of CO_2 from flue gas like absorption, adsorption, membrane, cryogenic and others, but the most prominent method by far is the absorption technique; absorption of CO_2 from the flue gas streams into the system bulk solvent. Physical and chemical properties of the solvent used for the absorption process significantly affect the environment, economic, safety and handling issues, along with end product separate from the system. Similarly, operating behavior such as thermal stability, vapor pressure contributes to the prevention of solvent loss by degradation and/or evaporation, which subsequently affect the total operational cost and environmental impact (Aschenbrenner & Styring, 2010; Wolfson et al., 2007). The absorption process can be either via chemical or physical absorption, depending on the properties of the solvent selected. In physical adsorption, the solubility of CO_2 into the solution depends on the temperature and pressure of the system. An example of the physical

absorption solvent is Rectisol, Selexol, fluorinated solvent, sulfolane and even ionic liquid. On the other hand, chemical absorption of CO_2 is through the acid-base neutralization reaction between CO_2 and solvent such as an aqueous solution of ammonia or alkanolamine.

2.3.1 Physical absorption solvent

Physical solvent has been successfully utilized in the CO_2 absorption process due to a number of advantages. The CO_2 loading capacity for physical solvent is governed by its ability to dissolve gas at given gas phase partial pressure (Henry's law constant). In short, physical solvent has no absorption limitation with loading capacity for a physical solvent increases with an increment of CO_2 partial pressure and able to hold more CO_2 than chemical solvent (Zaman & Lee, 2013).

The amount of CO_2 dissolved in a physical solvent is affected by temperature and pressure on the system. CO_2 molecules dissolved and retained in the solvent by a weak electrostatic or van der Waals bonding. Therefore, less energy is required to regenerate the CO_2-saturated solvent. The efficiency of physical absorption of CO_2 in the flue gas stream is subject to the concentration of CO_2 in the flue gas stream. Therefore, it is considered not economical for flue gas stream with CO_2 partial pressure less than 15 vol% of CO_2 because the flue gas pressurization increases energy requirement for CO_2 absorption process (M. Wang et al., 2011). The key attractive criteria of physical solvents for CO_2 capture are those having such properties as high thermal stability, extremely low vapor pressures, non-

flammability, and non-toxicity. Such materials do not only have the potential to capture CO_2 with minimal solvent loss in the gas stream but are expected to be environmentally benign.

2.3.1.1 Common physical absorption solvent

Organic solvents are usually used as a physical solvent for absorbing CO_2 from the flue gas stream. A number of physical solvents are commercially available are propylene carbonate (PC), dimethyl ether of polyethylene glycol (DMPEG), methyl isopropyl ether of polyethylene glycol (MPE), N-methyl-2-pyrrolidone (NMP), methanol, tributyl phosphate and methyl cyanoacetate (Kohl & Nielsen, 1997).

Propylene carbonate (PC) is a physical solvent used for the Fluor Solvent process. The process was applied in industries to process natural gas, ammonia synthesis gas and hydrogen. PC is a preferable choice when less to none H_2S present in the flue gas stream and the removal of CO_2 is crucial. PC has a lower solubility for hydrocarbon in natural gas processing and hydrogen in syngas treatment, which result in a lower gas compression cycle requirement for gas flashing stage at an intermediate pressure. The PC is able to operate at a lower temperature without turning too viscous enabling the process to be chilled down to lower temperature, improving the solvent CO_2 solubility. This result in a lower overall solvent circulation and plant operating cost (Burr & Lyddon, 2008).

DEPG is a mixture of DEGP ($CH_3O(C_2H_4O)_nCH_3$) with n ranging from 2 to 9. It is used to physically absorb CO_2, hydrogen sulfide (H_2S) and mercaptans from gas streams in the Selexol process (licensed by Honeywell Universal Oil Products). The Selexol process absorbs these gases from the feed gas stream at high pressure (300 to 2000 psi) with temperature ranging from -18 to 175 °C. The saturated solvent is then regenerated by bringing down the pressure and/or heating. The process can be constructed to separate H_2S and CO_2 as separate streams and usually requires a two-stage process with two absorption and regeneration columns. H_2S is selectively removed in the first column by a lean solvent that has been thoroughly stripped with steam, while CO_2 is removed in the second absorber. The second stage solvent can be regenerated with air or nitrogen for deep CO_2 removal (Kapetaki et al., 2015).

Purisol process utilizes NMP as a physical solvent with a general operating protocol similar to Selexol process. The process can be operated either at ambient temperature or at lower temperatures about -15 °C (Hiller et al., 2000). NMP possesses relatively high vapor pressure in comparison to PC and DEPG with resulted in the requirement of water washing stage of the treated gas and remaining flue gas to recover the loss solvent (Hochgesand, 1970). However, water washing stage is not necessary if the process system is operated at sub-ambient temperatures.

Tetrahydrothiophene 1,1-dioxide $(CH_2)_4SO_2$, also known as sulfolane (Figure 2.8) is versatile organosulfur dipolar aprotic solvent for various application. It is often used in the industries such as petrochemical, polymer and photographic chemical, textile, hydrocarbon

extraction and plasticizer (Ge et al., 2006; Moore et al., 2002) due to its high thermal and hydrolytic stability with high density and boiling point (Xu et al., 1992). Furthermore, sulfolane is one of the major components in the common industrial CO_2 absorption process called Sulfinol process. Sulfolane is used up to 45 % of total formulation which acts as physical absorbent facilitating the CO_2 absorption process and possess the high absorption capacity among other physical solvents (Angaji et al., 2013). Sulfolane was originally developed by Shell Oil Company by reaction between sulfur dioxide and butadiene in a cheletropic reaction producing sulfolene, followed by hydrogenation reaction catalyzed by Raney nickel to yield sulfolane. Subsequently, an improved pathway was developed via oxidation reaction between tetrahydrothiophene and hydrogen peroxide to produce tetramethylene sulfoxide, which will be further oxidized to yield sulfolane (Hatch & Matar, 1978). As comparison to other dipolar aprotic solvent, sulfolane poses a higher acute oral toxicity in comparison to dimethylsulfoxide (DMSO), *N*-methyl pyrrolidin-2-one (NMP), *N*,*N*-dimethyl formamide (DMF), and *N*,*N*-dimethyl acetamide (DMAC). However, sulfolane has a low skin permeability and low volatility, hence operationally safe to be handle in the industry (Tilstam, 2012).

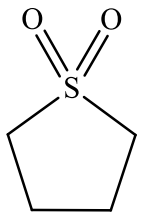

Figure 2.8: Chemical structure of sulfolane

2.3.1.2 Ionic liquids as physical solvent

2.3.1.2.1 Ionic liquids

Over the years, a new class of material (ionic liquids) has emerged as an attractive solvent used for various applications and were reported to be a potential solvent for CO_2 removal. Ionic liquids are compounds composed entirely of ions and are liquid at or below process temperatures. In general, ionic compounds composed entirely of ions, are solids with high melting points, for example, above 450 °C. These solids are commonly known as 'molten salts' when heated to above their melting points. Common example of this 'molten salt' is NaCl, with a melting point of 800 °C. In contrast to "molten salts", ionic liquids have low melting points, from −100 °C to 200 °C. They are liquid over a wide range of temperatures, with a liquid range of up to about 500 °C or higher. The definition of ionic liquid stated that "any ionic compound can be classified as ionic liquids if they composed only ions and can exist as liquid or solid with melting point below 100 °C" (Maurer & Tuma, 2009). The significant difference in melting point between the molten salts (example: sodium chloride, NaCl) and ionic liquids (example: 1-ethyl-3-methyimidazolium chloride, [C_2mim][Cl]) is due to the asymmetric large cation of ionic liquids causing a poorly coordination of packing structure between anion and cation. This prevents the formation of a stable crystal lattice. Subsequently lead to weak ionic bond between them as shown in Figure 2.9.

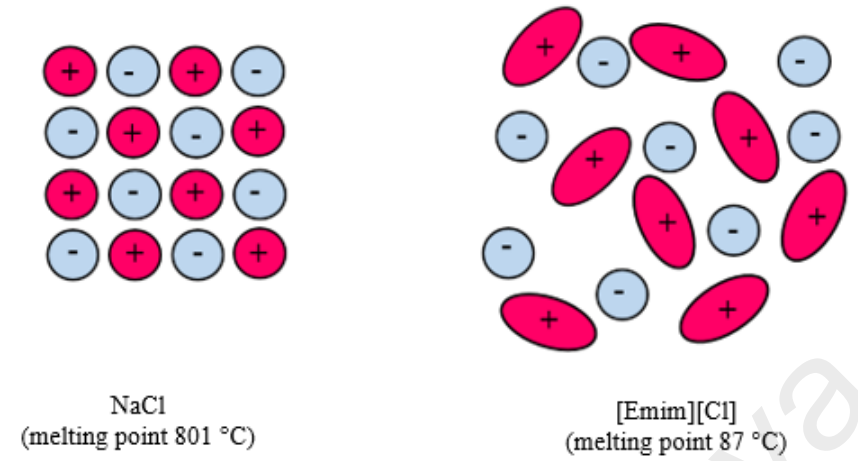

Figure 2.9: Comparison between lattice structure of NaCl (molten salt) and [C_2mim][Cl] (ionic liquid) (Wilkes et al., 1982)

Ionic liquids possess sets of exceptional physicochemical properties such as a wide range of liquid, thermal stability, negligible vapor pressure, tenability. Ionic liquids are generally non-volatile and numerous are air and water stable and can be good solvents for a wide variety of inorganic, organic, and polymeric materials. Another unique feature of ionic liquids is the tunability of their structures and properties that can be tuned to specific needs by manipulating cation and anion groups and/or attaching functional moiety to ions. It has been projected that $\sim 10^{14}$ matchless cation/anion combinations are achievable. Thus, they are known as designer media, whose great flexibility allows for optimizing the solvent for any particular use. The physicochemical properties, such as density, viscosity, melting point, boiling point, freezing point, and many more, of the ionic liquids are governed by their structure, hence the correlation between structures and properties needs to be understood prior to choosing and synthesizing the ionic liquids (Huddleston et al., 2001).

The initial discovery of ionic liquid was first reported by Walden in a Friedel-Craft reaction of concentrated nitric acid and ethylamine followed by removal of water producing pure liquid salt at room temperature. The liquid salt structure was later confirmed by nuclear magnetic resonance (NMR) spectroscopy technique as ethylammonium nitrate ($[EtNH_3][NO_3]$) with melting point of 12 °C (Walden, 1914). With relatively no publication regarding ionic liquids up to 1982, first dialkylammonium-based ionic liquids, 1-ethyl-3methylimidazolium tetrachloroaluminate ($[C_2mim][AlCl_4]$) was reported (Wilkes et al., 1982) and catalyzed the development of the 1st generation ionic liquids; combination of alkylammonium cations with chloroaluminate or other metal halide anions. Despite successful application as a catalyst and solvent in Friedel-Craft (Dupont et al., 2003) and oligomerization (Ellis et al., 1999) reactions, this type of ionic liquids drawbacks are its sensitivity to moisture and reactive to various organic compounds and therefore, not applicable for many organics reactions. In the later year, 2nd generation of ionic liquids was later initiated (Wilkes & Zaworotko, 1992) by combining *N*,*N*-dialkylimidazolium cations with water stable or weakly coordinating anions such as tetrafluoroborate ($[BF_4]^-$), hexafluorophosphate ($[PF_6]^-$), sulfate ($[SO_4]^-$), nitrate ($[NO_3]^-$) and trifluoromethanesulfonate $[CF_3O_3S]^-$. This type of ionic liquid is water and air tolerance with moderate polarity with most of them are hydrophobic and immiscible in water. However, this type of ionic liquid has a similar toxicity level as chlorinated or aromatic solvent, high cost and lack of large scale production (Docherty & Kulpa Jr, 2005). Due to the gained interest for ionic liquid within the past few years by the research community, 3rd generation ionic liquids have been developed especially with based of 1,3-dialkylimidazolium, quaternary ammonium or choline cation and sugars, amino acids, organic acids or sulfuric acid as cations. Figure 2.10 illustrates the structures of typical cations and anions used in producing ionic liquids.

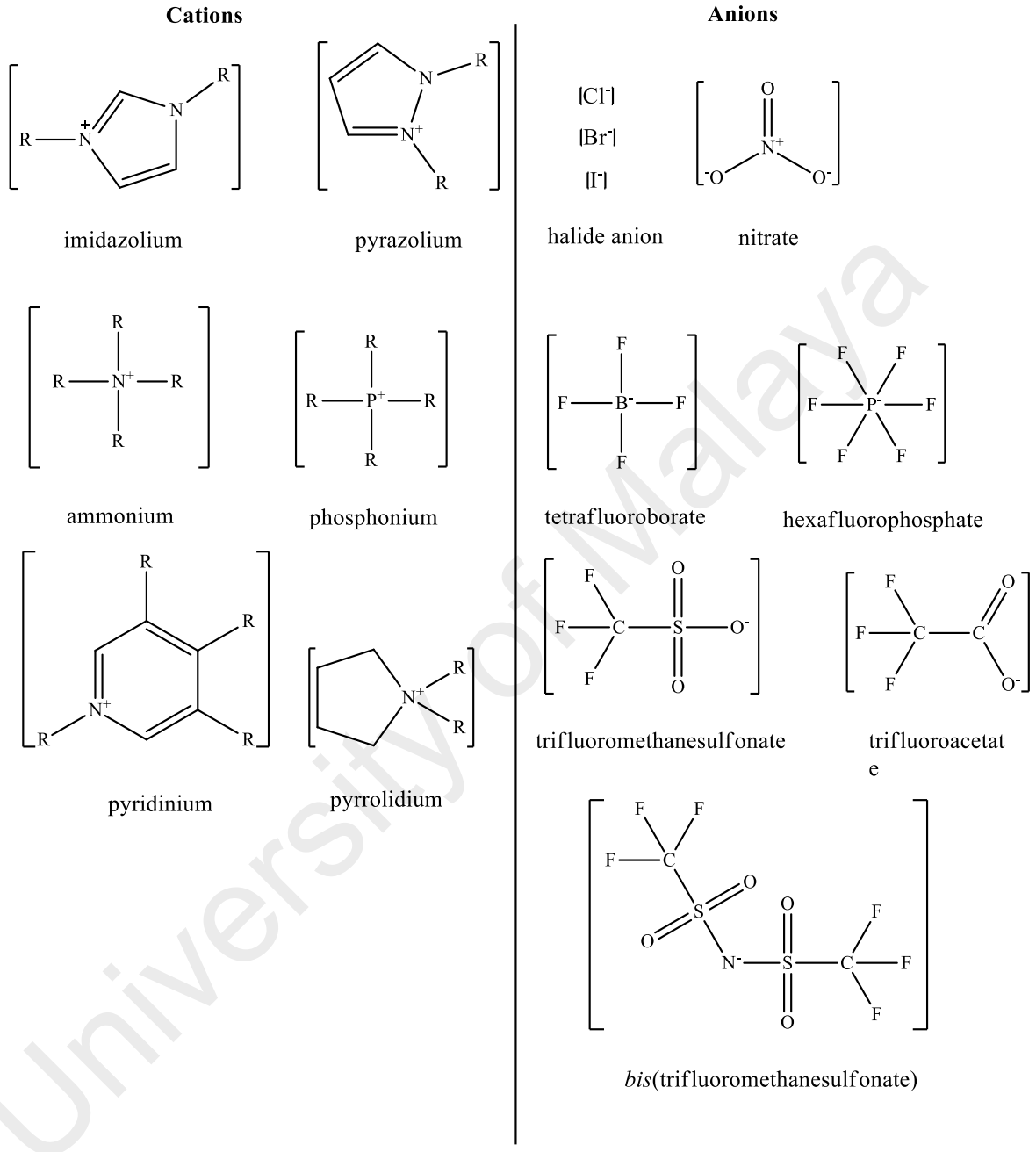

Figure 2.10: Structures of typical cations and anions used in ionic liquids

2.3.1.2.2 Ionic liquids for CO_2 capture

Over the past decades, ionic liquids have been studied for various fundamental and industrial applications and have been suggested as viable alternative absorption solvent for CO_2 capture due to its unique attribute; extensive liquid variety, thermal stability, tunable physicochemical properties, and negligible vapor pressure. CO_2 can significantly dissolve in ionic liquids as compared to the conventional organic solvent as physical solvent (Hasib-ur-Rahman et al., 2010). One of the main issues to consider in the ionic liquid application is its high viscosity, but by choosing an appropriate cation-anion combination, the viscosity if ionic liquids can be reduced to an acceptable range.

Many studies on ionic liquids, especially those with imidazolium-based cations have been conducted and these show that some ionic liquids have high CO_2 solubility. Initial study on the solubility of CO_2 in ionic liquid was conducted using 1-butyl-3-methylimidazolium hexaflourophosphate, [BMIM][PF_6], with the solubility of CO_2 about 0.6 mol fraction at 8 MPa (Blanchard et al., 1999). A series of ionic liquids, 1-*n*-butyl-3-methylimidazoliumhexafluorophosphate [C_4MIM][PF_6], 1-*n*-octyl-3-methylimidazoliumhexafluorophosphate [C_8MIM][PF_6], 1-*n*-octyl-3-ethylimidazoliumtetrafluoroborate [C_8MIM][BF_4], 1-*n*-butyl-3-methylimidazoliumnitrate ([C_4MIM][NO_3]), 1-ethyl-3-methylimidazolium ethylsulfate [C_2MIM][$EtSO_4$], and *N*-butylpyridiniumtetrafluoroborate [*N*-bupy][BF_4] under high-pressure with large quantity of CO_2 was found to dissolve in the ionic liquid phase, while no visible amount of ionic liquid solubilized in the CO_2 phase (Blanchard et al., 2001).

Studies of CO_2 solubility in 1-butyl-3-methylimidazoliumhexafluorophosphate ($[C_4MIM][PF_6]$) and 1,1,3,3-tetramethylguanidium lactate (TMGL) at 297–328 K under 0–11 MPa showed that the solubility of CO_2 in TMGL (2.77 mol kg^{-1}) was slightly higher than those in $[C_4MIM][PF_6]$ (2.65 mol kg^{-1}) at 319 K and 5.73 MPa and TMGL has been reported to possess high selectivity toward CO_2 than other gases such as N_2, O_2, CH_4 and H_2 (Yuan et al., 2006; Zhang et al., 2005).

The nature of cation and anion components significantly affects the solubility of CO_2 in ionic liquids. Studies on CO_2 solubility in fluorinated cation ionic liquids, $[C_8H_4F_{13}MIM][Tf_2N]$, $[C_6H_4F_9MIM][Tf_2N]$, and $[C_6MIM][Tf_2N]$ showed that the CO_2 solubility was higher in $[C_8H_4F_{13}MIM][Tf_2N]$ than $[C_6H_4F_9MIM][Tf_2N]$, and lowest in $[C_6MIM][Tf_2N]$. Overall, the CO_2 solubility increases with an increase of the numbers of fluorine in the alkyl side chain, but this tendency was not very visible (Anderson et al., 2007; Muldoon et al., 2007). Fluorinated side chains greatly enhance the uptake of CO_2 with respect to the corresponding non-substituted side chains, but at the expense of an increase in viscosity (Shin & Lee, 2008). Increasing the alkyl-side chain length of the imidazolium-based cation of the ionic liquids will also increase the CO_2 solubility to a certain extent; but the increase of solubility is not as prominent as that by substituting the anion component.

Experimental data and molecular simulation results showed that anion component gives rise to the more prominent effect to the CO_2 solubility with $[Tf_2N]^-$ is among the highest affinity towards CO_2 (Cadena et al., 2004). Similar observations were also reported in CO_2 solubility study in ionic liquids with $[MMIM]^+$ cation and various different anions with the

result showed that the CO_2 solubility increase with anion of following order; $[NO_3]^-$ < $[DCA]^-$ < $[BF_4]^-$ < $[PF_6]^-$ < $[CF_3SO_3]^-$ < $[Tf_2N]^-$ < [methide] (Aki et al., 2004). The effect of anion selection on the CO_2 solubility in ionic liquids has also been reported for [BMIM] $[PF_6]$, [BMIM]$[Tf_2N]$ and [BMIM][FAP] at temperature 298.15 to 323.15 K and pressure up to 2000 kPa. The result showed that the solubility of CO_2 in ionic liquids increases in following order: [BMIM][FAP] > [BMIM]$[NTf_2]$ > [BMIM]$[PF_6]$, with molar fractions of absorbed CO_2 corresponding to 0.47, 0.40 and 0.29, respectively. Similar to the general trends for solubility of gases in ionic liquids, CO_2 solubility increased with increasing pressure and decreasing temperature (Gonzalez-Miquel et al., 2013). High affinity between anion, particularly fluorinated anion with CO_2 molecules is due to the high coulombic interaction and was proven by multiple literatures (Jalili et al., 2010; Zhang et al., 2008). Table 2.2 summarizes some reported ionic liquids studied for CO_2 capture application.

Table 2.2: Various work on ionic liquids for CO_2 capture

Authors	Ionic liquids studied	Parameters	CO_2 solubility
(Blanchard et al., 2001; Lynnette A. Blanchard et al., 1999)	$[C_4MIM][PF_6]$; $[C_4MIM][PF_6]$; $[C_8MIM][PF_6]$; $[C_8MIM][BF_4]$;$[C_4MIM][NO_3]$; $[C_2MIM][EtSO_4]$;[*N*-bupy]$[BF_4]$; $[MIM][NO_3]$	P = 8–13.8 MPa, T = 313.15 to 333.15 K	At high-pressure, large quantity of CO_2 dissolved in the ionic liquid phase, while no visible amount of ionic liquid solubilized in the CO_2 phase
(Zhang et al., 2005)	[BMIM]$[PF_6]$ and 1,1,3,3-tetramethylguanidium lactate (TMGL)	T = 297–328 K P = 0–11 MPa	Solubility of CO_2 in TMGL is slightly larger than in [BMIM]$[PF_6]$

(Kumełan et al., 2006)	[HMIM][Tf_2N]	T = 293.15–413.2 K P = up to 10 MPa	CO_2 solubility linearly increases with increasing pressure at a given temperature.
(Muldoon et al., 2007)	[HMIM][Tf_2N]; [HMPy][Tf_2N]; [$C_6H_4F_9$MIM][Tf_2N]; [$C_8H_4F_{13}$MIM][Tf_2N]; [HMIM][eFAP]; [HMIM][pFAP]; [P_5MIM][bFAP]; [Et_3-NBH_2MIM][Tf_2N]; [HMIM][PF_6]; [choline][Tf_2N]; [HMIM][Tf_2N]; [N_{4111}][Tf_2N]; [$C_6H_4F_9$-MIM][Tf_2N]; [HMIM][eFAP]; [P_5MIM][bFAP]	T = 283.15 K, 298.15 K, 333.15 K P = (1.3 < P < 15 MPa)	CO_2 solubility was improved in ionic liquids that contain a level of fluorination.
(Zhang et al., 2008)	[HMIM][FEP]; [HEMIM][OTf]; [HEMIM]; [Tf_2N]	T = 283.2 K, 298.2 K, 323.2 K P = 1.8 MPa	High affinity between fluorinated anion with CO_2 molecules is due to the high coulombic interaction
(Jalili et al., 2010)	[HEMIM][PF_6]; [HEMIM][OTf]; [HEMIM][Tf_2N]	T = 303.15–353.15 K P = up to 1.3 MPa	High affinity between fluorinated anion with CO_2 molecules is due to the high coulombic interaction
(Kumełan et al., 2010)	1-n-butyl-1-methylpyrrolidinium	T = 293.1 K, 413.2 K	CO_2 solubility linearly

	bis(trifluoromethylsulfonyl)amide [BMPY][Tf_2N]	P = 10.8 MPa	increases with increasing pressure at a given temperature
(Cabaço et al., 2011)	1-butyl-3-methyl-imidazolium-trifluoro acetate ([BMIM][TFA])	T = 313 K P = 0.1–9 MPa	Increasing alkyl chain led to increasing concentrations of CO_2 molecules resides in the void existing among the different ion pairs.

Although ionic liquids have been studied extensively over the years for CO_2 capture application as physical solvent and have been proven to be a promising alternative solvent, they are still economically unviable for industrial scale. Moreover, ionic liquids as physical solvent is still unsuitable for post-combustion process due to lower CO_2 present in the flue gas stream (15 vol%) which renders ionic liquids inefficient.

2.3.2 Chemical absorption solvent

Chemical solvents are chosen to be used for the absorption process for CO_2 capture primarily because it has a high CO_2 absorption even at lower CO_2 partial pressure. Hence it offers an efficient and economical option in comparison to other methods (Olajire, 2010). In the chemical absorption process, the CO_2 in the flue gas stream is separated from the gas stream by a chemical reaction of the solvent, producing a stable intermediate compound in

the liquid phase. Subsequently, the saturated solvent containing the intermediate compound is heated to release the CO_2 for capturing, compression and transport. The regenerated solvent which contains trace amount of dissolved CO_2 is then fed back into the absorption process. There are several solvents that can be used for the chemical CO_2 absorption process such as amines, ammonia, potassium carbonate (K_2CO_3) or sodium carbonate (Na_2CO_3), but the most commercially used chemicals solvent used throughout the industry are alkanolamines. The essential criteria for chemical solvent selection includes high CO_2 absorption rate and capacity, low regeneration energy requirement, high chemical and thermal stability, low vapor pressure, low molecular weight, low viscosity and low corrosion rate (Zaman & Lee, 2013).

2.3.2.1 Alkanolamines

Alkanolamines are the most common option for CO_2 absorption and widely utilized in the industries. Alkanolamine is a chemical compound with amino and the hydroxyl functional group on an alkane backbone. Figure 2.11 illustrates common alkanolamines used as a chemical solvent in CO_2 capture in the absorption process; MEA, DEA, MDEA, AMP, DIPA, DGA and AEEA (Shakerian et al., 2015). The general reaction scheme of CO_2 with alkanolamines are shown in Figure 2.12. Primary and secondary alkanolamine react with CO_2 through a zwitterion mechanism to form carbamate. Theoretically, CO_2 loading for primary and secondary alkanolamines ranges from 0.5-1 $mol_{CO_2}/mol_{alkanolamine}$ due to the formation of carbamate (without present of water/OH^-) or hydrogen carbonate (presence of water/OH^-) (Figure 2.12 (i) and (ii)). Tertiary alkanolamines such as MDEA react via base-catalyzed hydration to form hydrogen carbonate as shown in Figure 2.12 (iii). This is due to

the lack of hydrogen on the nitrogen atom. Therefore, tertiary alkanolamine has a theoretical CO_2 loading of 1 $mol_{CO_2}/mol_{alkanolamine}$ as MDEA does not form carbamates.

Even though tertiary alkanolamine, MDEA, has a higher theoretical CO_2 loading than primary, MEA, and secondary alkanolamine, DEA, MDEA has a much slower absorption rate in comparison to primary and secondary alkanolamine. One of the alternatives for this issue is by substituting MDEA with AMP, a sterically hindered alkanolamine. AMP formed an unstable carbamate ion in its reaction with CO_2, which leads to a much higher CO_2 loading capacity than MEA but at a slower absorption rate at 40 °C (Quadrelli & Peterson, 2007). Other alternative includes application of aqueous piperazine (PZ) solution. It has been reported that PZ is a better alternative than MEA for CO_2 absorption process due to its higher absorption rate and capacity, low volatility with higher thermal stability and required less energy for regeneration (Nielsen & Rochelle, 2017).

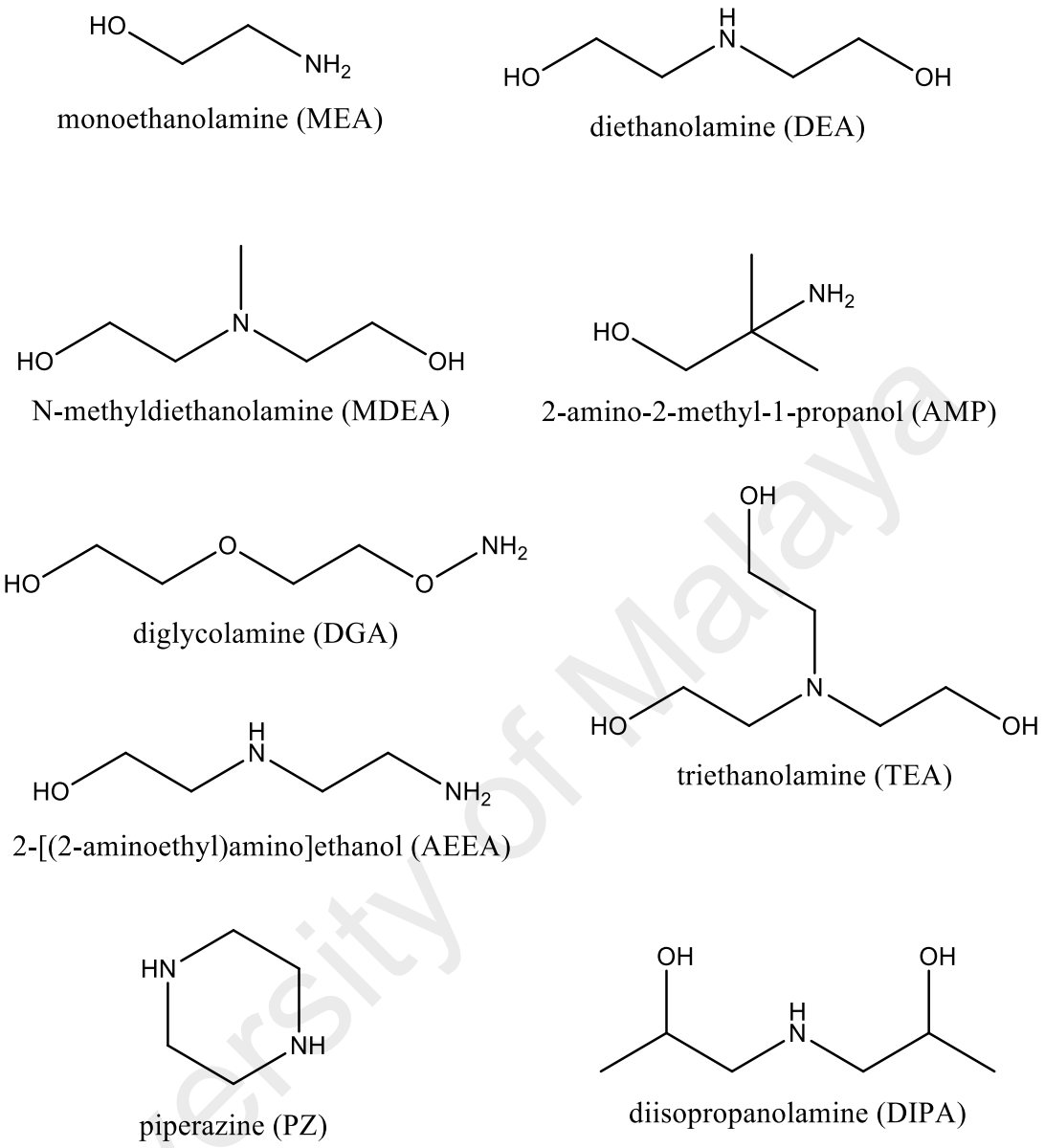

Figure 2.11: Structural formula of typical alkanolamines used for CO_2 capture

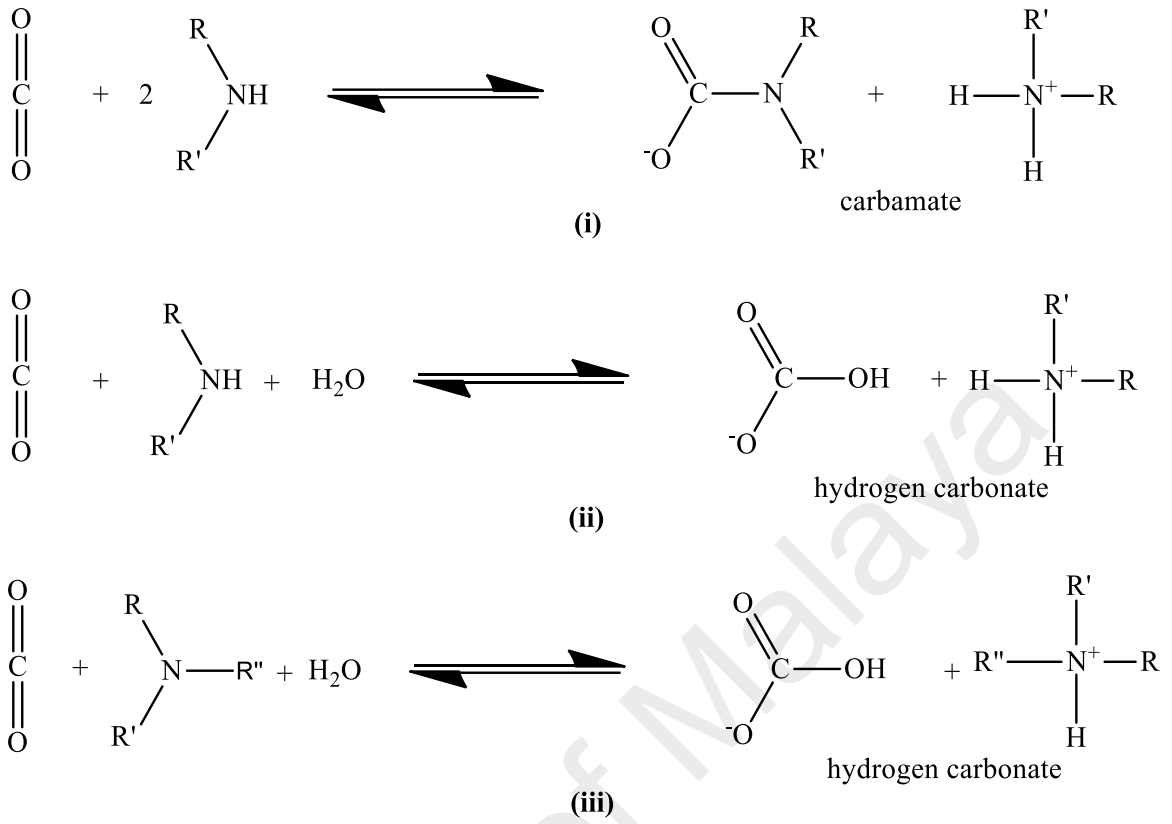

Figure 2.12: General reaction schemes for the chemical absorption of CO_2 by primary or secondary amines (i) without water, (ii) with water, and (iii) tertiary amine-containing solvents (Chen et al., 2014)

Blending of multiple alkanolamines has been utilized to improve the efficiency of the chemical solvent by utilizing the advantages of each singular alkanolamine. For example, the mixture of primary or secondary alkanolamine (eg.: MEA, DEA) with the tertiary amine (eg.: MDEA) is suggested to be a mixture that has a high absorption rate and higher CO_2 loading capacity attributed from primary/secondary and tertiary alkanolamine, respectively. Mixture of AMP and MEA has been reported to have the better absorption capacity, improved selectivity, higher absorption rate and less corrosion and degradation in comparison to conventional alkanolamine (Xiao et al., 2000). Pilot plant studies were conducted using a solvent mixture of MEA and MDEA with 4:1 molar ration shows a reduction of the heat

requirement in comparison to singular MEA aqueous solution which economically desirable (Idem et al., 2006). PZ was also used in combination with other alkanolamines to yield higher absorption rate and absorption capacity of the alkanolamines mixture. Example of the blends is PZ and MDEA which was utilized and patented by BASF for the removal of CO_2 in ammonia plants (Appl et al., 1982; Bishnoi & Rochelle, 2000)

Despite establishment and maturity of the CO_2 absorption using alkanolamine as a chemical solvent, this system still endures several drawbacks (Mondal et al., 2012):

- Corrosion of the equipment by the amine in the solvent limits the total amine concentration in the system and create addition maintenance cost.
- Alkanolamine compound loss from the system by evaporation during the regeneration process leads to an increase of production costs and potential environment issues.
- Alkanolamine degradation by the presence of SO_2, NO_2, HCl, HF and O_2 in the flue gas stream
- High energy requirement during the solvent regeneration process.

2.3.2.2 Ionic liquids as chemical solvents

As discussed in earlier, ionic liquids have unique properties like neglectable vapor pressure, thermal and chemical stability that is very desirable for CO_2 absorption process. Although ionic liquids show great potential as CO_2 absorbent with satisfactory solubility and selectivity for CO_2, conventional ionic liquids possess limitation in terms of CO_2 absorption

application and still are incomparable with the conventional chemical solvents (e.g.: alkanolamine) used commercially in the industries. Hence, ionic liquids tunable properties play an essential role in modifying ionic liquids to suit the end application. An attempt to create ionic liquids with chemical solvent abilities was undertaken by introducing amine functionality into anion or cation component of the ionic liquids. These amine-functionalized ionic liquids can be a promising alternative for CO_2 capture. It has been reported that a task specific ionic liquid (TSIL) with amine functionality is able to capture CO_2 via chemical reaction at low CO_2 pressure up to 33 mol%, which is significantly higher solubility in comparison to conventional ionic liquids (Bates et al., 2002). Similarly, studies of the amine-functionalized cation of 1-butyl-3-imidazolium tetrafluoroborate, [Am-IM][BF_4] and 1-butyl-3-imidazolium dicyanamide, [Am-IM][DCA] were compared with non-functionalized [BMIM][BF_4] and [BMIM][DCA]. The result shows higher CO_2 solubility in the amine-functionalized ionic liquids in comparison to the non-functionalized ionic liquids due to the introduction of an amine group into the cations of the ionic liquids (Sánchez et al., 2011). Higher CO_2 solubility coupled with the unique properties of ionic liquids makes them a viable alternative to conventional chemical solvent. Figure 2.13 illustrates the proposed reaction scheme of amine-functionalized TSIL with CO_2.

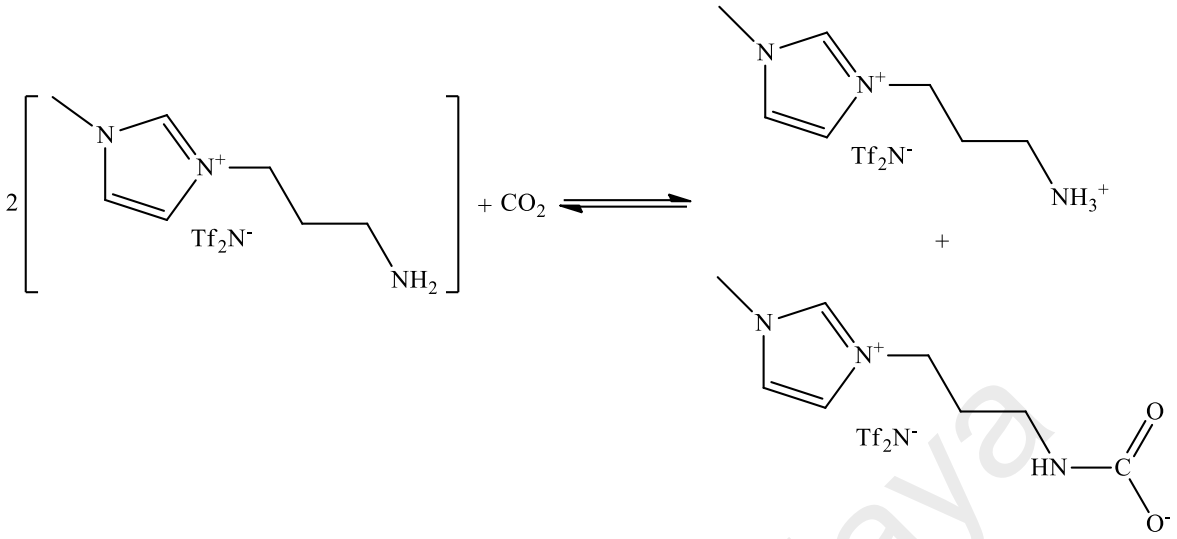

Figure 2.13: Proposed stoichiometric reaction of CO_2 with TSIL (Gutowski & Maginn, 2008)

1-aminoethyl-2,3-dimethylimidazolium cation with taurine amino acid anion [aemmim][Tau] (Figure 2.14) TSIL was synthesized and tested for CO_2 solubility at T= 303.15 to 323.15 K and pressure 0.2 – 1 bar. Results show that the CO_2 capacity reached up to 0.9 $mol_{CO_2}/mol_{[aemmim][Tau]}$. The saturated TSIL can be easily desorbed at low pressure and high temperature indicating the possibility for regeneration. The CO_2 was absorbed via chemical reaction (Xue et al., 2011). A similar observation was reported with dual amino-functionalized phosphonium ionic liquids with amino acids as an anion with the reported CO_2 solubility reached up to 1 mol_{CO_2}/mol_{TSIL} (Zhang et al., 2009).

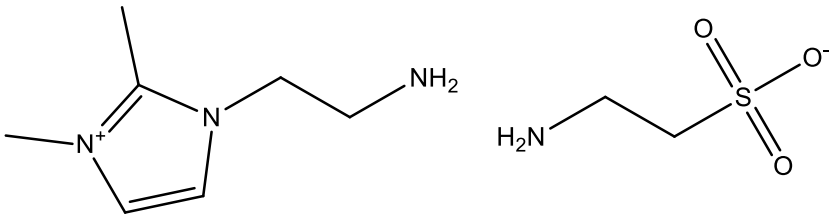

Figure 2.14: Chemical structure of [aemmim][Tau]

There are some challenges for amine-functionalized TSIL in CO_2 capture application. The amine functionality leads to the increase of viscosity of the TSIL at ambient temperature causing a decrease in the absorption rate. Furthermore, production of this TSIL involved multiple synthesis and purification steps, which increase the total production cost and time (Bara et al., 2010; Bates et al., 2002).

2.3.3 Hybrid solvent for CO_2 capture

Combination of a physical and chemical solvent will bring forward unique properties of both types of solvent into the hybrid mixture. It has been the commercially utilized in the industries. One of the most prominent examples is the application of Sulfinol process for flue gas stream treatment. Solvents used for the Sulfinol process composed of sulfolane (2,3,4,5-tetrahydrothiophene 1,1-dioxide) as a physical solvent and an alkanolamine (DIPA or MDEA) as a chemical solvent. Another commercial hybrid solvent is used in Amisol process, which composed of methanol as the physical solvent and a secondary amine as the chemical solvent (Olajire, 2010; Zaman & Lee, 2013).

Such approach was also adopted by researcher on improving ionic liquids for CO_2 capture, i.e., mixture of ionic liquids with alkanolamines. For example, a mixture of 1-ethyl-3-methylimidazolium *bis*(trifluoromethylsulfonyl)imide, $[C_2mim][Tf_2N]$ with primary alkanolamine, MEA which resulted in CO_2 absorption via stoichiometric chemical reaction (0.5 mol_{CO_2}/mol_{MEA}) at low pressure. Subsequently, desorption of the saturated solvent takes place at lower pressure and high temperature by decomplexation of the carbamate salt

(Bara et al., 2010). The same approach was also conducted for mixture of TSIL and alkanolamine. In the studies conducted, several amino-functionalized ionic liquids, tetraethylammonium glycinate ($[N_{2222}][Gly]$), tetraethylammonium lysinate ($[N_{2222}][Lys]$), tetramethylammonium glycinate ($[N_{1111}][Gly]$), tetramethylammonium lysinate ($[N_{1111}][Lys]$), were mixed with an aqueous MDEA solution and tested for CO_2 absorption which reported in significant increase of CO_2 solubility. Mixture of TSIL (15 wt%) and MDEA (15 wt%) possess higher CO_2 solubility and absorption rate in comparison to MDEA and ionic liquid mixture with 30 wt% of amine (Feng et al., 2010).

Some studies of ternary mixtures of aqueous MEA blend with series of ionic liquids show the ability to capture CO_2. They reported that a solvent mixture of 1-ethyl-3-methylimidazolium octyl sulfate ($[EMIM][OcSO_4]$)/MEA/H_2O the CO_2 capacity was dependent to the mass fraction of the ternary component. However, different observations were reported with a mixture containing 1-butyl-3-imidazolium acetate, [BMIM][OAc], due to the presence of an acetate functional group that has a high chemisorption capacity. Furthermore, the incorporation of water reduces the viscosity of the solvent mixture (Baj et al., 2013). Another CO_2 solubility study was conducted with aqueous MEA with mixtures of different ionic liquids, *bis*(2-hydroxyethyl) ammonium acetate (bheaa) and $[BMIM][BF_4]$ at pressure from 100 to 1600 kPa and at T = 298.15 K, 303.15 K and 308.15 K. The solubility of CO_2 in aqueous [bheaa] + MEA blends was higher than that of $[BMIM][BF_4]$ + MEA solution, mainly due to physical absorption, where the CO_2 loading was directly proportional to partial pressure. On the other hand, for the $[BMIM][BF_4]$ + MEA mixtures, the CO_2 loading was not proportional to partial pressure, mainly due to the formation of soluble carbamate. In case of [bheaa] + MEA blends the rate of absorption increased with

temperature, but the CO_2 loading was same, while for [BMIM][BF_4], CO_2 loading decreased with increasing temperature (Taib & Murugesan, 2012).

In conclusion, application of hybrid solvent for CO_2 capture via absorption is promising for the industries by incorporating unique properties of both ionic liquids and alkanolamines. However, the regeneration and reusability of these hybrid solvents together with thermophysical properties should be investigated to make a viable industrial application possible.

2.4 Non-aqueous solvents for CO_2 capture

Separation of CO_2 from the flue gas by absorption method using aqueous alkanolamine has been studied over many years (Astaria et al., 1983; Caplow, 1968). Aqueous alkanolamines, primarily MEA, DEA and MDEA have been utilized in the industries such as natural gas treatment, gas refinery and fossil fuel based power generator exhaust gases treatments due to their high CO_2 absorption efficiency and capacity at a lower CO_2 concentration (Böttinger et al., 2008). Nevertheless, as mentioned previously, the aqueous alkanolamine requires high temperature for the solvent regeneration process which translates to high energy cost. Furthermore, alkanolamine solution has a high vapor pressure, which leads to solvent loss due to evaporation. In addition, oxidative and thermal degradation and corrosion of equipment by the alkanolamine aqueous solution, still present as major problems (Lepaumier et al., 2009; Reynolds et al., 2012)

In the presence of water, CO_2 is captured by the alkanolamine aqueous solution by the formation of HCO_3^-(and to a much lesser extent as CO_3^{2-}) and thermally stable carbamate and this was verified using ^1H NMR and ^{13}C NMR studies (Ballard et al., 2011). Releasing the CO_2 from the stable carbamate and bicarbonate complexes requires high regenerating temperature, up to 140 °C, demanding high amount of energy. Throughout the regeneration process, a large amount of heat is initial utilized to increase the solution temperature to the regenerating temperature because of the specific heat capacity of the aqueous solution. Furthermore, the high heat energy subsequently resulted in water evaporation with leads to solvent loss. It was also reported by substituting water with an organic solvent, improvement in terms of reduced solvent decomposition, reduced energy requirement in the aqueous alkanolamine solution regeneration due to lower heat capacity or organic solvent, higher vapor pressure and higher boiling point (Oexmann & Kather, 2010).

Equipment corrosion during the CO_2 capture process by absorption using aqueous alkanolamine solution is one of the major issues to take into consideration. A recent study of economical view on corrosion in gas sweetening plants concluded that 25% of the maintenance budget was dedicated for corrosion control and approximately half of the maintenance work orders were due to corrosion issues (Kittel & Gonzalez, 2014; Tems & Al-Zahrani, 2006). Corrosion issue is faced in numerous pieces of equipment for the CO_2 capture operation plant with different types of corrosion. It was suggested that most systems suffered from wet acid gas corrosion and corrosion by amine solution. Wet acid gas corrosion effects on all parts of the units that are in contact with an aqueous phase with a high concentration of dissolved acid gases, like CO_2. However, the effect is more prominent in segments where the gaseous phases have high concentrations of acid gases and where water

may condense, mainly at the bottom of the absorber and the top of the regenerator (RB Nielsen et al., 1995). The major anodic and cathodic electrochemical reactions occurring in aqueous amine systems during the corrosion phenomenon are written as follows (Soosaiprakasam & Veawab, 2008):

(a) Anodic reaction

$$Fe \rightarrow Fe^{2+} + 2e^{-} \ (iron\ oxidation) \tag{2.4}$$

(b) Cathodic reaction

$$2H_2O + 2e^{-} \rightarrow 2OH^{-} + H_2 \uparrow \tag{2.5}$$

$$2HCO_3^{-} + 2e^{-} \rightarrow 2{CO_3}^{2-} + H_2 \uparrow \tag{2.6}$$

$$2H_2O + O_2 + 4e^{-} \rightarrow 4OH^{-} \tag{2.7}$$

(c) Corrosion product

$$Fe^{2+} + 2OH^{-} \rightarrow Fe(OH)_2 \tag{2.8}$$

$$Fe^{2+} + 2{CO_3}^{2-} \rightarrow FeCO_3 \tag{2.9}$$

Generally, aqueous alkanolamine solutions are not inherently corrosive, due to their high pH and low conductivity. However, CO_2-rich aqueous amine solution exhibits its corrosive properties when the alkanolamine have reacted with CO_2. Although no definite corrosion mechanisms by amine solutions were reported, mechanism model proposed by Riesenfeld and Blohm is as follows (RB Nielsen et al., 1995):

$$R_3NH^+ + HCO_3^- \rightarrow R_3N + H_2O + CO_2 \quad (2.10)$$

$$R_2NH_2^+ + R_2NCO_2^- \rightarrow 2R_2NH + CO_2 \quad (2.11)$$

$$Fe + H_2O + CO_2 \rightarrow FeCO_3 + H_2 \quad (2.12)$$

It can be concluded that, presents of water play an essential role in the corrosion phenomenon in CO_2 absorption process. Water in the solution act as an oxidizer for cathodic reaction and formation of carbonate, HCO_3^- from the dissolved CO_2 in the solution. Hence, substitution of water by other high-boiling point organic solvents, could eliminate the corrosion and also a considerable amount of thermal energy can be saved during the solvent regeneration cycle.

Recently, non-aqueous solutions were investigated for acid gas treatment. It was reported that, substitution of water with alcohol (methanol or ethanol) in alkanolamine solution could enhance the CO_2 absorption (Hamborg et al., 2011; Usubharatana & Tontiwachwuthikul, 2009). Other researchers have developed a mixture of alkanolamine

with glycols with almost similar observation for CO_2 capture; MEA + TEG and AMP + DEG and AMP + TEG (Li et al., 2012; Jing Tan et al., 2011; C Zheng et al., 2012, 2013). The chemical absorption rate of CO_2 with DIPA, TEA, MEA, and MDEA with polar organic solvents was also reported (Park et al., 2006a; Park et al., 2005; Park et al., 2006b). However, these non-aqueous mixture systems usually have a relatively high vapor pressure, and thus are not suitable for CO_2 capture from flue gases. Specific organic liquids have been designed and tested for CO_2 capture, including CO_2 binding organic liquids, CO_2BOLs (Heldebrant et al., 2008) and ionic liquids (Hart et al., 2010) have advantages over the aqueous alkanolamines solution due to their high-boiling, thermally stable liquids with lower heat capacity than water. However, due to the expensive synthesis of the starting compounds in comparison to alkanolamines and the high viscosity of the carbonated derivatives, application in the industrial processes is still limited. Similarly, mixed solvent of ionic liquids and alkanolamine shows great efficiency and reversible performance in the CO_2 capture show more commercial potential. However, the comparatively high viscosity, price, and their unknown toxicity impedes ionic liquids for large-scale industrial application.

One of the most promising solvent viable for non-aqueous approach is switchable-polarity solvent (SPS) which is very useful in separation process. A switchable-solvent specifically activated by CO_2 was originally developed by Jessop group whereby the polarity of the solvent was switched between low-polarity and high-polarity by the addition of CO_2 into the solution and switch back to low-polarity by removal of CO_2. The solution composed of alcohol and an amidine or guanidine will react with CO_2 forming ionic liquids which increase the polarity of the mixture considerably. The polarity is reversed by removing CO_2 via heating the solution (Alshamrani et al., 2016; Jessop et al., 2012). However, alcohol and

amidine/guanine dual component combination were not practical for industrial application due to losses of constituent via evaporation. This issue was overcome by combining both functionality of the components into single compound, such as alkanolguanidine derived from tetramethylguanidine (TMG) core with linear alcohols (Heldebrant et al., 2010). In comparison to the dual component solvent, this solvent is less volatile but generate ionic liquids with higher viscosity which lead to lower CO_2 loading. However, higher CO_2 loading was observed under high pressure. At higher CO_2 pressure, physical absorbent solvent was more favorable due to the more economical CO_2 release via pressure swing process. Study has shown that anhydrous tertiary alkanolamines were able to chemically absorb CO_2 under high pressure and the formed carbamate subsequently will further absorbed CO_2 physically. These absorbed CO_2 will be desorbed upon release of pressure (Rainbolt et al., 2011).

2.5 Phase-change solvent for CO_2 capture

Over the years, researchers have developed numerous alternative methods in an attempt to reduce the energy requirement of the CO_2 capture process. Normally, the desorption energy is about 4.0 GJ/ton of CO_2 in the conventional MEA absorption process. Furthermore, other challenges to be overcomes include, solvent degradation, slow kinetics and insufficient capture capacity. One of the emerging alternatives in the recent years is a phase-changing absorption. Upon contact and absorption of CO_2, the phase-change absorbents will be formed two phases with one phase are lean in CO_2 and the other phase is rich in CO_2, which can be separated based on differences in density. These CO_2-lean/CO_2-rich phased changed solvent can form either liquid-solid (precipitating) system or two liquid phases (biphasic liquid) system. The CO_2-lean phase can be recycled back to the absorber

and the CO_2-rich phase can be sent to the stripper for regeneration (Zheng et al., 2014). By regenerating only the CO_2-rich phase, significant energy can be saved and solvent loss via evaporation can be reduced (Liang et al., 2015).

There are some existing and novel solvents reported in the literature. In a chilled ammonia process, the absorption of CO_2 is conducted at low temperature (2–10 °C). The heat generated by CO_2 absorption by ammonia is significantly lower in comparison to amines systems. Hence, degradation of the solvent problems can be avoided due to the lower operating temperature, and a high CO_2 capacity is achieved. This process shows good perspectives for decreasing the heat requirement. The phase-changing was observed, whereby solid phases consisting of ammonium carbonate and bicarbonate are formed in the absorber. The unreacted ammonia solution, once separated by filtration from the solid compounds, can be completely reclaimed into the absorbent reactor. The enthalpy calculations showed that a heat requirement for the stripper was lower than 2 GJ/ton of CO_2 can be reached (Darde et al., 2010).

Potassium carbonate (K_2CO_3) carbonated slurry-based CO_2 absorption technology is a CO_2 capture process that involves gas, solid, and liquid phases. The difference in solubility between K_2CO_3 and potassium bicarbonate ($KHCO_3$) allows for the deposit of $KHCO_3$ via crystallization, and the concentrated $KHCO_3$ slurry is regenerated for the purpose of lowering water involvement during regeneration, essentially reducing the energy cost for desorption. Studies on K_2CO_3 slurry-based CO_2 capture process using the commercial simulation tool ASPEN indicated that the desorption energy of the K_2CO_3 slurry-based CO_2 capture process

is within 2.0–2.5 GJ/ton of CO_2 when the CO_2 concentration in coal-fired flue gas is 11% and CO_2 capture efficiency is 90%. (Anderson et al., 2013). Normally, the desorption energy is about 4.0 GJ/ton of CO_2 in the conventional MEA absorption process. Studies conducted at a bench-scale test on the K_2CO_3 slurry-based CO_2 capture process and were investigating the performance parameters such as K_2CO_3 concentration, viscosity, dispersion, absorption heat and CO_2 removal efficiency. They reported that the higher K_2CO_3 concentration is better for CO_2 capture and separation. However, the high K_2CO_3 concentration led to a high viscosity, subsequently caused a lower dispersion coefficient resulting in a lower CO_2 absorption rate (Gao et al., 2015; Smith et al., 2015).

Amino-acid salt present great potential as a phase-changing solvent in CO_2 capture application due to the formation of a precipitate after absorbing CO_2. Additionally, amino-acid salts are environmentally friendly due to their naturally exists in the environment. They possess ionic nature that makes amino-acid salts less volatile and they have good resistance from degradation by an oxygen-rich flue gas stream. The reactivity of amino-acid salts are parallel to those of alkanolamines due to the presence of identical amino functional groups in their molecules with some amino-acid salts, particularly the potassium salts of glycine, sarcosine, and proline, have faster reaction kinetics with CO_2 than does MEA (Ma'mun & Kim, 2013). Formation of precipitate was observed during absorption of CO_2 in 2.5 M aqueous potassium salts of N-methylalanine, DL-alanine, and a-aminoisobutyric acid (and its sterically hindered derivatives) at 295 K. Different precipitate types may be obtained depending on the amino-acid structure and solubility.

As discussed earlier, non-aqueous amine mixture is another alternative solvent in reduced the energy utilization. In some cases, this non-aqueous mixture also exhibits the phase-changing behavior. In mixture of triethylenetetramine (TETA) dissolved in ethanol, formation of solid precipitation after CO_2 absorption was observed and subsequently can be separate and regenerated. However, precipitation was not observed in the TETA aqueous mixture. (Zheng et al., 2014). Furthermore, the TETA / ethanol mixture has a higher absorption capacity and absorption rate. However, due to high vapor pressure of ethanol, solvent loss by evaporation is the limitation. Similarly, a mixture of alkanolamine with hydrophobic ionic liquids also exhibits the phase-changing phenomenon by the formation of the carbamate precipitate in DEA/ hydrophobic ionic liquids (eg.: [EMIM][Tf_2N], [BMIM][Tf_2N], [HMIM][Tf_2N]) emulsion. The solid precipitate rises to the surface of the mixture due to the difference in density and hydrophobicity of the ionic liquids (Hasib-ur-Rahman et al., 2012).

Beside phase change via precipitation, phase change via liquid biphasic formation was also reported throughout the literature. IFP Energies nouvelles has developed solvents such as 1,3-dipropyl-methylxanthine (DMX)-1 solvent, which displays a high CO_2 absorption capacity, low degradation and corrosion, and formation of biphasic layer. After CO_2 absorption, the DMX-1 solvent is stirred with a homogenizer in a stirred cell. Once the homogenization process is completed, liquid/liquid interfaces are formed. The DMX^{TM} solvent process differs from the common alkanolamine process by having an additional operation unit for decantation process. The decanter is positioned after the absorber unit and prior to the regenerator. Only the dense phase CO_2-rich is transferred in the regenerator, whereas the light phase, without being regenerated, is mixed with the regenerated solvent

coming from the stripper and is subsequently recycled back into the absorber. Separation of the biphasic phases enables the reduction in the liquid flow in the stripper, hence reducing the energy requirement for regeneration of the solvent. The DMX^{TM} solvent process can result in a significant reduction in energy consumption compared to 30 wt% MEA; the energy consumption decreases from 3.7 GJ/ton of CO_2 (30 wt% MEA) to 2.3-2.1 GJ/ton of CO_2 (Raynal et al., 2011)

2.6 Thermophysical properties

2.6.1 General background

2.6.1.1 Density

Density ρ, is the most useful intensive physicochemical properties widely applied in studies of pure liquids and liquid mixtures. Density is the most directly determined physical properties of material. Density is defined as "the mass of fluid per unit volume". For a mixture of solutions, density behaves as an additive volumetric property for ideal solutions.

$$\rho = \frac{m}{V} = \sum \rho_i \tag{2.13}$$

where, m, V and ρ_i are mass, volume and density of pure component, respectively. Results of many experimental works show that the analysis of deviation from ideality of density as a function of the composition as the mixture is more useful for studies of intermolecular

interactions in liquid mixtures than the analogous examination of changes of density. The knowledge of the density of liquid mixtures is necessary for calculations of other properties like viscosity and thermos acoustical parameters.

2.6.1.2 Viscosity

Viscosity, η, is an important transport property for process design in any petroleum, petrochemical and other chemical industries, which involve fluid transportation, mixing, agitation, filtration, heat exchange and concentration. Studies on viscosity can be a powerful tool for the characterization of intermolecular interactions present in the mixtures. Many authors underlined the existing relationship between experimental data of viscosity of liquids and their internal structure. Rheology is the study of the flow of fluids and deformation of solids. Resistance is offered when one part of the fluid is moved over another as shown in Figure 2.15.

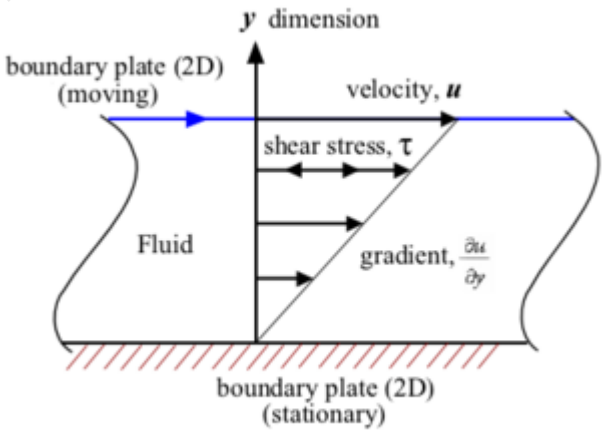

Figure 2.15: Laminar shear of fluid between two plates

The force required to slip one part of fluid over another is called shear stress while the rate of movement is called the rate of shear. Resistance to this movement is called viscosity. The viscosity of a liquid is defined as force per unit area necessary to maintain unit velocity gradient between two parallel planes of liquid separated by unit distance. The unit of viscosity is poise. But the majority of the liquids has very low viscosity and hence it is often expressed in centipoises. Pure liquids often have a constant viscosity at given temperature and pressure, such fluids are known as Newtonian fluids. The viscosity of these fluids increases with decrease in temperature. This suggests that molecular clustering or associations are prevailing in liquids. In the absence of experimental data on viscosity, it becomes necessary to predict or estimate viscosity data. An engineer, frequently encounters fluids for which data may not be available in the literature. To obtain the necessary data, extensive laboratory work is needed. Most of the liquid mixtures do not exhibit a linear relationship in viscosity. This has given rise to the idea that models can be generated, which predicts viscosity of liquid mixtures using the properties of pure components. Viscometer is the instrument used to measure the viscosity of liquid mixtures.

2.6.1.3 Refractive index

Refractive index measurements in combination with density are very useful industrially and also for common substances, which include oils, waxes, sugar syrup and many more. The refractive index, n_D, is a physical property of the medium and it depends on the wavelength of the light and the temperature. The speed of light in a vacuum is always the same, but when light moves through any other medium it travels more slowly since it is being constantly absorbed and reemitted by the atoms in the medium. The ratio of the speed of light

in vacuum to the speed of light in another substance is defined as the index of refraction or refractive index of the substance. The ratio of the sine of the angle of incidence of a ray of light to the sine of the angle of refraction in the medium is equal to the ratio of the wave velocity of light to the wave velocity in the medium. Since refractive index is a physical property of a substance, it is often used to identify a particular substance, confirm its purity or measure its concentration. Most commonly it is used to measure the concentration of solute in an aqueous solution. A refractometer is the instrument used to measure the refractive index. The refractive index of a medium is a measure for how much the speed of light is reduced inside the medium. Whenever light changes speed as it crosses a boundary from one medium into another its direction of travel also changes as shown in Figure 2.16.

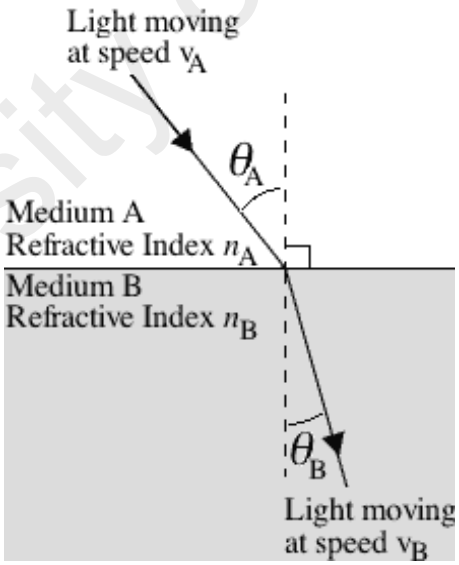

Figure 2.16: Light crossing from any transparent medium into another with different speed

In the special case where the light is traveling perpendicular to the boundary, there is no change in direction upon entering the new medium. The relationship between light speed in the two media V_A and V_B, the angle of incidence, θ_A and refraction, θ_B and the refractive indices of the two media are shown below.

$$\frac{V_A}{V_B} = \frac{sin\,\theta_A}{\sin\theta_B} = \frac{n_A}{n_B} \tag{2.14}$$

In the case shown, the speed of light in medium A is greater than the speed of light in medium B. It is not necessary to measure the speed of light in a sample in order to determine its index of refraction. Instead, by measuring the angle of refraction, and knowing the index of refraction of the layer that is in contact with the sample, it is possible to determine the refractive index of the sample quite accurately. Nearly all refractometers utilize this principle. It is also possible to design a refractometer based on the reflection of light from the boundary between the prism and the sample. These types of refractometers are often used for continuous monitoring of industrial processes. Many refractometers are equipped with a thermometer and a means of circulating water through the refractometer to maintain a given temperature.

2.6.2 Excess properties and derived parameters

Derivative properties such as excess molar volume, viscosity deviation and refractive index deviation have been used as qualitative and quantitative observation to identify the

molecular interaction between component in a liquid mixture. The excess molar volume V^E is defined as (Letcher, 1975):

$$V^E = V_{mixture} - \sum x_i V_i \quad (2.15)$$

where x_i is the mol fraction of component *i*, $V_{mixture}$ is the molar volume of the mixture and V_i is the molar volume of pure component *i*.

In a thermodynamically ideal solution, there is no volume change upon mixing of two or more liquids, but in a real liquid mixture a volume change may occur (Battino, 1971). This volume change upon mixing, V^E at constant temperature and pressure possess an interest to chemists and chemical engineers and is an indicator for non-ideality observed in real liquid mixtures. The volume change that occurs upon liquids mixing, excess molar volume, V^E can be measured either directly via dilatometric method or indirectly by measuring the density of the pure liquids and the liquid mixture (pycnometer or densitometer) and calculating the V^E using the following equation (Zarei et al., 2013) :

$$V^E = \sum_{i=1}^{n} x_i M_i (\rho^{-1} - \rho_i^{-1}) \quad (2.16)$$

where ρ is the density of a mixture and M_i, ρ_i are the molar mass and density of pure component, respectively. The viscosity deviation, $\Delta\eta$ is defined as follows:

$$\Delta\eta = \eta_{mixture} - \sum_{i-1}^{n} x_i \eta_i \quad (2.17)$$

where $\Delta\eta$ is the viscosity of the mixture, *xi, and* η_i is the mol fraction and the viscosity of the pure component. The refractive index deviation, Δn_D was defined as follows:

$$\Delta n_D = n_{D_{mixture}} - \sum_{i-1}^{n} x_i n_{D_i} \quad (2.18)$$

where Δn_D is the refractive index of the mixture, x_i and n_{Di} is the mol fraction and refractive index of the pure component, respectively.

The excess or deviation function could be positive of negative. This sign and magnitude represent the deviation from ideality which further can be used to interpret the molecular interaction between each component in the composition. For density, the calculated excess molar volume can be interpreted as molecular interaction of each component in the system. Positive deviation illustrates an increase of mixture molar volume and vice versa. The variation of mixture volume is due the change of molecule interaction either by breaking or formation of new hydrogen bond and/or dipole-dipole interactions. Similarly, viscosity deviation derived from viscosity measurement illustrates the change in viscosity due to the change of molecule interaction strength.

2.6.3 The importance of thermophysical properties

The thermophysical properties of molecular liquid mixtures represent important data used in chemical and petrochemical engineering designs (example: sulfolane, Table 2.3). They are utilized in different applications for surface facilities, production operations, pipeline systems, phase separation processes design and waste materials recycling, as well as in solution theory and molecular thermodynamics for verification and development of theoretical and empirical models of pure fluids and mixtures. Furthermore, most materials used industrial processes are in liquid form, hence the necessity of detail physical, chemical and transport properties. Most of the liquid used is in the form of mixtures which has a certain degree of deviation from ideality for it's pure components. Due to the deviation from ideality on mixing, the need for studying thermophysical properties of a mixture of materials for a specific application is required (HoiLand, 1986; Millero, 1980). Furthermore, for designing of any engineering operation requires quantitative estimation of the fluid mixture.

Table 2.3: Basic physical properties for pure sulfolane

Physical properties	Descriptions
Appearance	solid, deliquescent
Color	white
Melting point	26 °C
Boiling point	285 °C
Flash point	177 °C
Density	1.26 g/cm³ at 30 °C
Viscosity	10 mPa.s at 30 °C

Recently there has been considerable progress in the studies on intermolecular interactions and the internal structure of liquid mixtures. Studies for determination of different thermophysical properties of liquid mixtures within wide ranges of compositions and temperatures are valuable sources of information that may be used to examine the relation between the internal structure of the system and its physical properties. Most of information related to heat, momentum and mass transfer requires details of thermophysical properties and their variation with temperatures. This data on thermophysical properties related to pure liquids of liquid mixtures are great usage in solution theory and molecular dynamic which is essential in the interpretation of data collected via thermochemical, biochemical, electrochemical and kinetic studies (Kinart & Kinart, 2000; Mchaweh et al., 2004). Furthermore, the obtained thermophysical property data on the studied mixtures contributed to the enrichment of thermodynamic databases required for engineering design in various industrial applications.

A number of papers have been reported on characterization of sulfolane based mixture (sulfolane + solvent). Patrawi and co-workers brought up the measurements of densities, viscosities and for binary mixtures of sulfolane with esters (ethyl acetate, n-propyl acetate and n-butyl acetate) at temperature of 303.15 K, 308.15 K and 313.15 K. It reported that densities and viscosities of the mixtures increase with the increased of mole fraction of sulfolane and decreases with the increased of temperature. Negative excess molar volume was reported over the whole composition (Patwari et al., 2009).

Motin and co-workers reported the density and excess molar volume of binary mixtures sulfolane + alcohols (methanol, n-propanol, n-butanol, and n-propanol) at the temperature of 298.15 to 323.15 K. The binary mixture densities were reported to decrease with increased of alcohol composition with negative excess molar volume over the whole composition (Motin et al., 2007). Moreover, Mesquita and co-workers determined the density, viscosity and its excess properties for binary mixtures of sulfolane + alcohols (2-butanol and 2-propanol) and sulfolane + glycols (diethylene glycol and trietylene glycol) at the temperature ranging from 303.15 to 343.15 K (Mesquita et al., 2014). The binary mixture densities were reported to increase with increased of sulfolane composition in both sulfolane + alcohol and sulfolane + glycol binary mixtures. Similar trends were observed of the measurement of viscosity. For excess molar volume, sulfolane + alcohol displays a negative excess molar volume over the whole composition, while sulfolane + glycol displays a positive excess molar volume over the whole composition. The negative excess molar volume of sulfolane + alcohol binary mixture could be explained by the breaking of hydrogen bonds of the alcohol molecules, when mixed with sulfolane, which lead to the association of alcohol molecules with sulfolane that lead to volume contraction. On the other hand, the positive excess molar volume of sulfolane + glycol binary mixture is due to the volume expansion of the mixture.

Yang and co-workers measured the density, viscosity and its excess molar volume of binary mixtures sulfolane + aromatic hydrocarbons (benzene, toluene, ethylbenzene, p-xylene, o-xylene and m-xylene) at the temperatures of 303.15 K and 323.15 K. The density and viscosity of all binary mixtures were reported to increase with increased of sulfolane composition in all binary mixtures. Both excess molar volumes and viscosity deviation are

negative over the entire composition range of all the binary mixtures studied (Yang et al., 2004).

2.7 Intermolecular interaction

Based on the hydrogen bonding concept, liquid mixtures are categorized as non-polar, NP (e.g.: benzene), polar but not associating, NA (e.g.: acetone, chloroform) and polar and associating, AS (e.g.: water). Therefore, a mixture of liquids could be categorized into the following combination:

- NP-NP (e.g.: benzene – hexane)
- NA-NP (e.g.: acetone – hexane)
- AS-NP (e.g.: ethanol – hexane)
- NA-NA (e.g.: acetone – chloroform)
- AS-NA (e.g.: ethanol - acetone)
- AS-AS (e.g.: ethanol – water)

They are four types of interaction between molecules with the increasing strength of interaction:

ionic bonds > hydrogen bonding > van der Waals dipole-dipole interaction > van der Waals dispersion force

Ionic bonds are the interaction between charged atoms of a molecule; cations (positively charged ions) and anions (negatively charged ions) and the attraction between oppositely charged ions is described by Coulomb's Law. The interaction strength increases with charge and decrease with the increase in distance between ions. Hydrogen bonding occurs within molecules with highly electronegative atoms (F, O, or N) which bound to hydrogen producing dipoles. The dipole moment of one molecule will align with the dipole moment of a neighboring molecule leading to the formation of hydrogen bonding. Due to the rapid molecular motion in liquid phase, these bonds are temporary, but possess significant bonding strength. In general, the strength of hydrogen bonding increases as the electronegativity of the atoms/molecules bound to the hydrogen in increased. In van der Waals dipole-dipole interaction, other atoms/molecules beside hydrogen is involved in the bonding with the electronegative atoms, with a small magnitude of dipole strength, hence the interaction tend to be weaker than hydrogen bonding. van der Waals dispersion force is the weakest intermolecular forces. The attraction between molecules is by instantaneous dipole, an irregularity in electron dispersion at given instant between atoms/molecules. In hydrocarbon of non-polar molecules which absence of strong dipole, dispersion force is the only interaction between molecules. The dispersion force strength is dependent of the size of the molecules.

2.8 COSMO-RS predictive model

Molecular computational science is an essential instrument for acquiring quantitative estimation engineering parameter such as heat capacity, phase equilibria, and gas solubility. This facilitates in overall cost and the design process by reducing time to acquire these

necessary parameters. Predictive methods are often crucial for chemical engineers to design any chemical processes and plants because of the lack of actual experimental data either by databases or experimental measurement. COSMO-RS (COnductor-like Screening MOdel for Real Solvents) is a novel prediction method for thermodynamic equilibria of fluids and liquid mixture that was introduced by Klamt and co-workers (Klamt, 1995; Klamt et al., 2010). This method incorporates the computational efficiency of the quantum chemical dielectric continuum solvation model, COSMO, with the statistical thermodynamic approach for local interaction of surfaces. COSMO-RS model is a method based on the unimolecular quantum chemical calculation of the individual species in the system, not of the whole mixture itself., from the molecular surface as generated by quantum chemical methods (QM) (Eckert & Klamt, 2001).

The calculation can be viewed as stepwise calculation. In the initial step, the QM COSMO calculation was conducted for each of the molecular species where solvents and solutes information were extracted. This is done by applying the continuum solvation model COSMO to fabricate a virtual conductor environment of the molecule. Subsequently, the solute molecule induces a polarization charge density, σ, on the interface of the molecule and the conductor, which later act back on the solute, producing more polarized electron density than in vacuum. During the quantum chemical self-consistency algorithm cycle, the solute molecule is converged to its energetically optimal state in a conductor with respect to electron density. The molecular geometry can be optimized using conventional methods for calculation in a vacuum. The calculation will result in the self-consistency state surrounded by the virtual conductor outside the cavity. The quantum chemical calculation was conducted once for each individual species and stored in a database (Diedenhofen et al., 2003).

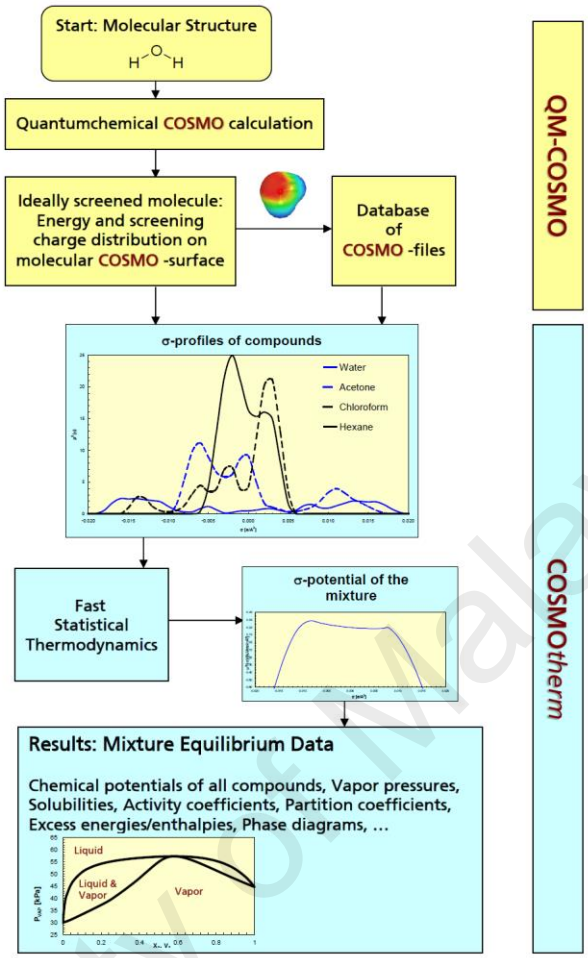

Figure 2.17: Flow chart of COSMOtherm calculation of thermodynamic properties (Eckert & Klamt, 2013)

The COSMO-RS calculation utilized the QM calculation stored in the database to predict the thermodynamic properties such as activity coefficient, solubility, vapor pressure and others. This can be done in a short amount of time and it is very useful in the task of screening a large set of compounds from the database generated. Relative to the ideal conductor, the deviation of real fluid behaviors can be simulated. The electrostatic energy different and hydrogen-bonding energies are quantified as a function of the local COSMO polarization charge density σ and σ' of the interacting surface of the molecule divided into segments (Eckert & Klamt, 2013). The parameter used in COSMO-RS calculation are

optimized only using QM method whereby the parameters are not specific to its functional groups of molecular types. Therefore, the parameterization produced is universal and can be utilized to predict the properties of almost any mixture combination.

In the COSMO-RS theory, the liquids are considered as a body of closely packed ideally screened molecules. This close packing is achieved by compressing the system, whereby the cavity of the molecules is slightly deformed. However, the volume of the individual cavity remains relatively unchanged. Each molecular surface is in close contact with each other. Assuming that there is still a conducting area between each molecule (each molecule is still enclosed by a virtual conductor), each contact area of a surface segment on both molecules by generating a net screening charge density, σ and σ'. However, in reality, the is no conductor area between the surface of the contact area. Consequently, an electrostatic interaction arises from the contact of two different screening charge densities. The specific interaction energy per unit area resulting from this "misfit" of screening charge densities is given as follows:

$$E_{MF}(\sigma, \sigma') = a_{eff} \frac{\alpha'}{2} (\sigma, \sigma')^2 \quad (2.19)$$

where a_{eff} is the effective contact area between the surface segment of the molecule and α' is an adjustable parameter. This equation is based on an assumption that the residual non-stearic interaction can be described by a pair of geometrically independent surface segment. By using two adjacent contacted surface segments, hydrogen bonding can be observed.

Hydrogen bond donors will have a strongly negative screening charge density and vice versa for hydrogen bond acceptors. Hence, hydrogen bond interactions can be deduced if two sufficiently polar surface segments with opposite polarity are in contact, and can be described by the following function:

$$E_{HB}(\sigma, \sigma') = a_{eff} c_{HB} min(0; (\min(0; \sigma_{donor} + \sigma_{HB}) \max(0; \sigma_{acceptor} - \sigma_{HB}) \quad (2.20)$$

where c_{HB} and σ_{HB} are adjustable parameters. Beside electrostatic misfit and hydrogen bond interaction, COSMO-RS also considers van der Waals (vdW) interaction between the contacted surface segments by the following function:

$$E_{vdW}(\sigma, \sigma') = a_{eff}(\tau_{vdW} + \tau'_{vdW}) \quad (2.21)$$

where τ_{vdW} and τ'_{vdW} are the element specific adjustable parameter. The van der Waals energy is only dependent on the element type of the atoms involved in the surface segment contact

Polarity of each surface segment on the surface of the molecule can be described by converting the three-dimension (3D) polarization density distribution on the surface of each molecule, X_i, into a distribution function, σ- profile ($p^{Xi}(\sigma)$). In considering the mixture of

molecules, the σ-profile of the solvent *S*, $p_s(\sigma)$ is the result of the sum of the individual $p^{Xi}(\sigma)$ weight by their mol fraction x_i as expressed below:

$$P_S(\sigma) = \sum_{i \in S} x_i P^{X_i}(\sigma) \tag{2.22}$$

It is practical to normalized the parameter for the calculation of statistical thermodynamic. Since the integral of $p^{Xi}(\sigma)$ over the entire σ range if the total surface area of the molecule, A^{Xi} of compound X_i, the normalized σ- profile ($p^{Xi}(\sigma)$) of the total system is as follows:

$$P_S(\sigma) = \frac{P_S(\sigma)}{A_S} = \frac{P_S(\sigma)}{\sum_{i \in S} x_i A^{X_i}} \tag{2.23}$$

The COSMO calculations have been performed with the TmolX program package. Geometry optimization was performed at Hartree-Fock theory with 6-31G* basic set. Geometry optimization calculation using Hartree-Fock level provides more meaningful accurate values while the * accounts for polarization effect of the species. Using the optimized geometry for each individual compound, a single point calculation was conducted with activation of the ***.cosmo file*** generation using density functional theory (DFT) with 6-31G* basic set. Then, the ***.cosmo file*** was imported into the COSMOthermX software package (version C30_1401) with parameterization file BP_TZVP_C30_1301.ctd. (Eckert & Klamt, 2013) to obtain the σ-profile and σ-potential of the individual components and to

calculate activity coefficient of the liquids mixture Within COSMOthermX software, a pseudo binary approach was adopted for the calculation of the mixture compose of ionic liquid-sulfolane whereby the cation and anion of the ionic liquid was input as separate compounds with equal mol fraction.

2.8 Summary

Based on the current trend, CO_2 absorption using a non-aqueous system is considered as alternative to be implemented in the CO_2 capture technology. All the components have been carefully selected based on literature study. The sulfolane based [BMIM][NTf_2] and MEA non-aqueous ternary mixture will undergo CO_2 solubility and reusability evaluation. Furthermore, thermophysical and excess properties of the ternary mixtures will be measured to elucidate the molecular interaction between each component. The molecular interaction will be verified using COSMO-RS model.

CHAPTER 3 : MATERIALS AND METHODS

3.1 Introduction

This chapter provides details of the materials involved, solution preparation, experimental techniques and data analysis used throughout the course of this work.

3.2 Material

Ionic liquid, 1-butyl-3-methylimidazolium *bis*(trifluoromethylsulfonyl)imide ([BMIM][NTf_2]) (> 98%) was purchased from Iolitech. Sulfolane, (> 98%) was purchased from Merck. Alkanolamines used in this study, monoethanolamine (MEA), diethanolamine (DEA), 2-amino-2-methyl-1-propanol (AMP) and 2-(2-aminoethylamine)ethanol (AEEA) were obtained from Merck. Purified CO_2 (99.995%) was purchased from Linde Malaysia Sdn. Bhd. (Linde). All chemicals were used as received. Chemical structure and provenance table for chemicals used in this study are shown in Figure 3.1 and Table 3.1, respectively.

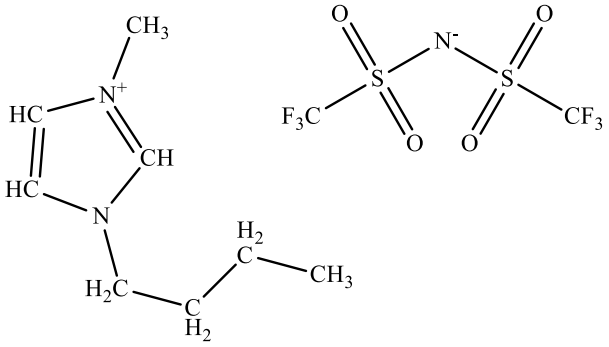

1-butyl-3-methylimidazolium bis(trifluorosulfonyl)imide
([BMIM][NTf_2])

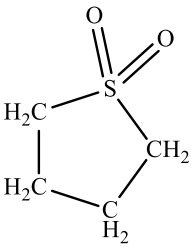

sulfolane

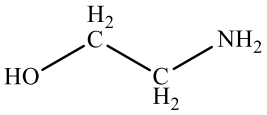

monoethanolamine
(MEA)

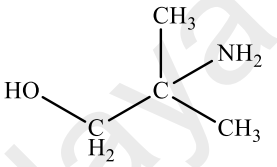

2-amino-2-methyl-1-propanol
(AMP)

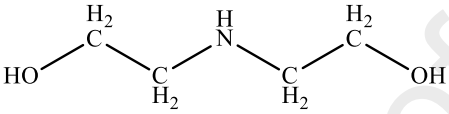

diethanolamine
(DEA)

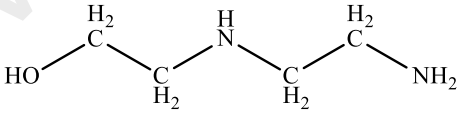

2-(2-aminoethylamine)ethanol
(AEEA)

Figure 3.1: Chemical structure of (a) [BMIM][NTf_2], (b) sulfolane, (c) MEA, (d) DEA, (e) AMP and (f) AEEA

Table 3.1: Material provenance table for the compounds system

Chemical	[BMIM][NTf_2]	Sulfolane	MEA	DEA	AMP	AEEA
Molecular formula	$C_{10}H_{15}F_6N_3O_4S_2$	$C_4H_8O_2S$	C_2H_7NO	$C_4H_{11}NO_2$	$C_4H_{11}NO$	$C_3H_{10}N_2O$
IUPAC name	1-butyl-3-methylimidazolium *bis*(trifluoromethylsulfonyl)imide	Tetrahydrothiophene 1,1-dioxide	2-aminoethanol	2,2'-iminodiethanol	2-amino-2-methylpropan-1-ol	2-[(2-aminoethyl) amino]ethanol
CASRN	174899-83-3	126-33-0	141-43-5	111-42-2	124-68-5	111-41-1
Source	Iolitech	Merck	Merck	Merck	Merck	Merck
Purity grade	Analytical Reagents	Analytical Reagents	Analytical Reagents	Analytical Reagents	Analytical Reagents	Analytical Reagents
Purity	99.0	99.0	99.5	99.5	98.0	99.5
Purification Method	None	None	None	None	None	None
Analysis Method	HPLC	GC	GC	GC	GC	GC

3.3 Methodology

3.3.1 CO_2 absorption at high pressure

3.3.1.1 CO_2 absorption setup

Figure 3.2 illustrates a complete schematic process flow diagram of CO_2 absorption set up at high-pressure. The cell was equipped with a welded stirrer assemble, a thermocouple, an inlet gas tube and air vent tube. The thermocouple has the accuracy of ± 0.1 K. The operation was initially started by purging the air out from the gas reservoir by introducing a sufficient flow of CO_2 throughout the system. The gas reservoir tank was loaded with purified CO_2 from the storage tank before it was heated and pressurized to the required condition.

A known volume of fresh sample was filled in the cell reactor prior to being sealed. The sample was stirred while the CO_2 gas was continuously introduced into the system until equilibrium was reached. Following the contact of CO_2 with the solutions, the total systems' pressure dropped gradually, and equilibrium was considered reached after the pressure in the cell reactor remained constant for at least half an hour. A decrease in the pressure within the gas reservoir corresponded to a decrease in the amount of CO_2 above the mixtures. Both temperatures of gas container and reactor were kept constant, throughout the process.

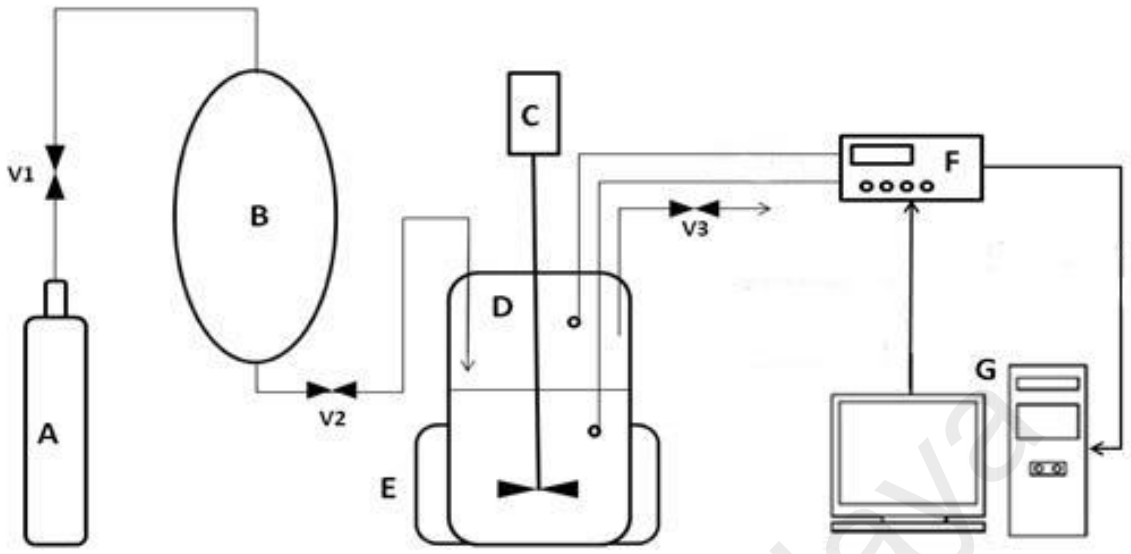

Figure 3.2: Schematic diagram of the experimental set-up for measuring the CO_2 solubility: A. Gas (CO_2) cylinder, B. Gas (CO_2) reservoir, C. Motor, D. High pressure reactor vessel (equilibrium cell), E. Heater, F. Reactor controller, G. PC graphical user interface, V1. Control valve, V2. Needle valve, V3. Pressure relief valve

3.3.1.2 CO_2 loading calculation techniques

During the experiment, all parameters were kept constant except for the pressure. By using the volume, pressure and temperature values, the mol of CO_2 in the gas phase can be determined. The initial and equilibrium pressures were recorded to compute the differences in mol throughout the absorption of which the solubility was expressed as per mol of total solvent. The solubility was calculated using Equation 3.1 and 3.2 as follows;

$$\chi = \frac{\left[\frac{(P_{Ti}-P_{Vi})\times V_{gc}}{zRT}\right]-\left[\frac{(P_{Tf}-P_{Vf})\times(V_{gc}(V_{cell}-V_{sol}))}{zRT}\right]}{n_{total}} \quad (3.1)$$

$$\alpha = \frac{\left[\frac{(P_{Ti}-P_{Vi})\times V_{gc}}{zRT}\right]-\left[\frac{(P_{Tf}-P_{Vf})\times(V_{gc}(V_{cell}-V_{sol}))}{zRT}\right]}{m_{total}} \quad (3.2)$$

where, χ is the CO_2 loading in mol of CO_2 / total mol of absorbent, α is the CO_2 loading in mol of CO_2 / total mass of absorbent, P_T is the total pressure, P_V is the vapor pressure, V_{gc} is volume of gas container, V_{cell} is volume cell, V_{sol} is volume solution, *i* is initial condition, *f* is final condition. All measurements were in triplicate and reported as average with standard deviation.

3.3.1.3 Reusability of non-aqueous solvent for CO_2 absorption

The reusability of the non-aqueous solvent was conducted by regenerating the solvent after the end of each absorption cycle. Reusability study was conducted using 0B-30M non-aqueous ternary mixture, initial CO_2 pressure of 2000 kPa at 303.15 K. At the end of each cycle, the CO_2 saturated solvent was regenerated under reduced pressure at 383.15 K for 4 h. The solubility was calculated as described in Section 3.3.1.2.

3.3.1.4 Effect of water content

The effect of water content to the non-aqueous solvent was conducted by introducing 1, 2.5 and 5 wt% of water into the solvent composition at various compositions. Reusability study was conducted using 0B-30M non-aqueous ternary mixture, initial CO_2 pressure of 2000 kPa at 303.15 K. The solubility was calculated as described in Section 3.3.1.2.

3.3.1.5 Determination of chemical components in CO_2 saturated solvents

Nuclear Magnetic Resonance (NMR) is a technique to determine the structure of organic compounds and provide detailed information on the three-dimensional structure of molecule in solution. $^{1}H/^{13}C$ NMR spectra were recorded at room temperature on Spectrometer NMR AVANCE III 400Hz (AVN 400). Deuterated methanol-*d4* solvent was obtained from Sigma Aldrich. Samples for carbon (^{13}C) spectrum analysis of CO_2 saturated solvents were prepared by diluting 150 μL of sample into 500 μL deuterated methanol-*d4* solvent in the NMR tubes. For each sample, 2000 scans were collected for ^{13}C NMR. Chemical shifts were quoted in part per million (ppm) relative to residual solvent peaks using tables of chemical shifts of solvents.

3.3.2 Solutions preparation for thermophysical properties

The required mass of each component to prepare [BMIM][NTf_2] + sulfolane, MEA + sulfolane and [BMIM] [NTf_2] + MEA binary mixtures together with [BMIM][NTf_2] + MEA + sulfolane ternary mixtures for thermophysical properties measurement were calculated over the entire range of composition with 0.1 mol fraction resolution as summarized in Table 3.2 and Table 3.3. Both binary and ternary mixtures were prepared gravimetrically by weighing the materials using a calibrated single pan digital balance (Sartorius BSA224S-CW, Germany) with precision of 0.1 mg. All mixtures were stirred until homogenized and kept in tightly sealed bottles to minimize moisture absorption from the atmosphere.

Table 3.2: Composition of binary mixtures for thermophysical properties studies

Binary mixtures	[BMIM][NTf_2] (mol)	MEA (mol)	Sulfolane (mol)
[BMIM][NTf_2] (1) + sulfolane (3)	0.0000	-	1.0000
	0.1000	-	0.9000
	0.1999	-	0.8001
	0.3001	-	0.6999
	0.4000	-	0.6000
	0.5001	-	0.4999
	0.5999	-	0.4001
	0.7000	-	0.3000
	0.7995	-	0.2005
	0.8985	-	0.1015
	1.0000	-	0.0000
MEA (2) + sulfolane (3)	-	1.0000	0.0000
	-	0.8999	0.1001
	-	0.8000	0.2000
	-	0.6999	0.3001
	-	0.5999	0.4001
	-	0.4999	0.5001
	-	0.3999	0.6001
	-	0.3001	0.6999
	-	0.2001	0.7999
	-	0.0999	0.9001
	-	0.0000	1.0000
[BMIM][NTf_2] (1) + MEA (2)	0.0000	-	1.0000
	0.1001	-	0.8999
	0.2000	-	0.8000
	0.3000	-	0.7000
	0.4000	-	0.6000
	0.4999	-	0.5001
	0.6000	-	0.4000
	0.6999	-	0.3001
	0.8000	-	0.2000
	0.8998	-	0.1002
	1.0000	-	0.0000

Table 3.3: Composition of ternary mixtures for thermophysical properties studies

Ternary mixtures	[BMIM][NTf_2] (mol)	MEA (mol)	Sulfolane (mol)
[BMIM][NTf_2] (1) + MEA (2) + sulfolane (3)	0.0999	0.1003	0.7998
	0.0998	0.2000	0.7002
	0.0997	0.3015	0.5988
	0.1000	0.4005	0.4995
	0.0999	0.5004	0.3997
	0.1000	0.5999	0.3001
	0.1000	0.7000	0.2000
	0.1000	0.8002	0.0999
	0.1995	0.1022	0.6982
	0.1997	0.2011	0.5992
	0.1997	0.3008	0.4995
	0.2000	0.4002	0.3998
	0.1998	0.4996	0.3006
	0.1996	0.6007	0.1997
	0.1995	0.7003	0.1002
	0.2993	0.1019	0.5988
	0.2996	0.2007	0.4997
	0.2994	0.2998	0.4008
	0.2997	0.4005	0.2998
	0.3000	0.5001	0.1999
	0.2997	0.6003	0.1000
	0.3989	0.1016	0.4995
	0.3990	0.2017	0.3993
	0.3988	0.3010	0.3002
	0.3995	0.4000	0.2005
	0.3996	0.5003	0.1001
	0.4992	0.1012	0.3996
	0.4993	0.2001	0.3006
	0.4992	0.3008	0.1999
	0.4980	0.3998	0.1021
	0.5978	0.1021	0.3001
	0.5992	0.1999	0.2009
	0.5984	0.3009	0.1007
	0.6963	0.1033	0.2004
	0.6964	0.2009	0.1027
	0.7965	0.1030	0.1005

3.3.3 Density

Density measurement of the binary and ternary mixtures were carried out at atmospheric pressure using oscillating U-tube digital densitometer DDM 2911 (Rudolph Research, USA) from temperatures of 293.15 to 343.15 K with 10 K intervals and temperature accuracy of ±0.01 K at 1 atm. The apparatus is precise within 1.0 $x10^{-4}$ g cm^{-3}, and the measurement uncertainty was estimated to be better than 0.001 g cm^{-3}. The calibration of the densitometer was performed using dry air and ultra-pure water (supplied) at given temperature and atmospheric pressure. All measurements for each sample were performed in triplicate, and the values were reported as an average.

3.3.4 Viscosity

Viscosity measurement of the binary and ternary mixtures were conducted using Rheometer MCR 301 (Anton Paar, Austria) from 293.15 to 343.15 K with 10 K increments at 1 atm. The temperature of the solution was maintained within ±0.1 K with the accuracy of less than 3 %. Each value reported was an average of triplicate.

3.3.5 Refractive index

Refractive index measurement was carried out using Mettler Toledo Refractometer Model RM40. The refractometer has measuring range from 1.3200 to 1.7000 with 0.0001 accuracy. The temperature was controlled using a Peltier temperature controller ranging from 5 to 100 °C with an accuracy of ± 0.1 °C. The value reported by the equipment was an average

of triplicate measurement. Calibration of the refractometer was performed by measuring the refractive index of double distilled water supplied by the manufacturer.

3.3.6 COSMO-RS model

The structure of the cation, anion, MEA and sulfolane were drawn and geometry optimized using the TmolX software package. Geometry optimization was performed at Hartree-Fock theory with 6-31G* basic set. Geometry optimization calculation using Hartree-Fock level provides more meaningful accurate values while the * accounts for polarization effect of the species. Using the optimized geometry for each individual compound, a single point calculation was conducted with activation of the ***.cosmo file*** generation using density functional theory (DFT) with 6-31G* basic set. Then, the ***.cosmo file*** was imported into the COSMOthermX software package with parameterization file BP_TZVP_C30_1301.ctd to obtain the σ-profile of the individual components and to calculate the activity coefficient of the [BMIM][NTf_2]-sulfolane, [BMIM][NTf_2]-MEA, sulfolane-MEA binary mixtures and [BMIM][NTf_2]-MEA-sulfolane ternary mixtures.

CHAPTER 4: RESULTS AND DISCUSSION

4.1 CO_2 absorption at high pressure

4.1.1 Introduction

This chapter aims to evaluate the ability of a non-aqueous mixture of sulfolane, [BMIM][NTf_2] and MEA in capturing CO_2 at a pressure range of 500 to 2000 kPa and temperature ranging from 303.15 to 333.15 K. All the data were reported as CO_2 loading capacity, χ (mol CO_2 / mol absorbent) and α (mol CO_2 / kg absorbent) as a function of CO_2 partial pressure at the corresponding temperature. Correlation for the CO_2 solubility was also obtained.

4.1.2 Apparatus reliability validation

To ensure the accuracy of the measurements for this study, several runs for CO_2 absorption using pure [BMIM][NTf_2] at reference temperature were performed. These data as well as those reported in the literature (Lee & Outcalt, 2006) are plotted in Figure 4.1, with average absolute relative deviation (AARD) of 0.33%. As can be seen from the figure, the data measured during the experiment are similar to the literature data, demonstrating the reliability and of the experimental apparatus.

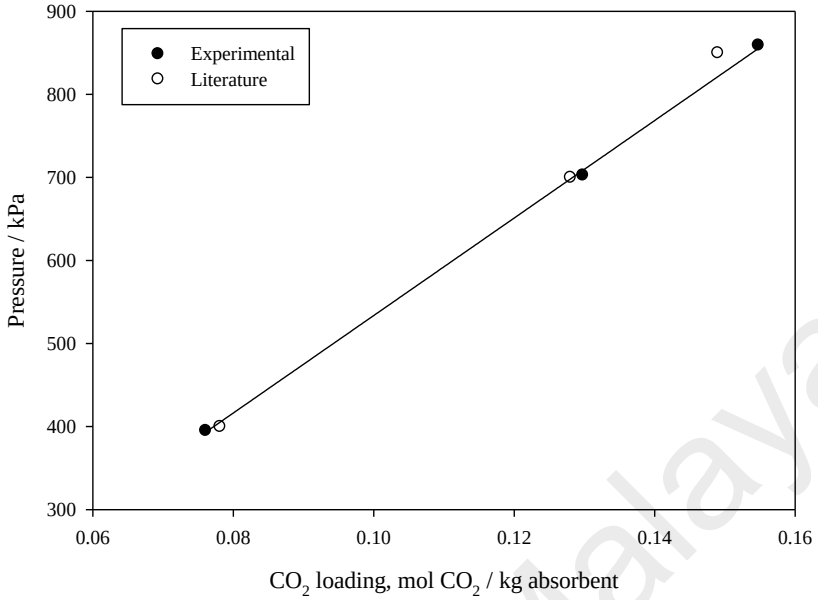

Figure 4.1: Comparison of measured CO_2 loading in pure [BMIM][NTf_2] with literature data at 313.15 K (Lee & Outcalt, 2006)

4.1.3 Solubility of CO_2 in [BMIM][NTf_2] + sulfolane binary mixtures

Figure 4.2 shows the solubility of CO_2 in the [BMIM][NTf_2] + sulfolane binary mixture at a pressure range of 500 to 2000 kPa at T= 323.15 K. The results indicated that the solubility of CO_2 increased with the increase of [BMIM][NTf_2] composition. This is due to the higher affinity of CO_2 to [BMIM][NTf_2] in comparison to sulfolane. CO_2 solubility in ionic liquids is dependent on the interaction between ionic liquids and molecules and the CO_2 molecules occupied the free space between anion and cation. The cations and anions of the ionic liquids form a rigid network by Coulombic interactions. Therefore, they are less mobile. During the addition of CO_2 into the mixture, the anions are slightly rearranged to form larger voids between anions and cations without resulting significant structural change of the rigid network. The CO_2 molecules diffuse through the network and fill into the free volume

without disturbing the arrangement of the ions (Huang & Rüther, 2009). Furthermore, the solubility of CO_2 increased with increases in pressure. From the data, it is shown that CO_2 solubility is higher with higher composition of [BMIM][NTf_2] in the mixture, but it is economically hindered because of relatively high cost to utilize [BMIM][NTf_2] at higher concentration. It is also worth mentioning that 0.1 mol fraction of [BMIM][NTf_2] in the binary mixture is equal to 30 wt% of [BMIM][NTf_2] in the composition. Therefore, reformulation using an alkanolamine is suggested to further increase the CO_2 capacity of the solvent mixture, thus maintaining the solvent mixture economically friendly.

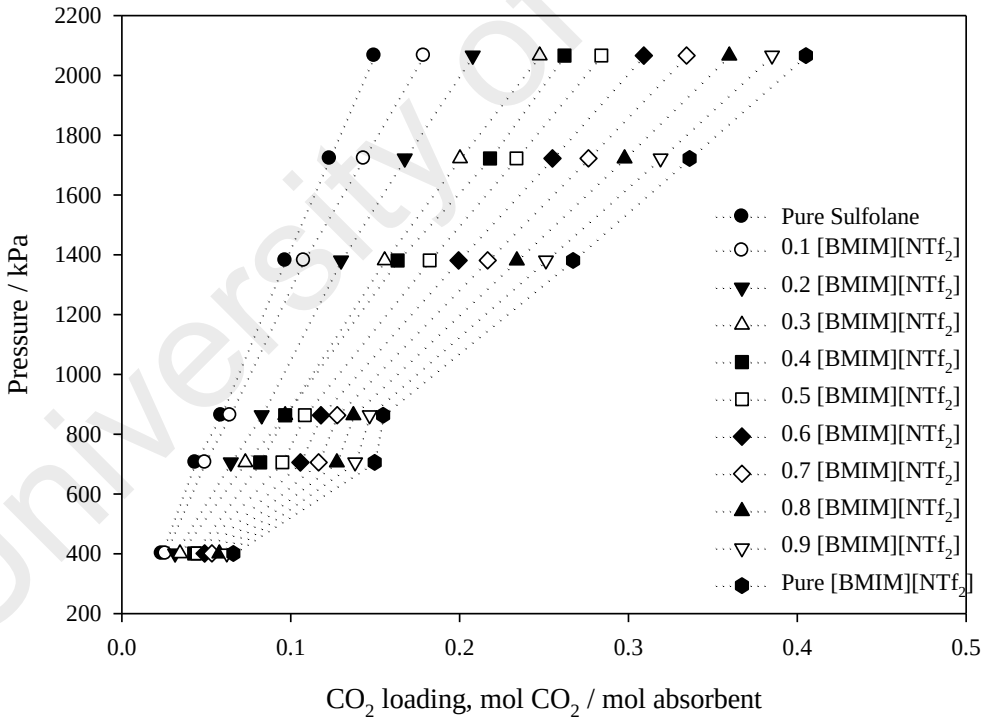

Figure 4.2: CO_2 loading in [BMIM][NTf_2] (1) + sulfolane (2) mixtures against pressure at various composition at 323.15 K

4.1.4 Screening for alkanolamine for ternary mixtures

Based on the binary mixtures study, an alkanolamine was included into the mixture to increase the CO_2 solubility via chemical reaction. A number of alkanolamines represent different types of molecule structures were formulated into the mixture for screening purposes. Tertiary amine was excluded from the screening because of their unable to react with CO_2 in a non-aqueous solution. This is due to the absence of H attached to N atom in the amine functionality to be utilized in the formation of amine carbamate (Kim et al., 2014). Solubility studies were conducted to investigate the CO_2 absorption capacity and the result are shown in Figure 4.3. Based on the figure, it can be seen that composition with MEA has the highest CO_2 absorption as compared with others alkanolamines. Although AMP and AEEA have a higher theoretical CO_2 absorption capacity as compared to MEA, these amines react with CO_2 to form semi-solid that inhibit stirring and absorption process. Therefore, MEA was chosen as part of the mixture for further study.

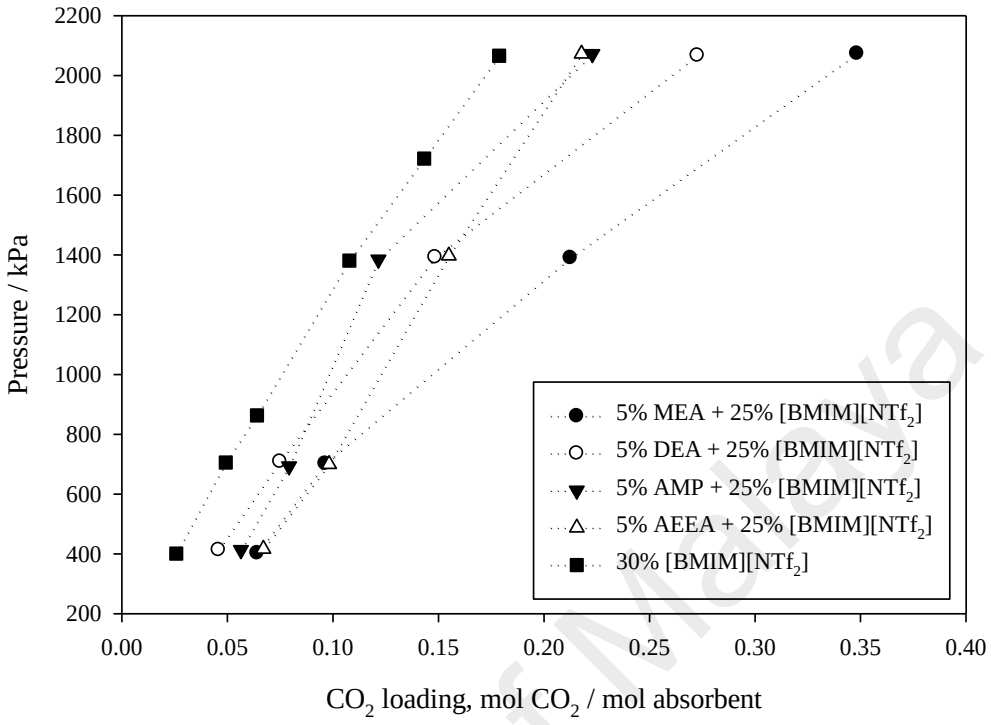

Figure 4.3: Solubility of CO_2 in [BMIM][NTf_2] + sulfolane with alkanolamines mixtures against pressure at 323.15 K

4.1.5 Solubility of CO_2 in [BMIM][NTf_2] + MEA + sulfolane ternary mixtures

Table 4.1 lists the composition of the mixture samples used in the study. Table 4.2 summarizes solubility data for the sulfolane based ternary mixtures. Throughout the study, it can be observed that CO_2 loading increases as composition of MEA in the mixture increased. This is primarily due to higher absorption of CO_2 into the solution by chemical reaction with MEA. Although the mixture with a high composition of ionic liquid has the lower absorption capacity, the absorption take a shorter time to reach equilibrium, as shown in Figure 4.4.

Table 4.1: Composition of sulfolane, [BMIM][NTf_2] and MEA in the ternary mixtures

Sample	Composition (wt%)		
	sulfolane	**[BMIM][NTf_2]**	**MEA**
0B-30M	70	0	30
5B-25M	70	5	25
15B-15M	70	15	15
25B-5M	70	25	5
30B-0M	70	30	0

Table 4.2: Experimental solubility data of CO_2 in ternary mixtures with different composition of [BMIM][NTf_2] and MEA

Sample	**T(K)**	P_{CO_2} **(kPa)**	**χ, CO_2 loading (mol CO_2 / mol absorbent)**	**α, CO_2 loading (mol CO_2 / kg absorbent)**
0B-30M	303.15 ± 0.01	496	0.225	2.414
		1002	0.250	2.682
		1499	0.256	2.744
		2004	0.266	2.861
	313.15 ± 0.01	5038	0.216	2.317
		1002	0.246	2.644
		1500	0.251	2.693
		1995	0.249	2.671
	323.15 ± 0.01	500	0.214	2.299
		1019	0.230	2.474
		1506	0.240	2.577
		1998	0.255	2.736
	333.15 ± 0.01	500	0.207	2.224
		1000	0.214	2.295
		1507	0.236	2.534
		1999	0.239	2.563
5B-25M	303.15 ± 0.01	499	0.203	2.038
		999	0.226	2.268
		1496	0.257	2.578
		1993	0.269	2.705
	313.15 ± 0.01	497	0.193	1.935
		1011	0.215	2.160
		1498	0.235	2.363
		2002	0.245	2.454
	323.15 ± 0.01	502	0.196	1.963
		1005	0.211	2.122

Sample	T(K)	P_{CO_2} (kPa)	χ, CO_2 loading (mol CO_2 / mol absorbent)	α, CO_2 loading (mol CO_2 / kg absorbent)
		1509	0.227	2.279
		2002	0.236	2.367
	333.15 ± 0.01	502	0.188	1.882
		1005	0.210	2.103
		1502	0.223	2.240
		2006	0.236	2.370
15B-15M	303.15 ± 0.01	500	0.146	1.263
		1000	0.192	1.659
		1497	0.223	1.930
		2005	0.222	1.922
	313.15 ± 0.01	499	0.142	1.222
		1000	0.186	1.606
		1498	0.201	1.732
		2002	0.209	1.808
	323.15 ± 0.01	499	0.136	1.174
		1004	0.168	1.455
		1505	0.199	1.716
		2003	0.201	1.740
	333.15 ± 0.01	501	0.140	1.212
		1004	0.166	1.432
		1500	0.190	1.637
		2003	0.198	1.709
25B-5M	303.15 ± 0.01	499	0.089	0.642
		1002	0.138	0.999
		1500	0.170	1.231
		2004	0.200	1.447
	313.15 ± 0.01	501	0.084	0.609
		1002	0.120	0.870
		1497	0.154	1.113
		1998	0.179	1.297
	323.15 ± 0.01	497	0.083	0.541
		1002	0.127	0.832
		1504	0.150	1.104
		2011	0.187	1.225
	333.15 ± 0.01	505	0.087	0.569
		1007	0.124	0.813
		1509	0.135	0.993
		2051	0.178	1.164
30B-0M	303.15 ± 0.01	496	0.044	0.290
		1002	0.091	0.595

Table 4.2, continued

Sample	T(K)	P_{CO_2} (kPa)	χ, CO_2 loading (mol CO_2 / mol absorbent)	α, CO_2 loading (mol CO_2 / kg absorbent)
		1499	0.130	0.852
		2004	0.194	1.267
	313.15 ± 0.01	503	0.041	0.265
		1002	0.080	0.522
		1500	0.119	0.781
		1995	0.158	1.031
	323.15 ± 0.01	500	0.032	0.207
		1019	0.075	0.491
		1506	0.105	0.585
		1998	0.133	0.872
	333.15 ± 0.01	500	0.028	0.181
		1000	0.066	0.432
		1508	0.096	0.626
		1999	0.126	0.824

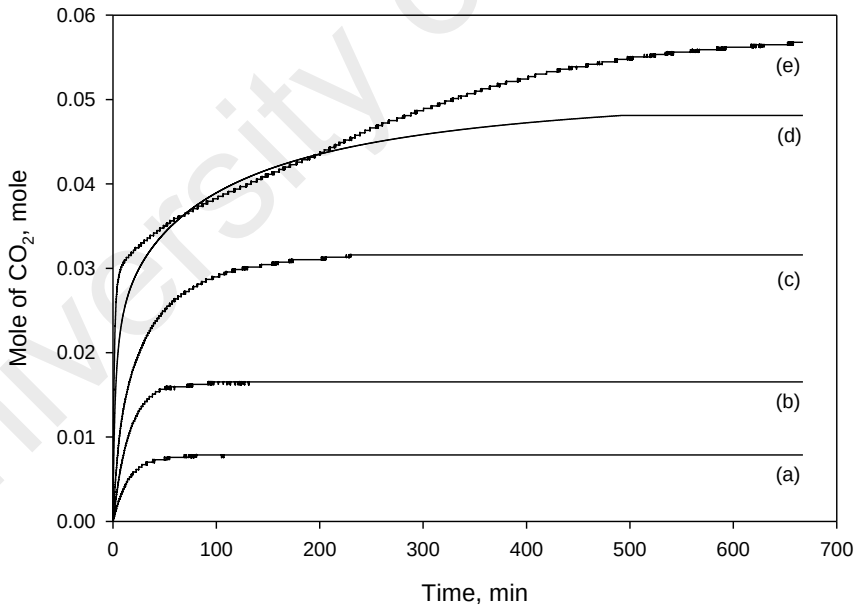

Figure 4.4: Comparison of equilibrium time for non-aqueous mixtures for P =500 kPa and temperature of 303.15 K; (a) 30B-0M; (b) 25B-5M; (c) 15B-15M; (d) 5B-25M; (e) 0B-30M

4.1.5.1 Effect of temperature and pressure on the solubility of CO_2

Figure 4.5 to Figure 4.9 show a general trend in the equilibrium whereby the CO_2 loading decreases with temperature and increases with pressure. Detail observation of the effect of temperature on the solubility of CO_2 are detail in Figure 4.10 to Figure 4.13. Each mixture shows a decreasing trend in the graphs with an increment of temperature from 303.15 to 333.15 K which indicates a high loading of CO_2 at a lower temperature at constant pressure. This is due to the higher vapor pressure at a higher temperature, which reflects on lower loading of CO_2.

On the other hand, detail observation of the effect of pressure on the solubility of CO_2 are detail in Figure 4.14 to Figure 4.17. Higher pressure at constant temperature contributes to a positive attribute to the CO_2 solubility due to the diffusion of gas into liquid which is directly proportional to the pressure of gas above the surface of the solution. It can be observed that mixture with high composition of [BMIM][NTf_2] has a more prominent change in CO_2 loading with increments of pressure. The absorption process is likely to be controlled by both chemical and physical absorption. At high temperature and low MEA composition, physical absorption plays major role in the absorption process, while at low temperature and high MEA composition, the chemical reaction shows prominent effect.

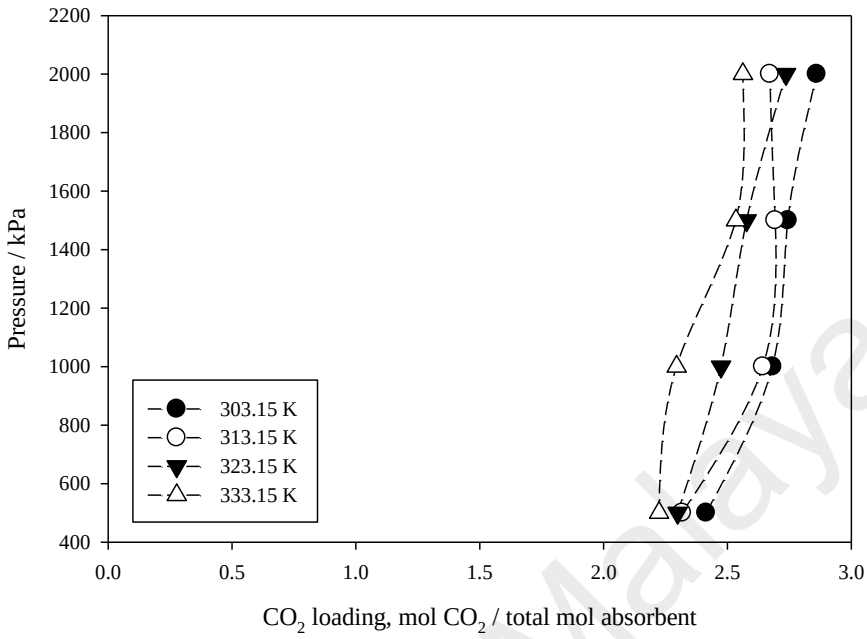

Figure 4.5: CO_2 loading in 0B-30M mixture mixtures for P=500 to 2000 kPa and temperatures of 303.15 to 333.15 K

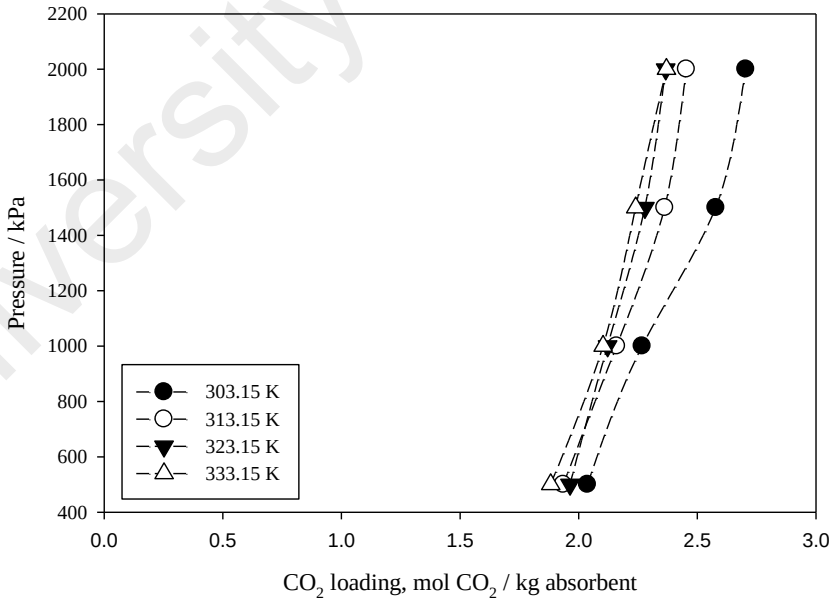

Figure 4.6: CO_2 loading in 5B-25M mixture for P=500 to 2000 kPa and temperatures of 303.15 to 333.15 K

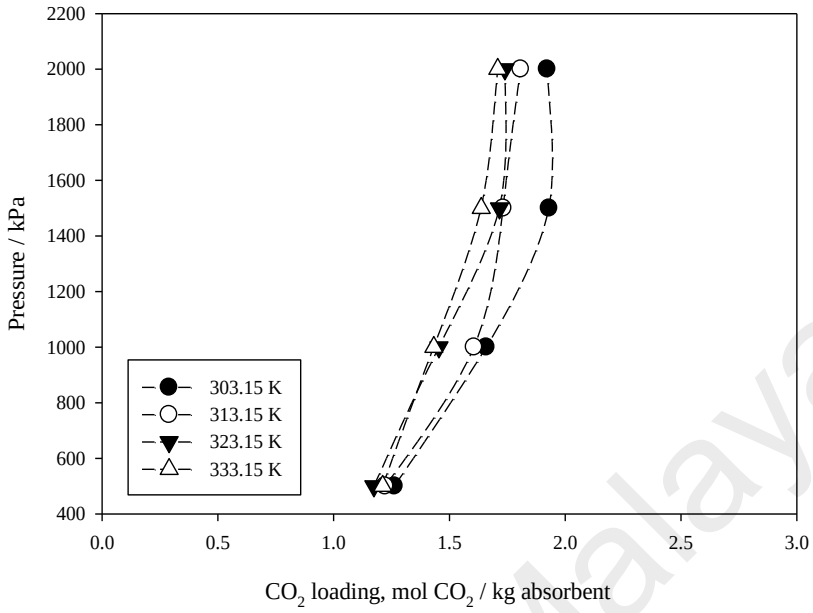

Figure 4.7: CO_2 loading in 15B-15M mixture for P=500 to 2000 kPa and temperatures of 303.15 to 333.15 K

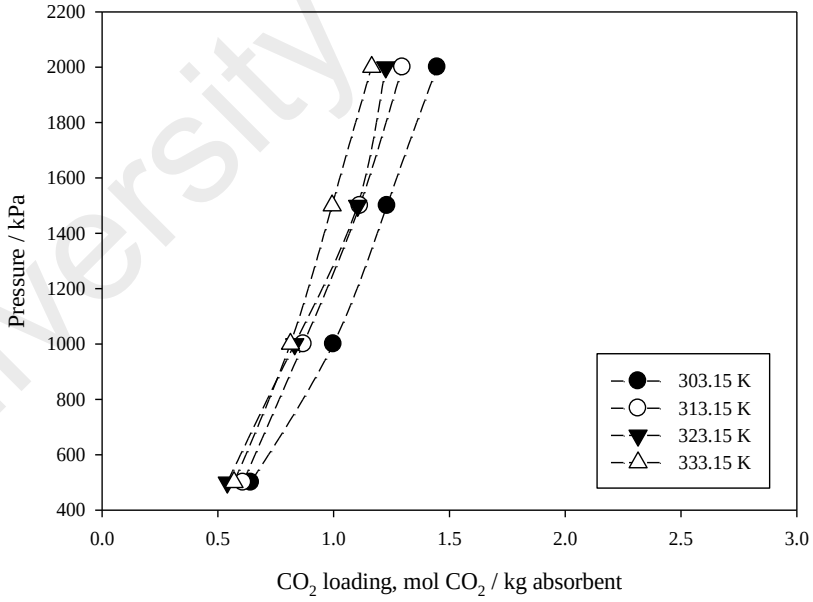

Figure 4.8: CO_2 loading in 25B-5M mixture for P=500 to 2000 kPa and temperatures of 303.15 to 333.15 K

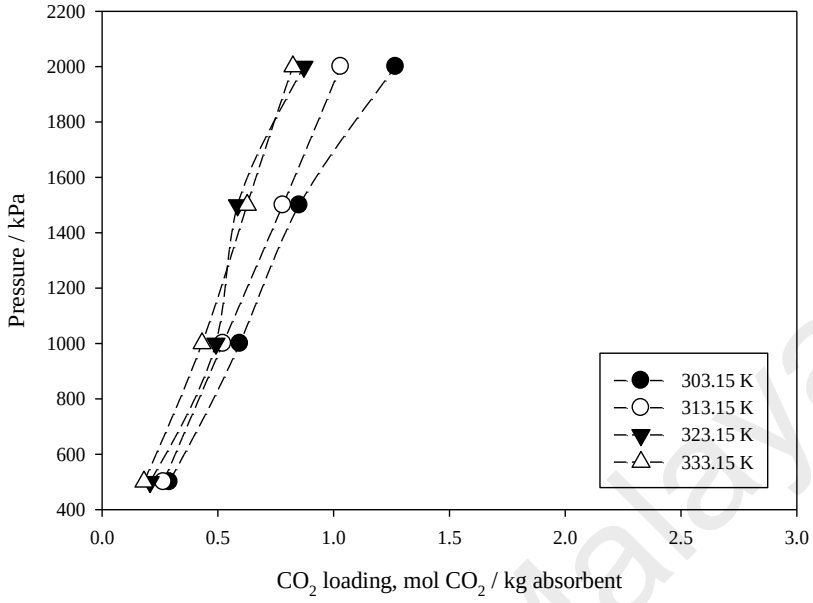

Figure 4.9: CO_2 loading in 30B-0M mixture for P=500 to 2000 kPa and temperatures of 303.15 to 333.15 K

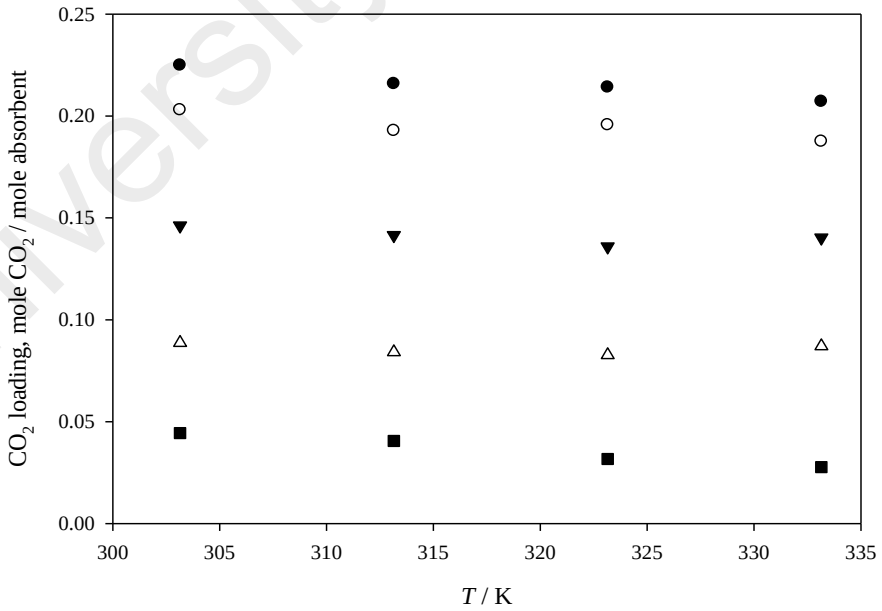

Figure 4.10: Solubility of CO_2 in non-aqueous mixtures against temperature at 500 kPa; (●) 0B-30M; (○) 5B-25M; (▼) 15B-15M; (△) 25B-5M; (■) 30B-0M

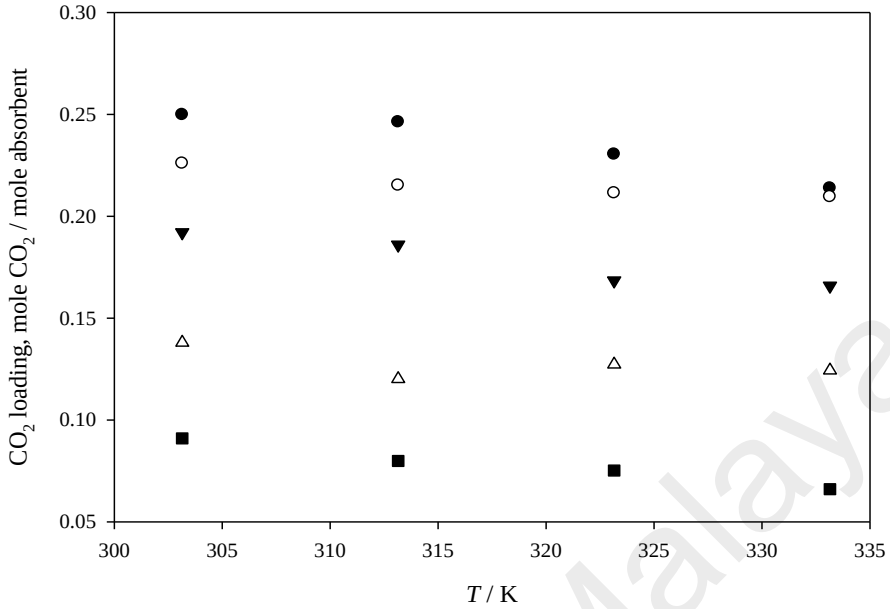

Figure 4.11: Solubility of CO_2 in non-aqueous mixtures against temperature at 1000 kPa; (●) 0B-30M; (○) 5B-25M; (▼) 15B-15M; (△) 25B-5M; (■) 30B-0M

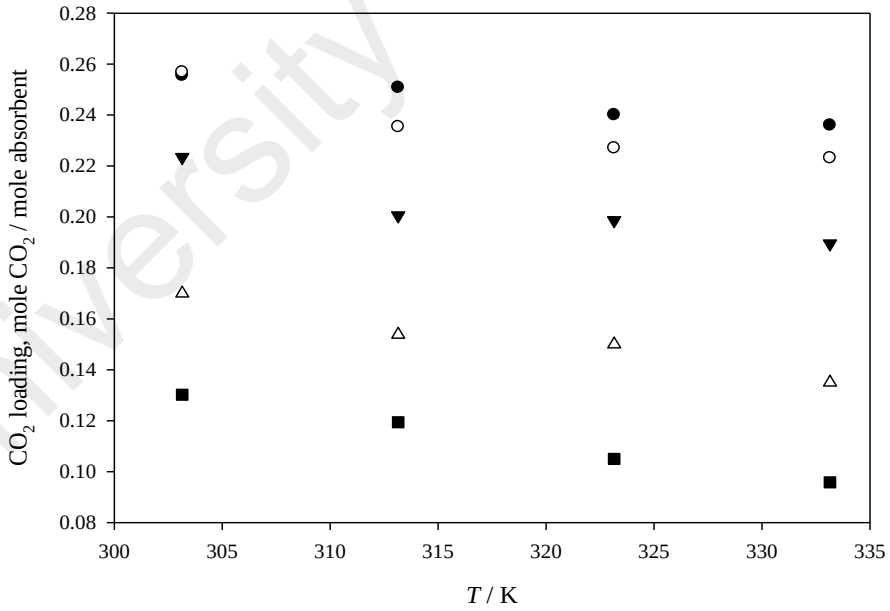

Figure 4.12: Solubility of CO_2 in non-aqueous mixtures against temperature at 1500 kPa; (●) 0B-30M; (○) 5B-25M; (▼) 15B-15M; (△) 25B-5M; (■) 30B-0M

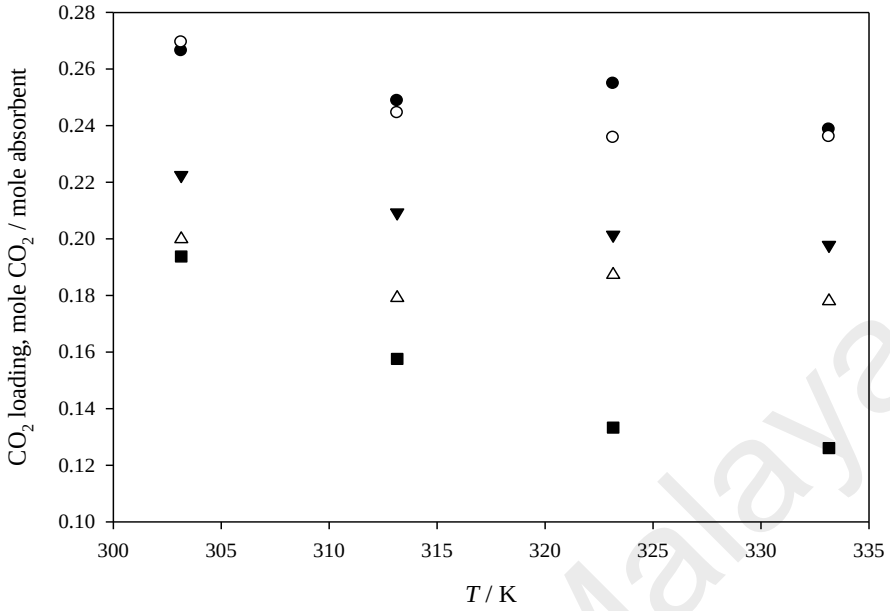

Figure 4.13: Solubility of CO_2 in non-aqueous mixtures against temperature at 2000 kPa; (●) 0B-30M; (○) 5B-25M; (▼) 15B-15M; (△) 25B-5M; (■) 30B-0M

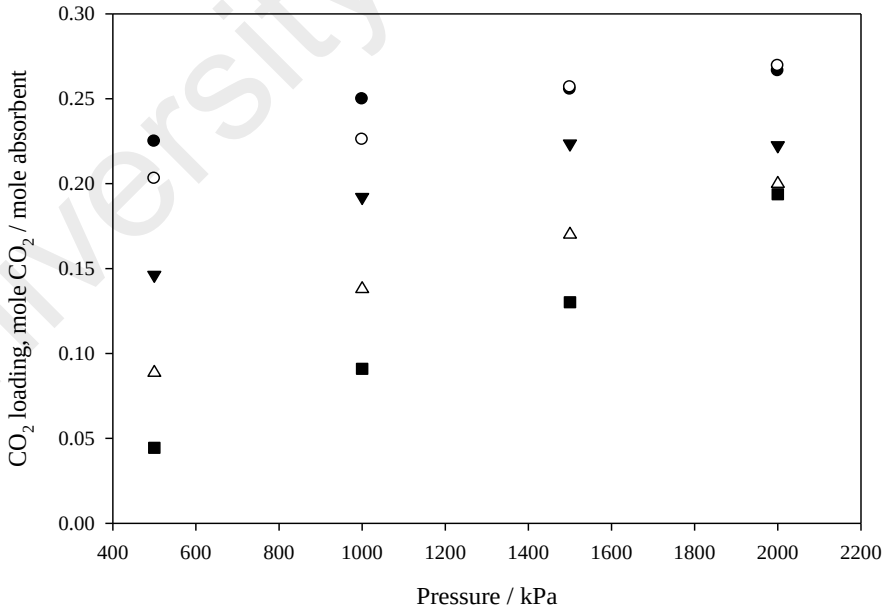

Figure 4.14: Solubility of CO_2 in non-aqueous mixtures against pressure at 303.15 K; (●) 0B-30M; (○) 5B-25M; (▼) 15B-15M; (△) 25B-5M; (■) 30B-0M

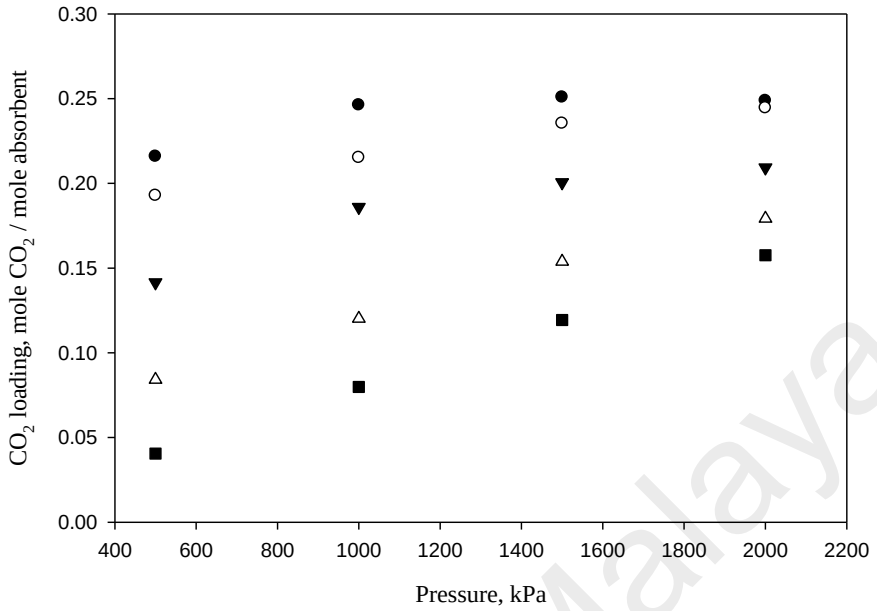

Figure 4.15: Solubility of CO_2 in non-aqueous mixtures against pressure at 313.15 K; (●) 0B-30M; (○) 5B-25M; (▼) 15B-15M; (△) 25B-5M; (■) 30B-0M

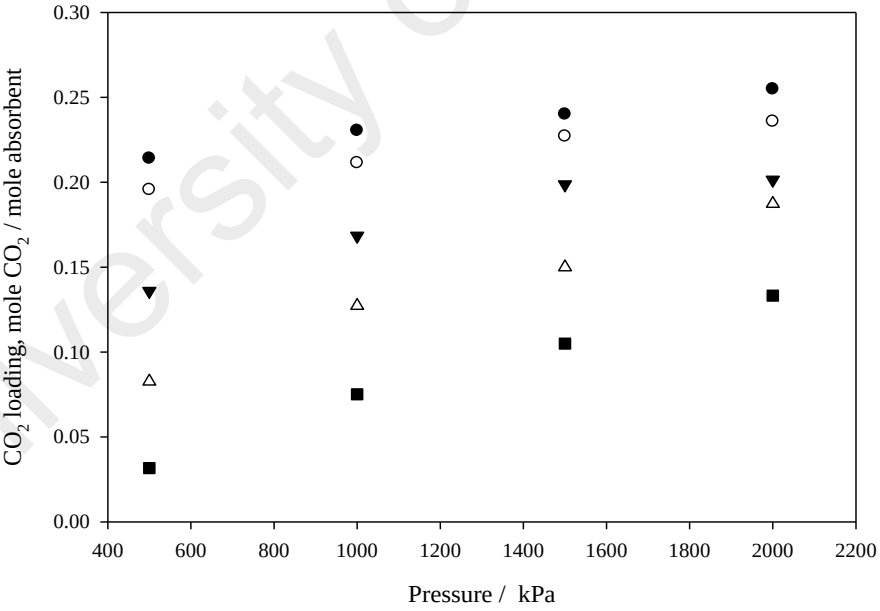

Figure 4.16: Solubility of CO_2 in non-aqueous mixtures against pressure at 323.15 K; (●) 0B-30M; (○) 5B-25M; (▼) 15B-15M; (△) 25B-5M; (■) 30B-0M

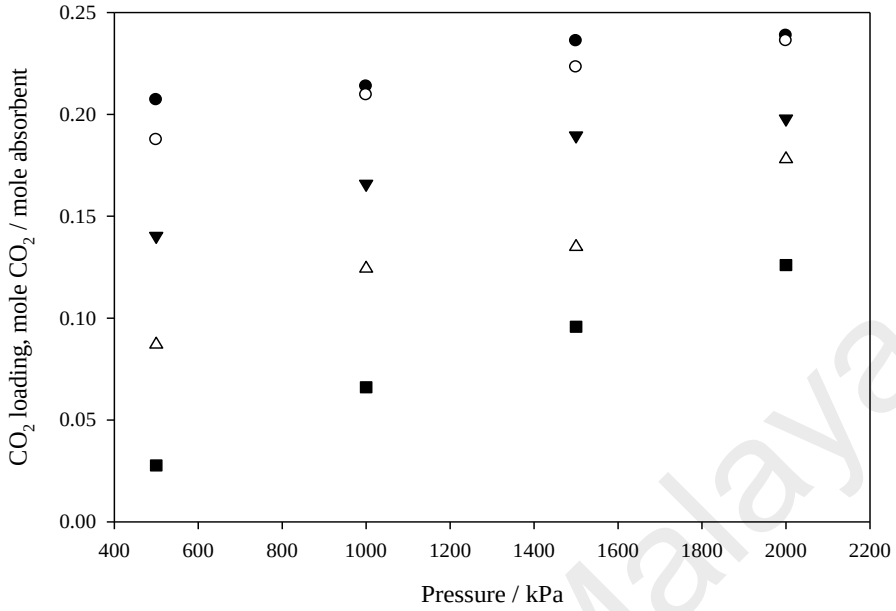

Figure 4.17: Solubility of CO_2 in non-aqueous mixtures against pressure at 333.15 K; (●) 0B-30M; (○) 5B-25M; (▼) 15B-15M; (△) 25B-5M; (■) 30B-0M

4.1.5.2 Correlation of solubility as function of pressure and temperature

Based on correlation suggested by Jou and Mather (F. Y. Jou & Mather, 2005), the measured CO_2 loading was fitted linearly as a function of pressure according to Equation 4.1. The coefficients for all the mixture system are summarized in Table 4.3.

$$\ln P = A + B \ln \alpha \tag{4.1}$$

where,

$$A = a + bT(K) + cT(K) \quad (4.2)$$

$$B = d + eT \quad (4.3)$$

Figure 4.18 shows a comparison of the calculated and experimental data at varying temperatures and compositions. It is evident that there is a good agreement between the calculated and experimental data. The average absolute deviation (AARD) values are calculated as:

$$AARD = \frac{1}{N_p}\sum_{i=1}^{N_p}\left(\frac{|\alpha_{exp,i}-\alpha_{cal,i}|}{\alpha_{exp,i}}\right) \times 100\% \quad (4.4)$$

where N_p is the number of experimental points and α_{exp} and α_{cal} are the experimental and calculated values of CO_2 loading, respectively.

Table 4.3: Coefficient for CO_2 loading correlation

Sample	Coefficient					AARD
	a	b	c	d	e	(%)
0B-30M	-82.003	0.483	-0.001	8.806	-0.003	1.84
5B-25M	392.725	-2.428	0.004	-12.852	0.059	0.93
15B-15M	-45.906	0.322	-0.001	-5.115	0.027	2.45
25B-5M	-16.411	0.137	0.000	-0.675	0.008	1.53
30B-0M	-34.512	0.254	0.000	1.665	-0.002	4. 89

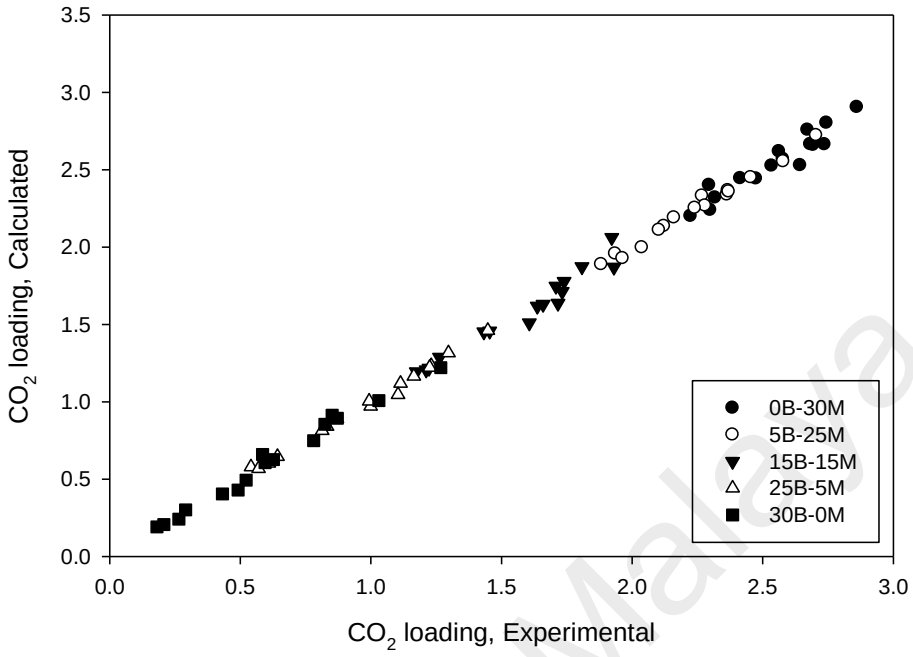

Figure 4.18: Comparison between calculated and experimental CO_2 loading

4.1.6 Biphasic layers formation

Formation of biphasic layers was observed after the absorption in the mixture containing MEA. These biphasic layers are shown in Figure 4.19. The biphasic phenomenon could be due to the formation of insoluble MEA-carbamate in the mixture. Strong ionic interactions and hydrogen bonding between MEA-carbamate making it difficult to dissolve in hydrophobic [BMIM] [NTf_2] and dipolar sulfolane. A similar observation was reported for CO_2 absorption using an emulsion of diethanolamine (DEA) and 1-hexyl-3-methylimidazolium *bis*(trifluoromethylsulfonyl)imide ([HMIM][NTf_2]) (Muhammad Hasib-ur-Rahman et al., 2012). It can be seen that in the mixture with higher [BMIM][NTf_2] content (30B-0M, 25B-5M and 15B-15M), the insoluble MEA-carbamate appears in the upper layer while [BMIM][NTf_2] and sulfolane is in the lower layer. For the mixture containing higher

MEA (5B-25M and 0B-30M), the insoluble MEA-carbamate appears in the lower layer while [BMIM][NTf_2] and sulfolane is in the upper layer. This could be due to the difference in density of the [BMIM][NTf_2] and sulfolane layer to the MEA-carbamate layer. Due to the high density of the pure [BMIM][NTf_2], CO_2 saturated mixtures of with a high content of [BMIM][NTf_2] have a higher as compare to the MEA-carbamate layer.

The observation on the formation of biphasic layers was in line with several findings. Arshad and co-workers reported a formation of biphasic layers when an aqueous blend of 2-(diethylamino) ethanol (DEEA) and 3-(methylamino)propylamine after absorption of CO_2 (Arshad et al., 2014). The CO_2-rich layer was at the bottom layer while the CO_2-lean layer was the upper layer, biphasic formation was also reported by Xu and co-workers in utilizing mixture of 1.4-butanediamine (BDA) and DEED (Zhicheng Xu et al., 2013). The French Institute of Petroleum (IFP) Energies nouvelles developed a class of undisclosed DMX™ absorbent that formed biphasic layers' after absorption of CO_2 (Raynal et al., 2011).

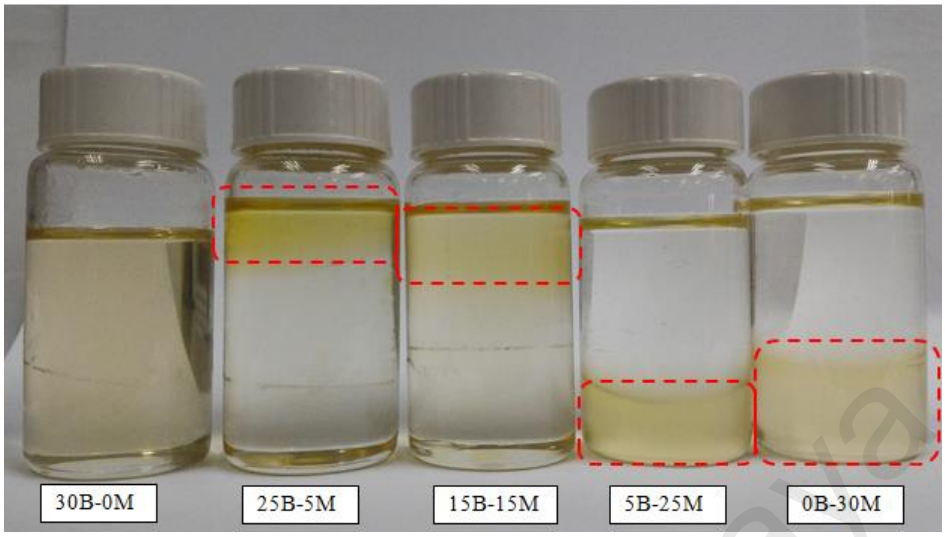

Figure 4.19 : CO_2-rich layer in the mixture samples (dotted box)

Figure 4.20 and Figure 4.21 illustrate the ^{13}C NMR spectra of lower (CO_2-rich) and upper (CO_2-lean) layer of the CO_2-loaded 5B-25M sample (taken in methanol-d4) with tetramethylsilane (TMS) as reference. 5B-25M sample displays six peaks in range of 22.48 to 63.02 ppm. Two intense peaks at 41.89 ppm and 58.99 ppm originated from the CH_2-CH_2 carbons of the protonated amine ($MEAH^+$) and two less intense peaks at 43.69 ppm and 63.02 ppm arise from the ethylene carbon of carbamate MEA. CO_2 captured chemically are shown by the low intensity resonance at 164.57 ppm, while physically absorb CO_2 are shown at 160 ppm. Two peaks at 22.34 ppm and 50.64 ppm belongs to sulfolane that partially dissolves in the lower layer. Similar observation can be seen in the 0B-30M sample. Trace of [BMIM][NTf_2] was not found in the lower layer of both samples which indicate that the hydrophobic ionic liquid, [BMIM][NTf_2] does not dissolve the polar carbamate MEA. It can be assumed that MEA in all of the non-aqueous samples react with CO_2, forming a MEA carbamate in the lower layer. It is worth mentioning that the samples were a homogeneous solution initially but turn into a heterogeneous solution with two layers. The reaction between the non-aqueous amine mixture and CO_2 were represented as follows (Equation 4.5 and 4.6):

$$RNH_2 + CO_2 \leftrightarrow RNH_2{}^+ COO^- \quad (4.5)$$

$$RNH_2{}^+ COO^- + RNH_2 \leftrightarrow RNHCOO^- + RNH_3{}^+ \quad (4.6)$$

The MEA carbamate and protonated MEA form an ion pair which possesses a high molecular weight, which leads to a higher density and viscosity of the lower layer. Sulfolane and [BMIM][NTf_2] are a chemically stable component and do not react with CO_2. The biphasic layers could lead to a reduction in regeneration cost. This can be done by separating the CO_2-rich layer of the mixture and transported to the stripper, instead of transporting the whole mixture (Kim et al., 2014).

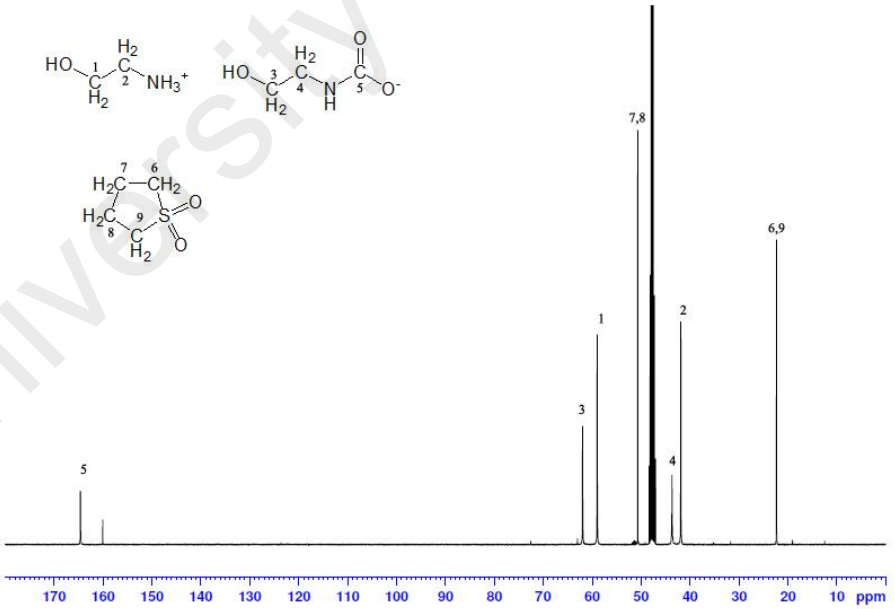

Figure 4.20: ^{13}C NMR spectrum of CO_2-loaded 5B-25M solution, CO_2-rich layer

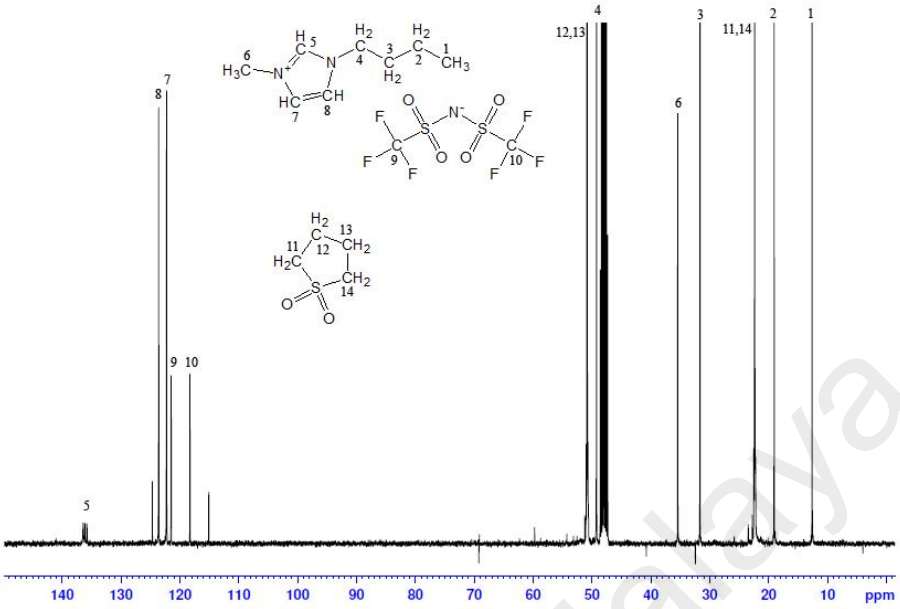

Figure 4.21: ^{13}C NMR spectrum of CO_2-loaded 5B-25M solution, CO_2-lean layer

4.1.7 Comparison with other studies

Few studies have been conducted using a non-aqueous physical-chemical solvent. Figure 4.22 shows a comparison of CO_2 solubility between this work and literatures. Due to the limited scope of previous work in literature, the selected data were measured at a temperature of 313.15 K and MEA composition of 30 wt% for comparison. As shown in Figure 4.22, at MEA composition of 30wt% and temperature of 313.15 K, sample 0B-30M was compared to 30wt% MEA + diglyme (Weijia Huang et al., 2015) and 30wt% MEA + H_2O (Fang-Yuan Jou et al., 1995). The comparison shows that 0B-30M sample has the lowest CO_2 loading even though with similar MEA composition. The difference in solubility could cause by the variation in the physical absorbent components which are sulfolane and diglyme. Sample 0B-30M also has a lower CO_2 loading compared to 30wt% MEA in H_2O. This could

due to the formation of stable carbamate facilitates CO_2 absorption by MEA in aqueous solution, while sulfolane is a dipolar aprotic solvent that unable to ionize MEA appropriately. Another possible reason for the lower CO_2 loading of the sulfolane based mixture system is due to the biphasic layer formed during the absorption process. Formation of CO_2-rich layer on the surface of the sample mixture during the absorption process could limit the contact of CO_2 with a physical absorbent component which leads to lower total CO_2 loading of the mixture.

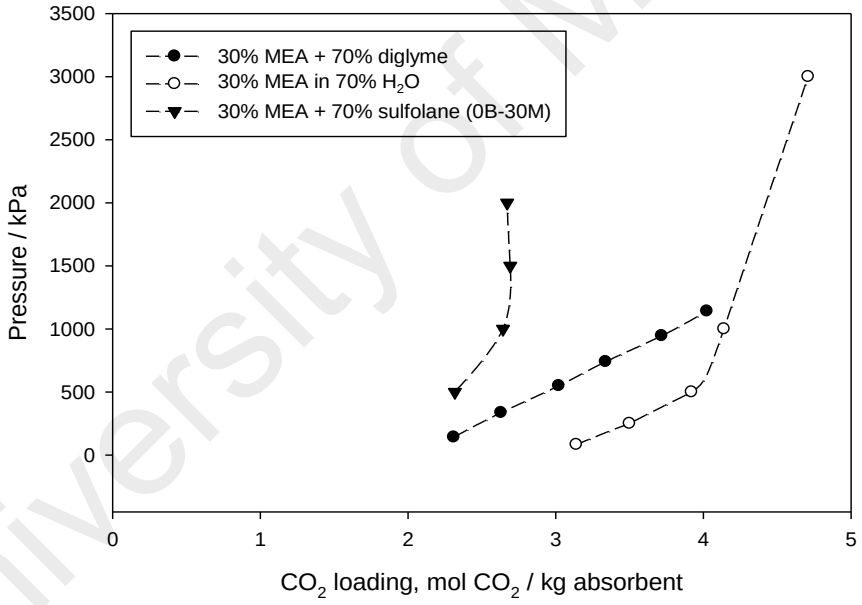

Figure 4.22: Comparison of CO_2 solubility in 0B-30M sample mixture and other physical MEA absorbent

Despite lower CO_2 loading in comparison to other solvent in literature, such disadvantage could be used as an advantage in term of total processing cost. Kim and co-workers demonstrated the concept of phase transitional absorption/ regeneration in their work

with phase transitional alkanolamine–alcohol mixture (Kim et al., 2014). Arshad and co-workers reported a formation of biphasic layers when an aqueous blend of DEEA and 3-(methylamino)propylamine after CO_2 absorption (Arshad et al., 2014). They observed the presents of viscous lower phase saturated with CO_2 in comparison with CO_2-lean upper phase. A similar observation was also reported by Xu and co-workers in utilizing mixture of BDA and DEED (Zhicheng Xu et al., 2013). This CO_2-rich layer can be easily separated and transported to the stripper in less quantity to be regenerated as illustrated in Figure 4.23. Furthermore, such approaches may overcome limitation faced due to corrosion and degradation in current industrial processes.

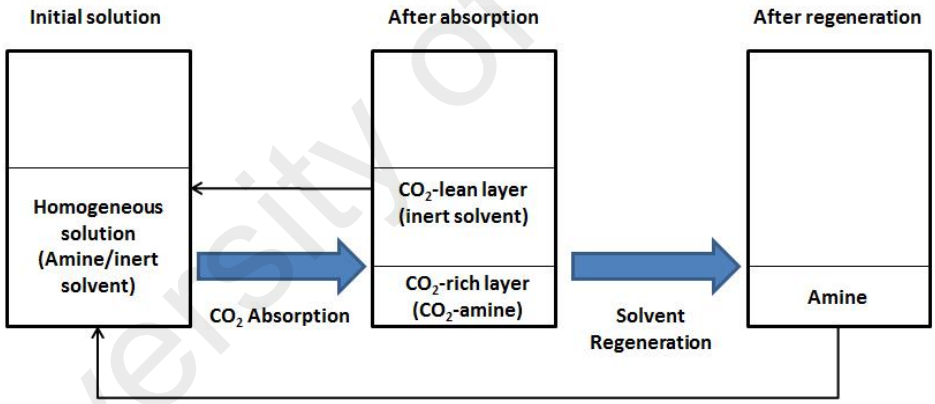

Figure 4.23: CO_2 absorption/regeneration using phase transitional absorbent by Kim *et al.* (Kim et al., 2014)

4.1.8 Recycling of solvents and effect of water

In the effort of minimizing the production cost and negative impact on the environment, recyclability of absorption solvent was further investigated. The absorption solvents were reused for further absorption study, which the data is presented in Figure 4.24.

At the end of every cycle, the CO_2 saturated solvent was desorpted under reduced pressure and at a temperature of 383.15 K for 4h. Figure 4.24 shows the CO_2 absorption performance of 0B-30M solvent mixture for 5 cycles of absorptions. The result shows a reduction in CO_2 solubility for 0B-30M solvent mixture, 46 % on the 5^{th} cycle of absorption. This is possibly due to the loss of significant amounts of viscous CO_2-rich amine phase during repeated recovery activities which include decantation and desorption. Higher number of steps involved exhibit a greater amount of solvent loss. Furthermore, the effect of water content in the feed CO_2 was simulated by addition of a small amount of water into the solvent mixture prior to the absorption process. Based on the result presented in Figure 4.25, water has shown no significant changes in CO_2 loading with the biphasic phenomenon still observed.

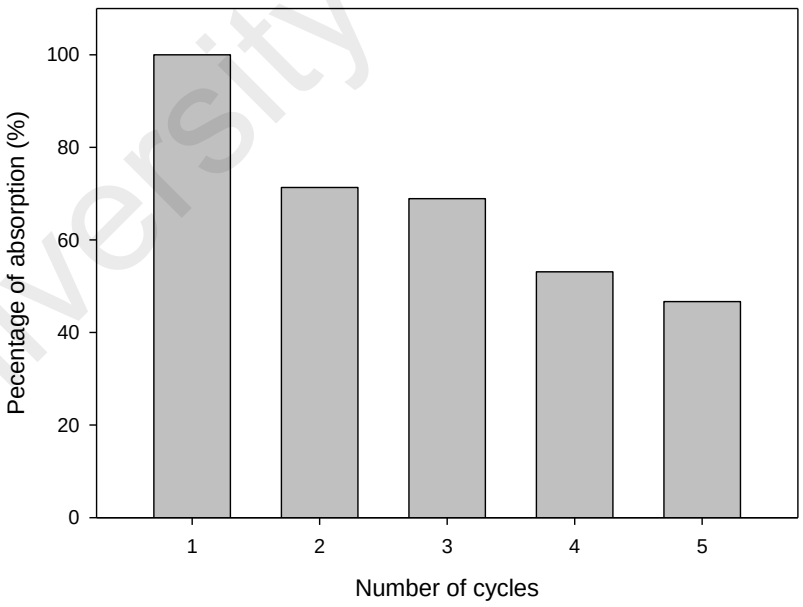

Figure 4.24: Reusability of phase transitional absorbent (Sample 0B-30M, P = 2000 kPa, T = 303.15 K)

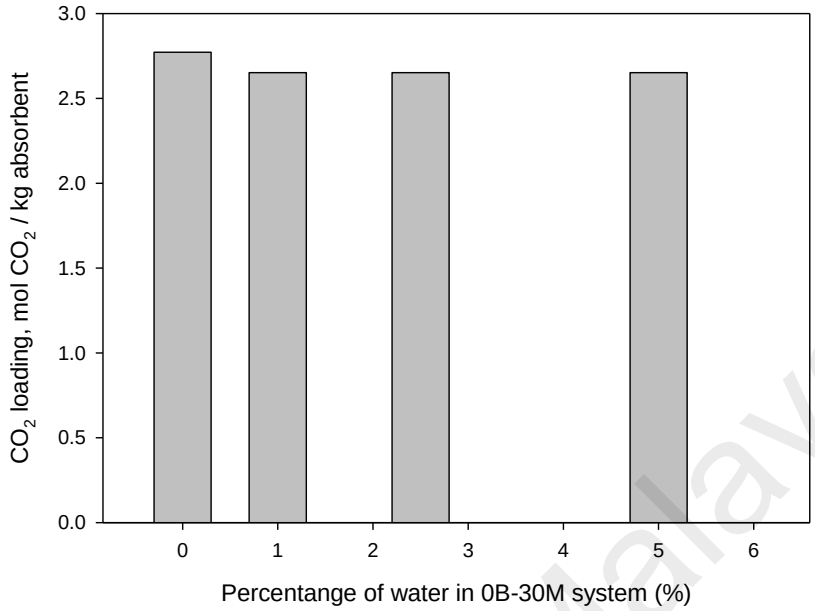

Figure 4.25: Effect of water content on CO_2 loading (Sample 0B-30M, P = 2000 kPa, T = 303.15 K)

4.2 Thermophysical properties

4.2.1 Density

4.2.1.1 Introduction

This chapter explores the density of three binary mixtures of [BMIM][NTf_2] (1) + sulfolane (3), MEA (2) + sulfolane (3) and [BMIM][NTf_2] (1) + MEA (2) together with ternary mixtures of [BMIM][NTf_2] (1) + MEA (2) + sulfolane (3) over whole range of composition. The atmospheric densities were measured at various temperatures ranging from 303.15 to 343 K with increment of 10 K. The measurement was conducted to evaluate the

changing of the density value of binary and ternary mixtures of [BMIM][NTf_2], MEA and sulfolane at different temperatures and compositions.

4.2.1.2 Validation of the density measurement

To verify the reliability of the equipment and procedures, the density measurements of pure [BMIM][NTf_2], MEA and sulfolane were measured at different temperatures and compared with the experimental values that are given by other authors in literatures (Table 4.4). The measurement of density obtained in this study was in good agreement with the literature data at all temperatures.

Table 4.4: Comparison of measured density (ρ) with literature values for [BMIM][NTf_2], MEA and sulfolane at different temperatures

ρ, g cm^{-3}	[BMIM][NTf_2]		MEA		sulfolane	
T/K	**Exp.**	**Lit.[1]**	**Exp.**	**Lit.[2]**	**Exp.**	**Lit.[3]**
303.15	1.4315	1.4319	1.0094		1.2594	1.2604
313.15	1.4219	1.4223	1.0012	1.0003	1.2517	1.2505
323.15	1.4124	1.4129	0.9931	0.9923	1.2440	1.2412
333.15	1.4029	1.4035	0.9849		1.2354	1.2326
343.15	1.3935	1.3942	0.9849	0.9760	1.2250	1.2224

1 = data from (Harris et al., 2007)
2 = data from (Amundsen et al., 2009)
3 = data from (Aguila-Hernandez et al., 2008)

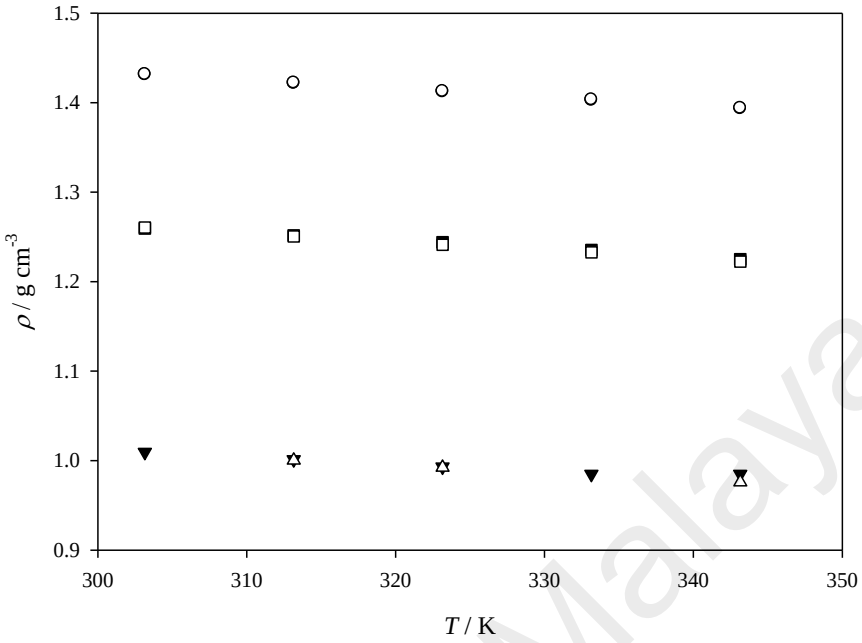

Figure 4.26: Comparison of density for pure [BMIM][NTf_2], MEA and sulfolane with literatures; (●) [BMIM][NTf_2]$_{Exp.;}$ (○) [BMIM][NTf_2]$_{Lit}$ (Harris et al., 2007).; (▼) $MEA_{Exp.;}$ (△) $MEA_{Lit.}$ (Amundsen et al., 2009); (■) $sulfolane_{Exp.;}$ (□) $sulfolane_{Lit}$ (Aguila-Hernandez et al., 2008)

.

4.2.1.3 Effect of temperature and composition

(a) Binary mixtures

All measured experimental density values of [BMIM][NTf_2] (1), MEA (2) and sulfolane (3) binary mixtures throughout the entire mol fraction composition with the temperatures ranging from 303.15 to 343.15 K are tabulated in Table 4.5 and represented by Figure 4.27 to Figure 4.32. Figure 4.27 to Figure 4.29 show the measured density of [BMIM][NTf_2] (1) + sulfolane (3), MEA (2) + sulfolane (3) and [BMIM][NTf_2] (1) + MEA (2) binary mixtures, respectively, throughout the entire temperatures ranging from 303.15 to

343.15 K at constant composition. In all binary mixtures, the density curves show a quasi-linear decrease in values with increment of temperature throughout whole composition. This illustrates the increase of molecular kinetic energy by the increase of temperature led to less interaction between the molecules. Subsequently, it led to increase in volume that decrease of density. The influence of temperature on the density of pure and binary mixtures of [BMIM][NTf_2] (1), MEA (2) and sulfolane (3) were found to be linear and correlated using a linear relationship as a function of temperature, Equation 4.7 and tabulated in Table 4.6.

$$f = A + BT \tag{4.7}$$

where *f* is the measured data, T is the temperature, and *A*, *B* are the adjustable parameters.

Table 4.5: Density (ρ) of [BMIM][NTf_2] (1), MEA (2) and sulfolane (3) binary mixtures at different temperatures and compositions

x_1	x_2	x_3	ρ, g cm^{-3}				
			303.15 K	**313.15 K**	**323.15 K**	**333.15 K**	**343.15 K**
[BMIM][NTf_2] (1) + sulfolane (3)							
0.0000	-	1.0000	1.2594	1.2517	1.244	1.2354	1.225
0.1000	-	0.9000	1.3061	1.297	1.288	1.279	1.2699
0.1999	-	0.8001	1.3367	1.3275	1.3183	1.309	1.2998
0.3001	-	0.6999	1.3591	1.3494	1.3402	1.331	1.3218
0.4000	-	0.6000	1.3766	1.3672	1.3578	1.3484	1.3391
0.5001	-	0.4999	1.3905	1.3811	1.3716	1.3622	1.3528
0.5999	-	0.4001	1.4017	1.3922	1.3828	1.3733	1.3639
0.7000	-	0.3000	1.4111	1.4016	1.3921	1.3826	1.3732
0.7995	-	0.2005	1.419	1.4094	1.3999	1.3904	1.381
0.8985	-	0.1015	1.4257	1.4161	1.4066	1.3971	1.3876
1.0000	-	0.0000	1.4315	1.4219	1.4124	1.4029	1.3935
MEA (2) + sulfolane (3)							
-	0.0000	1.0000	1.2594	1.2517	1.244	1.2354	1.2250
-	0.0999	0.9001	1.2428	1.2337	1.2247	1.2156	1.2065
-	0.2001	0.7999	1.2242	1.2149	1.2058	1.1966	1.1874
-	0.3001	0.6999	1.2048	1.1956	1.1865	1.1773	1.1681
-	0.3999	0.6001	1.1838	1.1746	1.1655	1.1563	1.147
-	0.4999	0.5001	1.1611	1.1520	1.1429	1.1337	1.1245
-	0.5999	0.4001	1.1364	1.1273	1.1184	1.1093	1.1002
-	0.6999	0.3001	1.1094	1.1005	1.0917	1.0828	1.0738
-	0.8000	0.2000	1.0796	1.0709	1.0623	1.0537	1.0448
-	0.8999	0.1001	1.0466	1.0381	1.0297	1.0213	1.0127
-	1.0000	0.0000	1.0085	1.0004	0.9923	0.9841	0.9758
[BMIM][NTf_2] (1) + MEA (2)							
0.0000	1.0000	-	1.0094	1.0012	0.9931	0.9849	0.9849
0.1001	0.8999	-	1.1561	1.1475	1.1382	1.1293	1.1206
0.2000	0.8000	-	1.2377	1.2284	1.2191	1.2095	1.2001
0.3000	0.7000	-	1.2906	1.2805	1.2714	1.2615	1.2515
0.4000	0.6000	-	1.3281	1.3182	1.3084	1.2986	1.2888
0.4999	0.5001	-	1.3564	1.3464	1.3366	1.3268	1.3170
0.6000	0.4000	-	1.3783	1.3687	1.3586	1.3488	1.3389
0.6999	0.3001	-	1.3959	1.3861	1.3761	1.3665	1.3567
0.8000	0.2000	-	1.4099	1.4000	1.3903	1.3807	1.371
0.8998	0.1002	-	1.4219	1.4123	1.4027	1.3931	1.3835
1.0000	0.0000	-	1.4329	1.4254	1.4134	1.4038	1.3943

Standard uncertainties u are: u(ρ) = 0.001 g cm^{-3}, u(T) = 0.05 K. x_1, x_2, and x_3 is the mol fraction of [BMIM][NTf_2], MEA and sulfolane, respectively.

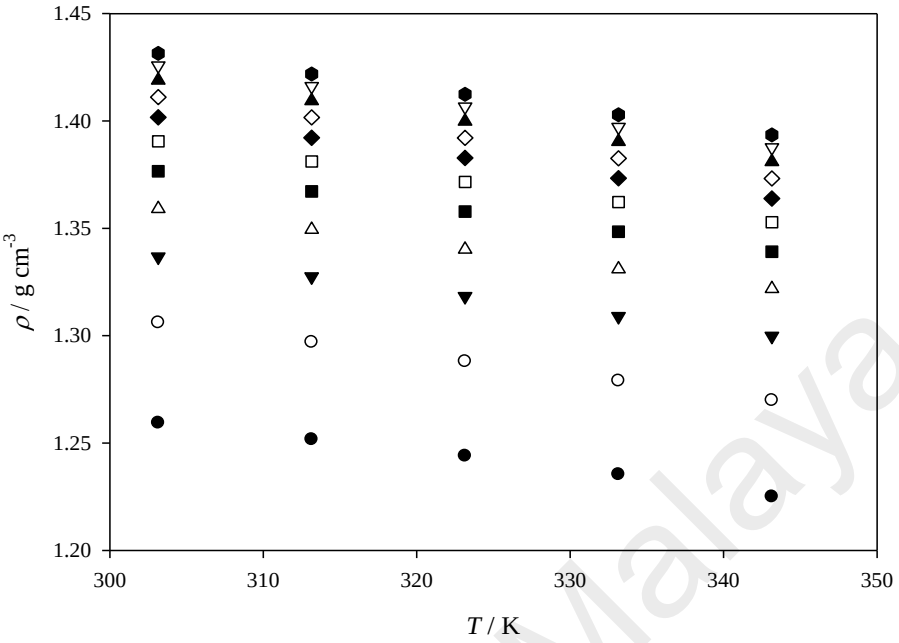

Figure 4.27: Density of [BMIM][NTf_2] (1) + sulfolane (3) binary mixtures against temperature at various compositions; (●) 0 x_1; (○) 0.1 x_1; (▼) 0.2 x_1; (△) 0.3 x_1; (■) 0.4 x_1; (□) 0.5 x_1; (◆) 0.6 x_1; (◇) 0.7 x_1; (▲) 0.8 x_1; (▽) 0.9 x_1; (⬢) 1.0 x_1

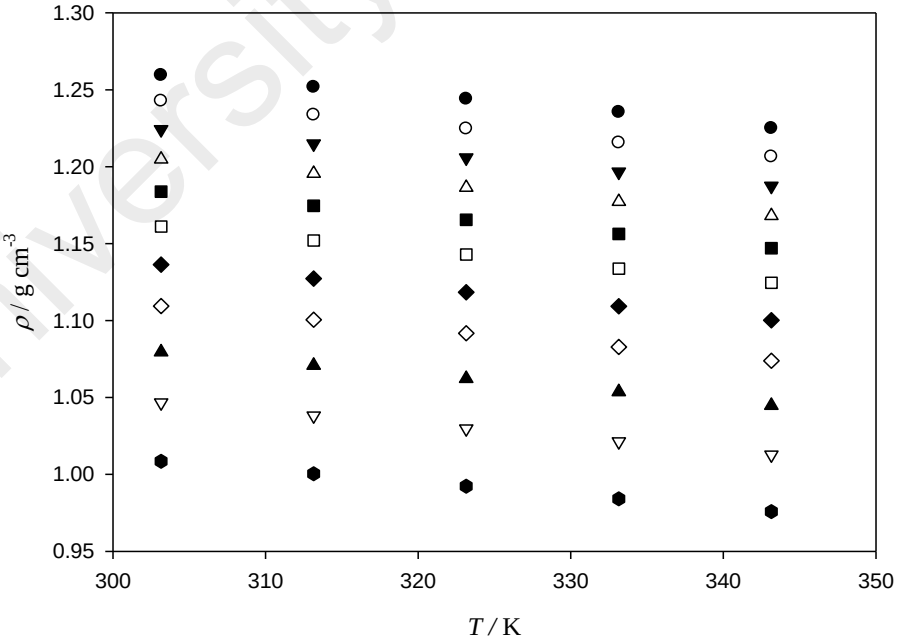

Figure 4.28: Density of sulfolane MEA (2) + sulfolane (3) binary mixtures against temperature at various compositions; (●) 0 x_2; (○) 0.1 x_2; (▼) 0.2 x_2; (△) 0.3 x_2; (■) 0.4 x_2; (□) 0.5 x_2; (◆) 0.6 x_2; (◇) 0.7 x_2; (▲) 0.8 x_2; (▽) 0.9 x_2; (⬢) 1.0 x_2.

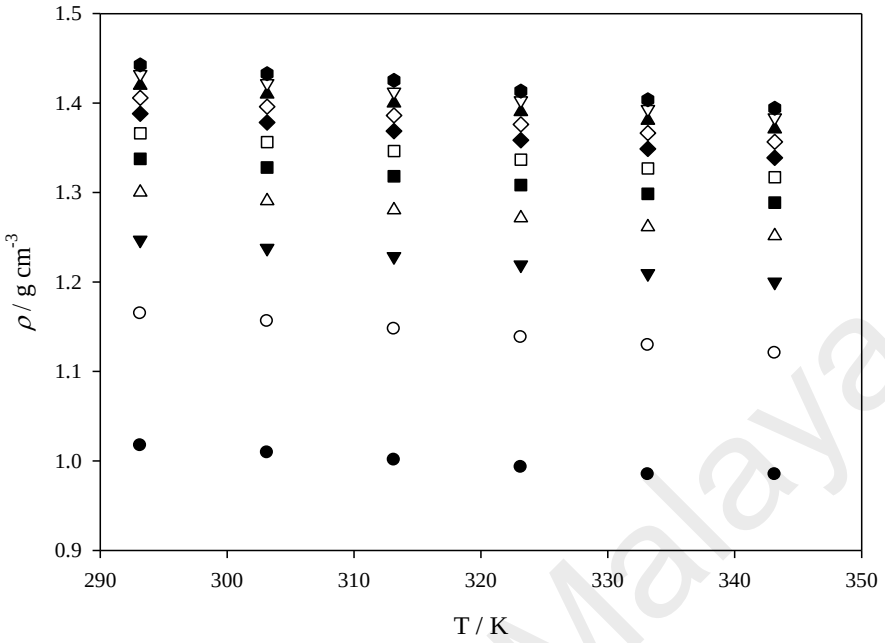

Figure 4.29: Density of [BMIM][NTf_2] (1) + MEA (2) binary mixtures against temperature at various concentrations; (●) 0 x_1; (○) 0.1 x_1; (▼) 0.2 x_1; (△) 0.3 x_1; (■) 0.4 x_1; (□) 0.5 x_1; (◆) 0.6 x_1; (◇) 0.7 x_1; (▲) 0.8 x_1; (▽) 0.9 x_1; (⬢) 1.0 x_1.

Table 4.6: Fitting parameters of Equation 4.7 together with correlation coefficient squared, R^2, and standard relative deviations, σ, for the influence of temperature on density of [BMIM][NTf_2] (1), MEA (2) and sulfolane (3) binary mixtures

x_1	x_2	x_3	A	B (x10^{-4})	R^2	σ^a (x10^{-5})
[BMIM][NTf_2] (1) + sulfolane (3)						
0.0000	-	1.0000	1.5273	-8.7874	0.9954	89.3085
0.1000	-	0.9000	1.5801	-9.0379	1.0000	4.8235
0.1999	-	0.8001	1.6163	-9.2218	1.0000	4.9834
0.3001	-	0.6999	1.6454	-9.4389	0.9996	3.1891
0.4000	-	0.6000	1.6615	-9.3973	1.0000	4.5147
0.5001	-	0.4999	1.6772	-9.4549	1.0000	4.9658
0.5999	-	0.4001	1.6890	-9.4758	1.0000	4.9931
0.7000	-	0.3000	1.6998	-9.5201	1.0000	7.1428
0.7995	-	0.2005	1.7078	-9.5259	1.0000	6.1257
0.8985	-	0.1015	1.7149	-9.5392	1.0000	4.0884
1.0000	-	0.0000	1.7209	-9.5447	1.0000	8.5251
MEA (2) + sulfolane (3)						
-	0.0000	1.0000	1.5181	-8.5100	0.9999	100.00
-	0.0999	0.9001	1.5178	-9.0700	0.9999	3.1623
-	0.2001	0.7999	1.5028	-9.1900	0.9999	4.8305
-	0.3001	0.6999	1.4830	-9.1760	0.9999	4.5494
-	0.3999	0.6001	1.4624	-9.1900	0.9999	6.0553
-	0.4999	0.5001	1.4385	-9.1500	0.9999	4.8305
-	0.5999	0.4001	1.4104	-9.0400	0.9999	6.3246
-	0.6999	0.3001	1.3789	-8.8900	0.9999	6.0553
-	0.8000	0.2000	1.3428	-8.6800	0.9999	9.6609
-	0.8999	0.1001	1.3031	-8.4600	0.9999	6.3246
-	1.0000	0.0000	1.2562	-8.1700	0.9999	7.9582
[BMIM][NTf_2] (1) + MEA (2)						
0.0000	1.0000	-	1.2198	-6.9572	0.9649	0.0028
0.1001	0.8999	-	1.4251	-8.8752	0.9999	0.0002
0.2000	0.8000	-	1.5222	-9.3861	0.9999	0.0001
0.3000	0.7000	-	1.5850	-9.7137	0.9998	0.0003
0.4000	0.6000	-	1.6248	-9.7924	0.9999	0.0001
0.4999	0.5001	-	1.6547	-9.8429	0.9999	0.0001
0.6000	0.4000	-	1.6769	-9.8475	0.9999	0.0001
0.6999	0.3001	-	1.6930	-9.8004	0.9999	0.0001
0.8000	0.2000	-	1.7057	-9.7580	0.9999	0.0001
0.8998	0.1002	-	1.7151	-9.6648	0.9999	0.0002
1.0000	0.0000	-	1.7287	-9.7437	0.9976	0.0010

[a]σ = standard deviation, Equation 4.9. x_1 is the mol fraction of [BMIM][NTf_2].

Figure 4.30 to Figure 4.32 show the effect of composition on the density of [BMIM][NTf_2] (1) + sulfolane (3), MEA (2) + sulfolane (3) and [BMIM][NTf_2] (1) + MEA (2) binary mixtures, respectively, at constant temperature. It is observed that in Figure 4.30, the density increases with increased in composition of [BMIM][NTf_2] in the mixture. This is due to higher density of pure [BMIM][NTf_2] than pure sulfolane. In Figure 4.31, it is observed that the density decreases with increased in composition of MEA as density of pure MEA is lower than pure sulfolane. While Figure 4.29 shows the density increases with increased composition of [BMIM][NTf_2] as density of pure [BMIM][NTf_2] is higher than pure MEA. In the pure state, the density of [BMIM][NTf_2] (1), MEA (2) and sulfolane (3) had been found to be in the order of;

[BMIM][NTf_2] > sulfolane > MEA

The influence of composition on the density of pure and [BMIM][NTf_2] (1), MEA (2) and sulfolane (3) binary mixtures was correlated using a cubic polynomial function as a function of composition x_1, Equation 4.8 and the fitting parameters were tabulated in Table 4.7.

$$f = \sum_{i=0}^{3} a_i x_1^i \tag{4.8}$$

where *f* is the measure data, α_i is the adjustable parameters, and x_1 is composition of the first component. Standard deviation, σ, between experimental and correlated data is calculated using the Equation 4.9 (Y. J. Xu et al., 2013):

$$\sigma = \left[\sum_1^m \frac{(Z_{exp} - Z_{cal})^2}{(m-n)}\right]^{\frac{1}{2}} \quad (4.9)$$

where m denotes the number of experimental points.

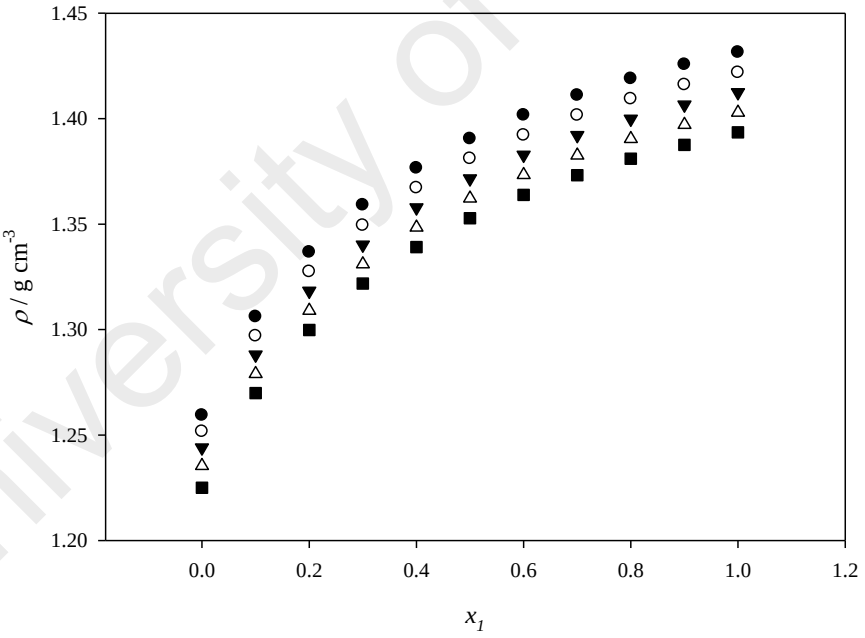

Figure 4.30: Density of [BMIM][NTf_2] (1) + sulfolane (3) binary mixtures against composition at various temperatures; (●) 303.15 K; (○) 313.15 K; (▼) 323.15 K; (△) 333.15 K; (■) 343.15 K

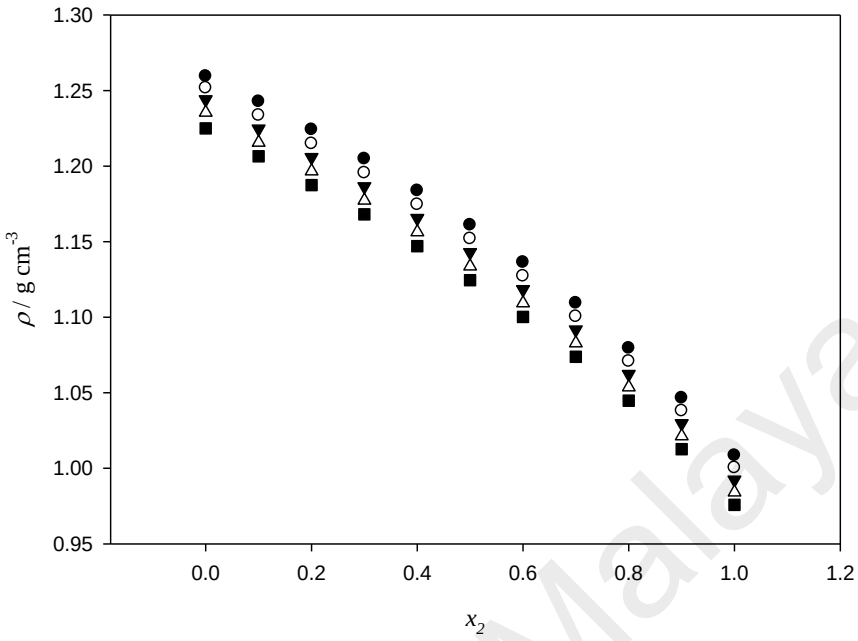

Figure 4.31: Density of MEA (2) + sulfolane (3) binary mixtures against composition at various temperatures; (●) 303.15 K; (○) 313.15 K; (▼) 323.15 K; (△) 333.15 K; (■) 343.15 K.

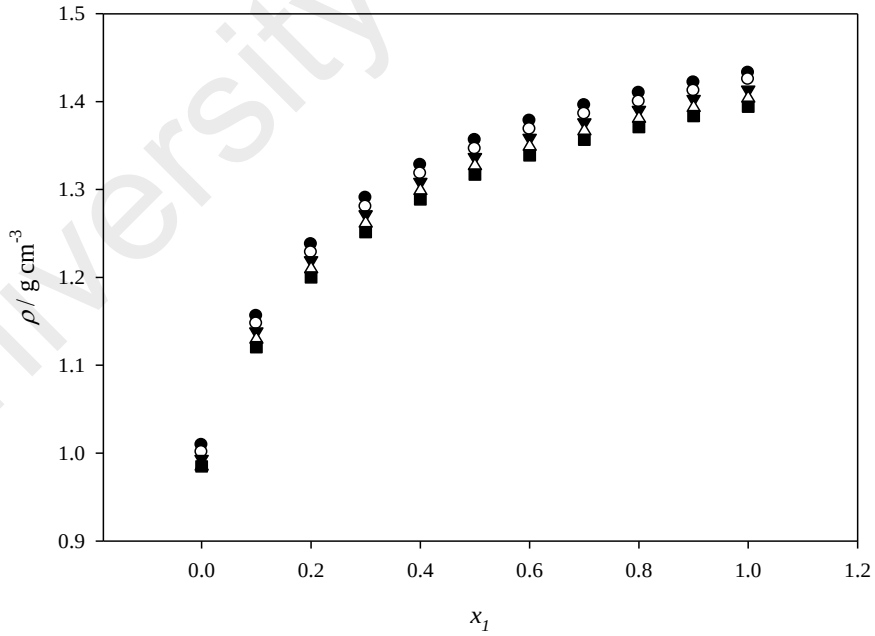

Figure 4.32: Density of [BMIM][NTf_2] (1) + MEA (2) binary mixtures against concentration at various temperatures; (●) 303.15 K; (○) 313.15 K; (▼) 323.15 K; (△) 333.15 K; (■) 343.15 K.

Table 4.7: Fitting parameters of Equation 4.8 together with correlation coefficient squared, R^2, and standard relative deviations, σ, for influence of composition on density of [BMIM][NTf_2] (1), MEA (2) and sulfolane (3) binary mixtures

T/K	A_0	A_1	A_2	A_3	R^2	σ[a]
[BMIM][NTf_2] (1) + sulfolane (3)						
303.15	1.2620	0.4553	-0.4540	0.2112	0.9998	0.0022
313.15	1.2540	0.4457	-0.4783	0.2018	0.9999	0.0020
323.15	1.2461	0.4374	-0.4643	0.1945	0.9991	0.0019
333.15	1.2374	0.4340	-0.4595	0.1923	0.9992	0.0018
343.15	1.2273	0.4408	-0.4739	0.2007	0.9999	0.0020
MEA (2) + sulfolane (3)						
303.15	1.2598	-0.1729	-0.0177	-0.0602	0.9999	0.0004
313.15	1.2518	-0.1815	-0.0019	-0.0677	0.9999	0.0003
323.15	1.2439	-0.1895	0.0128	-0.0746	0.9999	0.0003
333.15	1.2352	-0.1934	0.0198	-0.0773	0.9999	0.0003
343.15	1.2251	-0.1869	0.0063	-0.0684	0.9999	0.0003
[BMIM][NTf_2] (1) + MEA (2)						
303.15	1.0212	1.3606	-1.7573	0.8152	0.9957	0.0103
313.15	1.0130	1.3556	-1.7580	0.8212	0.9958	0.0102
323.15	1.0049	1.3449	-1.7349	0.8054	0.9957	0.0102
333.15	0.9967	1.3353	-1.7177	0.7964	0.9957	0.0102
343.15	0.9950	1.2809	-1.6175	0.7421	0.9966	0.0089

[a]σ = standard deviation, Equation 4.9

(b) Ternary mixtures

All the measured experimental density values of [BMIM][NTf_2] (1) + MEA (2) + sulfolane (3) ternary mixtures throughout the entire mol fraction composition with the temperatures ranging from 303.15 to 343.15 K are tabulated in Table 4.8. Figure 4.33 to Figure 4.37 represent the density for ternary mixtures at constant temperature with temperatures range from 303.15 to 343.15 K, respectively. Overall, it can be observed that the composition of [BMIM][NTf_2] is influenced the density of ternary mixtures highly, in comparison with MEA and sulfolane. At constant [BMIM][NTf_2] mol fraction, the density of the ternary mixtures is affected significantly by sulfolane composition. This is due to sulfolane being relatively higher density than MEA. Therefore, at constant [BMIM][NTf_2] mol fraction, the density of ternary mixtures increases as the sulfolane composition increased. The density data shows a quasi-linear decrease in values with the increment of temperature throughout the whole ternary mixture compositions.

Table 4.8: Density (ρ) of [BMIM][NTf_2] (1) + MEA (2) + sulfolane (3) ternary mixtures at different temperatures and compositions

[BMIM][NTf_2] (1) + MEA (2) + sulfolane (3)							
x_1	x_2	x_3	ρ, g cm^{-3}				
			303.15 K	313.15 K	323.15 K	333.15 K	343.15 K
0.0999	0.1003	0.7998	1.3020	1.2927	1.2833	1.2740	1.2648
0.0998	0.2000	0.7002	1.2879	1.2786	1.2691	1.2596	1.2503
0.0997	0.3015	0.5988	1.2730	1.2636	1.2541	1.2446	1.2352
0.1000	0.4005	0.4995	1.2576	1.2482	1.2387	1.2292	1.2198
0.0999	0.5004	0.3997	1.2407	1.2315	1.2220	1.2127	1.2033
0.1000	0.5999	0.3001	1.2238	1.2146	1.2051	1.1958	1.1865
0.1000	0.7000	0.2000	1.2048	1.1957	1.1864	1.1770	1.1678
0.1000	0.8002	0.0999	1.1845	1.1756	1.1664	1.1573	1.1482
0.1995	0.1022	0.6982	1.3350	1.3256	1.3160	1.3065	1.2971
0.1997	0.2011	0.5992	1.3239	1.3143	1.3046	1.2951	1.2856
0.1997	0.3008	0.4995	1.3124	1.3028	1.2931	1.2834	1.2739
0.2000	0.4002	0.3998	1.3004	1.2910	1.2813	1.2716	1.2621
0.1998	0.4996	0.3006	1.2879	1.2785	1.2688	1.2593	1.2497
0.1996	0.6007	0.1997	1.2744	1.2650	1.2553	1.2458	1.2363
0.1995	0.7003	0.1002	1.2605	1.2513	1.2416	1.2322	1.2227
0.2993	0.1019	0.5988	1.3599	1.3505	1.3408	1.3312	1.3217
0.2996	0.2007	0.4997	1.3503	1.3407	1.3310	1.3213	1.3117
0.2994	0.2998	0.4008	1.3412	1.3316	1.3218	1.3120	1.3024
0.2997	0.4005	0.2998	1.3316	1.3218	1.3119	1.3022	1.2926
0.3000	0.5001	0.1999	1.3217	1.3120	1.3022	1.2925	1.2828
0.2997	0.6003	0.1000	1.3111	1.3015	1.2917	1.2819	1.2722
0.3989	0.1016	0.4995	1.3788	1.3692	1.3594	1.3498	1.3402
0.3990	0.2017	0.3993	1.3703	1.3606	1.3508	1.3410	1.3314
0.3988	0.3010	0.3002	1.3625	1.3526	1.3427	1.3329	1.3232
0.3995	0.4000	0.2005	1.3549	1.3450	1.3351	1.3253	1.3156
0.3996	0.5003	0.1001	1.3468	1.3370	1.3271	1.3172	1.3075
0.4992	0.1012	0.3996	1.3937	1.3841	1.3743	1.3645	1.3550
0.4993	0.2001	0.3006	1.3871	1.3773	1.3674	1.3576	1.3480
0.4992	0.3008	0.1999	1.3804	1.3706	1.3606	1.3507	1.3410
0.4980	0.3998	0.1021	1.3734	1.3636	1.3536	1.3436	1.3339
0.5978	0.1021	0.3001	1.4059	1.3961	1.3863	1.3766	1.3671
0.5992	0.1999	0.2009	1.4002	1.3903	1.3804	1.3706	1.3609
0.5984	0.3009	0.1007	1.3941	1.3842	1.3742	1.3643	1.3546
0.6963	0.1033	0.2004	1.4159	1.4061	1.3963	1.3865	1.3769
0.6964	0.2009	0.1027	1.4106	1.4007	1.3908	1.3810	1.3713
0.7965	0.1030	0.1005	1.4246	1.4147	1.4049	1.3951	1.3855

Standard uncertainties u are: u(ρ) = 0.001 g cm^{-3}, u(T) = 0.05 K. x_1, x_2, and x_3 is the mol fraction of [BMIM][NTf_2], MEA and sulfolane, respectively.

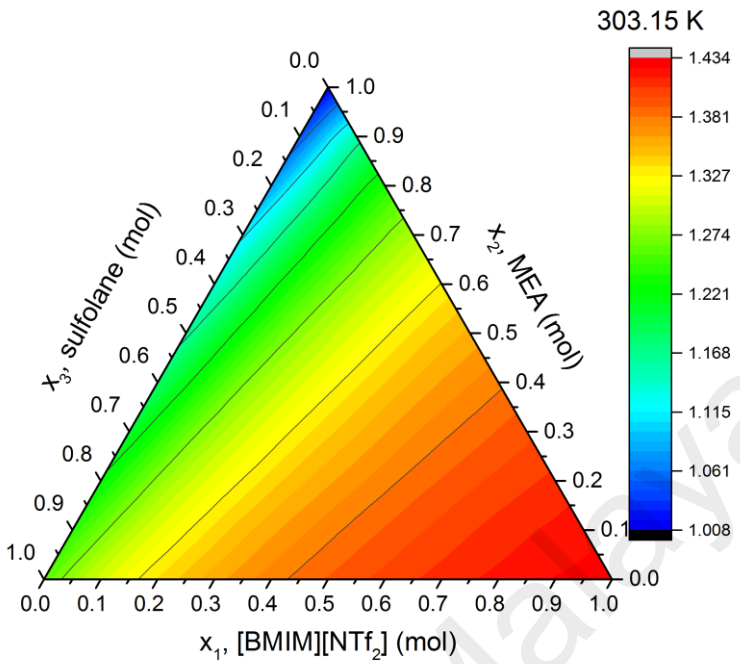

Figure 4.33: Density of [BMIM][NTf_2] (1) + MEA (2) + sulfolane (3) ternary mixtures against temperature at various concentrations at T=303.15 K

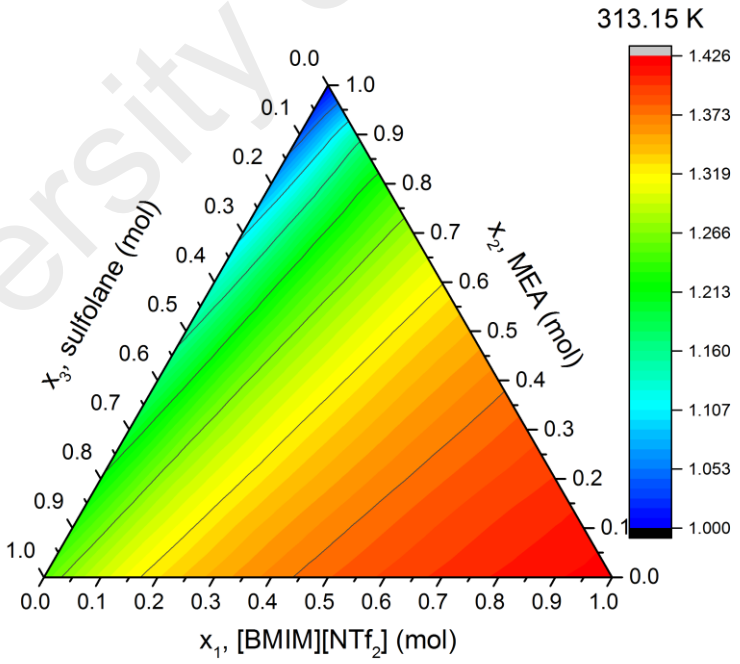

Figure 4.34: Density of [BMIM][NTf_2] (1) + MEA (2) + sulfolane (3) ternary mixtures against temperature at various concentrations at T=313.15 K

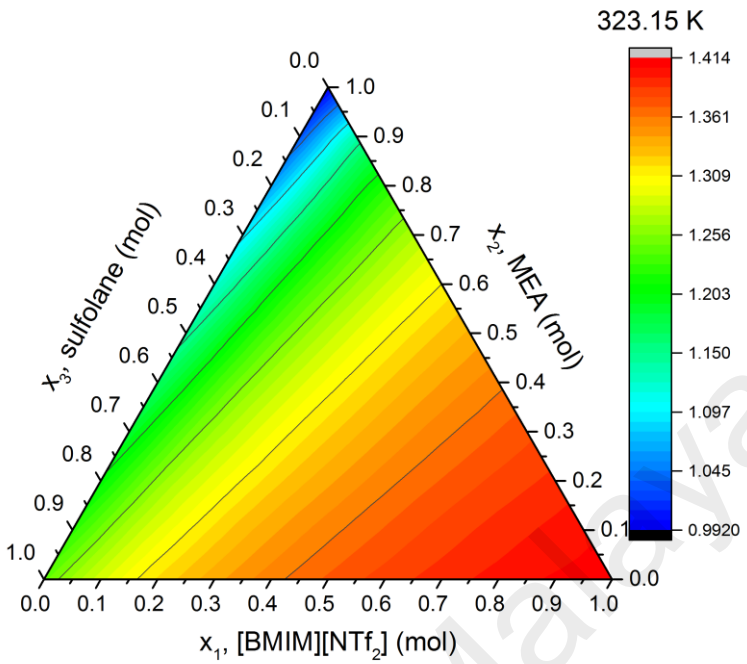

Figure 4.35: Density of [BMIM][NTf_2] (1) + MEA (2) + sulfolane (3) ternary mixtures against temperature at various concentrations at T=323.15 K

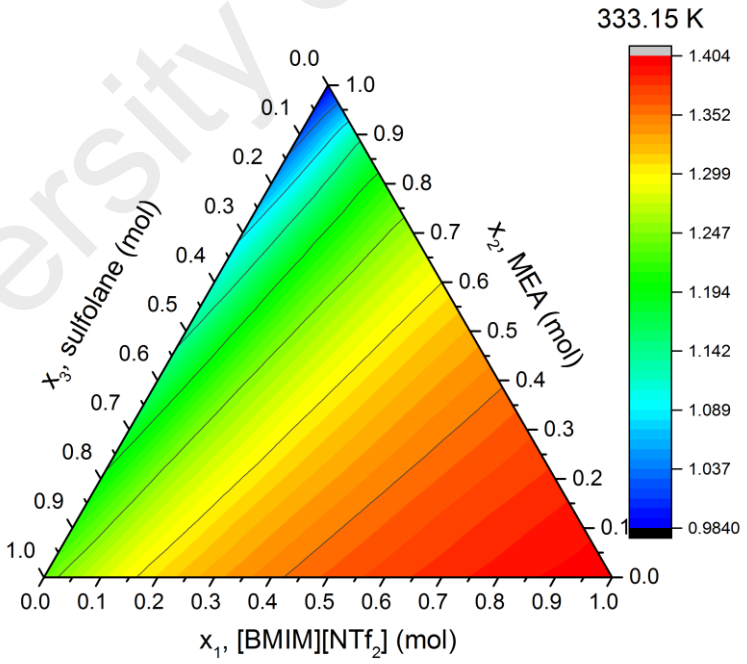

Figure 4.36: Density of [BMIM][NTf_2] (1) + MEA (2) + sulfolane (3) ternary mixtures against temperature at various concentrations at T=333.15 K

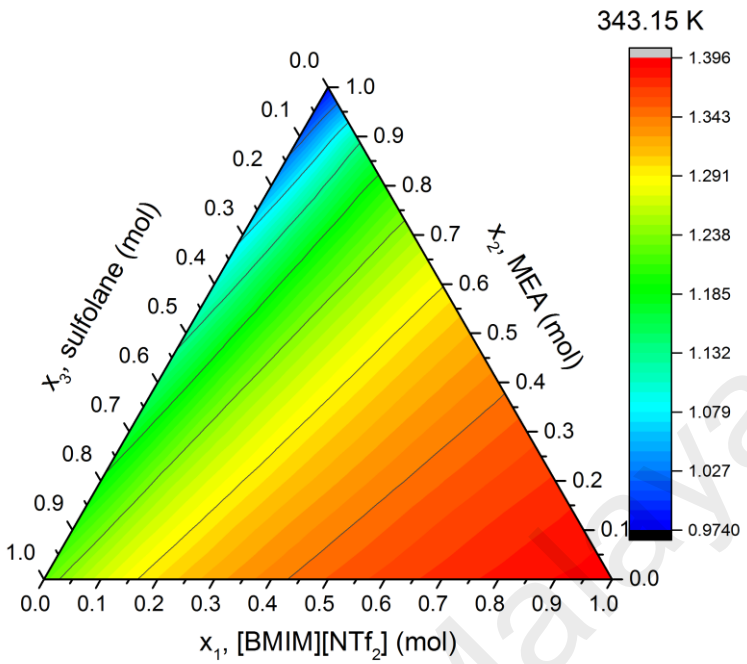

Figure 4.37: Density of [BMIM][NTf_2] (1) + MEA (2) + sulfolane (3) ternary mixtures against temperature at various concentrations at T=343.15 K

4.2.1.4 Excess molar volume

Values of excess molar volume (V^E) were calculated from experimental density of the mixture, ρ, density of pure component, ρ_i, corresponding mol fraction, x_i, and molar masses, M_i, using Equation 4.10 (Zarei et al., 2013):

$$V^E = x_1 M_1 \left(\frac{1}{\rho} - \frac{1}{\rho_1}\right) + x_2 M_2 \left(\frac{1}{\rho} - \frac{1}{\rho_2}\right) \quad (4.10)$$

where x_1, ρ_1 and M_1 relate to the first component, whereas x_2, ρ_2 and M_2 relate to the second component. Excess molar volume for all binary mixtures were correlated using a Redlich-Kister equation (Vranes et al., 2014) where Y^E represents the excess properties where A_i refers to the adjustable parameter and n is the number of coefficient in the equation, as shown in Equation 4.11.

$$Y^E = x_1 x_2 \sum_{i=0}^{n} A_i \, (2x_1 - 1)^i \tag{4.11}$$

(a) Binary mixtures

Values of excess molar volume of [BMIM][NTf_2] (1) + sulfolane (3), MEA (2) + sulfolane (3) and [BMIM][NTf_2] (1) + MEA (2) binary mixtures are summarized in Table 4.9 and represented by Figure 4.38 to Figure 4.40, respectively. In Figure 4.38, it is shown that V^E values are negative over the entire mol fraction range of [BMIM][NTf_2] at various temperatures with the minimum of the asymmetric curve is at x_1 = 0.2 for all studied systems. The excess molar volume depends primarily on the intermolecular forces between two components of the mixture. The magnitude and sign of V^E can be qualitatively examined by accounting the physical, structural and chemical contributions (Kumar et al., 2012). The physical contribution comprises of dispersion of forces or weak dipole-dipole interaction that leads to the positive contribution of V^E. The structural contribution involves the geometric effect, enabling the fitting of molecule of two different sizes into each other structure leading to negative contribution to V^E (B. Gonzalez & Gonzalez, 2014).

Table 4.9: Excess molar volume (V^E) of [BMIM][NTf_2] (1), MEA (2) and sulfolane (3) binary mixtures at different temperatures and compositions

x_1	x_2	x_3	ρ, g cm^{-3}				
			303.15 K	**313.15 K**	**323.15 K**	**333.15 K**	**343.15 K**
[BMIM][NTf_2] (1) + sulfolane (3)							
0.0000	-	1.0000	0.0000	0.0000	0.0000	0.0000	0.0000
0.1000	-	0.9000	-0.1484	-0.1459	-0.1434	-0.1408	-0.1381
0.1999	-	0.8001	-0.1634	-0.1560	-0.1484	-0.1405	-0.1324
0.3001	-	0.6999	-0.1475	-0.1254	-0.1026	-0.0792	-0.0551
0.4000	-	0.6000	-0.1261	-0.1161	-0.1056	-0.0954	-0.0846
0.5001	-	0.4999	-0.1232	-0.1125	-0.1016	-0.0903	-0.0786
0.5999	-	0.4001	-0.0889	-0.0809	-0.0728	-0.0643	-0.0558
0.7000	-	0.3000	-0.0849	-0.0755	-0.0658	-0.0559	-0.0456
0.7995	-	0.2005	-0.0529	-0.0473	-0.0416	-0.0357	-0.0296
0.8985	-	0.1015	-0.0222	-0.0188	-0.0152	-0.0116	-0.0078
1.0000	-	0.0000	0.0000	0.0000	0.0000	0.0000	0.0000
MEA (2) + sulfolane (3)							
-	0.0000	1.0000	0.0000	0.0000	0.0000	0.0000	0.0000
-	0.0999	0.9001	0.0060	0.1069	0.2029	0.2448	0.1577
-	0.2001	0.7999	0.0604	0.1703	0.2683	0.3186	0.2540
-	0.3001	0.6999	0.0650	0.1650	0.2550	0.3050	0.2550
-	0.3999	0.6001	0.0688	0.1592	0.2450	0.2953	0.2656
-	0.4999	0.5001	0.0593	0.1372	0.2173	0.2681	0.2452
-	0.5999	0.4001	0.0413	0.1141	0.1753	0.2200	0.2046
-	0.6999	0.3001	0.0149	0.0700	0.1201	0.1527	0.1454
-	0.8000	0.2000	-0.0126	0.0262	0.0597	0.0750	0.0768
-	0.8999	0.1001	-0.0440	-0.0199	-0.0015	0.0048	0.0041
-	1.0000	0.0000	0.0000	0.0000	0.0000	0.0000	0.0000
[BMIM][NTf_2] (1) + MEA (2)							
0.0000	1.0000	-	0.0000	0.0000	0.0000	0.0000	0.0000
0.1001	0.8999	-	0.1000	0.1300	0.1200	0.1300	0.5900
0.2000	0.8000	-	0.3000	0.4100	0.3400	0.3900	0.8400
0.3000	0.7000	-	0.4500	0.6800	0.5200	0.5900	1.0500
0.4000	0.6000	-	0.5248	0.7701	0.6378	0.6911	1.0712
0.4999	0.5001	-	0.5111	0.8122	0.6227	0.6761	1.0039
0.6000	0.4000	-	0.4700	0.7700	0.5700	0.6100	0.9000
0.6999	0.3001	-	0.4000	0.7650	0.5000	0.5100	0.7300
0.8000	0.2000	-	0.3691	0.7932	0.4342	0.4479	0.5905
0.8998	0.1002	-	0.2792	0.6769	0.2442	0.2447	0.3199
1.0000	0.0000	-	0.0000	0.0000	0.0000	0.0000	0.0000

[a] Standard uncertainty u are u(x) = 0.0005, u(T) = 0.05 K, and U(V^E) = 0.0001 cm^3 mol^{-1}. x_1 and x_3 is the mol fraction of [BMIM][NTf_2] and sulfolane, respectively.

The chemical contribution comprises specific interactions; formation of hydrogen bonding, formation of charge transfer complexes, other complex forming interactions, and strong dipole-dipole interaction between the components, while leads to negative V^E values. Therefore, the negative V^E of binary mixtures [BMIM][NTf_2] + sulfolane could be attributed to strong interaction between different molecules (Pal & Kumar, 2011), i.e. [BMIM][NTf_2] and sulfolane. Moreover, the relatively small sulfolane molecule easily fits into the free volume between comparatively large ions of the [BMIM][NTf_2], resulting in a negative V^E value (Gonzalez et al., 2013). With an increase of temperature, the trend of V^E values for binary mixtures [BMIM][NTf_2] + sulfolane becomes more negative, which possibly due to the increases of kinetic energy with the increase of temperature. This leads to a lower interaction of similar molecules resulting in increasing shrinkage of volume and consequently decrease the excess molar volume (Singh et al., 2013).

Meanwhile, values of excess molar volume for MEA (2) + sulfolane (3) binary mixtures represented by Figure 4.39. Figure 4.39 shows positive V^E values over the entire mol fraction range of composition at various temperatures with the maximum asymmetric curve at mol fraction x_2 = 0.2 MEA for all temperatures range. Similarly, Figure 4.40 shows the V^E values are positive over the entire mol fraction range of [BMIM][NTf_2] at various temperatures with maximum of the asymmetric curve at mol fraction x_1 = 0.4 [BMIM][NTf_2] for all temperatures range. The positive excess molar volume indicates an expansion in volume of the mixtures with the possible breakdown of the self-associated molecules. Disruption of the closely associated MEA multimers in the addition of sulfolane or [BMIM][NTf_2], and formation of a new association between the unlike MEA and sulfolane / [BMIM][NTf_2] molecules, respectively.

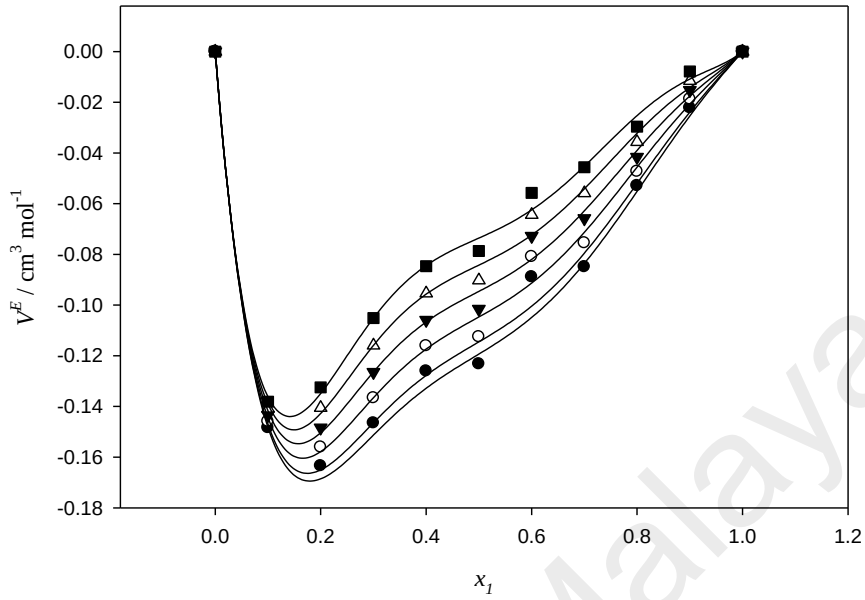

Figure 4.38: Excess molar volume of [BMIM][NTf_2] (1) + sulfolane (3) binary mixtures against temperature as function of sulfolane mol fraction; (●)T = 303.15 K, (○)T = 313.15 K, (▼)T = 323.15 K, (△)T = 333.15 K, (■)T = 343.15 K

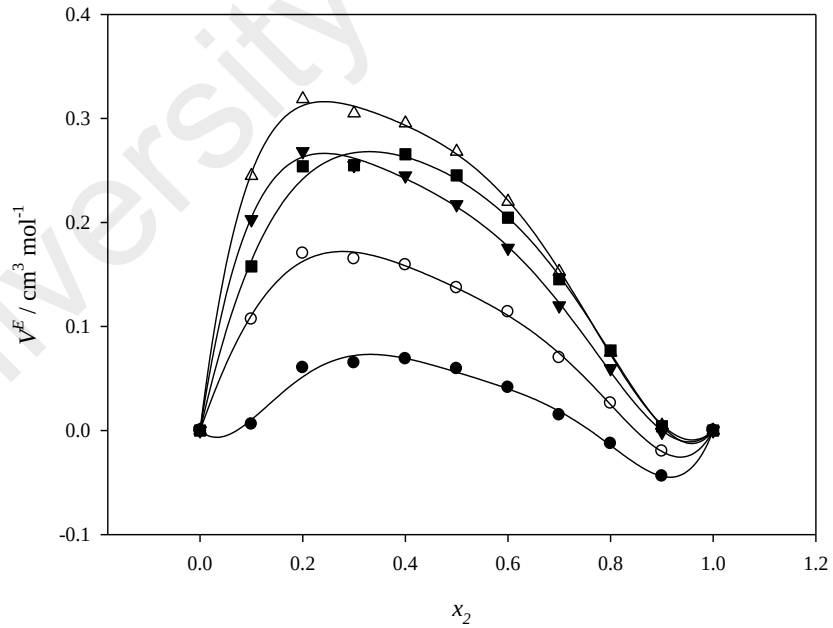

Figure 4.39: Excess molar volume of MEA (2) + sulfolane (3) binary mixtures against temperature as function of sulfolane mol fraction; (●)T = 303.15 K, (○)T = 313.15 K, (▼)T = 323.15 K, (△)T = 333.15 K, (■)T = 343.15 K

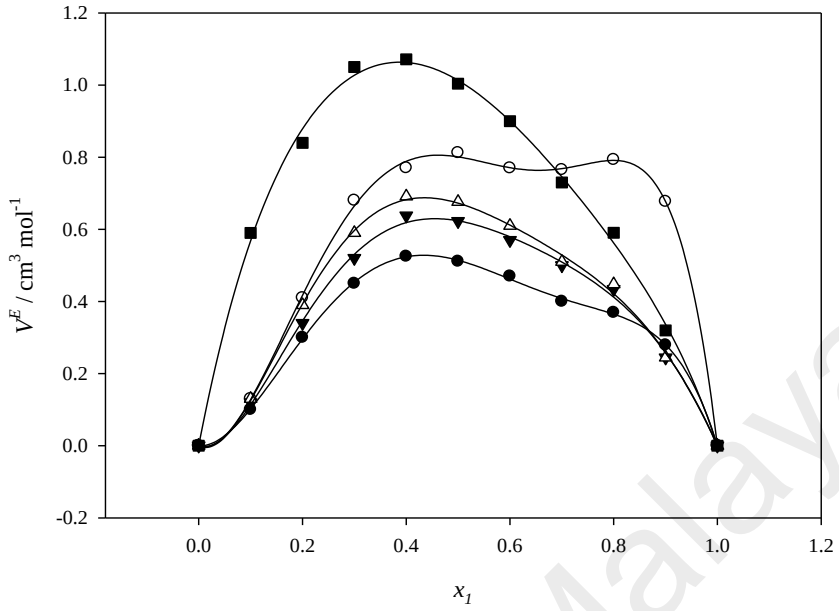

Figure 4.40: Excess molar volume of [BMIM][NTf_2] (1) + MEA (2) binary mixtures against temperature as function of [BMIM][NTf_2] mol fraction; (●)T = 303.15 K, (○)T = 313.15 K, (▼)T = 323.15 K, (△)T = 333.15 K, (■)T = 343.15 K

Excess molar volumes for [BMIM][NTf_2] (1) + sulfolane (3), MEA (2) + sulfolane (3) and [BMIM][NTf_2] (1) + MEA (2) binary were correlated using a Redlich-Kister equation as represented in Equation 4.11. The adjustable parameters, A*i*, are summarized in Table 4.10.

Table 4.10: Redlich-Kister fitting coefficients A_i of the V^E of [BMIM][NTf_2] (1), MEA (2) and sulfolane (3) binary mixtures as a function of various temperatures along with their fitting deviations, σ

T / K	A_0	A_1	A_2	A_3	A_4	R^2	σ[a]
[BMIM][NTf_2] (1) + sulfolane (3)							
303.15	-0.3369	0.2016	-0.2990	1.0392	-0.7887	0.9974	0.0227
313.15	-0.3784	0.2169	-0.3373	1.0091	-0.7096	0.9971	0.0079
323.15	-0.4188	0.2318	-0.3744	0.9798	-0.6326	0.9966	0.0128
333.15	-0.4581	0.2462	-0.4106	0.9512	-0.5577	0.9962	0.0287
343.15	-0.4773	0.2533	-0.4283	0.9372	-0.5210	0.9959	0.0421
MEA (2) + sulfolane (3)							
303.15	0.2244	-0.3000	0.1413	-0.1204	-1.224	0.9938	0.0054
313.15	0.5480	-0.4700	0.3303	-0.6856	-0.6250	0.9986	0.0050
323.15	0.8602	-0.6311	0.3123	-1.2358	0.1936	0.9990	0.0044
333.15	1.0628	-0.6893	0.2124	-1.5481	0.5051	0.9994	0.0043
343.15	0.9669	-0.5716	0.2080	-0.8300	-0.4100	0.9970	0.0077
[BMIM][NTf_2] (1) + MEA (2)							
303.15	2.0569	-0.7691	-0.0835	3.1342	0.2938	0.9995	0.0056
313.15	3.2035	-0.4493	1.0760	6.6596	1.4246	0.9993	0.0113
323.15	2.4946	-0.5052	0.0721	2.3582	-1.1761	0.9975	0.0153
333.15	2.6907	-0.8461	0.2010	2.7630	-1.6736	0.9979	0.0153
343.15	4.0521	-1.6991	0.8954	0.1423	0.9860	0.9974	0.0257

[a]σ = standard deviation, equation 4.9

(b) Ternary mixtures

Values of excess molar volume (V^E) were calculated from experimental density of the mixture using Equation 4.10 and were tabulated in Table 4.11. Figure 4.41 to Figure 4.45 represent the excess molar volume for ternary mixtures at constant temperature with temperatures range from 303.15 to 343.15 K, respectively. In general, both negative and positive values of excess molar volume are observed over the whole composition. At T=303.15 K, negative excess molar volume is observed in the ternary mixtures with low MEA composition, whereby strong interaction between [BMIM][NTf_2] and sulfolane is dominant. On the other hand, high positive excess molar volume was observed in ternary mixtures with low sulfolane composition, whereby the unfavorable packing between [BMIM][NTf_2] and MEA and lead to expansion in volume. At higher temperature, negative excess molar volume was observed predominantly in [BMIM][NTf_2]-rich composition with minimum peak at mol fraction ratio of 0.8 [BMIM][NTf_2]: 0.1 MEA: 0.1 sulfolane ternary mixture. On the contrary, positive excess molar volume are observed predominantly in MEA-rich composition with maximum peak at mol fraction ratio 0.1 [BMIM][NTf_2]: 0.8 MEA: 0.1 sulfolane ternary mixture. This due to the weak interaction between MEA and both [BMIM][NTf_2] and sulfolane that led to expansion of volume in the mixture.

Table 4.11: Excess molar volume (V^E) of [BMIM][NTf_2] (1) + MEA (2) + sulfolane (3) ternary mixtures at different temperatures and compositions

[BMIM][NTf_2] (1) + MEA (2) + sulfolane (3)							
x_1	x_2	x_3	V^E , cm^3 mol^{-1}				
			303.15 K	313.15 K	323.15 K	333.15 K	343.15 K
0.0999	0.1003	0.7998	-0.1580	-9.3002	11.1083	33.8832	38.1408
0.0998	0.2000	0.7002	-0.0634	-2.1426	12.4231	40.6026	44.8953
0.0997	0.3015	0.5988	0.0034	5.9004	13.1498	47.5634	51.9589
0.1000	0.4005	0.4995	0.0693	14.6361	13.3341	54.6812	59.1149
0.0999	0.5004	0.3997	0.1285	24.5248	13.0086	62.3099	66.7041
0.1000	0.5999	0.3001	0.1259	35.3048	11.8803	70.0764	74.4747
0.1000	0.7000	0.2000	0.1585	47.6241	10.2007	78.7002	83.0197
0.1000	0.8002	0.0999	0.1679	61.4587	7.6092	87.7513	92.0358
0.1995	0.1022	0.6982	-0.1350	-12.7307	-3.4330	19.0117	23.3121
0.1997	0.2011	0.5992	-0.0021	-6.8898	-2.7121	24.3052	28.6672
0.1997	0.3008	0.4995	0.0761	-0.4972	-2.4639	29.7214	34.1200
0.2000	0.4002	0.3998	0.1364	6.4596	-2.7585	35.1765	39.6512
0.1998	0.4996	0.3006	0.1873	14.1210	-3.4760	40.8827	45.3257
0.1996	0.6007	0.1997	0.2372	22.7215	-4.6577	47.0662	51.5133
0.1995	0.7003	0.1002	0.2522	31.9545	-6.4729	53.3409	57.7639
0.2993	0.1019	0.5988	-0.1541	-14.8469	-13.6901	7.6842	12.0159
0.2996	0.2007	0.4997	0.0406	-9.8191	-13.1440	12.3101	16.6895
0.2994	0.2998	0.4008	0.1043	-4.5072	-13.1897	16.6006	21.0592
0.2997	0.4005	0.2998	0.1900	1.4047	-13.6061	21.1245	25.5802
0.3000	0.5001	0.1999	0.2374	7.6704	-14.4902	25.6416	30.1173
0.2997	0.6003	0.1000	0.2782	14.5854	-15.6907	30.5168	34.9813
0.3989	0.1016	0.4995	-0.1224	-15.9126	-21.0081	-0.8420	3.5004
0.3990	0.2017	0.3993	0.0987	-11.4448	-20.5833	3.2261	7.6473
0.3988	0.3010	0.3002	0.2072	-6.7641	-20.6947	6.9922	11.4276
0.3995	0.4000	0.2005	0.2532	-1.8462	-21.2840	10.5252	14.9931
0.3996	0.5003	0.1001	0.2705	3.5107	-22.1694	14.2570	18.7517
0.4992	0.1012	0.3996	-0.0959	-16.3269	-26.4549	-7.6376	-3.2619
0.4993	0.2001	0.3006	0.0613	-12.4894	-26.3158	-4.4127	0.0057
0.4992	0.3008	0.1999	0.1416	-8.3436	-26.5166	-1.1917	3.2778
0.4980	0.3998	0.1021	0.2190	-3.9564	-26.9470	2.0942	6.5959
0.5978	0.1021	0.3001	-0.0850	-16.2613	-30.6051	-13.1841	-8.8133
0.5992	0.1999	0.2009	0.0718	-12.8264	-30.5454	-10.3642	-5.9609
0.5984	0.3009	0.1007	0.1829	-9.0610	-30.7215	-7.4495	-2.9837
0.6963	0.1033	0.2004	-0.0746	-15.8550	-33.7787	-17.7208	-13.3365
0.6964	0.2009	0.1027	0.0961	-12.7049	-33.7064	-15.1317	-10.7150
0.7965	0.1030	0.1005	-0.0670	-15.2243	-36.2713	-21.6584	-17.2748

[a] Standard uncertainty u are u(x) = 0.0005, u(T) = 0.05 K, and U(V^E) = 0.0001 cm^3 mol^{-1}. x_1, x_2 and x_3 is the mol fraction of [BMIM][NTf_2], MEA and sulfolane respectively.

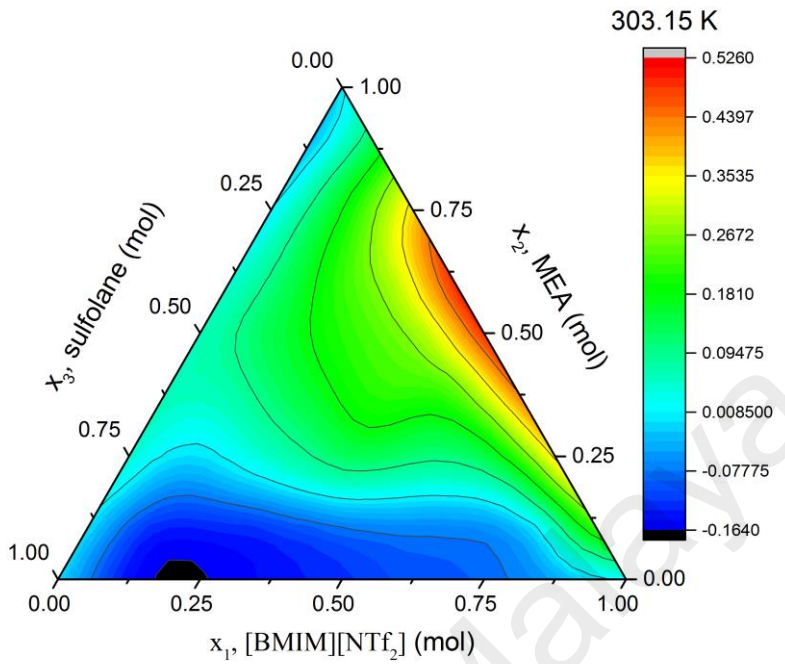

Figure 4.41: Excess molar volume of [BMIM][NTf_2] (1) + MEA (2) + sulfolane (3) ternary mixtures at T= 303.15 K

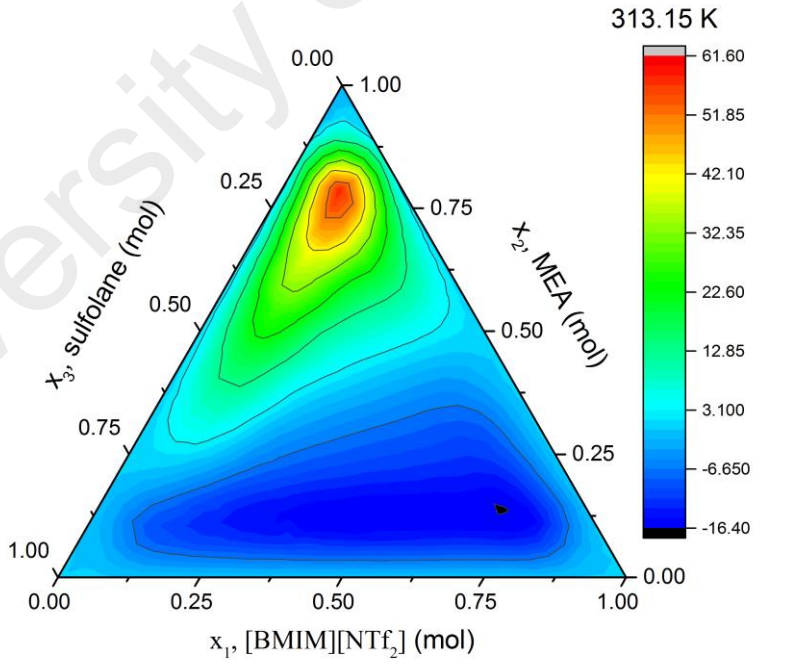

Figure 4.42: Excess molar volume of [BMIM][NTf_2] (1) + MEA (2) + sulfolane (3) ternary mixtures at T= 313.15 K

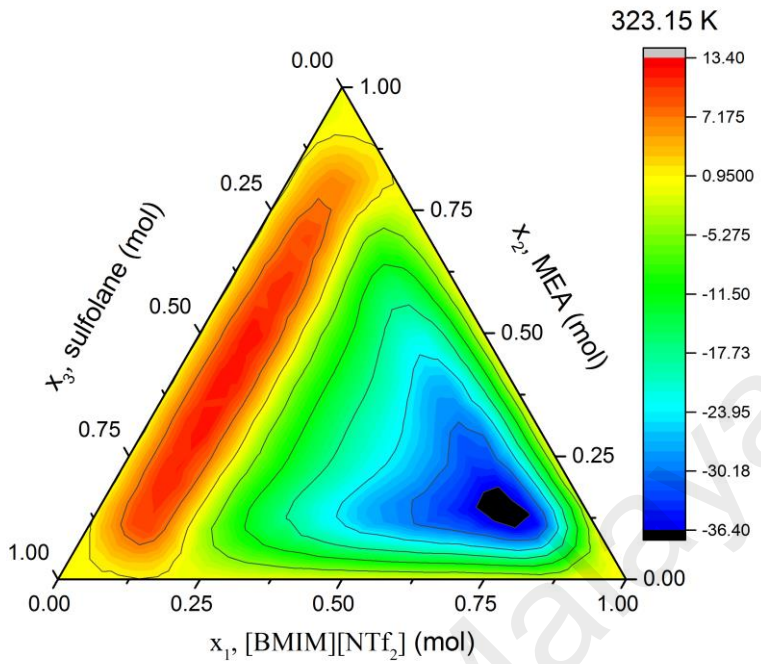

Figure 4.43: Excess molar volume of [BMIM][NTf_2] (1) + MEA (2) + sulfolane (3) ternary mixtures at T= 323.15 K

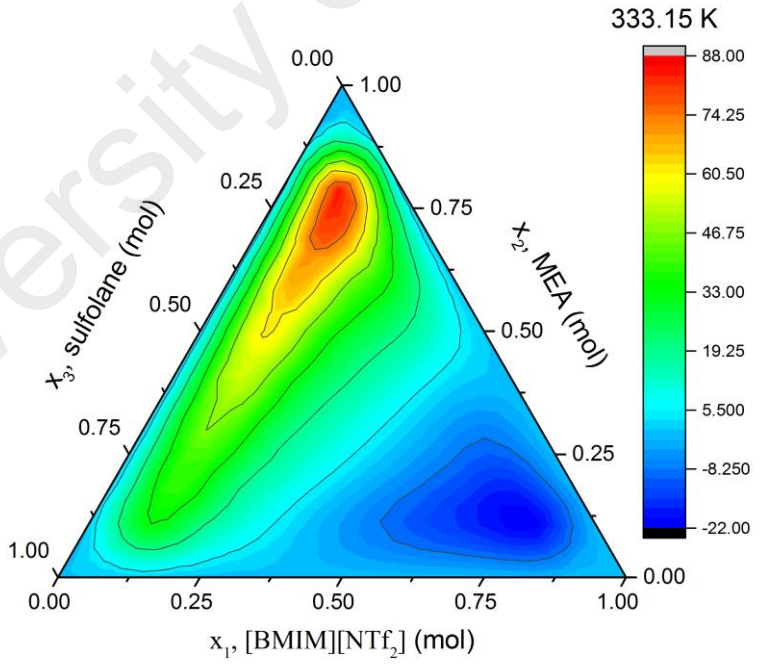

Figure 4.44: Excess molar volume of [BMIM][NTf_2] (1) + MEA (2) + sulfolane (3) ternary mixtures at T= 333.15 K

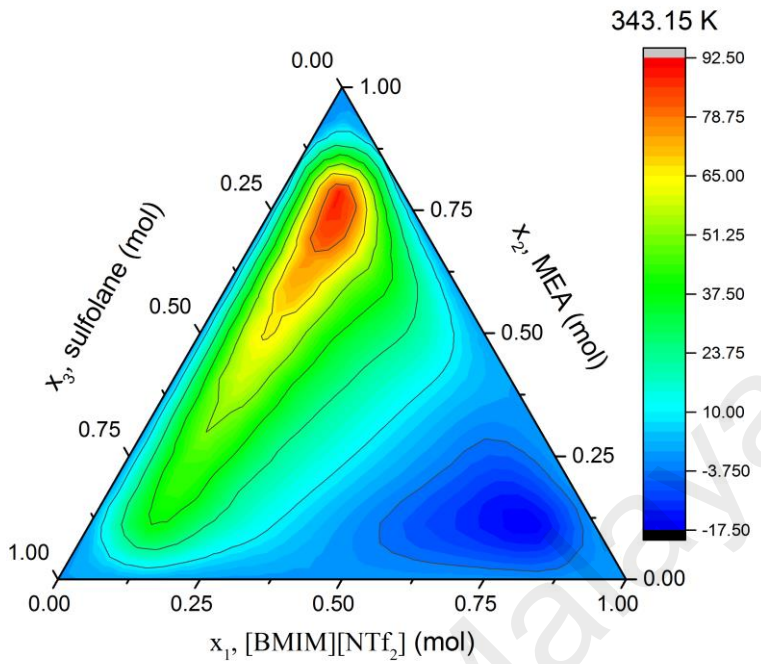

Figure 4.45: Excess molar volume of [BMIM][NTf_2] (1) + MEA (2) + sulfolane (3) ternary mixtures at T= 343.15 K

4.2.1.5 Thermal expansion

The coefficients of thermal expansion (α) for the systems studied in this work are calculated from the experimental density data using Equation 4.12 (Geppert-Rybczynska et al., 2014):

$$\alpha = -\frac{1}{\rho}\left(\frac{\partial \rho}{\partial T}\right) = -\left(\frac{\partial ln\rho}{\partial T}\right) \quad (4.12)$$

where ρ and T refer to density and temperature.

(a) Binary mixtures

The coefficients of thermal expansion (α) for 1 [BMIM][NTf_2] (1), MEA (2) and sulfolane (3) binary mixtures studied in this work were calculated from the experimental density data using Equation 4.12. It can be observed from Table 4.12 that the change in thermal expansion coefficient values is not significant and the variation of volume expansion of the systems studied in the present work could be considered as temperature dependent. Since the densities decrease linearly with temperature, it is obvious that α values are all positives but slightly increasing with temperature.

Table 4.12: Thermal expansion coefficients, α, of [BMIM][NTf_2] (1), MEA (2) and sulfolane (3) binary mixtures at different temperatures and compositions

			α ,10^4/K^{-1}				
x_1	x_2	x_3	303.15 K	313.15 K	323.15 K	333.15 K	343.15 K
[BMIM][NTf_2] (1) + sulfolane (3)							
0.0000	-	1.0000	0.6977	0.7020	0.7064	0.7113	0.7173
0.1000	-	0.9000	0.6920	0.6968	0.7017	0.7066	0.7117
0.1999	-	0.8001	0.6899	0.6947	0.6995	0.7045	0.7095
0.3001	-	0.6999	0.6945	0.6995	0.7043	0.7092	0.7141
0.4000	-	0.6000	0.6826	0.6873	0.6921	0.6969	0.7017
0.5001	-	0.4999	0.6800	0.6846	0.6893	0.6941	0.6989
0.5999	-	0.4001	0.6760	0.6806	0.6853	0.6900	0.6948
0.7000	-	0.3000	0.6747	0.6792	0.6839	0.6886	0.6933
0.7995	-	0.2005	0.6713	0.6759	0.6805	0.6851	0.6898
0.8985	-	0.1015	0.6691	0.6736	0.6782	0.6828	0.6875
1.0000	-	0.0000	0.6668	0.6713	0.6758	0.6804	0.6849
MEA (2) + sulfolane (3)							
-	0.0000	1.0000	8.1011	8.1667	8.2334	8.3020	8.3726
-	0.0999	0.9001	8.0833	8.1495	8.2160	8.2836	8.3539
-	0.2001	0.7999	8.0400	8.1053	8.1709	8.2376	8.3078
-	0.3001	0.6999	8.0133	8.0781	8.1433	8.2102	8.2790
-	0.3999	0.6001	7.9549	8.0192	8.0830	8.1493	8.2167
-	0.4999	0.5001	7.8805	7.9427	8.0059	8.0709	8.1369
-	0.5999	0.4001	7.7631	7.8239	7.8850	7.9478	8.0122
-	0.6999	0.3001	7.6160	7.6749	7.7336	7.7941	7.8555

Table 4.12, continued

x_1	x_2	x_3	α ,$10^4/K^{-1}$ 303.15 K	313.15 K	323.15 K	333.15 K	343.15 K
-	0.8000	0.2000	7.5069	7.5644	7.6215	7.6801	7.7396
-	0.8999	0.1001	7.2980	7.3519	7.4059	7.4613	7.5176
-	1.0000	0.0000	6.7572	6.7988	6.8408	6.8885	6.9469
[BMIM][NTf$_2$] (1) + MEA (2)							
0.0000	1.0000	-	6.8926	6.9488	7.0638	7.0638	7.0638
0.1001	0.8999	-	7.6769	7.7343	7.7972	7.8590	7.9204
0.2000	0.8000	-	7.5834	7.6407	7.6992	7.7605	7.8214
0.3000	0.7000	-	7.5265	7.5861	7.6401	7.7000	7.7619
0.4000	0.6000	-	7.3734	7.4286	7.4844	7.5407	7.5981
0.4999	0.5001	-	7.2568	7.3105	7.3641	7.4185	7.4737
0.6000	0.4000	-	7.1445	7.1949	7.2483	7.3007	7.3547
0.6999	0.3001	-	7.0209	7.0706	7.1219	7.1718	7.2236
0.8000	0.2000	-	6.9209	6.9699	7.0186	7.0676	7.1175
0.8998	0.1002	-	6.7973	6.8432	6.8902	6.9376	6.9858
1.0000	0.0000	-	6.8002	6.8356	6.8937	6.9410	6.9884

[a]Standard uncertainty *u* are u(x) = 0.0005, u(T) = 0.05 K, . x_1, x_2 and x_3 is the mol fraction of [BMIM][NTf$_2$], MEA and sulfolane respectively.

(b) Ternary mixtures

The coefficients of thermal expansion (α) for [BMIM][NTf$_2$] (1) + MEA (2) + sulfolane (3) ternary mixtures studied in this work are calculated from the experimental density data using Equation 4.12. It can be observed from Table 4.13 that the change in thermal expansion coefficient values is not significant and the variation of volume expansion of the systems studied in the present work could be considered as temperature dependent.

Table 4.13: Thermal expansion coefficients, α, of [BMIM][NTf_2] (1) + MEA (2) + sulfolane (3) ternary mixtures over whole range of composition for temperatures range from 303.15 to 343.15 K

[BMIM][NTf_2] (1) + MEA (2) + sulfolane (3)							
x_1	x_2	x_3	α ,10^4/K^{-1}				
			303.15 K	**313.15 K**	**323.15 K**	**333.15 K**	**343.15 K**
0.0999	0.1003	0.7998	7.1788	7.2312	7.2840	7.3371	7.3911
0.0998	0.2000	0.7002	7.3520	7.4070	7.4627	7.5184	7.5747
0.0997	0.3015	0.5988	7.4971	7.5537	7.6115	7.6695	7.7289
0.1000	0.4005	0.4995	7.6054	7.6637	7.7232	7.7827	7.8442
0.0999	0.5004	0.3997	7.6438	7.7032	7.7625	7.8231	7.8852
0.1000	0.5999	0.3001	7.7229	7.7834	7.8441	7.9058	7.9694
0.1000	0.7000	0.2000	7.7725	7.8332	7.8956	7.9580	8.0219
0.1000	0.8002	0.0999	7.7806	7.8416	7.9037	7.9663	8.0307
0.1995	0.1022	0.6982	7.1290	7.1809	7.2331	7.2855	7.3383
0.1997	0.2011	0.5992	7.2436	7.2971	7.3508	7.4049	7.4598
0.1997	0.3008	0.4995	7.3764	7.4316	7.4879	7.5438	7.6006
0.2000	0.4002	0.3998	7.4772	7.5338	7.5913	7.6488	7.7079
0.1998	0.4996	0.3006	7.5010	7.5583	7.6155	7.6738	7.7332
0.1996	0.6007	0.1997	7.5522	7.6104	7.6686	7.7274	7.7878
0.1995	0.7003	0.1002	7.6030	7.6620	7.7208	7.7806	7.8417
0.2993	0.1019	0.5988	7.0667	7.1176	7.1691	7.2205	7.2722
0.2996	0.2007	0.4997	7.1878	7.2404	7.2933	7.3469	7.4005
0.2994	0.2998	0.4008	7.2972	7.3511	7.4060	7.4608	7.5166
0.2997	0.4005	0.2998	7.3462	7.4013	7.4568	7.5122	7.5688
0.3000	0.5001	0.1999	7.4113	7.4669	7.5231	7.5800	7.6377
0.2997	0.6003	0.1000	7.4787	7.5355	7.5931	7.6508	7.7094
0.3989	0.1016	0.4995	7.0067	7.0569	7.1072	7.1580	7.2087
0.3990	0.2017	0.3993	7.1245	7.1760	7.2284	7.2806	7.3334
0.3988	0.3010	0.3002	7.2036	7.2563	7.3099	7.3633	7.4173
0.3995	0.4000	0.2005	7.2691	7.3226	7.3771	7.4315	7.4867
0.3996	0.5003	0.1001	7.3511	7.4059	7.4618	7.5173	7.5738
0.4992	0.1012	0.3996	6.9767	7.0266	7.0769	7.1267	7.1770
0.4993	0.2001	0.3006	7.0550	7.1058	7.1572	7.2082	7.2599
0.4992	0.3008	0.1999	7.1625	7.2148	7.2678	7.3204	7.3737
0.4980	0.3998	0.1021	7.2359	7.2892	7.3433	7.3970	7.4516
0.5978	0.1021	0.3001	6.9048	6.9536	7.0028	7.0516	7.1009
0.5992	0.1999	0.2009	7.0033	7.0533	7.1041	7.1544	7.2051
0.5984	0.3009	0.1007	7.0897	7.1411	7.1929	7.2445	7.2967
0.6963	0.1033	0.2004	6.8773	6.9254	6.9742	7.0229	7.0718
0.6964	0.2009	0.1027	6.9562	7.0056	7.0554	7.1052	7.1553
0.7965	0.1030	0.1005	6.8426	6.8902	6.9386	6.9866	7.0351

[a]Standard uncertainty *u* are u(x) = 0.0005, u(T) = 0.05 K, x_1 , x_2 and x_3 is the mol fraction of [BMIM][NTf_2], MEA and sulfolane respectively.

4.2.2 Viscosity

4.2.2.1 Introduction

This chapter explores the viscosity of 3 binary mixtures of [BMIM][NTf_2] (1) + sulfolane (3), MEA (2) + sulfolane (3) and [BMIM][NTf_2] (1) + MEA (2) together with ternary mixtures of [BMIM][NTf_2] (1) + MEA (2) + sulfolane (3) over the whole range of composition. The atmospheric viscosities were measured at various temperatures ranging from 303.15 to 343 K with increment of 10 K. The measurement was conducted to evaluate the changing of viscosity value of binary and ternary mixtures of [BMIM][NTf_2] (1), MEA (2) and sulfolane (3) at different temperatures and compositions.

4.2.2.2 Validation of the viscosity measurement

To verify reliability of the equipment, the viscosity of pure [BMIM][NTf_2], MEA and sulfolane were measured at different temperatures and compared with experimental values given by other authors in literature as shown in Table 4.14. Figure 4.46 show the measurement of viscosity obtained in this study was in good agreement with the literature data at all temperatures.

Table 4.14: Comparison of measured viscosity (η) with literature values for pure [BMIM][NTf_2], MEA and sulfolane at different temperatures

T/K	[BMIM][NTf_2]		MEA		sulfolane	
	Exp.	Lit.[1]	Exp.	Lit.[2]	Exp.	Lit.[3]
303.15	0.0390	0.0414	0.0157	0.0141	0.0105	0.0104
313.15	0.0267	0.0285	0.0107	0.0100	0.0081	0.0080
323.15	0.0201	0.0206	0.0073	-	0.0064	0.0064
333.15	0.0155	0.0155	0.0053	0.0050	0.0046	0.0052
343.15	0.0124	0.0120	0.0040	-	0.0038	0.0043

1 = data from (Atilhan et al., 2013)
2 = data from (Maham et al., 2002)
3 = data from (Mesquita et al., 2014)

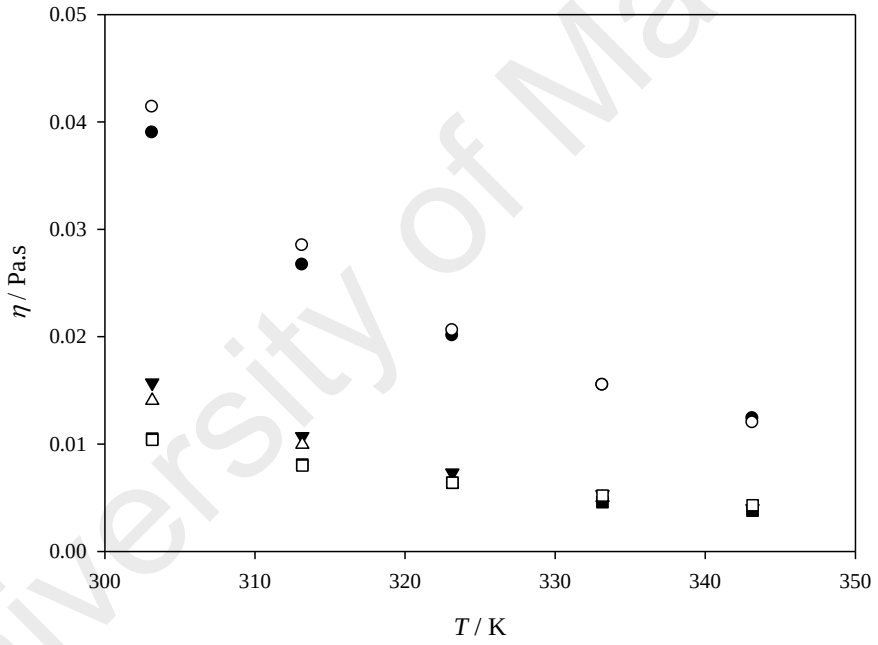

Figure 4.46: Comparison of viscosity for pure [BMIM][NTf_2], MEA and sulfolane with literatures; (●) $[BMIM][NTf_2]_{Exp.;}$ (○) $[BMIM][NTf_2]_{Lit}$ (Atilhan et al., 2013); (▼) $MEA_{Exp.;}$ (△) MEA_{Lit} (Maham et al., 2002).; (■) $sulfolane_{Exp.;}$ (□) $sulfolane_{Lit}$ (Mesquita et al., 2014)

4.2.2.3 Effect of temperature and composition

(a) Binary mixtures

All measured experimental viscosity values of [BMIM][NTf_2] (1), MEA (2) and sulfolane (3) binary mixtures throughout the entire mol fraction composition with the temperatures ranging from 303.15 to 343.15 K are tabulated in Table 4.5 and represented in Figure 4.47 to Figure 4.52. Figure 4.47 to Figure 4.49 show the measured viscosity of [BMIM][NTf_2] (1) + sulfolane (3), MEA (2) + sulfolane (3) and [BMIM][NTf_2] (1) + MEA (2) binary mixtures, respectively, throughout the entire temperatures ranging from 303.15 to 343.15 K at constant composition. Results show that the viscosity of all binary mixtures decreased exponentially with the increase of temperature. All the viscosity values for [BMIM][NTf_2] (1) + sulfolane (3), MEA (2) + sulfolane (3) and [BMIM][NTf_2] (1) + MEA (2) binary mixtures, respectively, were fitted using Vogel-Fulcher-Tammann (VFT) equation (4.13) (Huang et al., 2014):

$$\eta = A \exp\left(\frac{B}{T - T_0}\right) \tag{4.13}$$

where A, B and T_0 are adjustable parameter. Table 4.16 summarizes the fitting parameters of VFT equation of pure components and [BMIM][NTf_2] (1) + sulfolane (3), MEA (2) + sulfolane (3) and [BMIM][NTf_2] (1) + MEA (2) binary mixtures.

Table 4.15: Viscosity (η) of [BMIM][NTf_2] (1), MEA (2) and sulfolane (3) binary mixtures at different temperatures and compositions

x_1	x_2	x_3	η, Pa.s				
			303.15 K	313.15 K	323.15 K	333.15 K	343.15 K
[BMIM][NTf_2] (1) + sulfolane (3)							
0.0000	-	1.0000	0.0105	0.0081	0.0064	0.0046	0.0038
0.1000	-	0.9000	0.0128	0.0097	0.0077	0.0057	0.0046
0.1999	-	0.8001	0.0143	0.0107	0.0084	0.0063	0.0051
0.3001	-	0.6999	0.0165	0.0123	0.0097	0.0073	0.0059
0.4000	-	0.6000	0.0188	0.0134	0.0102	0.0075	0.0062
0.5001	-	0.4999	0.0215	0.0154	0.0119	0.0092	0.0073
0.5999	-	0.4001	0.0247	0.0176	0.0136	0.0105	0.0082
0.7000	-	0.3000	0.0273	0.0187	0.0141	0.0108	0.0086
0.7995	-	0.2005	0.0311	0.0212	0.0160	0.0122	0.0095
0.8985	-	0.1015	0.0351	0.0244	0.0184	0.0141	0.0107
1.0000	-	0.0000	0.0390	0.0267	0.0201	0.0155	0.0124
MEA (2) + sulfolane (3)							
-	0.0000	1.0000	0.0105	0.0081	0.0064	0.0046	0.0038
-	0.0999	0.9001	0.0109	0.0083	0.0064	0.0046	0.0037
-	0.2001	0.7999	0.0110	0.0082	0.0063	0.0045	0.0036
-	0.3001	0.6999	0.0112	0.0082	0.0063	0.0045	0.0036
-	0.3999	0.6001	0.0108	0.0078	0.0059	0.0042	0.0033
-	0.4999	0.5001	0.0110	0.0079	0.0058	0.0042	0.0033
-	0.5999	0.4001	0.0108	0.0077	0.0056	0.0040	0.0031
-	0.6999	0.3001	0.0115	0.0081	0.0058	0.0042	0.0033
-	0.8000	0.2000	0.0125	0.0087	0.0061	0.0044	0.0034
-	0.8999	0.1001	0.0134	0.0092	0.0064	0.0047	0.0036
-	1.0000	0.0000	0.0157	0.0107	0.0073	0.0053	0.0040
[BMIM][NTf_2] (1) + MEA (2)							
0.0000	1.0000	-	0.0105	0.0081	0.0064	0.0046	0.0038
0.1001	0.8999	-	0.0128	0.0097	0.0077	0.0057	0.0046
0.2000	0.8000	-	0.0143	0.0107	0.0084	0.0063	0.0051
0.3000	0.7000	-	0.0165	0.0123	0.0097	0.0073	0.0059
0.4000	0.6000	-	0.0188	0.0134	0.0102	0.0075	0.0062
0.4999	0.5001	-	0.0215	0.0154	0.0119	0.0092	0.0073
0.6000	0.4000	-	0.0247	0.0176	0.0136	0.0105	0.0082
0.6999	0.3001	-	0.0273	0.0187	0.0141	0.0108	0.0086
0.8000	0.2000	-	0.0311	0.0212	0.0160	0.0122	0.0095
0.8998	0.1002	-	0.0351	0.0244	0.0184	0.0141	0.0107
1.0000	0.0000	-	0.0390	0.0267	0.0201	0.0155	0.0124

[a] Standard uncertainty u are u(x) = 0.0005, u(T) = 0.05 K, u(η) = 5%, x_1 and x_3 is the mol fraction of [BMIM][NTf_2] and sulfolane, respectively.

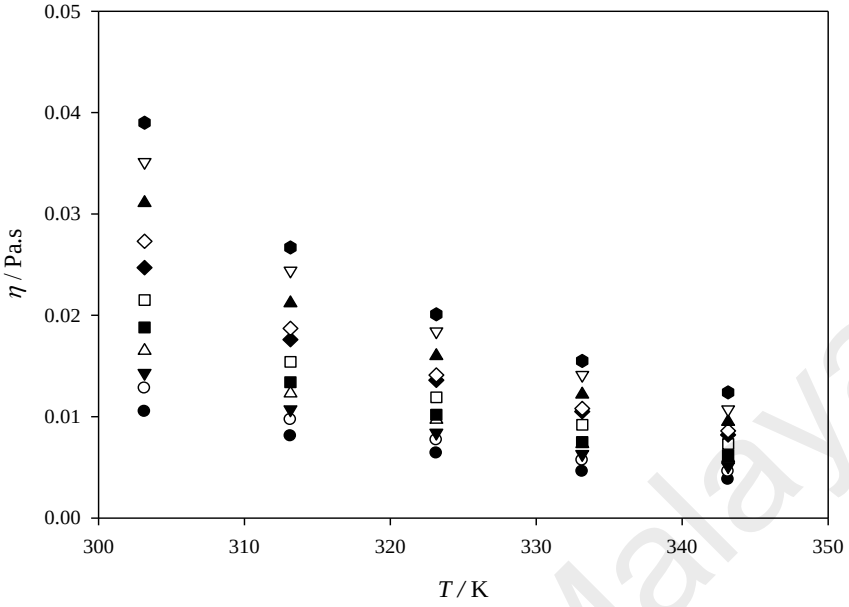

Figure 4.47: Viscosity of [BMIM][NTf_2] (1) + sulfolane (2) binary mixtures against temperature at various concentrations; (●) x_1= 0, (○) x_1= 0.1, (▼) x_1= 0.2, (△) x_1= 0.3, (■) x_1= 0.4, (□) x_1= 0.5, (◆) x_1= 0.6, (◇) x_1= 0.7, (▲) x_1= 0.8, (▽) x_1= 0.9, (⬢) x_1= 1.0

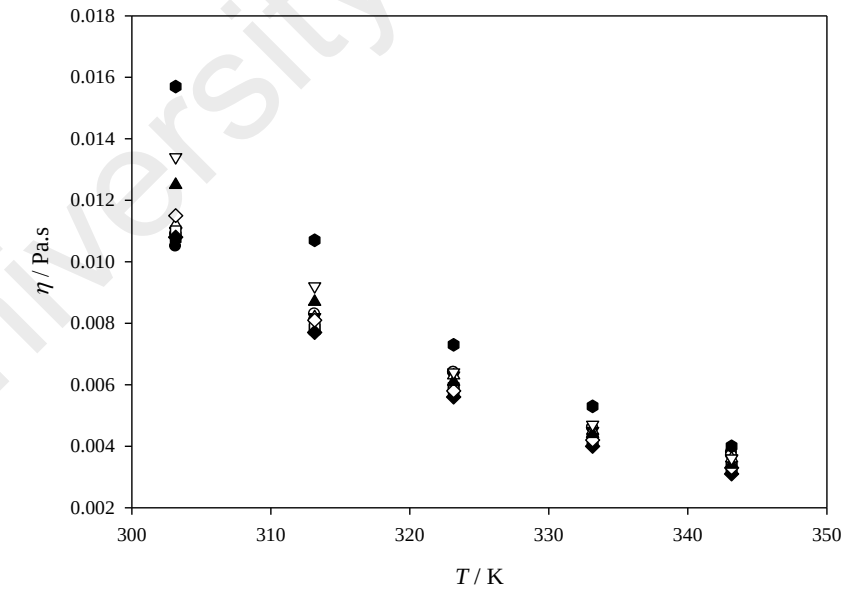

Figure 4.48: Viscosity of MEA (2) + sulfolane (3) binary mixtures against temperature at various compositions; (●) x_2= 0, (○) x_2= 0.1, (▼) x_2= 0.2, (△) x_2= 0.3, (■) x_2= 0.4, (□) x_2= 0.5, (◆) x_2= 0.6, (◇) x_2= 0.7, (▲) x_2= 0.8, (▽) x_2= 0.9, (⬢) x_2= 1.0

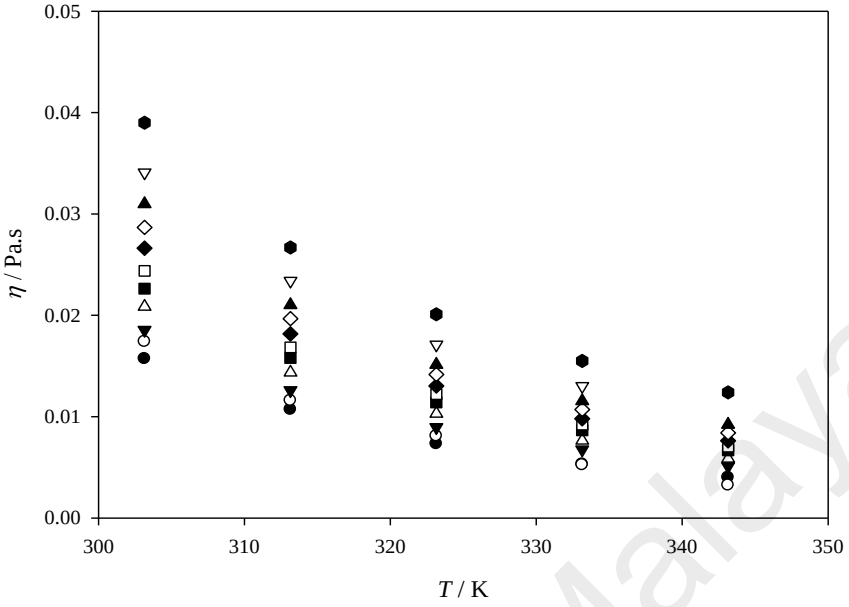

Figure 4.49: Viscosity of [BMIM][NTf_2] (1) + MEA (2) binary mixtures against temperature at various compositions; (●) x_1= 0, (○) x_1= 0.1, (▼) x_1= 0.2, (△) x_1= 0.3, (■) x_1= 0.4, (□) x_1= 0.5, (◆) x_1= 0.6, (◇) x_1= 0.7, (▲) x_1= 0.8, (▽) x_1= 0.9, (⬢) x_1= 1.0

Table 4.16: Fitting parameters of VFT equation, correlation coefficient, R^2, and standard relative deviations, σ, for the viscosity of [BMIM][NTf_2] (1) + sulfolane (3) binary mixtures

x_1	x_2	x_3	A	B	C	R^2	σ^a
[BMIM][NTf_2] (1) + sulfolane (3)							
0.0000	-	1.0000	6.292 x10^{-6}	2.273 x10^3	-4.22	0.9941	0.0002
0.1000	-	0.9000	7.069 x10^{-6}	2.188 x10^3	12.69	0.9952	0.0003
0.1999	-	0.8001	7.018 x10^{-6}	2.152 x10^3	23.63	0.9950	0.0004
0.3001	-	0.6999	7.225 x10^{-6}	2.151 x10^3	28.96	0.9955	0.0004
0.4000	-	0.6000	3.570 x10^{-6}	2.355 x10^3	32.08	0.9943	0.0006
0.5001	-	0.4999	7.200 x10^{-6}	2.113 x10^3	43.75	0.9957	0.0006
0.5999	-	0.4001	6.713 x10^{-6}	2.198 x10^3	40.19	0.9950	0.0007
0.7000	-	0.3000	5.612 x10^{-6}	2.194 x10^3	49.35	0.9942	0.0009
0.7995	-	0.2005	5.522 x10^{-6}	2.225 x10^3	50.12	0.9944	0.0010
0.8985	-	0.1015	5.576 x10^{-6}	2.342 x10^3	40.04	0.9940	0.0012
1.0000	-	0.0000	6.303 x10^{-6}	2.288 x10^3	45.53	0.9945	0.0013

Table 4.16, continued

x_1	x_2	x_3	A	B	C	R^2	σ^a
MEA (2) + sulfolane (3)							
-	0.0000	1.0000	4.9070×10^{-59}	6.4220×10^{5}	-4.6480×10^{3}	0.9973	0.0013
-	0.0999	0.9001	1.1410×10^{-30}	1.4770×10^{5}	-1.9890×10^{3}	0.9935	0.0012
-	0.2001	0.7999	7.0380×10^{-16}	3.1230×10^{4}	-7.2470×10^{2}	0.9988	0.0010
-	0.3001	0.6999	8.8570×10^{-12}	1.4290×10^{4}	-3.7860×10^{2}	0.9988	0.0009
-	0.3999	0.6001	4.2940×10^{-10}	8.9780×10^{3}	-2.2370×10^{2}	0.9992	0.0007
-	0.4999	0.5001	1.3210×10^{-8}	5.5080×10^{3}	-1.0100×10^{2}	0.9995	0.0006
-	0.5999	0.4001	1.1630×10^{-7}	3.7280×10^{3}	-2.2820×10^{1}	0.9996	0.0006
-	0.6999	0.3001	5.9730×10^{-7}	2.6780×10^{3}	3.1680×10^{1}	0.9997	0.0004
-	0.8000	0.2000	1.2630×10^{-6}	2.2060×10^{3}	6.3440×10^{1}	0.9998	0.0004
-	0.8999	0.1001	1.4690×10^{6}	1.0140×10^{4}	8.6500×10^{2}	0.9956	0.0003
-	1.0000	0.0000	1.4010×10^{6}	9.8770×10^{3}	8.4230×10^{2}	0.9930	0.0002
[BMIM][NTf$_2$] (1) + MEA (2)							
0.0000	1.0000	-	3.0690×10^{6}	1.0700×10^{4}	8.632×10^{2}	0.9953	0.0002
0.1001	0.8999	-	1.6220×10^{-134}	2.2930×10^{6}	-7.2390×10^{3}	0.9987	0.0001
0.2000	0.8000	-	3.2980×10^{6}	1.1250×10^{4}	8.9500×10^{2}	0.9999	0.0001
0.3000	0.7000	-	3.6360×10^{5}	1.0170×10^{3}	1.4310×10^{2}	0.9999	0.0002
0.4000	0.6000	-	6.3640×10^{5}	8.9620×10^{2}	1.5060×10^{2}	0.9999	0.0002
0.4999	0.5001	-	7.4910×10^{5}	8.5140×10^{2}	1.7950×10^{2}	0.9999	0.0001
0.6000	0.4000	-	1.5920×10^{4}	6.3300×10^{2}	1.8430×10^{2}	0.9999	0.0002
0.6999	0.3001	-	2.1680×10^{4}	5.8070×10^{2}	9.2700×10^{2}	0.9999	0.0003
0.8000	0.2000	-	7.5180×10^{6}	1.2060×10^{4}	9.2700×10^{2}	0.9876	0.0001
0.8998	0.1002	-	4.8410×10^{6}	1.1050×10^{4}	8.9140×10^{2}	0.9934	0.0002
1.0000	0.0000	-	1.0150×10^{-3}	3.2250×10^{2}	2.1470×10^{2}	0.9997	0.0002

[a]σ = standard deviation, equation 4.9

Figure 4.50 to Figure 4.52 show the effect of composition at constant temperature on the viscosity of [BMIM][NTf$_2$] (1) + sulfolane (3), MEA (2) + sulfolane (3) and [BMIM][NTf$_2$] (1) + MEA (2) binary mixtures. As shown in Figure 4.50, the viscosity of [BMIM][NTf$_2$] (1) + sulfolane (3) binary mixtures increased exponentially as the mol fraction of [BMIM][NTf$_2$] increases. Moreover, the viscosity of pure [BMIM][NTf$_2$] is higher than pure sulfolane. Therefore, the viscosity of binary mixtures was enhanced as the concentration of sulfolane in the mixture increased.

Figure 4.51 illustrates the viscosity of MEA (2) + sulfolane (3) binary mixtures over whole composition at constant temperature. The result shows that viscosity increases as mol fraction of MEA increased at constant temperature. It was observed that at higher temperature, the viscosity of pure MEA is almost comparable to the viscosity of pure sulfolane. Therefore, less significant change in viscosity was observed at high temperature with the increase of MEA composition. On the other hand, Figure 4.52 shows that viscosity of [BMIM][NTf_2] (1) + MEA (2) binary mixtures increases as mol fraction of [BMIM][NTf_2] increased at constant temperature. In the pure state, the viscosity of [BMIM][NTf_2] (1), MEA (2) and sulfolane (3) had been found to be in the order of;

[BMIM][NTf_2] > MEA > sulfolane

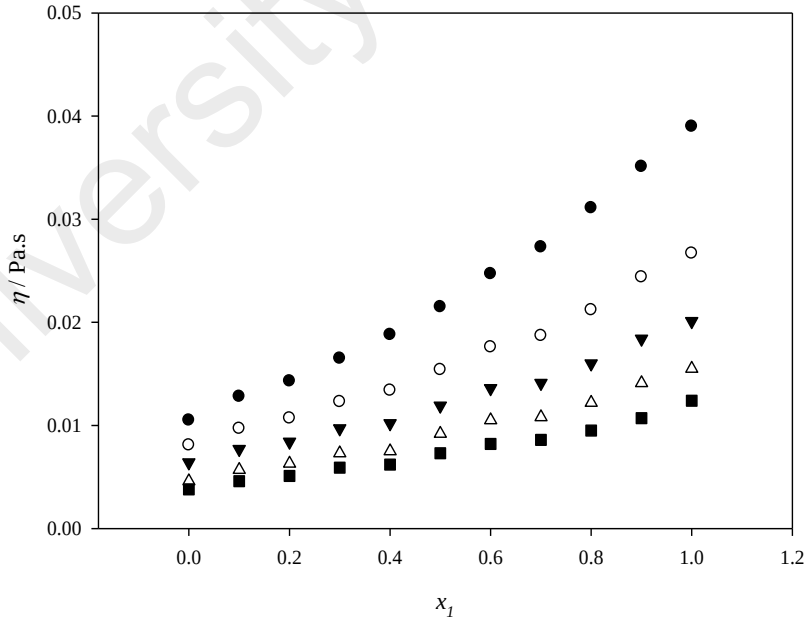

Figure 4.50: Viscosity of [BMIM][NTf_2] (1) + sulfolane (3) binary mixtures against composition at various temperatures; (●) 303.15 K; (○) 313.15 K; (▼) 323.15 K; (△) 333.15 K; (■) 343.15 K

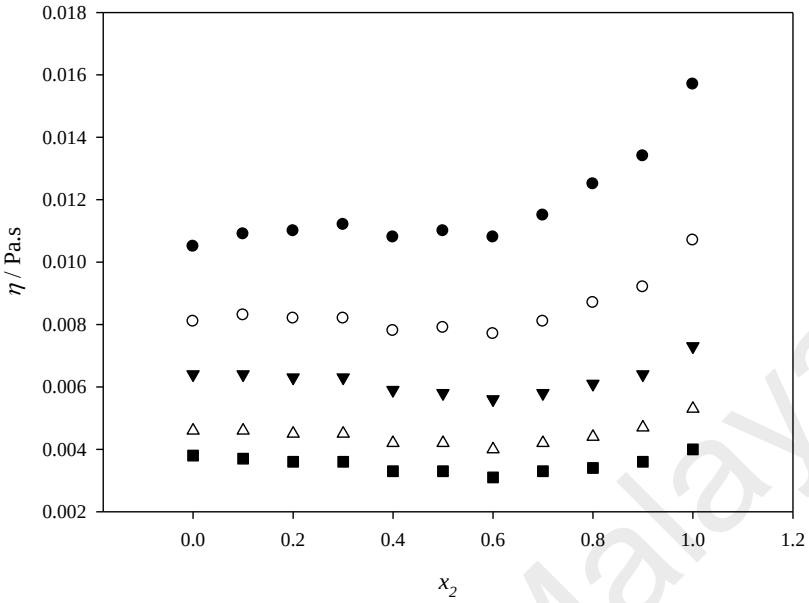

Figure 4.51: Viscosity of MEA (2) + sulfolane (3) binary mixtures against composition at various temperatures; (●) 303.15 K; (○) 313.15 K; (▼) 323.15 K; (△) 333.15 K; (■) 343.15 K

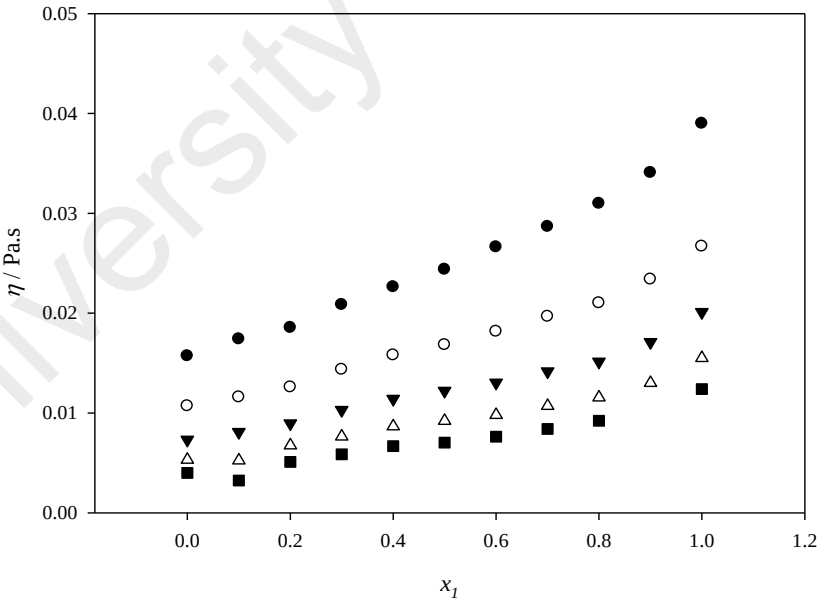

Figure 4.52: Viscosity of [BMIM][NTf_2] (1) + MEA (2) binary mixtures against composition at various temperatures; (●) 303.15 K; (○) 313.15 K; (▼) 323.15 K; (△) 333.15 K; (■) 343.15 K

The influence of composition on the viscosity of pure and [BMIM][NTf_2] (1) + sulfolane (3), MEA (2) + sulfolane (3) and [BMIM] [NTf_2] (1) + MEA (2) binary mixtures were correlated using a cubic polynomial function as a function of composition, Equation 4.8 and the fitting parameters were summarized in Table 4.17.

Table 4.17: Fitting parameters of equation 4.8 together with correlation coefficient squared, R^2, and standard relative deviations, σ, for influence of composition on viscosity of [BMIM][NTf_2] (1) + sulfolane (3) binary mixtures

***T*/K**	A_0	A_1	A_2	A_3	R^2	σ[a]
[BMIM][NTf_2] (1) + sulfolane (3)						
303.15	0.0107	0.0170	0.0074	0.0040	0.9996	0.0002
313.15	0.0082	0.0130	-0.0007	0.0064	0.9977	0.0003
323.15	0.0065	0.0105	-0.0027	0.0060	0.9955	0.0004
333.15	0.0047	0.0087	-0.0025	0.0047	0.9933	0.0004
343.15	0.0038	0.0083	-0.0065	0.0067	0.9955	0.0002
MEA (2) + sulfolane (3)						
303.15	0.0105	0.0063	-0.0207	0.0196	0.9908	0.0002
313.15	0.0081	0.0026	-0.0128	0.0127	0.9838	0.0001
323.15	0.0064	0.0013	-0.0096	0.0091	0.9733	0.0004
333.15	0.0046	0.0006	-0.0062	0.0063	0.9933	0.0004
343.15	0.0038	0.0003	-0.0035	0.0040	0.9955	0.0001
[BMIM][NTf_2] (1) + MEA (2)						
303.15	0.0155	0.0205	-0.0148	0.0173	0.9977	0.0004
313.15	0.0104	0.0158	-0.0132	0.0134	0.9961	0.0004
323.15	0.0070	0.0150	-0.0182	0.0160	0.9942	0.0004
333.15	0.0048	0.0128	-0.0154	0.0130	0.9878	0.0004
343.15	0.0034	0.0095	-0.0093	0.0086	0.9792	0.0005

[a]σ = standard deviation, equation 4.9

(b) Ternary mixtures

All the measured experimental viscosity values of [BMIM][NTf_2] + MEA + sulfolane ternary mixtures throughout the entire mol fraction composition with the temperatures ranging from 303.15 to 343.15 K are tabulated in Table 4.18. Figure 4.53 to Figure 4.57 represent the viscosity for the ternary mixtures at constant temperature with temperatures range from 303.15 to 343.15 K, respectively. Overall, it can be observed that the composition of [BMIM][NTf_2] highly influenced the viscosity of the ternary mixtures in comparison with MEA and sulfolane. At constant [BMIM][NTf_2] mol fraction, the viscosity of the ternary mixtures is affected significantly by the MEA composition due to MEA higher viscosity than sulfolane with viscosity on the ternary mixtures increases as the MEA composition increased. The density data show a decrease in values with the increment of temperature throughout the whole composition.

Table 4.18: Viscosity (η) of [BMIM][NTf_2] (1) + MEA (2) + sulfolane (3) ternary mixtures at different temperatures and compositions

[BMIM][NTf_2] (1) + MEA (2) + sulfolane (3)							
x_1	x_2	x_3	**η, Pa.s**				
			303.15 K	**313.15 K**	**323.15 K**	**333.15 K**	**343.15 K**
0.0999	0.1003	0.7998	0.0104	0.0081	0.0062	0.0052	0.0043
0.0998	0.2000	0.7002	0.0100	0.0076	0.0059	0.0048	0.0039
0.0997	0.3015	0.5988	0.0102	0.0077	0.0058	0.0047	0.0038
0.1000	0.4005	0.4995	0.0106	0.0079	0.0059	0.0047	0.0038
0.0999	0.5004	0.3997	0.0112	0.0082	0.0060	0.0047	0.0038
0.1000	0.5999	0.3001	0.0120	0.0086	0.0062	0.0049	0.0038
0.1000	0.7000	0.2000	0.0130	0.0092	0.0066	0.0051	0.0039
0.1000	0.8002	0.0999	0.0141	0.0099	0.0070	0.0053	0.0041
0.1995	0.1022	0.6982	0.0126	0.0096	0.0073	0.0059	0.0048
0.1997	0.2011	0.5992	0.0122	0.0092	0.0070	0.0056	0.0045

Table 4.18, continued

x_1	x_2	x_3	η, Pa.s				
			303.15 K	**313.15 K**	**323.15 K**	**333.15 K**	**343.15 K**
0.1997	0.3008	0.4995	0.0123	0.0092	0.0069	0.0055	0.0044
0.2000	0.4002	0.3998	0.0127	0.0094	0.0069	0.0055	0.0043
0.1998	0.4996	0.3006	0.0135	0.0098	0.0071	0.0056	0.0044
0.1996	0.6007	0.1997	0.0145	0.0104	0.0074	0.0058	0.0045
0.1995	0.7003	0.1002	0.0159	0.0112	0.0079	0.0060	0.0046
0.2993	0.1019	0.5988	0.0150	0.0112	0.0084	0.0068	0.0054
0.2996	0.2007	0.4997	0.0146	0.0108	0.0081	0.0064	0.0052
0.2994	0.2998	0.4008	0.0148	0.0109	0.0081	0.0064	0.0051
0.2997	0.4005	0.2998	0.0155	0.0112	0.0082	0.0064	0.0050
0.3000	0.5001	0.1999	0.0164	0.0117	0.0084	0.0065	0.0051
0.2997	0.6003	0.1000	0.0177	0.0125	0.0088	0.0068	0.0053
0.3989	0.1016	0.4995	0.0176	0.0130	0.0097	0.0077	0.0062
0.3990	0.2017	0.3993	0.0172	0.0126	0.0093	0.0074	0.0059
0.3988	0.3010	0.3002	0.0174	0.0127	0.0093	0.0073	0.0058
0.3995	0.4000	0.2005	0.0183	0.0132	0.0095	0.0074	0.0058
0.3996	0.5003	0.1001	0.0196	0.0139	0.0099	0.0076	0.0059
0.4992	0.1012	0.3996	0.0204	0.0150	0.0111	0.0088	0.0069
0.4993	0.2001	0.3006	0.0202	0.0147	0.0108	0.0084	0.0066
0.4992	0.3008	0.1999	0.0208	0.0150	0.0108	0.0084	0.0066
0.4980	0.3998	0.1021	0.0218	0.0155	0.0110	0.0085	0.0066
0.5978	0.1021	0.3001	0.0237	0.0172	0.0126	0.0099	0.0077
0.5992	0.1999	0.2009	0.0235	0.0170	0.0123	0.0096	0.0076
0.5984	0.3009	0.1007	0.0242	0.0172	0.0123	0.0095	0.0074
0.6963	0.1033	0.2004	0.0270	0.0195	0.0141	0.0110	0.0086
0.6964	0.2009	0.1027	0.0269	0.0192	0.0138	0.0107	0.0083
0.7965	0.1030	0.1005	0.0307	0.0219	0.0158	0.0122	0.0094

[a] Standard uncertainty u are u(x) = 0.0005, u(T) = 0.05 K, u(η) = 5%, x_1, x_2 and x_3 is the mol fraction of [BMIM][NTf_2], MEA and sulfolane, respectively.

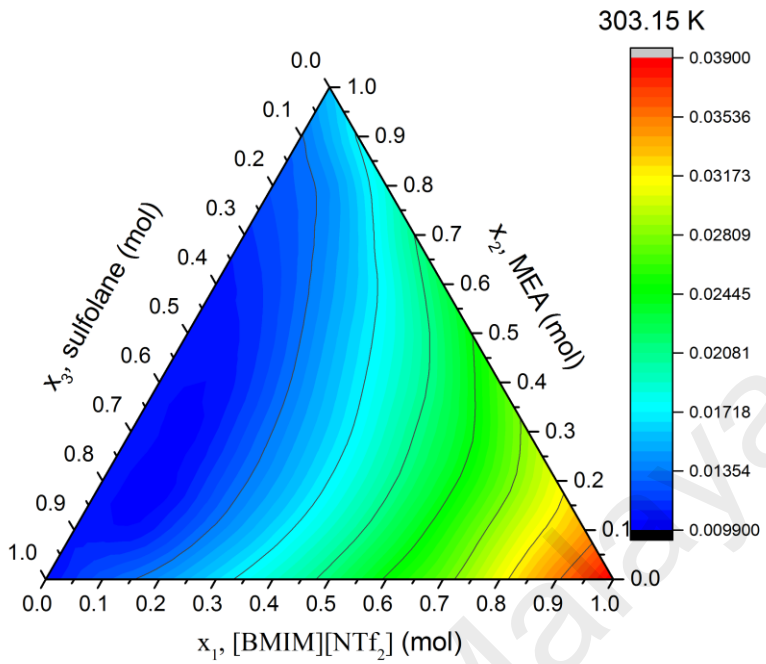

Figure 4.53: Viscosity of [BMIM][NTf_2] (1) + MEA (2) + sulfolane (3) ternary mixtures at T = 303.15 K

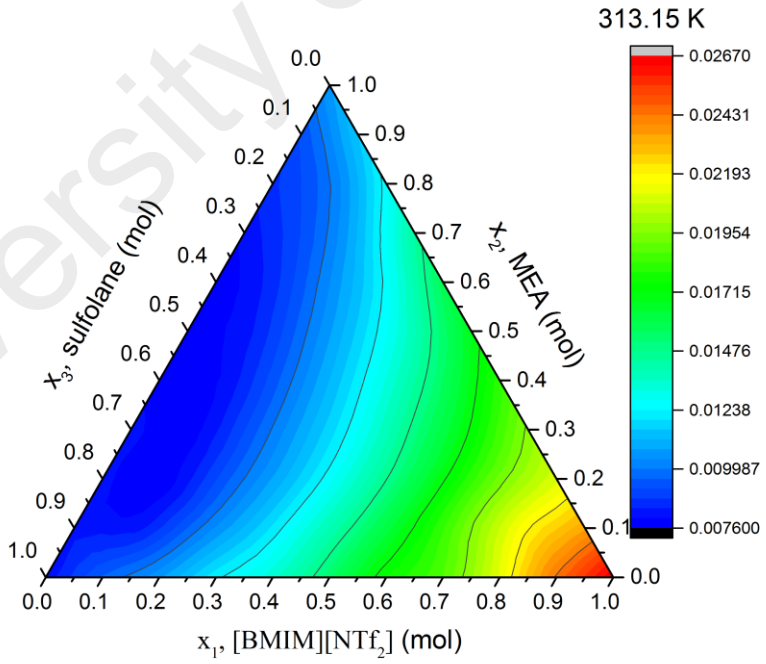

Figure 4.54: Viscosity of [BMIM][NTf_2] (1) + MEA (2) + sulfolane (3) ternary mixtures at T = 313.15 K

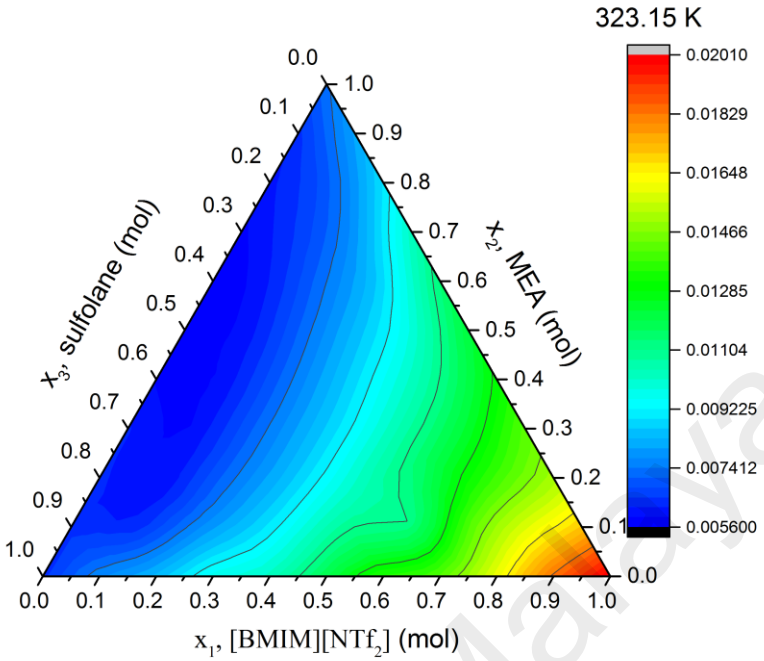

Figure 4.55: Viscosity of [BMIM][NTf_2] (1) + MEA (2) + sulfolane (3) ternary mixtures at T = 323.15 K

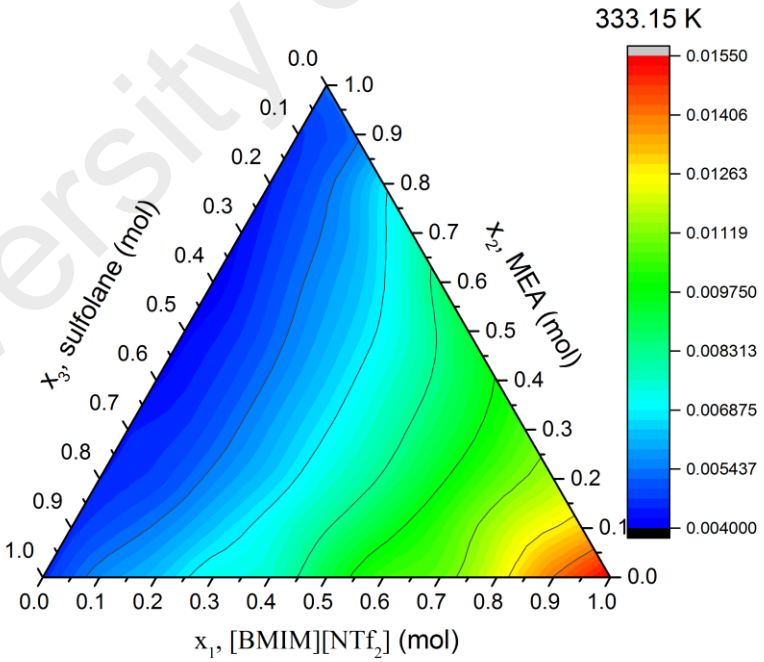

Figure 4.56: Viscosity of [BMIM][NTf_2] (1) + MEA (2) + sulfolane (3) ternary mixtures at T = 333.15 K

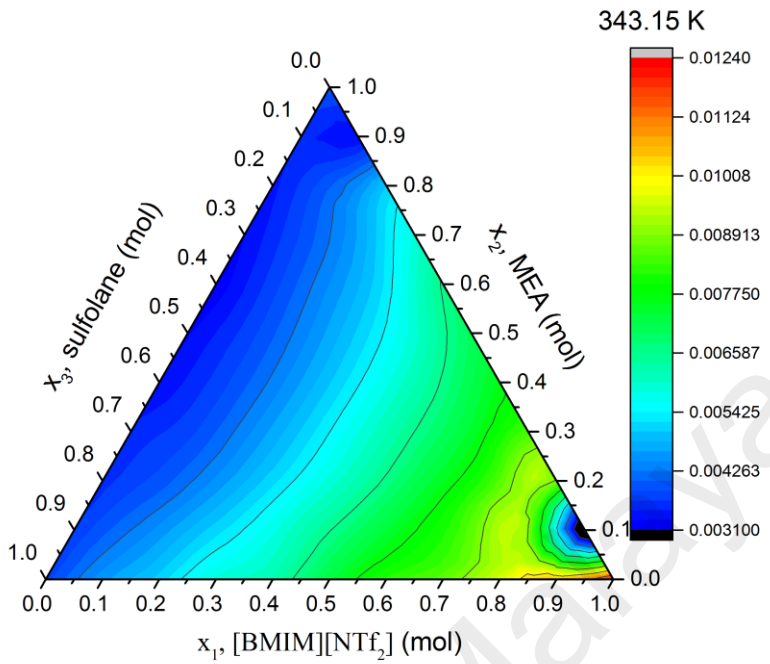

Figure 4.57: Viscosity of [BMIM][NTf_2] (1) + MEA (2) + sulfolane (3) ternary mixtures at T = 343.15 K

4.2.2.4 Viscosity deviation

Using the experimental viscosity data of pure components and their binary mixtures, viscosity deviations of the mixtures, $\Delta\eta$ are calculated using following Equation 4.14 (Qian et al., 2012): where, x_i and η_i represent the mol fraction and viscosity of pure component, respectively.

$$\Delta\eta = \eta_{mixture} - \sum_{i=1}^{n}(x_i\eta_i) \quad (4.14)$$

(a) Binary mixtures

The values of viscosity deviation of [BMIM][NTf_2] (1) + sulfolane (3), MEA (2) + sulfolane (3) and [BMIM][NTf_2] (1) + MEA (2) binary mixtures are summarized in Table 4.19 and represented in Figure 4.58 to Figure 4.60, respectively. Figure 4.58 to Figure 4.60 show that viscosity deviations, $\Delta\eta$, for all binary mixtures at various temperatures are negative over the entire mol fraction and become less negative with increasing the temperature. This negative $\Delta\eta$ value for all binary mixtures can be explained by the fact that the van der Waals dispersion force interaction is dominant in these mixtures (Mesquita et al., 2014; Qian et al., 2012). Moreover, in MEA (2) + sulfolane (3) and [BMIM][NTf_2] (1) + MEA (2) binary mixtures, the negative $\Delta\eta$ values is also due to breaking of hydrogen bonding of MEA that makes the mixture to flow more easily. Subsequently, the viscosity deviations were regressed using the Redlich-Kister equation, Equation 4.11 with the adjustable parameters, A_i were summarized in Table 4.20.

Table 4.19: Viscosity deviation ($\Delta\eta$) of [BMIM][NTf_2] (1), MEA (2) and sulfolane (3) binary mixtures at different temperatures and compositions

x_1	x_2	x_3	$\Delta\eta$, Pa.s				
			303.15 K	**313.15 K**	**323.15 K**	**333.15 K**	**343.15 K**
[BMIM][NTf_2] (1) + sulfolane (3)							
0.0000	-	1.0000	0.0000	0.0000	0.0000	0.0000	0.0000
0.1000	-	0.9000	-0.0005	-0.0003	-0.0001	0.0000	0.0000
0.1999	-	0.8001	-0.0018	-0.0011	-0.0007	-0.0005	-0.0003
0.3001	-	0.6999	-0.0023	-0.0014	-0.0009	-0.0006	-0.0004
0.4000	-	0.6000	-0.0031	-0.0023	-0.0018	-0.0015	-0.0012
0.5001	-	0.4999	-0.0030	-0.0020	-0.0013	-0.0010	-0.0007
0.5999	-	0.4001	-0.0027	-0.0017	-0.0011	-0.0007	-0.0005
0.7000	-	0.3000	-0.0029	-0.0022	-0.0017	-0.0014	-0.0011
0.7995	-	0.2005	-0.0019	-0.0016	-0.0013	-0.0011	-0.0009
0.8985	-	0.1015	-0.0009	-0.0005	-0.0003	-0.0002	-0.0002
1.0000	-	0.0000	0.0000	0.0000	0.0000	0.0000	0.0000
MEA (2) + sulfolane (3)							
-	0.0000	1.0000	0.0000	0.0000	0.0000	0.0000	0.0000
-	0.0999	0.9001	-0.0001	-0.0001	-0.0001	-0.0001	-0.0001
-	0.2001	0.7999	-0.0005	-0.0005	-0.0003	-0.0003	-0.0002
-	0.3001	0.6999	-0.0009	-0.0007	-0.0004	-0.0003	-0.0003
-	0.3999	0.6001	-0.0018	-0.0013	-0.0009	-0.0007	-0.0006
-	0.4999	0.5001	-0.0021	-0.0015	-0.0010	-0.0008	-0.0006
-	0.5999	0.4001	-0.0028	-0.0020	-0.0013	-0.0010	-0.0008
-	0.6999	0.3001	-0.0027	-0.0018	-0.0012	-0.0009	-0.0007
-	0.8000	0.2000	-0.0021	-0.0015	-0.0010	-0.0007	-0.0005
-	0.8999	0.1001	-0.0018	-0.0012	-0.0008	-0.0006	-0.0004
-	1.0000	0.0000	0.0000	0.0000	0.0000	0.0000	0.0000
[BMIM][NTf_2] (1) + MEA (2)							
0.0000	1.0000	-	0.0000	0.0000	0.0000	0.0000	0.0000
0.1001	0.8999	-	-0.0005	-0.0003	-0.0001	0.0000	0.0000
0.2000	0.8000	-	-0.0018	-0.0011	-0.0007	-0.0005	-0.0003
0.3000	0.7000	-	-0.0023	-0.0014	-0.0009	-0.0006	-0.0004
0.4000	0.6000	-	-0.0031	-0.0023	-0.0018	-0.0015	-0.0012
0.4999	0.5001	-	-0.0030	-0.0020	-0.0013	-0.0010	-0.0007
0.6000	0.4000	-	-0.0027	-0.0017	-0.0011	-0.0007	-0.0005
0.6999	0.3001	-	-0.0029	-0.0022	-0.0017	-0.0014	-0.0011
0.8000	0.2000	-	-0.0019	-0.0016	-0.0013	-0.0011	-0.0009
0.8998	0.1002	-	-0.0009	-0.0005	-0.0003	-0.0002	-0.0002
1.0000	0.0000	-	0.0000	0.0000	0.0000	0.0000	0.0000

[a] Standard uncertainty u are u(x) = 0.0005, u(T) = 0.05 K, u(η) = 5%

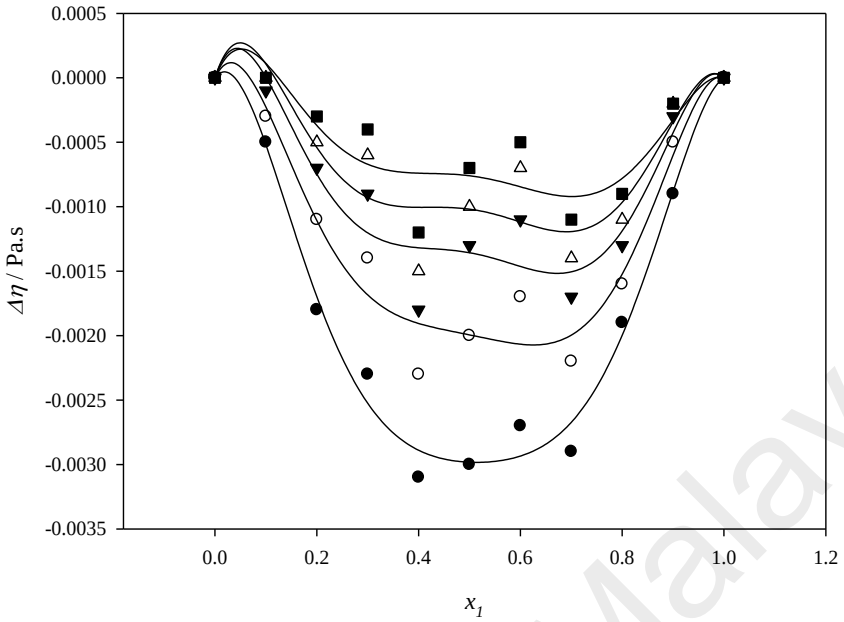

Figure 4.58: Viscosity deviation of [BMIM][NTf_2] (1) + sulfolane (3) binary mixtures against temperature as function of [BMIM][NTf_2] mol fraction; (●) 303.15 K; (○) 313.15 K; (▼) 323.15 K; (△) 333.15 K; (■) 343.15 K

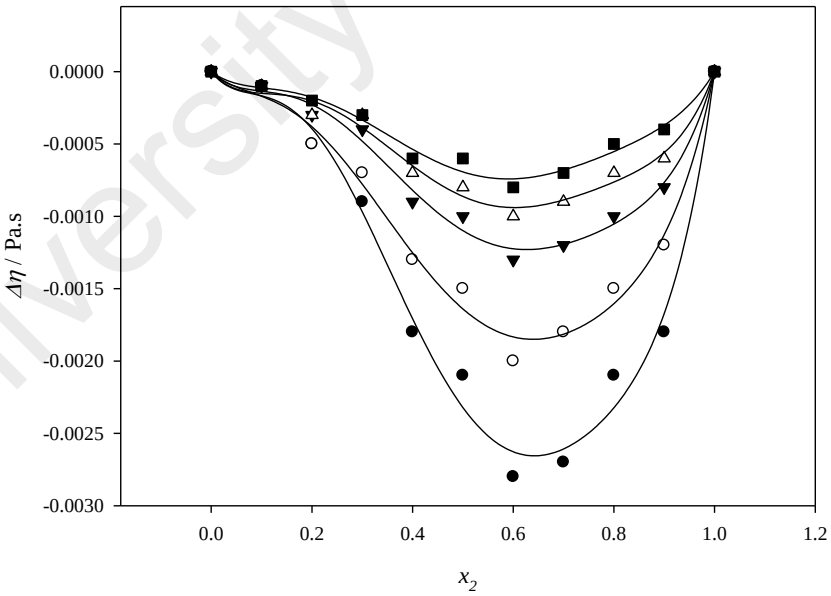

Figure 4.59: Viscosity deviation of MEA (2) + sulfolane (3) binary mixtures at various temperatures; (●) 303.15 K; (○) 313.15 K; (▼) 323.15 K; (△) 333.15 K; (■) 343.15 K.

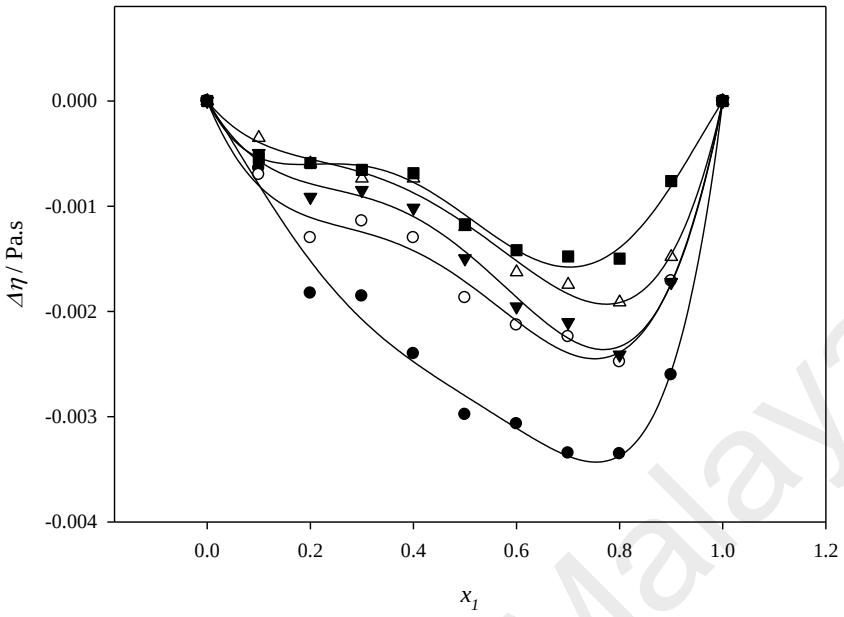

Figure 4.60: Viscosity deviation of [BMIM][NTf_2] (1) + MEA (2) mixture at various temperatures; (●) 303.15 K; (○) 313.15 K; (▼) 323.15 K; (△) 333.15 K; (■) 343.15 K

Table 4.20: Redlich-Kister fitting coefficients A_i of the viscosity deviation ($\Delta\eta$) of [BMIM][NTf_2] (1) + sulfolane (3) binary mixtures as a function of various temperatures along with their fitting deviations, σ

T / K	A_0	A_1	A_2	A_3	A_4	R^2	σ^a
[BMIM][NTf_2] (1) + sulfolane (3)							
303.15	-0.0119	-0.0003	-0.0059	-0.0034	0.0193	0.9845	0.0002
313.15	-0.0080	-0.0016	-0.0083	-0.0015	0.0212	0.9421	0.0003
323.15	-0.0054	-0.0014	-0.0101	-0.0025	0.0233	0.8787	0.0003
333.15	-0.0041	-0.0011	-0.0096	-0.0032	0.0217	0.7994	0.0003
343.15	-0.0030	-0.0010	-0.0072	-0.0032	0.0157	0.7481	0.0003
MEA (2) + sulfolane (3)							
303.15	-0.0093	-0.0096	0.0069	-0.0014	-0.0131	0.9843	0.0002
313.15	-0.0066	-0.0060	0.0036	0.0010	-0.0072	0.9832	0.0001
323.15	-0.0044	-0.0042	0.0037	-0.0003	-0.0073	0.9846	0.0001
333.15	-0.0035	-0.0030	0.0037	0.0003	-0.0070	0.9824	0.0001
343.15	-0.0028	-0.0022	0.0029	0.0006	-0.0044	0.9821	0.0001
[BMIM][NTf_2] (1) + MEA (2)							
303.15	-0.0112	-0.0062	-0.0109	-0.0096	-0.0013	0.9871	0.0002

Table 4.20, continued

T / K	A_0	A_1	A_2	A_3	A_4	R^2	σ^a
313.15	-0.0069	-0.0070	-0.0113	0.0008	-0.00002	0.9816	0.0001
323.15	-0.0057	-0.0080	-0.0114	-0.0002	0.0005	0.9894	0.0001
333.15	-0.0047	-0.0067	-0.0081	-0.0011	-0.0011	0.9903	0.0001
343.15	-0.0043	-0.0070	-0.0058	0.0080	0.0014	0.9861	0.0001

[a]σ = standard deviation, Equation 4.9

(b) Ternary mixtures

Values of viscosity deviation ($\Delta\eta$), were calculated from experimental viscosity of the mixture using Equation 4.14. Figure 4.61 to Figure 4.65 represent viscosity deviation for the ternary mixtures at constant temperature with temperatures range from 303.15 to 343.15 K, respectively. In general, the negative value of viscosity deviation was observed over the whole compositions and temperatures range. The negative viscosity deviation is more prominent in ternary mixture with each composition reaching equimolar of each other (example: 0.3 [BMIM][NTf_2]: 0.3 MEA: 0.4 sulfolane). The negative values of viscosity deviation indicate characteristic of mixtures without strong specific interactions and van der Waals dispersion force interaction is dominant (Mesquita et al., 2014; Pires et al., 2013). Furthermore, viscosity deviation values decrease by increasing the temperature over the whole range of compositions.

Table 4.21: Viscosity deviation ($\Delta\eta$) of [BMIM][NTf_2] (1) + MEA + sulfolane (3) ternary mixtures at different temperatures and compositions

[BMIM][NTf_2] (1) + MEA (2) + sulfolane (3)							
x_1	x_2	x_3	$\Delta\eta$, Pa.s				
			303.15	313.15	323.15	333.15	343.15
0.0999	0.1003	0.7998	-0.00345	-0.00212	-0.00162	-0.00056	-0.00042
0.0998	0.2000	0.7002	-0.00439	-0.00288	-0.00208	-0.00103	-0.00076
0.0997	0.3015	0.5988	-0.00474	-0.00304	-0.00222	-0.00120	-0.00093
0.1000	0.4005	0.4995	-0.00488	-0.00310	-0.00226	-0.00128	-0.00099
0.0999	0.5004	0.3997	-0.00478	-0.00306	-0.00225	-0.00135	-0.00101
0.1000	0.5999	0.3001	-0.00446	-0.00292	-0.00211	-0.00122	-0.00099
0.1000	0.7000	0.2000	-0.00396	-0.00258	-0.00184	-0.00109	-0.00090
0.1000	0.8002	0.0999	-0.00346	-0.00214	-0.00151	-0.00096	-0.00075
0.1995	0.1022	0.6982	-0.00417	-0.00248	-0.00188	-0.00095	-0.00070
0.1997	0.2011	0.5992	-0.00500	-0.00314	-0.00234	-0.00132	-0.00106
0.1997	0.3008	0.4995	-0.00541	-0.00340	-0.00252	-0.00149	-0.00120
0.2000	0.4002	0.3998	-0.00557	-0.00346	-0.00258	-0.00157	-0.00128
0.1998	0.4996	0.3006	-0.00528	-0.00332	-0.00248	-0.00154	-0.00126
0.1996	0.6007	0.1997	-0.00480	-0.00297	-0.00225	-0.00141	-0.00116
0.1995	0.7003	0.1002	-0.00395	-0.00243	-0.00191	-0.00128	-0.00102
0.2993	0.1019	0.5988	-0.00459	-0.00273	-0.00215	-0.00114	-0.00096
0.2996	0.2007	0.4997	-0.00551	-0.00339	-0.00260	-0.00161	-0.00126
0.2994	0.2998	0.4008	-0.00575	-0.00355	-0.00271	-0.00168	-0.00138
0.2997	0.4005	0.2998	-0.00564	-0.00352	-0.00269	-0.00175	-0.00144
0.3000	0.5001	0.1999	-0.00523	-0.00328	-0.00255	-0.00173	-0.00140
0.2997	0.6003	0.1000	-0.00446	-0.00273	-0.00224	-0.00150	-0.00124
0.3989	0.1016	0.4995	-0.00482	-0.00278	-0.00227	-0.00132	-0.00106
0.3990	0.2017	0.3993	-0.00571	-0.00345	-0.00271	-0.00169	-0.00141
0.3988	0.3010	0.3002	-0.00599	-0.00360	-0.00285	-0.00186	-0.00150
0.3995	0.4000	0.2005	-0.00566	-0.00337	-0.00272	-0.00184	-0.00155
0.3996	0.5003	0.1001	-0.00487	-0.00293	-0.00246	-0.00171	-0.00142
0.4992	0.1012	0.3996	-0.00483	-0.00265	-0.00227	-0.00131	-0.00117
0.4993	0.2001	0.3006	-0.00556	-0.00321	-0.00265	-0.00179	-0.00150
0.4992	0.3008	0.1999	-0.00546	-0.00317	-0.00273	-0.00186	-0.00156
0.4980	0.3998	0.1021	-0.00501	-0.00290	-0.00258	-0.00181	-0.00155
0.5978	0.1021	0.3001	-0.00433	-0.00228	-0.00368	-0.00129	-0.00121
0.5992	0.1999	0.2009	-0.00507	-0.00276	-0.00253	-0.00167	-0.00144
0.5984	0.3009	0.1007	-0.00496	-0.00281	-0.00254	-0.00184	-0.00161
0.6963	0.1033	0.2004	-0.00384	-0.00182	-0.00196	-0.00126	-0.00126
0.6964	0.2009	0.1027	-0.00446	-0.00238	-0.00236	-0.00163	-0.00149
0.7965	0.1030	0.1005	-0.00305	-0.00128	-0.00166	-0.00116	-0.00122

[a] Standard uncertainty u are u(x) = 0.0005, u(T) = 0.05 K, u(η) = 5%, x_1, x_2 and x_3 is the mol fraction of [BMIM][NTf_2], MEA and sulfolane, respectively.

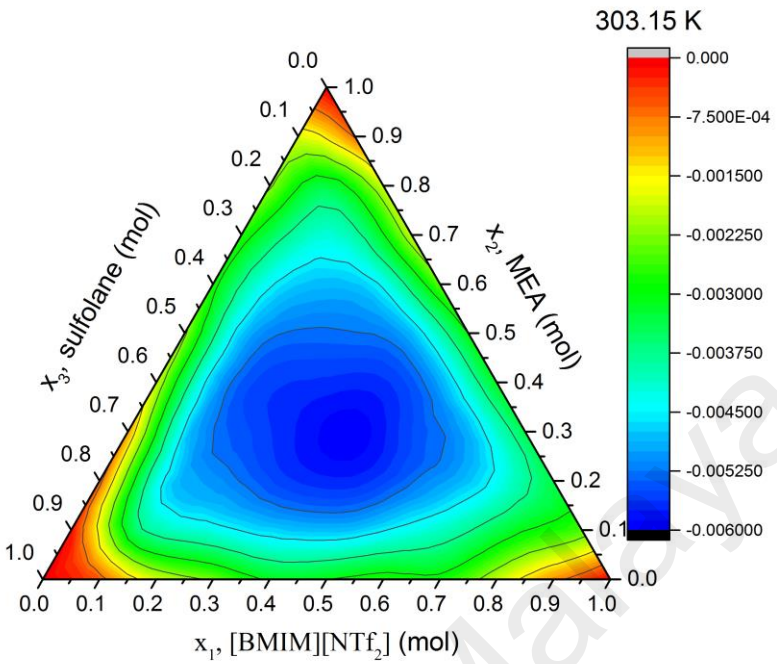

Figure 4.61: Viscosity deviation of [BMIM][NTf_2] (1) + MEA (2) + sulfolane (3) ternary mixtures at T= 303.15 K

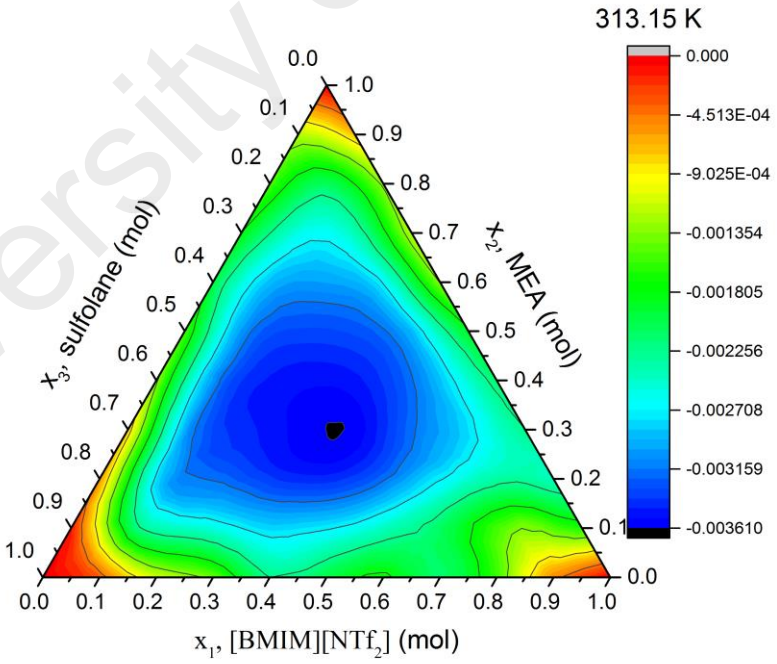

Figure 4.62: Viscosity deviation of [BMIM][NTf_2] (1) + MEA (2) + sulfolane (3) ternary mixtures at T= 313.15 K

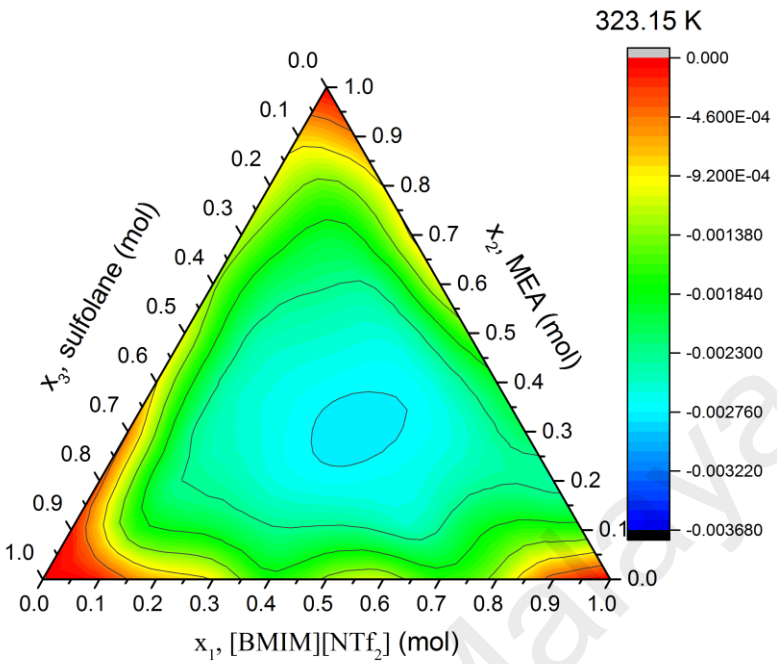

Figure 4.63: Viscosity deviation of [BMIM][NTf_2] (1) + MEA (2) + sulfolane (3) ternary mixtures at T= 323.15 K

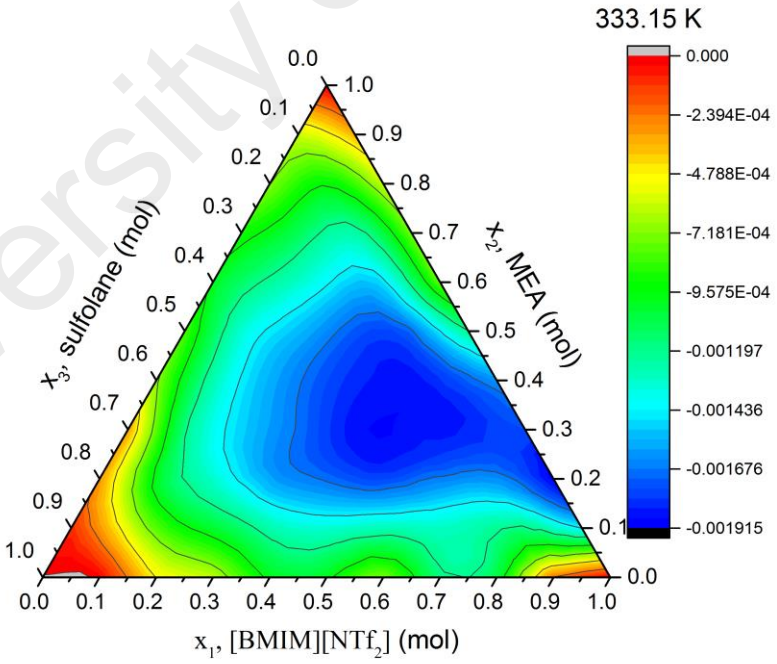

Figure 4.64: Viscosity deviation of [BMIM][NTf_2] (1) + MEA (2) + sulfolane (3) ternary mixtures at T= 333.15 K

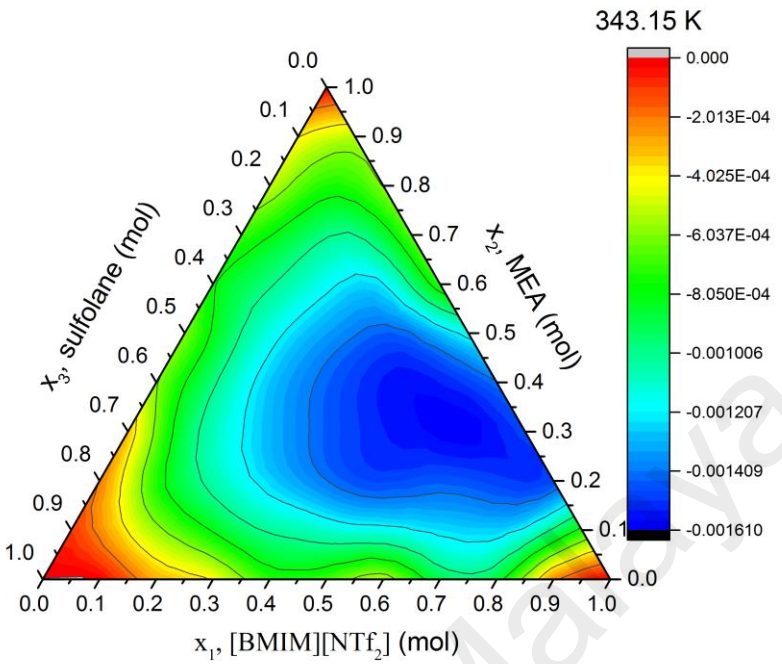

Figure 4.65: Viscosity deviation of [BMIM][NTf_2] (1) + MEA (2) + sulfolane (3) ternary mixtures at T= 343.15 K

4.2.3 Refractive index

4.2.3.1 Introduction

This chapter explores the refractive index of 3 binary mixtures of [BMIM][NTf_2] (1) + sulfolane (3), MEA (2) + sulfolane (3) and [BMIM][NTf_2] (1) + MEA (2) together with ternary mixtures of [BMIM][NTf_2] (1) + MEA (2) + sulfolane (3) over the whole range of composition. The atmospheric refractive indices were measured at various temperatures ranging from 303.15 to 343 K with increment of 10 K. The measurement was conducted to evaluate the changing of the refractive index value of binary and ternary

mixtures of [BMIM][NTf_2], MEA and sulfolane at different temperatures and compositions.

4.2.3.2 Validation of the refractive index measurement

To verify reliability of the equipment and procedures, the refractive index of pure [BMIM][NTf_2], MEA and sulfolane were measured at different temperatures and compared with the experimental values that are reported by other authors in literatures (Table 4.22 and Figure 4.66). The measurement of refractive index obtained in this study are in good agreement with the literature data at all the temperatures.

Table 4.22: Comparison of measured refractive indexes (n_D) with literature values for [BMIM][NTf_2], MEA and sulfolane at different temperatures

T/K	[BMIM][NTf_2]		MEA		sulfolane	
	Exp.	Lit.[1]	Exp.	Lit.[2]	Exp.	Lit.[3]
303.15	1.4254	1.4216	1.4505	1.4488	1.4790	1.4814
313.15	1.4222	1.4188	1.4463	1.4449	1.4750	1.4780
323.15	1.4193	1.4159	1.4417	1.4417	1.4714	1.4744
333.15	1.4163	1.4131	1.4384	-	1.4679	-
343.15	1.4152	1.4103	1.4349	-	1.4644	-

1 = data from (Seki et al., 2012)
2 = data from (García-Abuín et al., 2011)
3 = data from (Vahidi & Moshtari, 2013)

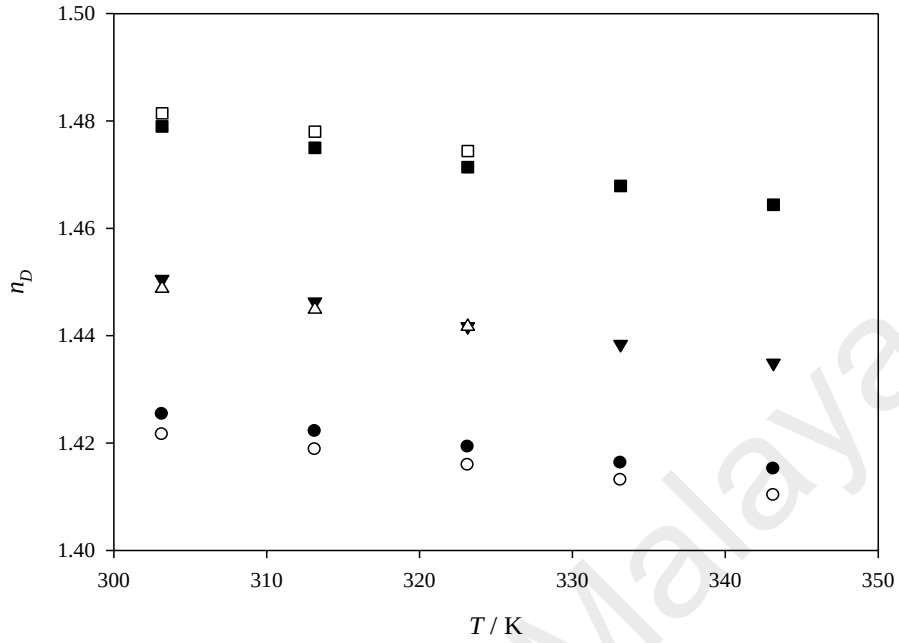

Figure 4.66: Comparison of refractive index for pure [BMIM][NTf_2], MEA and sulfolane with literatures; (●) [BMIM][NTf_2]$_{Exp.;}$ (○) [BMIM][NTf_2]$_{Lit.}$ (Seki et al., 2012)$_;$ (▼) $MEA_{Exp.;}$ (△) MEA_{Lit} (García-Abuín et al., 2011)$_.;$ (■) $sulfolane_{Exp.;}$ (□) $sulfolane_{Lit}$ (Vahidi & Moshtari, 2013)

4.2.3.3 Effect of temperature and composition

(a) Binary mixtures

All measured experimental refractive index values of [BMIM][NTf_2] (1), MEA (2) and sulfolane (3) binary mixtures throughout the entire mol fraction composition with the temperatures ranging from 303.15 to 343.15 K are tabulated in Table 4.23 and represented in Figure 4.67 to Figure 4.72. Figure 4.67 to Figure 4.69 show that the measured refractive index of [BMIM][NTf_2] (1) + sulfolane (3), MEA (2) + sulfolane (3) and [BMIM][NTf_2] (1) + MEA (2) binary mixtures, respectively, throughout the entire temperatures ranging

from 303.15 to 343.15 K at constant compositions. For all the binary mixtures, the refractive index curves show a quasi-linear decrease in values with the increment of temperature throughout the whole composition. The influence of temperature on the refractive index of pure and [BMIM][NTf_2] (1), MEA (2) and sulfolane (3) binary mixtures were found to be linear and correlated using a linear relationship as a function of temperature using Equation 4.7 and tabulated in Table 4.24.

Table 4.23: Refraction index (n_D) of [BMIM][NTf_2] (1), MEA (2) and sulfolane (3) binary mixtures at different temperatures and compositions

x_1	x_2	x_3	η, Pa.s				
			303.15 K	**313.15 K**	**323.15 K**	**333.15 K**	**343.15 K**
[BMIM][NTf_2] (1) + sulfolane (3)							
0.0000	-	1.0000	1.4790	1.4750	1.4714	1.4679	1.4644
0.1000	-	0.9000	1.4644	1.4607	1.4572	1.4538	1.4505
0.1999	-	0.8001	1.4556	1.4520	1.4486	1.4454	1.4422
0.3001	-	0.6999	1.4479	1.4446	1.4413	1.4382	1.4350
0.4000	-	0.6000	1.4423	1.4391	1.4359	1.4328	1.4297
0.5001	-	0.4999	1.4385	1.4353	1.4322	1.4291	1.4260
0.5999	-	0.4001	1.4350	1.4318	1.4288	1.4257	1.4228
0.7000	-	0.3000	1.4318	1.4284	1.4254	1.4224	1.4194
0.7995	-	0.2005	1.4294	1.4262	1.4232	1.4203	1.4172
0.8985	-	0.1015	1.4272	1.4240	1.4211	1.4182	1.4152
1.0000	-	0.0000	1.4254	1.4222	1.4193	1.4163	1.4134
MEA (2) + sulfolane (3)							
-	0.0000	1.0000	1.4791	1.4751	1.4715	1.4681	1.4644
-	0.0999	0.9001	1.4771	1.4730	1.4694	1.4662	1.4625
-	0.2001	0.7999	1.4749	1.4708	1.4670	1.4640	1.4603
-	0.3001	0.6999	1.4725	1.4683	1.4645	1.4616	1.4578
-	0.3999	0.6001	1.4699	1.4657	1.4618	1.4589	1.4551
-	0.4999	0.5001	1.4670	1.4628	1.489	1.4559	1.4522
-	0.5999	0.4001	1.4639	1.4597	1.4558	1.4527	1.4489
-	0.6999	0.3001	1.4606	1.4565	14525	1.4491	1.4455
-	0.8000	0.2000	1.4571	1.4530	1.4490	1.4454	1.4417
-	0.8999	0.1001	1.4533	1.4493	1.4453	1.4413	1.4377
-	1.0000	0.0000	1.4493	1.4454	1.4414	1.4370	1.4335
[BMIM][NTf_2] (1) + MEA (2)							
0.0000	1.0000	-	1.4505	1.4463	1.4417	1.4384	1.4349
0.1001	0.8999	-	1.4404	1.4367	1.4331	1.4295	1.4259

Table 4.23, continued

x_1	x_2	x_3	η, Pa.s				
			303.15 K	**313.15 K**	**323.15 K**	**333.15 K**	**343.15 K**
0.2000	0.8000	-	1.4342	1.4309	1.4276	1.4243	1.4210
0.3000	0.7000	-	1.4310	1.4279	1.4248	1.4216	1.4184
0.4000	0.6000	-	1.4287	1.4257	1.4228	1.4197	1.4166
0.4999	0.5001	-	1.4277	1.4246	1.4215	1.4184	1.4154
0.6000	0.4000	-	1.4266	1.4234	1.4201	1.4174	1.4145
0.6999	0.3001	-	1.4262	1.4230	1.4198	1.4168	1.4138
0.8000	0.2000	-	1.4258	1.4227	1.4195	1.4166	1.4137
0.8998	0.1002	-	1.4254	1.4224	1.4193	1.4164	1.4135
1.0000	0.0000	-	1.4253	1.4223	1.4192	1.4163	1.4134

[a] Standard uncertainty u are u(x) = 0.0005, u(T) = 0.05 K, u(n_D) = 0.0005, x_1 and x_3 is the mol fraction of [BMIM][NTf_2] and sulfolane, respectively.

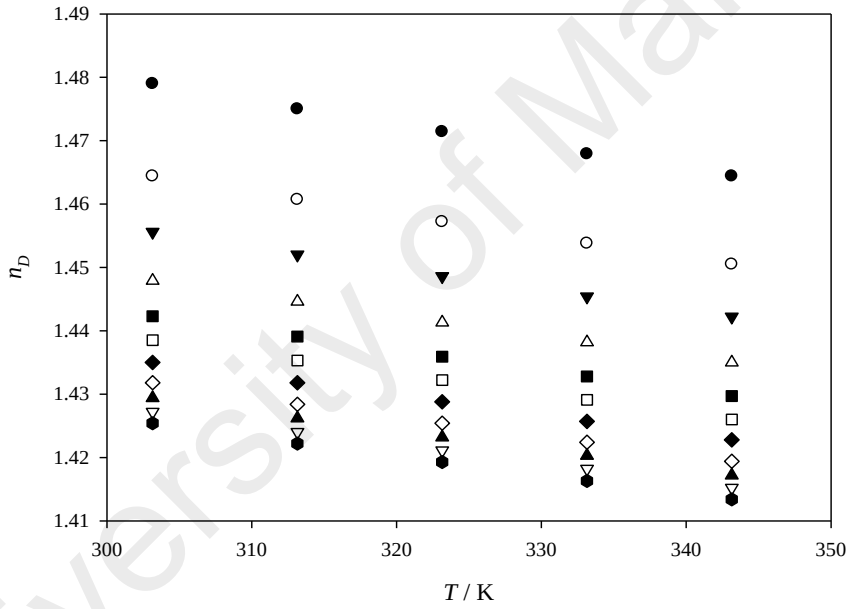

Figure 4.67: Refractive index of [BMIM][NTf_2] (1) + sulfolane (3) binary mixtures against temperature at various compositions; (●) x_1= 0, (○) x_1= 0.1, (▼) x_1= 0.2, (△) x_1= 0.3, (■) x_1= 0.4, (□) x_1= 0.5, (◆) x_1= 0.6, (◇) x_1= 0.7, (▽) x_1= 0.8, (▲) x_1= 0.9, (⬢) x_1= 1.0.

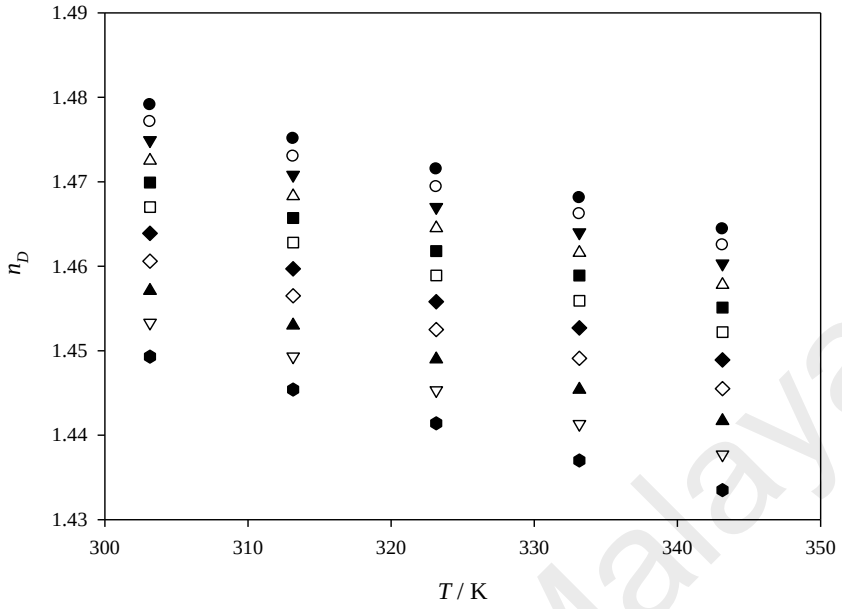

Figure 4.68: Refractive index of MEA (2) + sulfolane (3) binary mixtures against temperature at various compositions; (●) 0 x_1; (○) 0.1 x_1; (▼) 0.2 x_1; (△) 0.3 x_1; (■) 0.4 x_1; (□) 0.5 x_1; (◆) 0.6 x_1; (◇) 0.7 x_1; (▲) 0.8 x_1; (▽) 0.9 x_1; (⬢) 1.0 x_1.

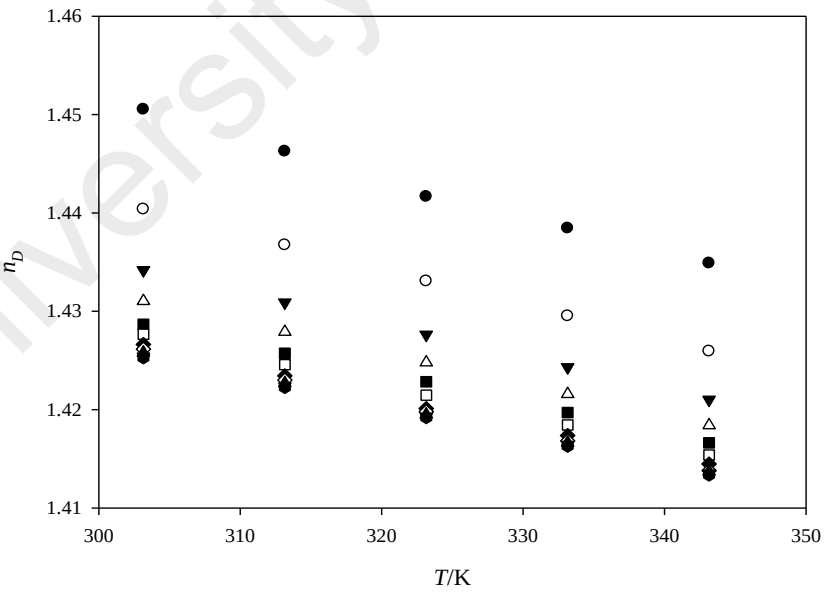

Figure 4.69: Refractive index of [BMIM][NTf_2] (1) + MEA (2) binary mixtures against temperature at various compositions; (●) x_1= 0, (○) x_1= 0.1, (▼) x_1= 0.2, (△) x_1= 0.3, (■) x_1= 0.4, (□) x_1= 0.5, (◆) x_1= 0.6, (◇) x_1= 0.7, (▽) x_1= 0.8, (▲) x_1= 0.9, (⬢) x_1= 1.0

Table 4.24: Fitting parameters of Equation 4.7 together with correlation coefficient, R^2, and standard relative deviations, σ, for influence of temperature on the refractive index of [BMIM][NTf_2] (1), MEA (2) and sulfolane (3) binary mixtures

x_1	x_2	x_3	A	B	R^2	σ^a
[BMIM][NTf_2] (1) + sulfolane (3)						
0.0000	-	1.0000	1.5888	-0.0004	0.9992	0.0002
0.1000	-	0.9000	1.5695	-0.0003	0.9995	0.0001
0.1999	-	0.8001	1.5567	-0.0003	0.9993	0.0002
0.3001	-	0.6999	1.5455	-0.0003	0.9998	0.0001
0.4000	-	0.6000	1.5378	-0.0003	0.9999	0.0001
0.5001	-	0.4999	1.5330	-0.0003	0.9999	0.0001
0.5999	-	0.4001	1.5274	-0.0003	0.9998	0.0001
0.7000	-	0.3000	1.5250	-0.0003	0.9993	0.0001
0.7995	-	0.2005	1.5212	-0.0003	0.9997	0.0001
0.8985	-	0.1015	1.5174	-0.0003	0.9997	0.0001
1.0000	-	0.0000	1.5159	-0.0003	0.9997	0.0001
MEA (2) + sulfolane (3)						
-	0.0000	1.0000	1.5706	-0.0004	0.9991	0.0002
-	0.0999	0.9001	1.5717	-0.0004	0.9995	0.0002
-	0.2001	0.7999	1.5729	-0.0004	0.9991	0.0002
-	0.3001	0.6999	15744	-0.0004	0.9983	0.0003
-	0.3999	0.6001	1.5760	-0.0004	0.9973	0.0004
-	0.4999	0.5001	1.5778	-0.0004	0.9966	0.0004
-	0.5999	0.4001	1.5797	-0.0004	0.9964	0.0004
-	0.6999	0.3001	1.5819	-0.0004	0.9966	0.0004
-	0.8000	0.2000	1.5842	-0.0004	0.9973	0.0003
-	0.8999	0.1001	1.5866	-0.0004	0.9983	0.0003
-	1.0000	0.0000	1.5393	-0.0004	0.9993	0.0002
[BMIM][NTf_2] (1) + MEA (2)						
0.0000	1.0000	-	1.5687	-0.0004	0.9953	0.0005
0.1001	0.8999	-	1.5498	-0.0004	0.9999	0.0001
0.2000	0.8000	-	1.5340	-0.0003	0.9999	0.0001
0.3000	0.7000	-	1.5268	-0.0003	0.9999	0.0001
0.4000	0.6000	-	1.5201	-0.0003	0.9997	0.0001
0.4999	0.5001	-	1.5207	-0.0003	0.9999	0.0001
0.6000	0.4000	-	1.5186	-0.0003	0.9985	0.0002
0.6999	0.3001	-	1.5197	-0.0003	0.9997	0.0001
0.8000	0.2000	-	1.5174	-0.0003	0.9995	0.0001
0.8998	0.1002	-	1.5154	-0.0003	0.9998	0.0001
1.0000	0.0000	-	1.5156	-0.0003	0.9999	0.0001

[a]σ = standard deviation, Equation 4.9

Figure 4.70 to Figure 4.72 show effect of composition to the refractive index of [BMIM][NTf_2] (1) + sulfolane (3), MEA (2) + sulfolane (3) and [BMIM][NTf_2] (1) + MEA (2) binary mixtures, respectively, at constant temperature. As shown in Figure 4.70, it is observed that the refractive index increases with increased composition of [BMIM][NTf_2] as the refractive index of pure [BMIM][NTf_2] is significantly higher than the refractive index of pure sulfolane. Figure 4.71 shows that the refractive index decreases with the increased composition of MEA as the refractive index of pure sulfolane is significantly higher than refractive index of pure MEA. Figure 4.72 shows the effect of the composition to the refractive index of the [BMIM][NTf_2] (1) + MEA (2) binary mixtures at constant temperature. It is observed that the refractive index increases with the increased composition of [BMIM][NTf_2] as the refractive index of pure [BMIM][NTf_2] is significantly higher than the refractive index of pure MEA. In pure state the refractive index of [BMIM][NTf_2] (1), MEA (2) and sulfolane (3) had been found to be in the order of,

sulfolane > MEA > [BMIM][NTf_2]

The influence of the composition on the refractive index of pure and [BMIM][NTf_2] (1), MEA (2) and sulfolane (3) binary mixtures were correlated using a cubic polynomial function as a function of composition, Equation 4.8 and summarized in Table 4.25.

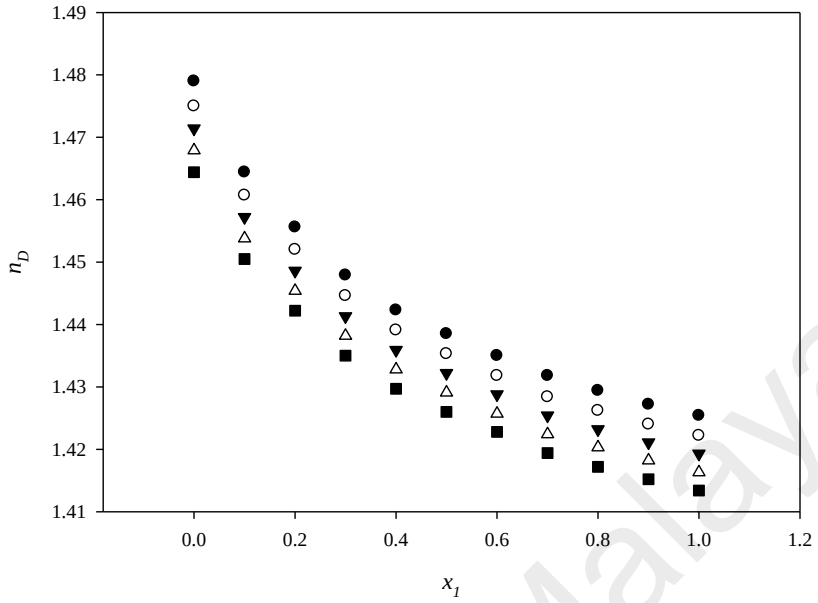

Figure 4.70: Refractive index of [BMIM][NTf_2] (1) + sulfolane (3) binary mixtures against composition at various temperatures; (●) 303.15 K; (○) 313.15 K; (▼) 323.15 K; (△) 333.15 K; (■) 343.15 K

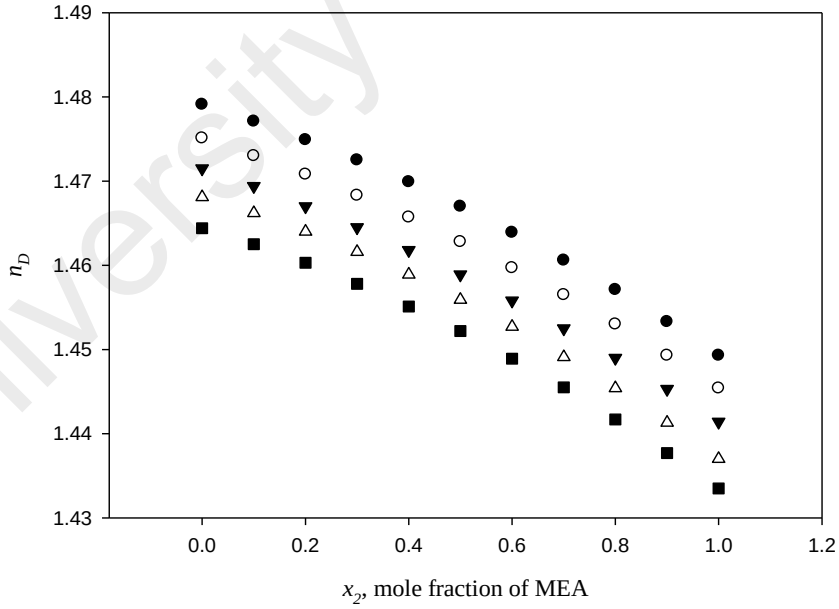

Figure 4.71: Refractive index of MEA (2) + sulfolane (3) binary mixtures against composition at various temperatures; (●) 303.15 K; (○) 313.15 K; (▼) 323.15 K; (△) 333.15 K; (■) 343.15 K

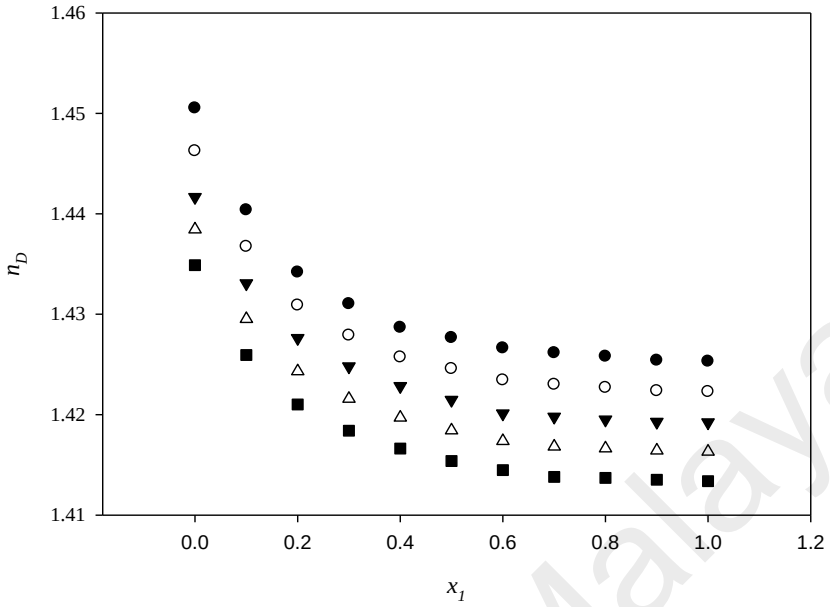

Figure 4.72: Refraction index of [BMIM][NTf_2] (1) + MEA (2) binary mixtures against composition at various temperatures; (●) 303.15 K; (○) 313.15 K; (▼) 323.15 K; (△) 333.15 K; (■) 343.15 K

Table 4.25: Fitting parameters of Equation 4.8 together with correlation coefficient squared, R^2, and standard relative deviations, σ, for influence of composition on refractive index of [BMIM][NTf_2] (1), MEA (2) and sulfolane (3) binary mixtures

T/K	A_0	A_1	A_2	A_3	R^2	σ^a
[BMIM][NTf_2] (1) + sulfolane (3)						
303.15	1.4782	-0.1409	0.1528	-0.0652	0.9988	0.0007
313.15	1.4742	-0.1372	0.1471	-0.0624	0.9987	0.0007
323.15	1.4706	-0.1360	0.1469	-0.0626	0.9986	0.0007
333.15	1.4671	-0.1345	0.1453	-0.0620	0.9987	0.0007
343.15	1.4636	-0.1327	0.1428	-0.0608	0.9986	0.0007
MEA (2) + sulfolane (3)						
303.15	1.4493	0.0411	-0.0113	4.5227	0.9999	0.0001
313.15	1.4454	0.0399	-0.0102	2.1850	0.9999	0.0001
323.15	1.4414	0.0398	-0.0097	4.1743	0.9999	0.0001
333.15	1.4370	0.0445	-0.0134	2.8524	0.9999	0.0001
343.15	1.4335	0.0437	-0.0128	2.9537	0.9999	0.0001
[BMIM][NTf_2] (1) + MEA (2)						
303.15	1.4498	-0.0996	0.1409	-0.0664	0.9954	0.0007
313.15	1.4456	-0.0928	0.1289	-0.0599	0.9945	0.0007

Table 4.25, continued

T/K	A_0	A_1	A_2	A_3	R^2	σ^a
323.15	1.4410	-0.0836	0.1116	-0.0502	0.9949	0.0006
333.15	1.4377	-0.0844	0.1158	-0.0533	0.9935	0.0007
343.15	1.4341	-0.0826	0.1147	-0.0532	0.9922	0.0007

[a]σ = standard deviation, Equation 4.9

(b) Ternary mixtures

All the measured experimental refractive index values of [BMIM][NTf_2] + MEA + sulfolane ternary mixtures throughout entire mol fraction composition with temperatures ranging from 303.15 to 343.15 K are tabulated in Table 4.26. Figure 4.73 to Figure 4.77 represent refractive index for the ternary mixtures at constant temperature in temperatures range from 303.15 to 343.15 K, respectively. Overall, it is observed that the composition of sulfolane highly influenced density of the ternary mixtures in comparison to MEA and [BMIM][NTf_2]. In a constant sulfolane mol fraction, the refractive index of the ternary mixtures is affected significantly by the MEA composition due to MEA higher refractive index than [BMIM][NTf_2] with refractive index on the ternary mixtures increases as the MEA composition increased. The refractive index data show a quasi-linear decrease in values with the increment of temperature throughout the whole composition.

Table 4.26: Refractive index (n_D) of [BMIM][NTf_2] (1) + MEA (2) + sulfolane (3) ternary mixtures at different temperatures and compositions

[BMIM][NTf_2] (1) + MEA (2) + sulfolane (3)							
x_1	x_2	x_3	n_D				
			303.15 K	313.15 K	323.15 K	333.15 K	343.15 K
0.0999	0.1003	0.7998	1.4643	1.4604	1.4564	1.4530	1.4495
0.0998	0.2000	0.7002	1.4617	1.4580	1.4542	1.4506	1.4470
0.0997	0.3015	0.5988	1.4590	1.4553	1.4515	1.4480	1.4445
0.1000	0.4005	0.4995	1.4564	1.4527	1.4490	1.4453	1.4417
0.0999	0.5004	0.3997	1.4535	1.4499	1.4464	1.4425	1.4388
0.1000	0.5999	0.3001	1.4507	1.4470	1.4432	1.4395	1.4358
0.1000	0.7000	0.2000	1.4473	1.4436	1.4399	1.4362	1.4325
0.1000	0.8002	0.0999	1.4440	1.4403	1.4365	1.4330	1.4293
0.1995	0.1022	0.6982	1.4542	1.4507	1.4470	1.4439	1.4407
0.1997	0.2011	0.5992	1.4517	1.4481	1.4445	1.4413	1.4379
0.1997	0.3008	0.4995	1.4493	1.4457	1.4420	1.4387	1.4353
0.2000	0.4002	0.3998	1.4462	1.4429	1.4396	1.4361	1.4326
0.1998	0.4996	0.3006	1.4437	1.4403	1.4369	1.4333	1.4298
0.1996	0.6007	0.1997	1.4410	1.4375	1.4339	1.4305	1.4271
0.1995	0.7003	0.1002	1.4380	1.4345	1.4310	1.4276	1.4241
0.2993	0.1019	0.5988	1.4468	1.4434	1.4399	1.4368	1.4337
0.2996	0.2007	0.4997	1.4446	1.4412	1.4377	1.4346	1.4313
0.2994	0.2998	0.4008	1.4421	1.4388	1.4354	1.4321	1.4287
0.2997	0.4005	0.2998	1.4396	1.4363	1.4330	1.4295	1.4261
0.3000	0.5001	0.1999	1.4370	1.4336	1.4301	1.4269	1.4236
0.2997	0.6003	0.1000	1.4344	1.4308	1.4274	1.4233	1.4195
0.3989	0.1016	0.4995	1.4412	1.4379	1.4345	1.4315	1.4284
0.3990	0.2017	0.3993	1.4389	1.4356	1.4321	1.4291	1.4260
0.3988	0.3010	0.3002	1.4370	1.4337	1.4305	1.4272	1.4239
0.3995	0.4000	0.2005	1.4333	1.4304	1.4275	1.4244	1.4214
0.3996	0.5003	0.1001	1.4318	1.4285	1.4251	1.4220	1.4189
0.4992	0.1012	0.3996	1.4367	1.4336	1.4304	1.4273	1.4242
0.4993	0.2001	0.3006	1.4346	1.4314	1.4281	1.4251	1.4220
0.4992	0.3008	0.1999	1.4325	1.4292	1.4259	1.4228	1.4197
0.4980	0.3998	0.1021	1.4304	1.4269	1.4232	1.4206	1.4176
0.5978	0.1021	0.3001	1.4332	1.4299	1.4267	1.4228	1.4191
0.5992	0.1999	0.2009	1.4312	1.4280	1.4247	1.4218	1.4187
0.5984	0.3009	0.1007	1.4292	1.4259	1.4224	1.4196	1.4166
0.6963	0.1033	0.2004	1.4302	1.4271	1.4239	1.4210	1.4181
0.6964	0.2009	0.1027	1.4284	1.4252	1.4220	1.4191	1.4161
0.7965	0.1030	0.1005	1.4277	1.4246	1.4215	1.4186	1.4157

[a] Standard uncertainty u are u(x) = 0.0005, u(T) = 0.05 K, $u(n_D)$ = 0.0005, x_1, x_2 and x_3 is the mol fraction of [BMIM][NTf_2], MEA and sulfolane respectively.

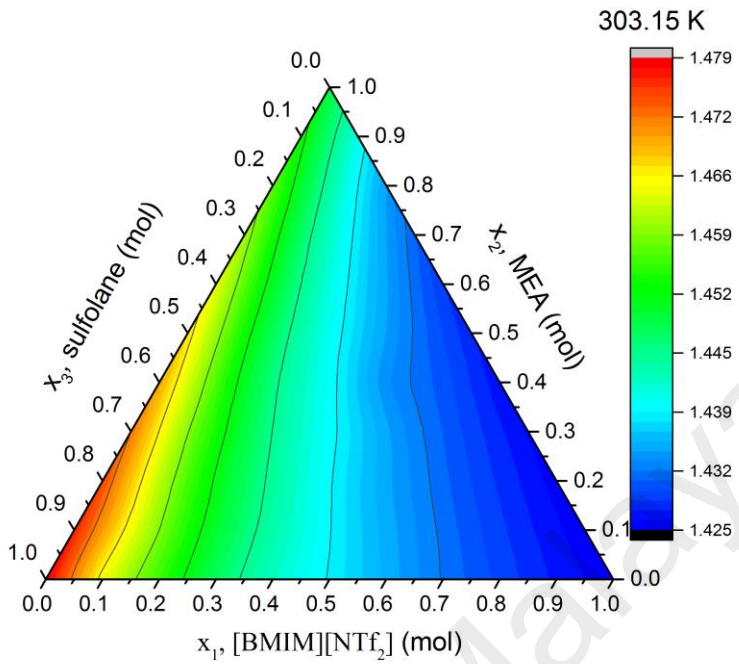

Figure 4.73: Refractive index of [BMIM][NTf_2] (1) + MEA (2) + sulfolane (3) mixture at T=303.15 K at various concentration

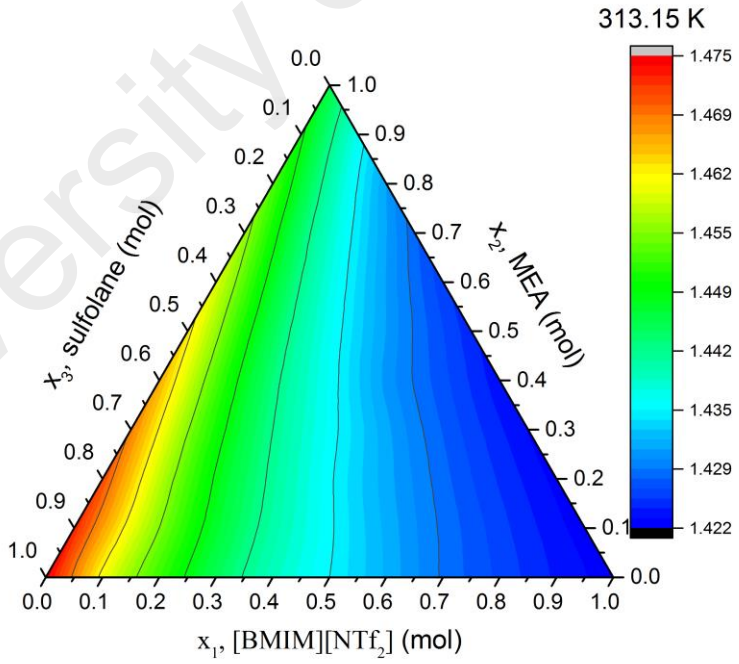

Figure 4.74: Refractive index of [BMIM][NTf_2] (1) + MEA (2) + sulfolane (3) mixture at T=313.15 K at various concentration

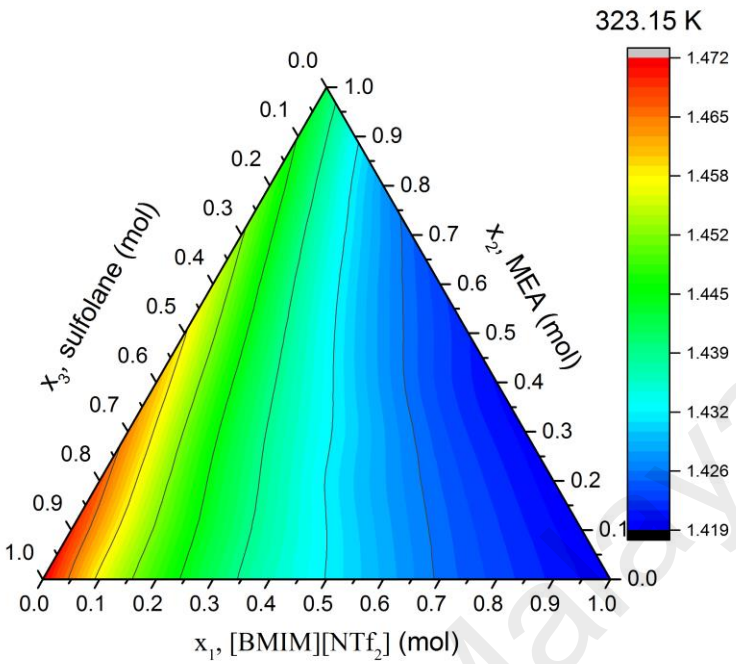

Figure 4.75: Refractive index of [BMIM][NTf_2] (1) + MEA (2) + sulfolane (3) mixture at T=323.15 K at various concentration

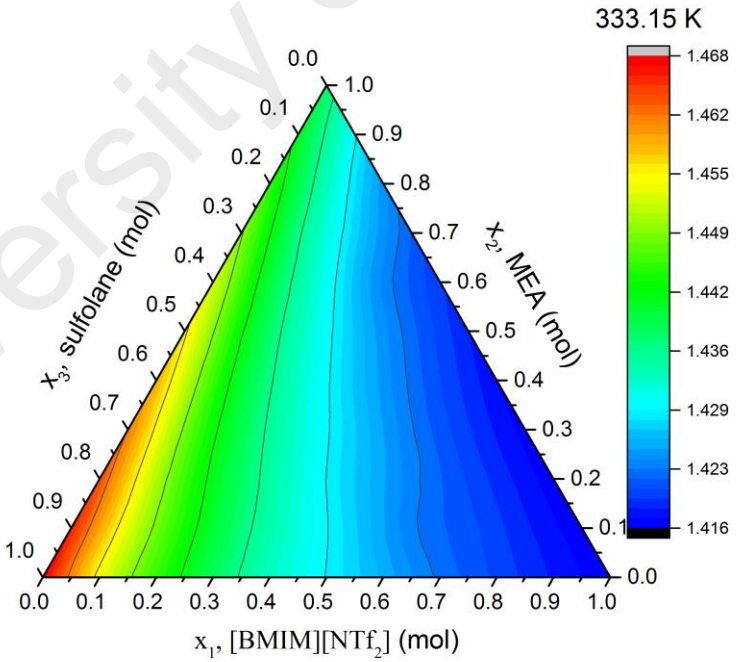

Figure 4.76: Refractive index of [BMIM][NTf_2] (1) + MEA (2) + sulfolane (3) mixture at T=333.15 K at various concentration

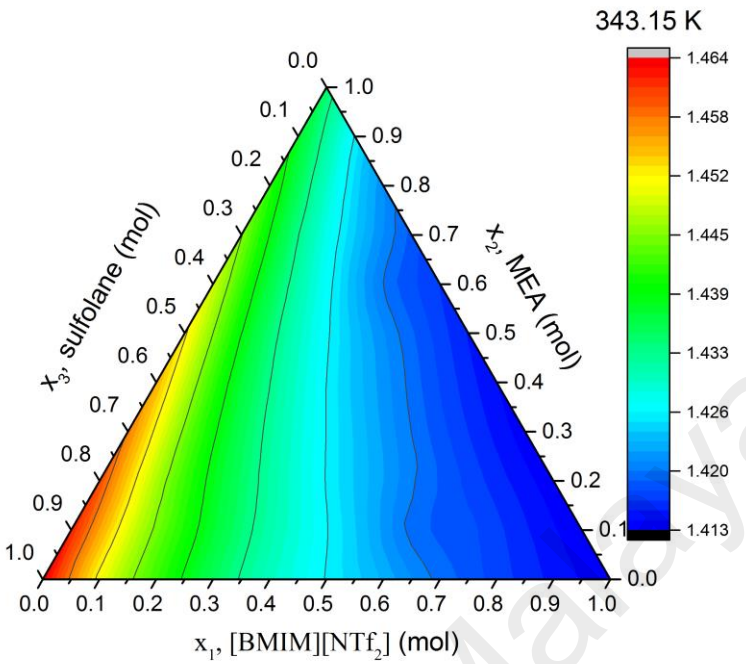

Figure 4.77: Refractive index of [BMIM][NTf_2] (1) + MEA (2) + sulfolane (3) mixture at T=343.15 K at various concentration

4.2.3.4 Refractive index deviation

Using the experimental refractive index data of the pure components and their binary mixtures, the values of refractive index deviation (Δn_D) for [BMIM][NTf_2] (1), MEA (2) and sulfolane (3) binary mixtures were calculated from the experimental refractive index of the mixtures using Equation 4.15.

$$\Delta n_D = n_{D\,mixture} - \sum_{i=1}^{n}(x_i n_{Di}) \quad (4.15)$$

where, x_i and η_{Di} represent the mol fraction and refractive index of pure component, respectively.

(a) Binary mixtures

The values of refractive index deviation of [BMIM][NTf_2] (1) + sulfolane (3), MEA (2) + sulfolane (3) and [BMIM][NTf_2] (1) + MEA (2) binary mixtures are summarized in Table 4.27 and represented by Figure 4.78 to Figure 4.80, respectively. Figure 4.78 shows that the Δn_D values are negative over the entire mol fraction range of [BMIM][NTf_2] at various temperatures with minimum of the asymmetric curve is at mol fraction x_1 = 0.4 [BMIM][NTf_2] for all temperatures range. Figure 4.79 shows that the Δn_D values are positive over the entire mol fraction range of MEA at various temperatures with maximum of the asymmetric curve is at mol fraction x_1 = 0.5 MEA for all temperatures range. Figure 4.80 shows that the Δn_D values are negative over the entire mol fraction range of [BMIM][NTf_2] at various temperatures with the minimum of the asymmetric curve at mol fraction x_1 = 0.3 [BMIM][NTf_2]. The refractive index deviation data were then correlated using a Redlich-Kister equation (Equation 4.11). The adjustable parameters, A*i*, are summarized in Table 4.27.

Table 4.27: Refractive index deviation (Δn_D) of [BMIM][NTf_2] (1), MEA (2) and sulfolane (3) binary mixtures at different temperatures and compositions

x_1	x_2	x_3	ρ, g cm^{-3}				
			303.15 K	**313.15 K**	**323.15 K**	**333.15 K**	**343.15 K**
[BMIM][NTf_2] (1) + sulfolane (3)							
0.0000	-	1.0000	0.0000	0.0000	0.0000	0.0000	0.0000
0.1000	-	0.9000	-0.0092	-0.0090	-0.0090	-0.0089	-0.0088
0.1999	-	0.8001	-0.0127	-0.0124	-0.0124	-0.0122	-0.0120
0.3001	-	0.6999	-0.0150	-0.0146	-0.0145	-0.0142	-0.0141
0.4000	-	0.6000	-0.0153	-0.0148	-0.0147	-0.0145	-0.0143
0.5001	-	0.4999	-0.0137	-0.0133	-0.0132	-0.0130	-0.0129
0.5999	-	0.4001	-0.0118	-0.0115	-0.0113	-0.0112	-0.0110
0.7000	-	0.3000	-0.0097	-0.0096	-0.0095	-0.0094	-0.0093
0.7995	-	0.2005	-0.0067	-0.0066	-0.0065	-0.0063	-0.0064
0.8985	-	0.1015	-0.0036	-0.0035	-0.0034	-0.0033	-0.0033
1.0000	-	0.0000	0.0000	0.0000	0.0000	0.0000	0.0000
MEA (2) + sulfolane (3)							
-	0.0000	1.0000	0.0000	0.0000	0.0000	0.0000	0.0000
-	0.0999	0.9001	0.0010	0.0009	0.0009	0.0012	0.0012
-	0.2001	0.7999	0.0018	0.0016	0.0016	0.0021	0.0020
-	0.3001	0.6999	0.0024	0.0021	0.0020	0.0028	0.0027
-	0.3999	0.6001	0.0027	0.0024	0.0023	0.0032	0.0031
-	0.4999	0.5001	0.0028	0.0026	0.0024	0.0034	0.0032
-	0.5999	0.4001	0.0027	0.0024	0.0023	0.0032	0.0031
-	0.6999	0.3001	0.0024	0.0021	0.0020	0.0028	0.0027
-	0.8000	0.2000	0.0018	0.0016	0.0016	0.0021	0.0020
-	0.8999	0.1001	0.0010	0.0009	0.0009	0.0012	0.0012
-	1.0000	0.0000	0.0000	0.0000	0.0000	0.0000	0.0000
[BMIM][NTf_2] (1) + MEA (2)							
0.0000	1.0000	-	0.0000	0.0000	0.0000	0.0000	0.0000
0.1001	0.8999	-	-0.0076	-0.0071	-0.0063	-0.0067	-0.0068
0.2000	0.8000	-	-0.0113	-0.0106	-0.0096	-0.0097	-0.0096
0.3000	0.7000	-	-0.0119	-0.0112	-0.0101	-0.0102	-0.0100
0.4000	0.6000	-	-0.0118	-0.0109	-0.0098	-0.0099	-0.0097
0.4999	0.5001	-	-0.0102	-0.0097	-0.0090	-0.0089	-0.0087
0.6000	0.4000	-	-0.0088	-0.0084	-0.0081	-0.0078	-0.0075
0.6999	0.3001	-	-0.0067	-0.0065	-0.0062	-0.0061	-0.0060
0.8000	0.2000	-	-0.0045	-0.0044	-0.0042	-0.0041	-0.0040
0.8998	0.1002	-	-0.0024	-0.0023	-0.0022	-0.0021	-0.0020
1.0000	0.0000	-	0.0000	0.0000	0.0000	0.0000	0.0000

[a] Standard uncertainty u are u(x) = 0.0005, u(T) = 0.05 K, and u(n_D) = 0.0005, x_1, x_2, and x_3 is the mol fraction of [BMIM][NTf_2], MEA and sulfolane, respectively.

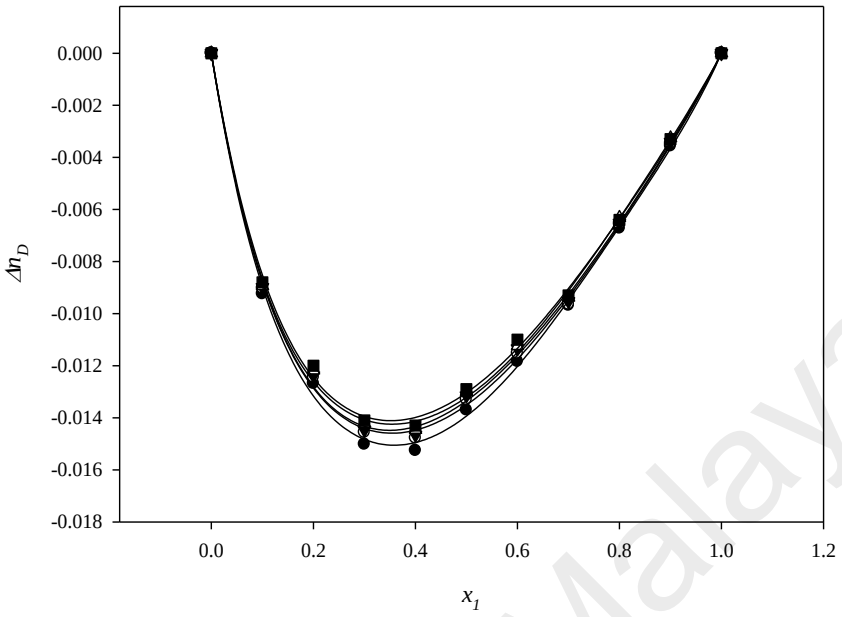

Figure 4.78: Refractive index deviation of [BMIM][NTf_2] (1) + sulfolane (3) binary mixtures against temperature as function of [BMIM][NTf_2] mol fraction; (●) 303.15 K; (○) 313.15 K; (▼) 323.15 K; (△) 333.15 K; (■) 343.15 K

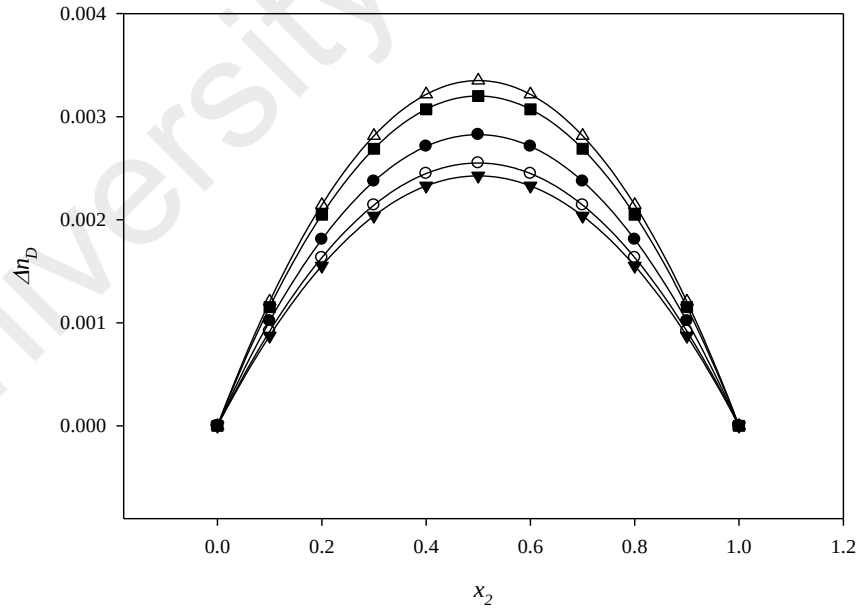

Figure 4.79: Refractive index deviation of MEA (2) + sulfolane (3) binary mixtures against temperature; (●)T = 298.15 K, (○)T = 303.15 K, (▼)T = 313.15 K, (△)T = 323.15 K, (■)T = 333.15 K, (□)T = 343.15 K

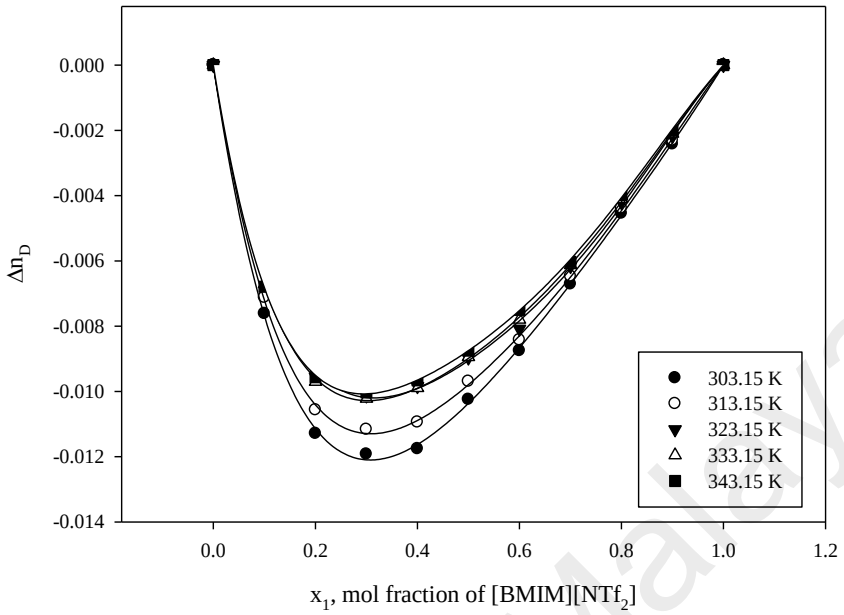

Figure 4.80: Refraction index deviation (Δn_D) of binary mixtures [BMIM][NTf_2] (1) + MEA (2) at various temperatures

Table 4.28:Redlich-Kister fitting coefficients A_i of the refractive index deviation (Δn_D) of [BMIM][NTf_2] (1) + sulfolane (3) binary mixtures as a function of various temperatures along with their fitting deviations, σ

T / K	A_0	A_1	A_2	A_3	A_4	R^2	σ[a]
[BMIM][NTf_2] (1) + sulfolane (3)							
303.15	-0.0557	0.0301	-0.0106	0.0105	-0.0185	0.9982	0.0003
313.15	-0.0540	0.0279	-0.0140	0.0132	-0.0132	0.9982	0.0003
323.15	-0.0534	0.0281	-0.0156	0.0131	-0.0110	0.9981	0.0003
333.15	-0.0528	0.0270	-0.0124	0.0159	-0.0145	0.9980	0.0003
343.15	-0.0522	0.0272	-0.0139	0.0129	-0.0127	0.9977	0.0003
MEA (2) + sulfolane (3)							
303.15	0.0113	-6.9630×10^{-19}	5.7715×10^{-18}	6.5450×10^{-18}	-10.246×10^{-18}	0.9999	2.7990
313.15	0.0102	21.666×10^{-19}	-4.6137×10^{-18}	7.7320×10^{-18}	12.022×10^{-18}	0.9999	3.1298
323.15	0.0097	6.2277×10^{-19}	38.52×10^{-18}	4.0029×10^{-18}	1.2711×10^{-18}	0.9999	2.8342
333.15	0.0134	-8.6482×10^{-19}	4.903×10^{-18}	6.7453×10^{-18}	2.7636×10^{-18}	0.9999	1.7705
343.15	0.0128	-9.7762×10^{-19}	1.1447×10^{-18}	6.3621×10^{-18}	2.9341×10^{-18}	0.9999	2.7994
[BMIM][NTf_2] (1) + MEA (2)							
303.15	-0.0112	-0.0062	-0.0109	-0.0096	-0.0013	0.9871	0.0002
313.15	-0.0069	-0.0070	-0.0113	0.0008	-0.00002	0.9816	0.0001
323.15	-0.0057	-0.0080	-0.0114	-0.0002	0.0005	0.9894	0.0001
333.15	-0.0047	-0.0067	-0.0081	-0.0011	-0.0011	0.9903	0.0001
343.15	-0.0043	-0.0070	-0.0058	0.0080	0.0014	0.9861	0.0001

[a]σ = standard deviation, Equation 4.9

(b) Ternary mixtures

The values of refractive index deviation (Δn_D) were calculated from the experimental refractive index value of the mixture using Equation 4.15. Figure 4.81 to Figure 4.85 show the refractive index deviation for the ternary mixtures at constant temperature with temperatures range from 303.15 to 343.15 K, respectively. In general, the negative value of the refractive index deviation are observed over the whole compositions and temperature range. The negative refractive index deviation is more prominent in ternary mixture with mol fraction ratio of 0.4 [BMIM][NTf_2]: 0.5 MEA: 0.1 sulfolane. The negative values of refractive index deviation indicate characteristic of mixtures without strong specific interactions (Pires et al., 2013). Furthermore, the refractive index deviation values become more negative with increasing of the temperatures over the whole range of composition.

Table 4.29: Refractive index deviation (Δn_D) of [BMIM][NTf_2] (1) + MEA (2) + sulfolane (3) ternary mixtures at different temperatures and compositions

[BMIM][NTf_2] (1) + MEA (2) + sulfolane (3)							
x_1	x_2	x_3	Δn_D				
			303.15 K	**313.15 K**	**323.15 K**	**333.15 K**	**343.15 K**
0.0999	0.1003	0.7998	-0.00648	-0.01038	-0.01438	-0.01778	-0.02128
0.0998	0.2000	0.7002	-0.00624	-0.00994	-0.01374	-0.01734	-0.02094
0.0997	0.3015	0.5988	-0.00605	-0.00975	-0.01355	-0.01705	-0.02055
0.1000	0.4005	0.4995	-0.00582	-0.00952	-0.01322	-0.01692	-0.02052
0.0999	0.5004	0.3997	-0.00587	-0.00947	-0.01297	-0.01687	-0.02057
0.1000	0.5999	0.3001	-0.00583	-0.00953	-0.01333	-0.01703	-0.02073
0.1000	0.7000	0.2000	-0.00638	-0.01008	-0.01378	-0.01748	-0.02118
0.1000	0.8002	0.0999	-0.00697	-0.01067	-0.01447	-0.01797	-0.02167
0.1995	0.1022	0.6982	-0.01103	-0.01453	-0.01823	-0.02133	-0.02453
0.1997	0.2011	0.5992	-0.01084	-0.01444	-0.01804	-0.02124	-0.02464
0.1997	0.3008	0.4995	-0.01040	-0.01400	-0.01770	-0.02100	-0.02440
0.2000	0.4002	0.3998	-0.01065	-0.01395	-0.01725	-0.02075	-0.02425

Table 4.29, continued

x_1	x_2	x_3	Δn_D				
			303.15 K	**313.15 K**	**323.15 K**	**333.15 K**	**343.15 K**
0.1998	0.4996	0.3006	-0.01033	-0.01373	-0.01713	-0.02073	-0.02423
0.1996	0.6007	0.1997	-0.01016	-0.01366	-0.01726	-0.02066	-0.02406
0.1995	0.7003	0.1002	-0.01033	-0.01383	-0.01733	-0.02073	-0.02423
0.2993	0.1019	0.5988	-0.01322	-0.01662	-0.02012	-0.02322	-0.02632
0.2996	0.2007	0.4997	-0.01259	-0.01599	-0.01949	-0.02259	-0.02589
0.2994	0.2998	0.4008	-0.01228	-0.01558	-0.01898	-0.02228	-0.02568
0.2997	0.4005	0.2998	-0.01189	-0.01519	-0.01849	-0.02199	-0.02539
0.3000	0.5001	0.1999	-0.01164	-0.01504	-0.01854	-0.02174	-0.02504
0.2997	0.6003	0.1000	-0.01140	-0.01500	-0.01840	-0.02250	-0.02630
0.3989	0.1016	0.4995	-0.01348	-0.01678	-0.02018	-0.02318	-0.02628
0.3990	0.2017	0.3993	-0.01293	-0.01623	-0.01973	-0.02273	-0.02583
0.3988	0.3010	0.3002	-0.01201	-0.01531	-0.01851	-0.02181	-0.02511
0.3995	0.4000	0.2005	-0.01285	-0.01575	-0.01865	-0.02175	-0.02475
0.3996	0.5003	0.1001	-0.01148	-0.01478	-0.01818	-0.02128	-0.02438
0.4992	0.1012	0.3996	-0.01261	-0.01571	-0.01891	-0.02201	-0.02511
0.4993	0.2001	0.3006	-0.01188	-0.01508	-0.01838	-0.02138	-0.02448
0.4992	0.3008	0.1999	-0.01097	-0.01427	-0.01757	-0.02067	-0.02377
0.4980	0.3998	0.1021	-0.01032	-0.01382	-0.01752	-0.02012	-0.02312
0.5978	0.1021	0.3001	-0.01079	-0.01409	-0.01729	-0.02119	-0.02489
0.5992	0.1999	0.2009	-0.00993	-0.01313	-0.01643	-0.01933	-0.02243
0.5984	0.3009	0.1007	-0.00909	-0.01239	-0.01589	-0.01869	-0.02169
0.6963	0.1033	0.2004	-0.00847	-0.01157	-0.01477	-0.01767	-0.02057
0.6964	0.2009	0.1027	-0.00748	-0.01068	-0.01388	-0.01678	-0.01978
0.7965	0.1030	0.1005	-0.00559	-0.00869	-0.01179	-0.01469	-0.01759

[a] Standard uncertainty u are u(x) = 0.0005, u(T) = 0.05 K, $u(n_D)$ = 0.0005, x_1, x_2 and x_3 is the mol fraction of [BMIM][NTf_2], MEA and sulfolane respectively.

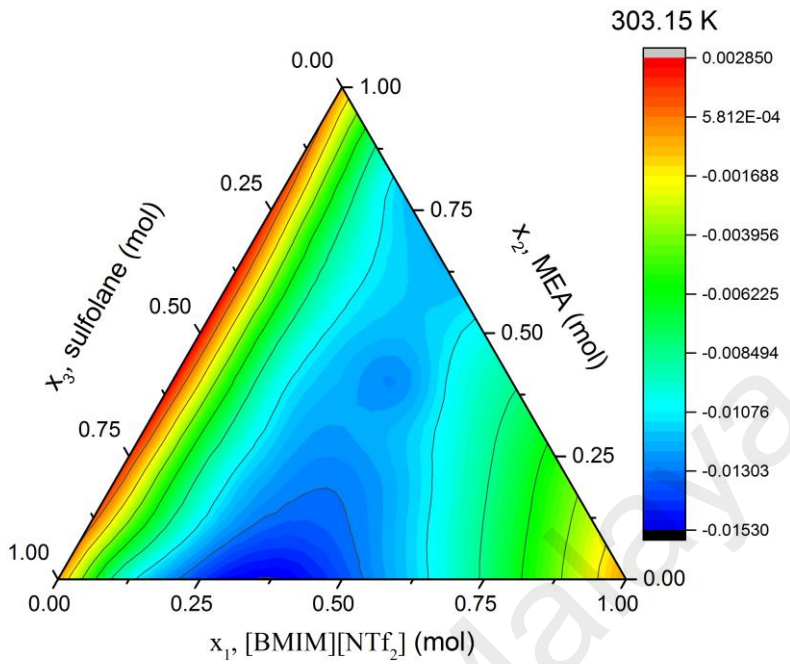

Figure 4.81: Refractive index deviation (Δn_D) of [BMIM][NTf_2] (1) + MEA (2) + sulfolane (3) ternary mixtures at T = 303.15 K

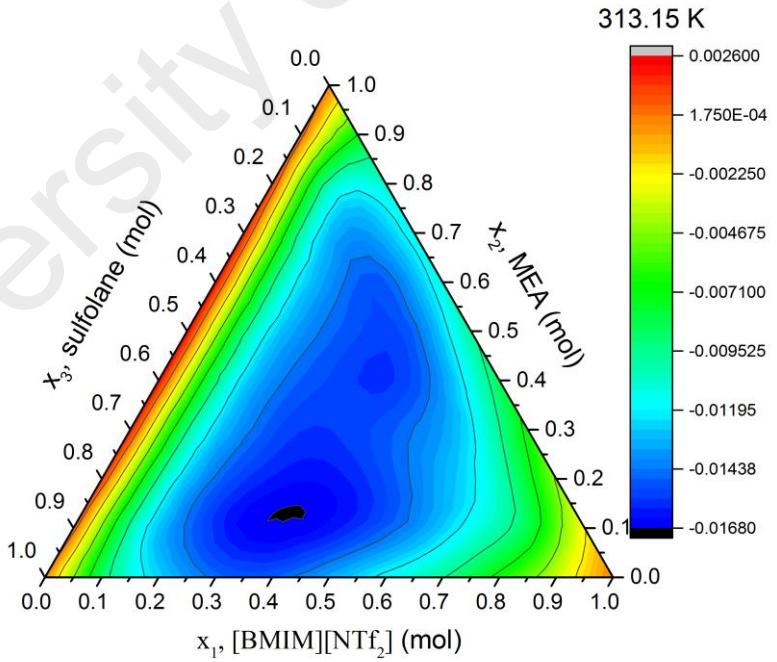

Figure 4.82: Refractive index deviation (Δn_D) of [BMIM][NTf_2] (1) + MEA (2) + sulfolane (3) ternary mixtures at T = 313.15 K

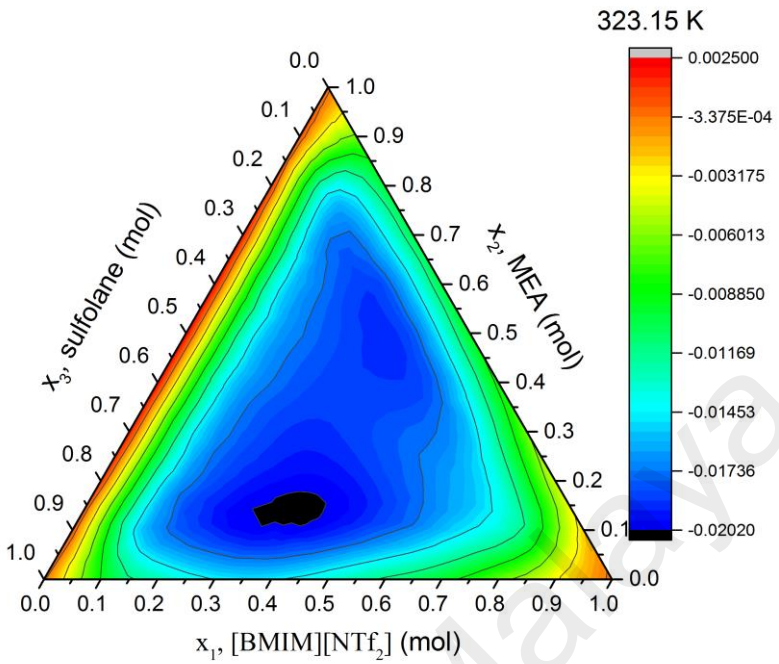

Figure 4.83: Refractive index deviation (Δn_D) of [BMIM][NTf_2] (1) + MEA (2) + sulfolane (3) ternary mixtures at T = 323.15 K

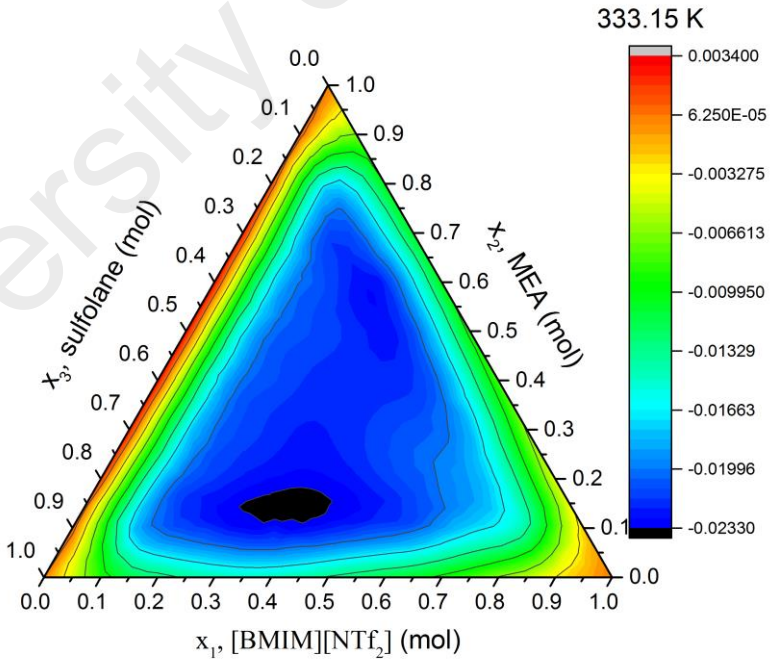

Figure 4.84: Refractive index deviation (Δn_D) of [BMIM][NTf_2] (1) + MEA (2) + sulfolane (3) ternary mixtures at T = 333.15 K

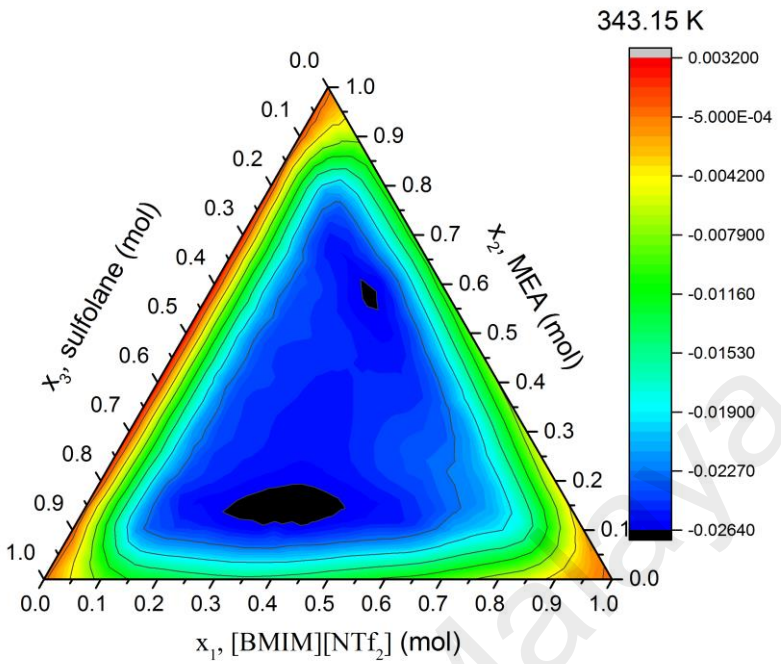

Figure 4.85: Refractive index deviation (Δn_D) of [BMIM][NTf_2] (1) + MEA (2) + sulfolane (3) ternary mixtures at T = 343.15 K

4.3 COSMO-RS modelling

4.3.1 Introduction

In this study, we attempted to elucidate the molecular interaction between the component of binary and ternary mixtures over the whole range of composition using a conductor-like screening model for realistic solvation (COSMO-RS) computational method. This model is independent of experimental data and uses the molecular structure to determine the Screening Charge Densities (SCDs) of sigma (σ) profile and potential of the pure molecule. This is the only indicator in computing the chemical potential of the component in solution. The σ-profile generated by COSMO*therm* is used to describe the polarity for the compound molecule by identifying the interaction energies between different molecules in the solution mixtures. The polarity effect has been analyzed for the [BMIM][NTf_2]-sulfolane, MEA-sulfolane, [BMIM][NTf_2]-MEA binary mixtures and [BMIM][NTf_2]-MEA-sulfolane ternary mixtures over the whole composition.

4.3.2 σ-profile, σ-potential, activity coefficient and excess enthalpies

For further understanding of the molecular interaction in term of molecular polarity, electrostatic interaction, hydrogen bond affinity and hydrophobicity in [BMIM][NTf_2]-sulfolane, MEA-sulfolane, [BMIM][NTf_2]-MEA binary mixtures and [BMIM][NTf_2]-MEA-sulfolane ternary mixtures, a 3D polarized charged distribution (σ, sigma) on the molecular surface of the individual components resulted from the quantum chemical calculation were generated using COSMO-RS model as represented in Figure 4.86 to Figure 4.89. The 3D

screening charge distribution on the molecular surface were visualized using a histogram σ-profile, which used to qualitatively describe the molecule and predict the possible interaction of the components in liquid mixture (Gonzalez-Miquel et al., 2014). The σ-profile histogram is divided into 3 main regions; hydrogen bond donor region ($\sigma < -0.0082$ e/Å^2), hydrogen bond acceptor region ($\sigma > 0.0082$ e/Å^2) and non-polar region ($-0.0082 < \sigma < 0.0082$ e/Å^2). Figure 4.90 shows the σ-profile of $[BMIM]^+$ cation, $[NTf_2]^-$ anion, MEA and sulfolane molecules.

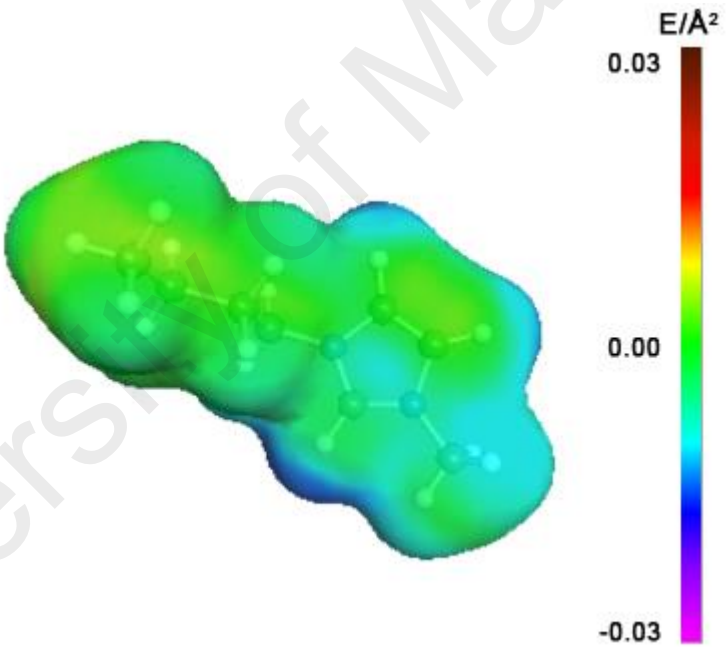

Figure 4.86: 3D screening charge distribution for $[BMIM]^+$ cation molecule

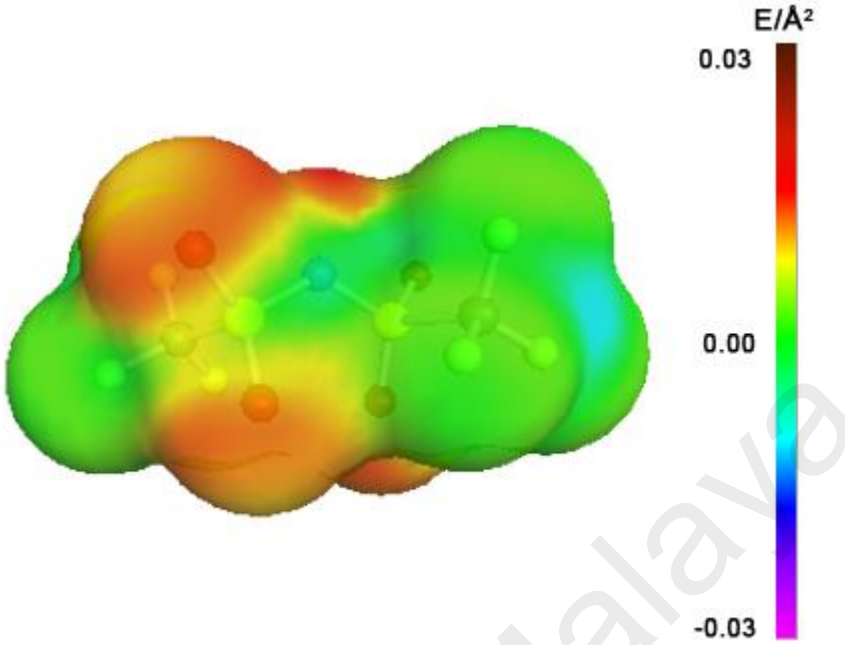

Figure 4.87: 3D screening charge distribution for $[NTf_2]^-$ anion molecule

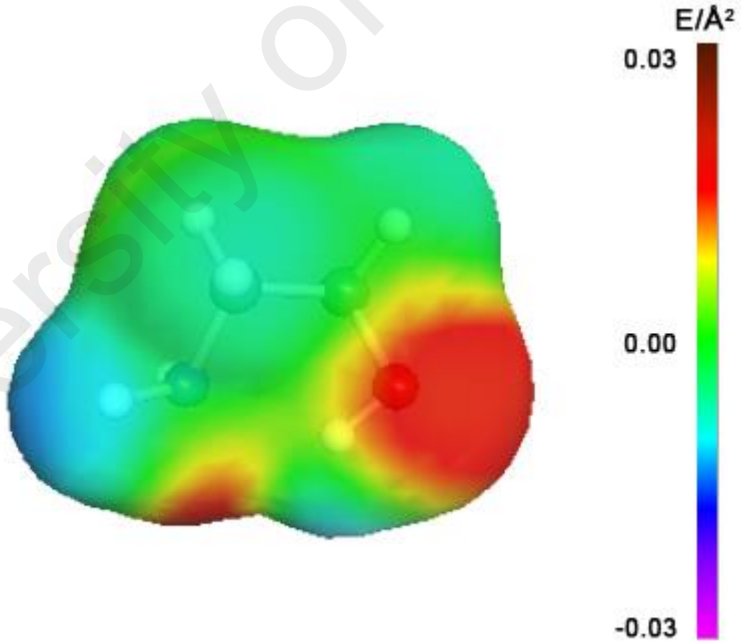

Figure 4.88: 3D screening charge distribution for MEA molecule

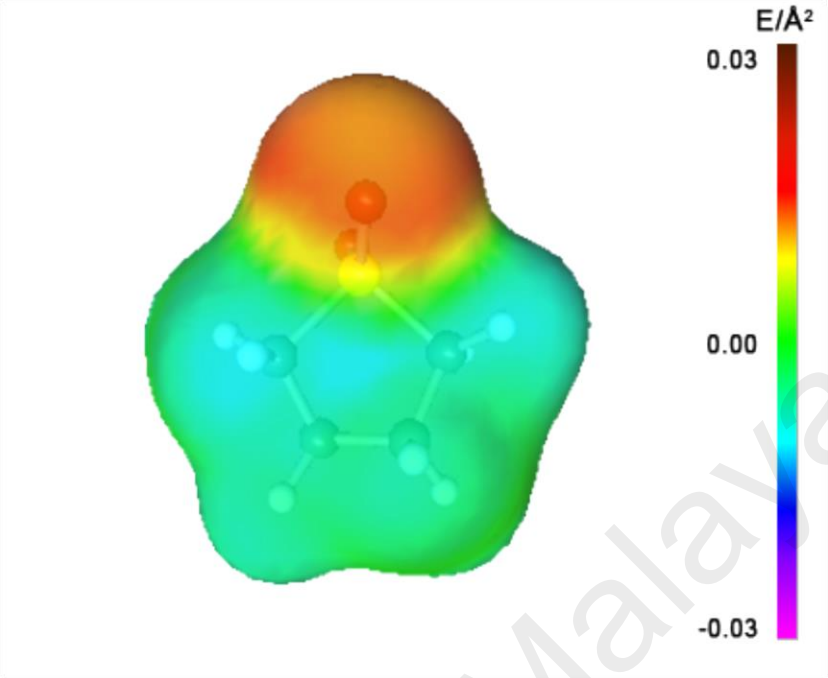

Figure 4.89: 3D screening charge distribution for sulfolane molecule

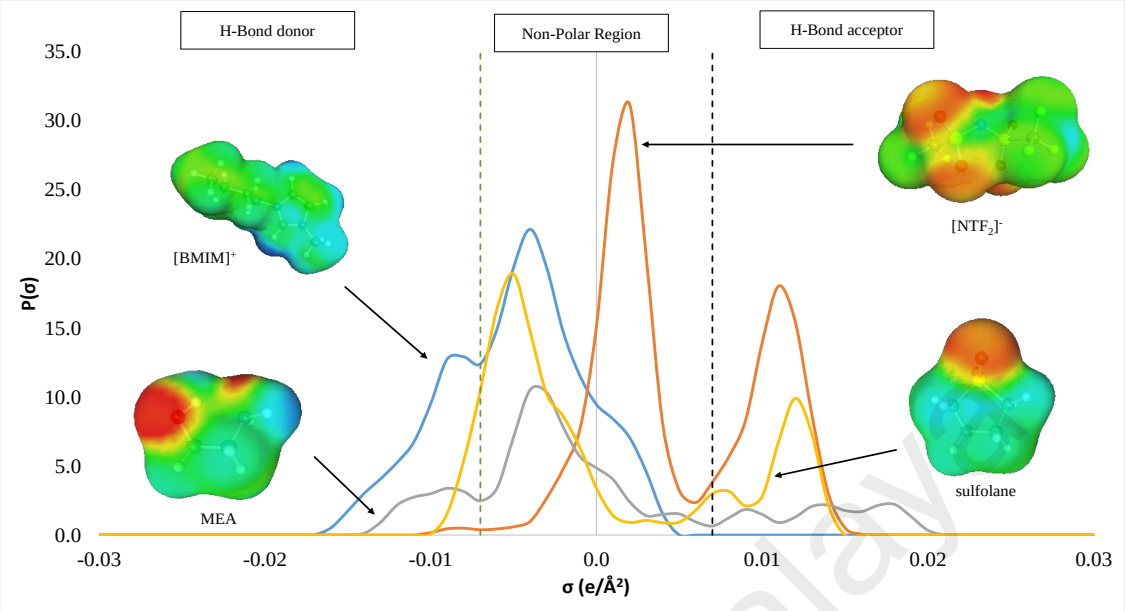

(a)

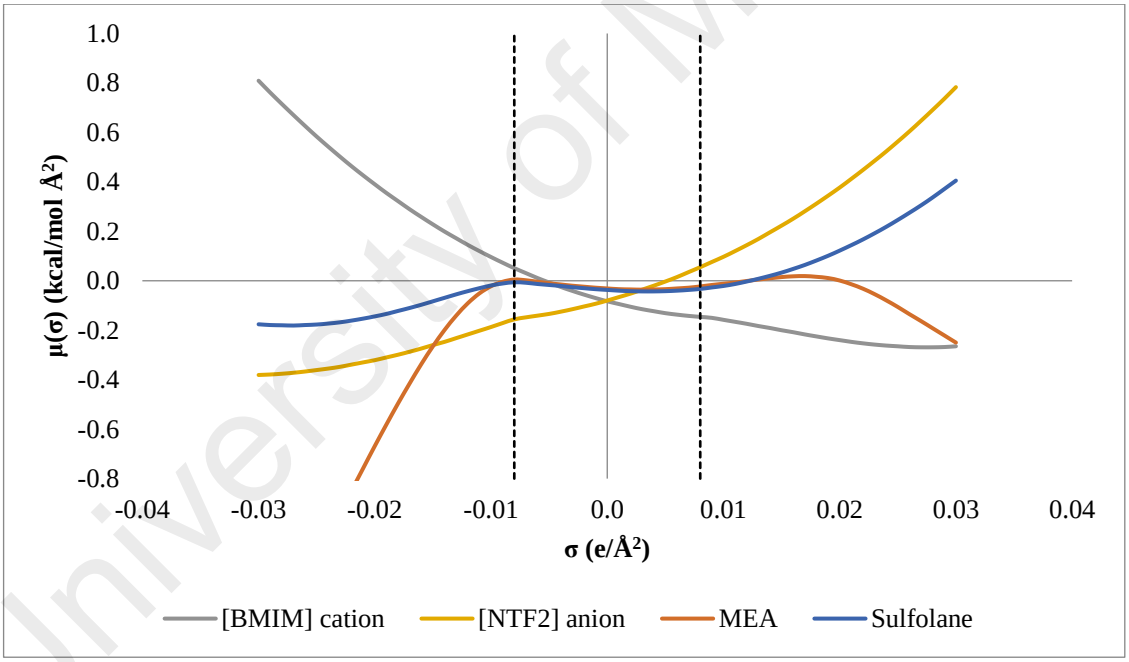

(b)

Figure 4.90: σ-profile (a) and σ-potential (b) of $[BMIM]^+$ cation, $[NTf_2]^-$ anion, MEA and sulfolane predicted by COSMO-RS model

Figure 4.90 shows σ-profile and σ-potential for $[BMIM]^+$ cation, $[NTf_2]^-$ anion, MEA and sulfolane generated by COSMO-RS model. σ-profile for $[BMIM]^+$ cation is dominated by a main peak at -0.004 e/Å^2 with a large distribution in the non-polar region of the histogram attributed to the aliphatic alkyl chain and the aromatic head group (green color sigma surface). A peak, -0.009 e/Å^2 in the hydrogen bond donor region is due to the acidic hydrogen atom of the aromatic ring (blue color sigma surface). σ-profile for $[NTf_2]^-$ anion with a prominent peak at +0.003 e/Å^2 in the non-polar region attributed to the non-polar fluorinated alkyl group (green color sigma surface). A peak, +0.011 e/Å^2 in the hydrogen bond acceptor region is due to the polar sulfonyl group (red color sigma surface). σ-potential shows a negative value $\sigma > 0.0082$ e/Å^2 for $[BMIM]^+$ cation which indicates an affinity to a hydrogen bond acceptor while a negative value at $\sigma < -0.0082$ e/Å^2 for $[NTf_2]^-$ anion exhibits an affinity toward hydrogen bond donor.

The σ-profile of MEA illustrates MEA behavior as amphoteric compounds, indicating their ability to act as H-bond acceptors (basic character) and also as H-bond donor groups (acid character). A peak at -0.009 e/Å^2 in the hydrogen bond donor region is attributed to the polar hydrogen of the hydroxyl and an amine group (blue color sigma surface). MEA molecule displays multiple peaks in the hydrogen bond acceptor region arising from the lone pair of the oxygen atom of the hydroxyl group as well as the lone pair of the nitrogen atom of the amine group (red color sigma surface). Strong non-polar peak at -0.005 e/Å^2 is attributed to the C-C backbone of the ethanolamine molecule. σ-potential for MEA displays a negative at both $\sigma < -0.0082$ e/Å^2 and $\sigma > 0.0082$ e/Å^2 which indicates affinity to both hydrogen bond donor and hydrogen bond acceptor Therefore, it can be concluded that self-association might be favorable interactions between the MEA molecules.

In Figure 4.90, σ-profile for sulfolane presents a highly polarized charged distribution at +0.012 e/Å^2 which is assigned to the sulfonyl group (red colored sigma surface) showing its ability to act as hydrogen bond acceptor (basic character). Moreover, sulfolane presents a peak at -0.006 e/Å^2 within the non-polar region due to the four-carbon ring bonded to the sulfur atom (green colored sigma surface). σ-potential for sulfolane presents a negative value at $\sigma < -0.0082$ e/Å^{2}which indicates an affinity to a hydrogen bond donor and a positive value at $\sigma > 0.0082$ e/Å^2 corresponds with no affinity to hydrogen bond acceptor. From the overall analysis of the σ-profile of sulfolane, a distribution charge on the σ polarity scale around hydrogen bond acceptor region indicates the ability of sulfolane to act as a base. Hence it is possible to forecast that component with hydrogen bond donor groups (acidic character) able to develop a favorable intermolecular interaction with sulfolane. Furthermore, sulfolane is shown to possess high dipole moment due to presence of only H-bond acceptor region in the molecule.

For predicting molecular interaction, COSMO-RS focuses on three specific interactions which is the electrostatic-misfit energy (E_{MF}), hydrogen bonding energy (E_{HB}) and van der Waals energy, (H_{VdW}). These energies were described in Eq. 2.19 to 2.21 in Chapter 2. In COSMO-RS calculation. Interaction energy of excess enthalpies were defined as difference in enthalpy of solute molecules *i* in its pure and mixture state (Kurnia & Coutinho, 2013).

$$H_i^{\,E}\,(interaction) = \; H_{i,mixture}(interaction) - \; H_{i,pure}(interaction) \qquad (4.16)$$

The H_i^E (interaction) in the calculation in the sums of the specific interaction; electrostatic-misfit energy (H_{MF}^E), hydrogen bonding energy (H_{HB}^E) and van der Waals energy, (H_{VdW}^E) as follows:

$$H_m^E = H_{MF}^E + H_{HB}^E + H_{VdW}^E \quad (4.17)$$

The final equation for calculating the excess enthalpies can be express as

$$H_m^E = H_{i,MF}^E + H_{i,HB}^E + H_{i,VdW}^E \quad (4.18)$$

4.3.2.1 [BMIM][NTf_2] (1) + sulfolane (3) binary mixtures

Figure 4.91 shows σ-profile and σ-potential for $[BMIM]^+$ cation, $[NTf_2]^-$ anion and sulfolane generated by COSMO-RS model. σ-profile for $[BMIM]^+$ and $[NTf_2]^-$ show a H-bond donor and H-bond acceptor, respectively the complement each of the ion pairs. Both $[BMIM]^+$ cation and $[NTf_2]^-$ anion show a peak in the non-polar region. Similarly, sulfolane has a peak in the non-polar region, which suggests the possibility of weak interaction predominates in these systems. Moreover, the relatively small sulfolane molecule easily fits into the free volume between the comparatively large ions of the [BMIM][NTf_2].

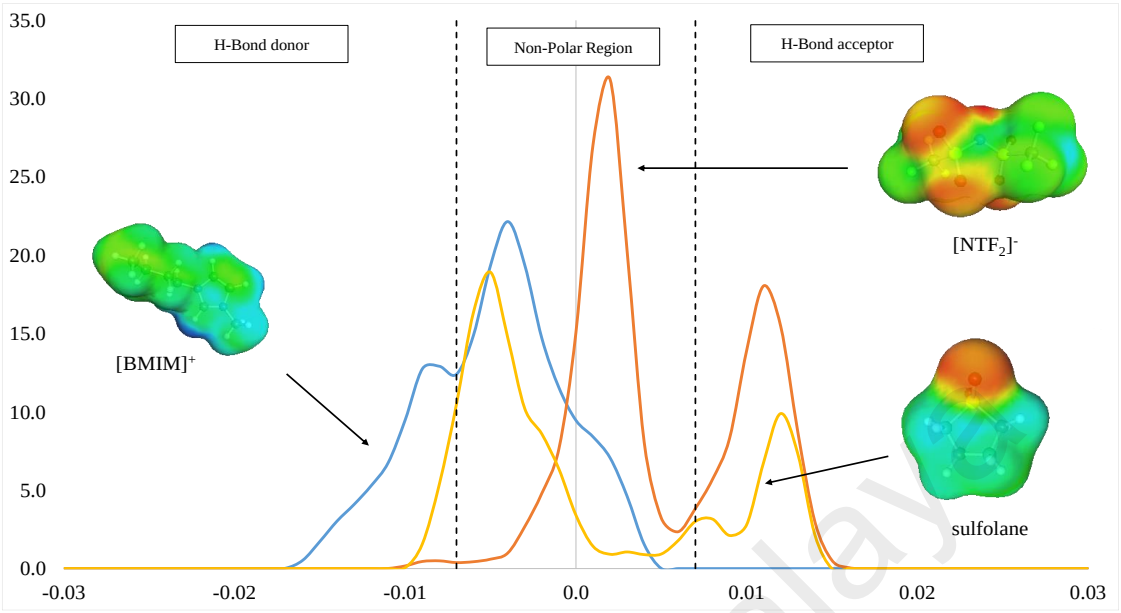

(a)

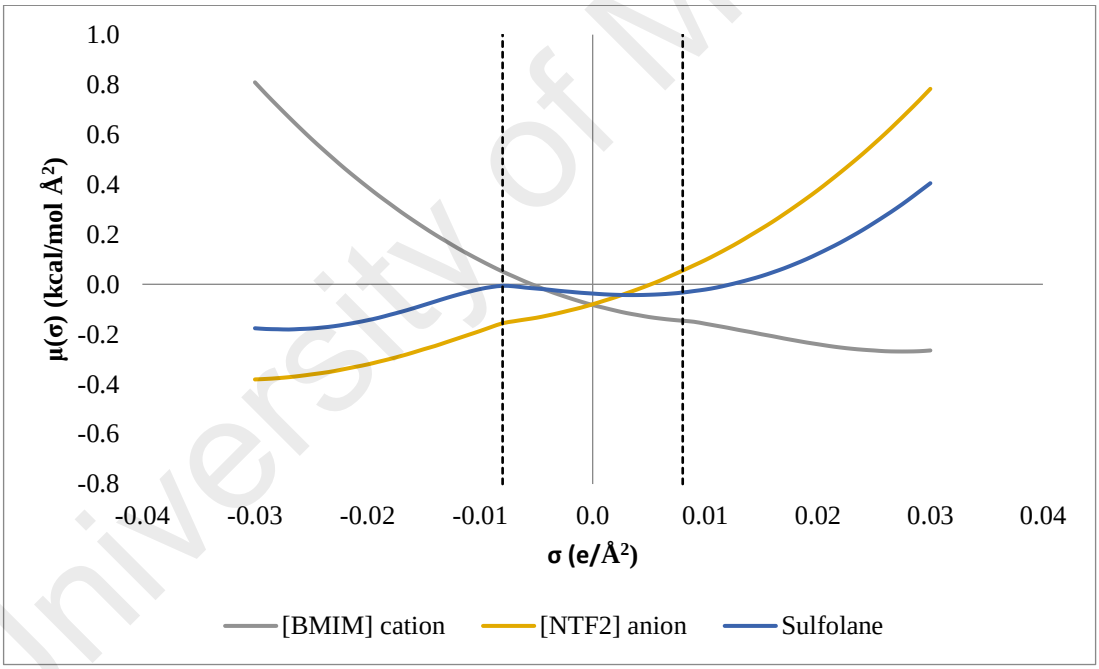

(b)

Figure 4.91: σ-profile (a) and σ-potential (b) of $[BMIM]^+$ cation, $[NTf_2]^-$ anion, sulfolane predicted by COSMO-RS model

Figure 4.92 shows the predicted activity coefficient for [BMIM][NTf_2] and sulfolane in the [BMIM][NTf_2] + sulfolane binary mixture at 298.15 K. The predicted activity coefficient for [BMIM][NTf_2] increases while predicted activity coefficient sulfolane decreases with the increasing mol fraction of [BMIM][NTf_2] in the mixture and has an activity coefficient value lower than 1 over the whole composition. This indicates a stronger unlike interactions compare to like interaction which leads to an attraction between unlike molecules (Tosun, 2013).

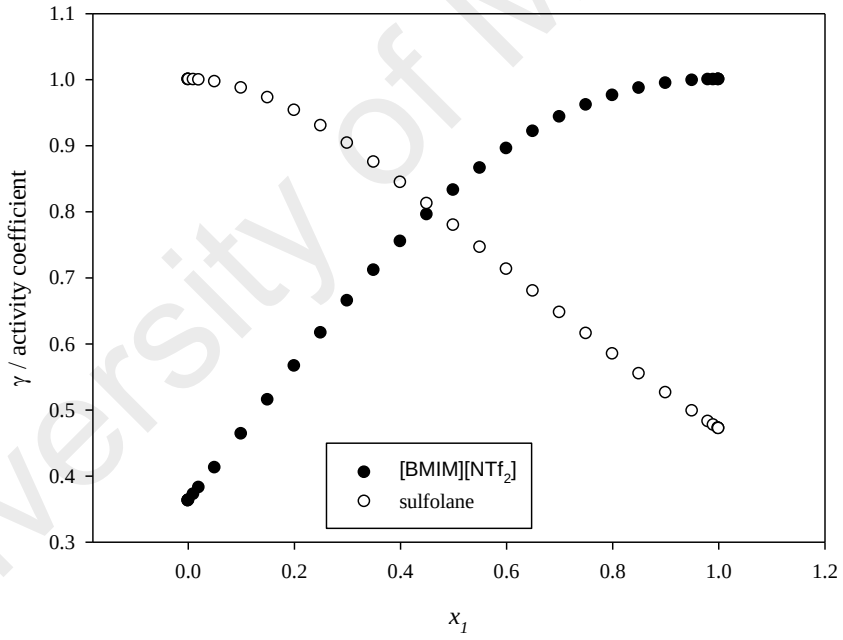

Figure 4.92: Activity coefficient for [BMIM][NTf_2] (1) + sulfolane (3) binary mixtures as function of [BMIM][NTf_2] mol fraction at T = 298.15 K

Figure 4.93 shows the predicted excess enthalpies for the [BMIM][NTf_2] + sulfolane binary mixture at 298.15 K. The graph shows that the mixture has a negative excess enthalpy predominantly attributed to electrostatic misfit energy followed by hydrogen bonding energy. The negative enthalpy by electrostatic misfit is due to the increase of molecular contact via efficient packing of sulfolane molecule into the [BMIM][NTf_2] lattice in the mixture. Subsequently, the negative excess enthalpy by hydrogen bonding is due to increase of hydrogen bonding between H atom in the $[BMIM]^+$ imidazolium ring with sulfonyl group from sulfolane.

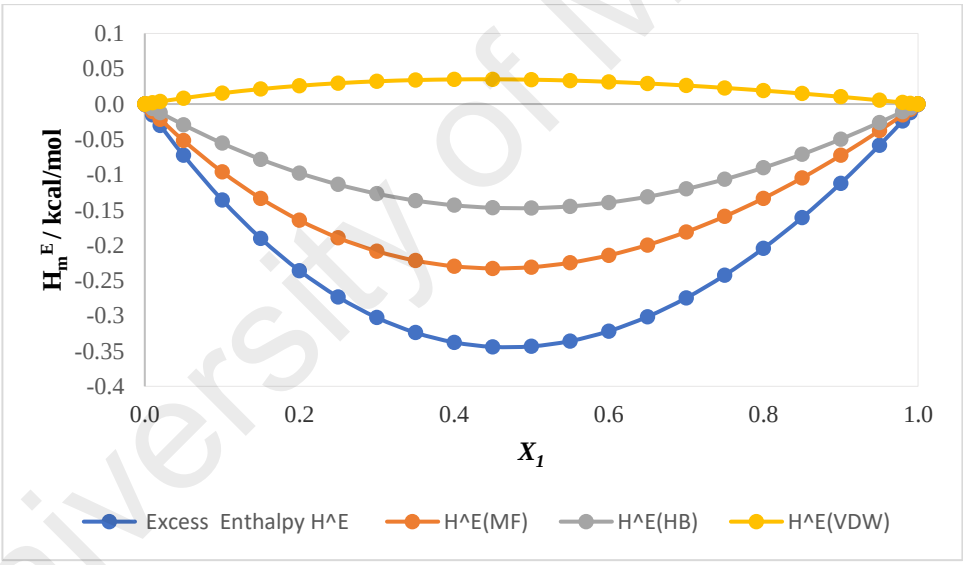

Figure 4.93: Predicted excess enthalpies for [BMIM][NTf_2] (1) + sulfolane (3) binary mixtures as function of [BMIM][NTf_2] mol fraction at T = 298.15 K

4.3.2.2 MEA (2) + sulfolane (3) binary mixtures

As shown in Figure 4.94, MEA has an amphoteric characteristic with both H-bond donor and H-bond acceptor present in the molecule. This suggests a strong intramolecular H-bonding with each MEA molecule. On the other hand, sulfolane present with an H-bond acceptor which may break the existing MEA intramolecular H-bonding which lead to expansion of mixture volume. Similarly, presence of peak in the non-polar region in both molecules with sulfolane exhibit a prominent peak in non-polar region at -0.006 e/Å^2 with higher intensity than MEA non-polar peak. This indicates the possibility of weak van der Waal's interaction predominates in these binary mixtures.

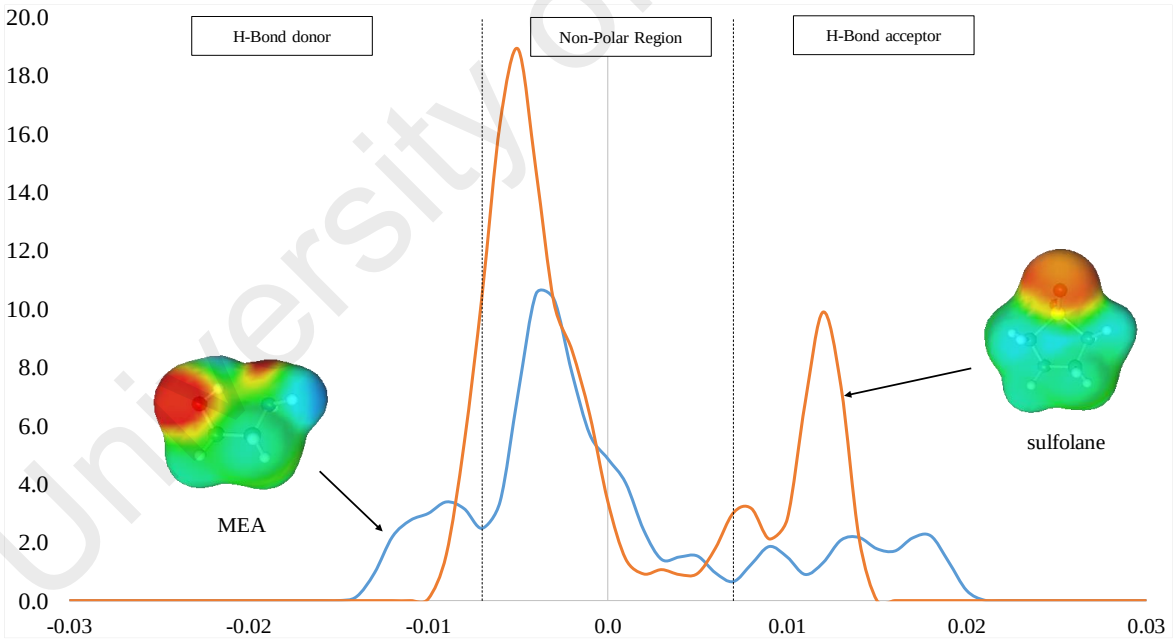

(a)

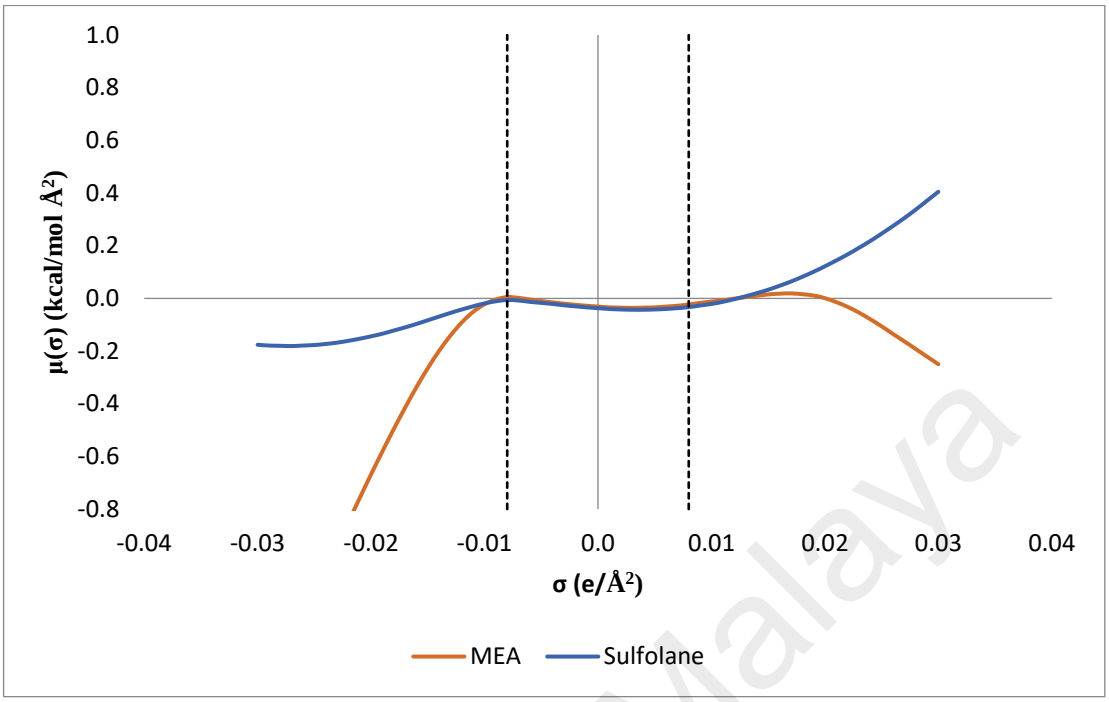

(b)

Figure 4.94: σ-profile (a) and σ-potential (b) of MEA and sulfolane predicted by COSMO-RS model

Figure 4.95 shows the predicted activity coefficient for MEA and sulfolane in the MEA + sulfolane binary mixture at 298.15 K. The predicted activity coefficient for sulfolane increases with increasing in a mol fraction of MEA in the mixture, while the activity coefficient for MEA decreases with increasing in a mol fraction of MEA. Both of the components of the mixture have an activity coefficient value higher than 1 over the whole composition. This indicates a strong like interactions compare to unlike interaction which leads to self-association between like molecules (Tosun, 2013).

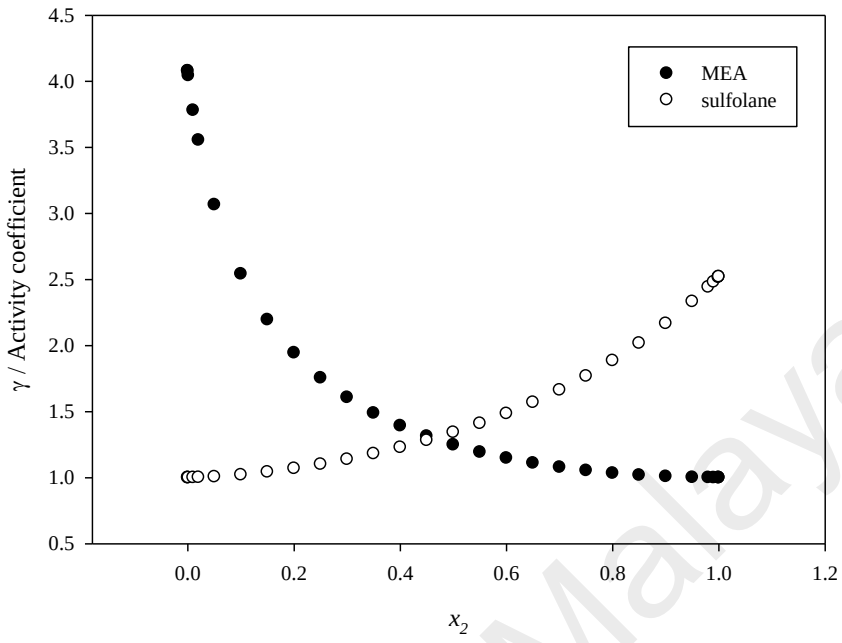

Figure 4.95: Activity coefficient for MEA (2) + sulfolane (3) binary mixtures as function of sulfolane mol fraction at T = 298.15 K

Figure 4.96 shows the predicted excess enthalpies for the MEA + sulfolane binary mixture at 298.15 K. The graph shows that the mixture has a positive excess enthalpy predominantly attributed to hydrogen bond energy, followed by weaker positive enthalpy by electrostatic misfit and weaker negative enthalpy by van der Waals energy. The positive enthalpy by hydrogen bonding and electrostatic misfit is due to the breaking of the intermolecular hydrogen bonding and loss of packing efficiency of MEA-MEA molecules by incorporation of sulfolane into the mixture. The negative excess enthalpy by van der Waals illustrates the increase non-polar interaction between MEA C-C backbone and sulfolane C-C aromatic ring.

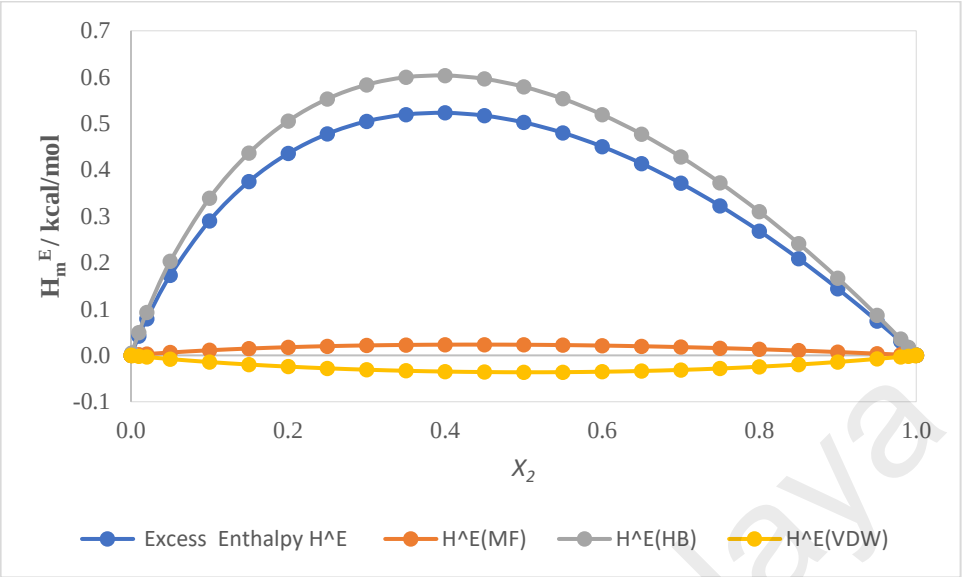

Figure 4.96: Predicted excess enthalpies for MEA (2) + sulfolane (3) binary mixtures as function of sulfolane mol fraction at T = 298.15 K

4.3.2.3 [BMIM][NTf_2] (1) + MEA (2) binary mixtures

Figure 4.97 shows σ-profile and σ-potential for $[BMIM]^+$, $[NTf_2]^-$ anion and MEA generated by COSMO-RS model. σ-profile and σ-potential for $[BMIM]^+$ and $[NTf_2]^-$ show an H-bond donor and H-bond acceptor, respectively the complement each of the ion pairs. Both $[BMIM]^+$ cation and $[NTf_2]^-$ anion show a peak in the non-polar region. While, σ-profile and σ-potential show MEA has an amphoteric characteristic with both H-bond donor and H-bod acceptor present in the molecule suggesting intramolecular H-bonding with each MEA molecule. Introduction of [BMIM][NTf_2] into the MEA matrix would cause disruption to the intramolecular H-bond the leads to expansion of volume. MEA also shows weaker non-polar peak in comparison to sulfolane which cause weaker van der Waal's interaction. This can be observed with [BMIM][NTf_2] + sulfolane binary mixtures having negative excess molar volume and [BMIM][NTf_2] + MEA binary mixtures having a positive value.

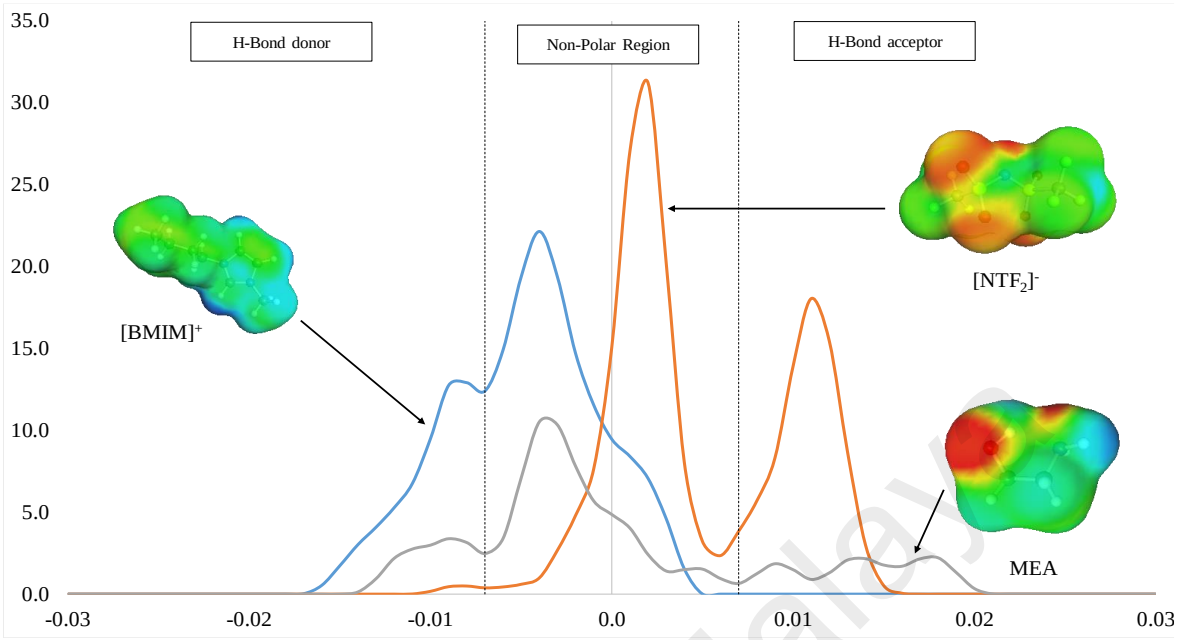

(a)

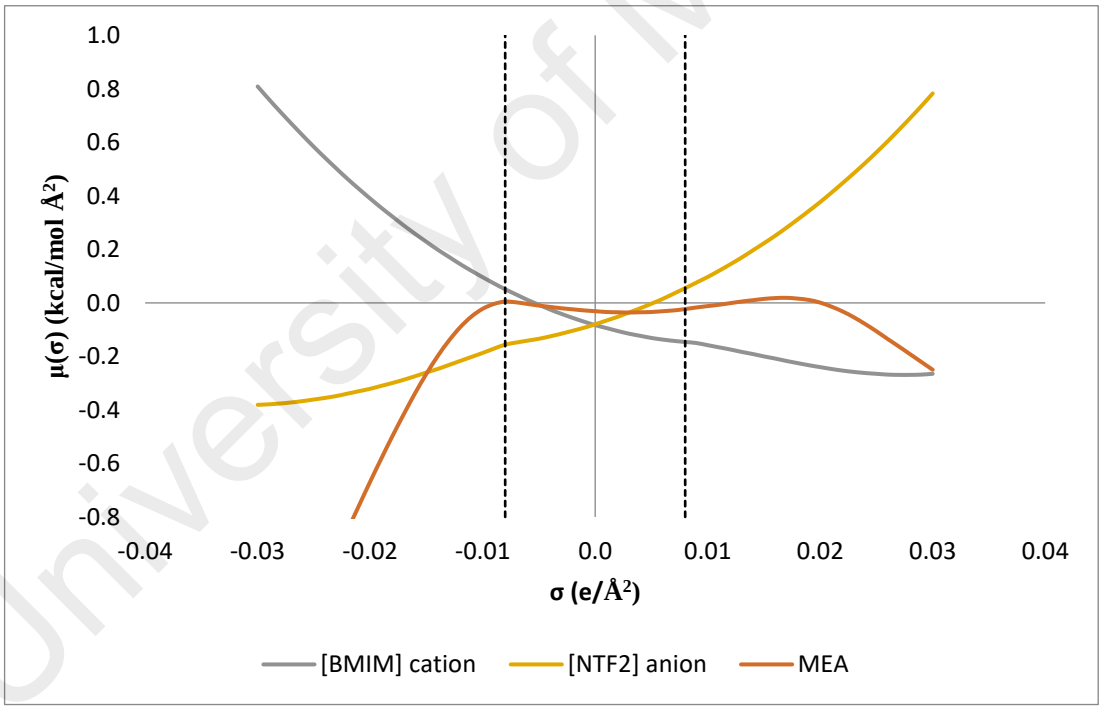

(b)

Figure 4.97: σ-profile and σ-potential of $[BMIM]^+$ cation, $[NTf_2]^-$ anion, and MEA predicted by COSMO-RS model

Figure 4.98 shows the predicted activity coefficient of [BMIM][NTf_2] and MEA in [BMIM][NTf_2] + MEA binary mixture at 298.15 K. The predicted activity coefficient for [BMIM][NTf_2] decreases while predicted activity coefficient for MEA increases with increasing in mol fraction of [BMIM][NTf_2] in the mixture. Both [BMIM][NTf_2] and MEA have an activity coefficient value higher than 1 over the whole composition which indicates a stronger like interactions compare to unlike interaction which leads to self-association between like molecules (Tosun, 2013)

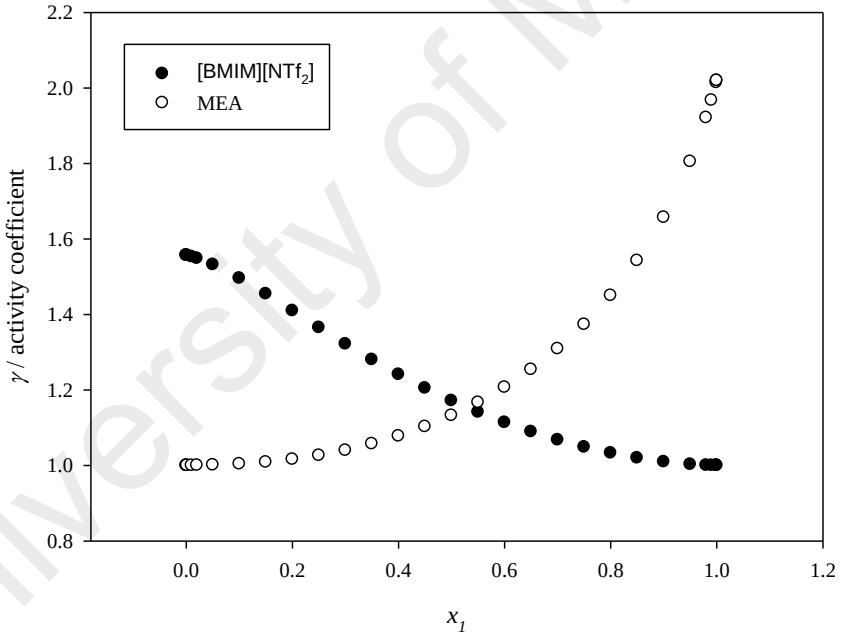

Figure 4.98: Activity coefficient for [BMIM][NTf_2] (1) + MEA (2) binary mixtures as function of sulfolane mol fraction at T = 298.15 K

Figure 4.99 shows the predicted excess enthalpies in the [BMIM][NTf_2] + MEA binary mixture at 298.15 K. The graph shows that the mixture has a positive excess enthalpy predominantly attributed to hydrogen bond energy. The positive enthalpy by hydrogen bonding is due to the breaking of the intermolecular hydrogen bonding of MEA-MEA molecules by incorporation of [BMIM][NTf_2] into the mixture.

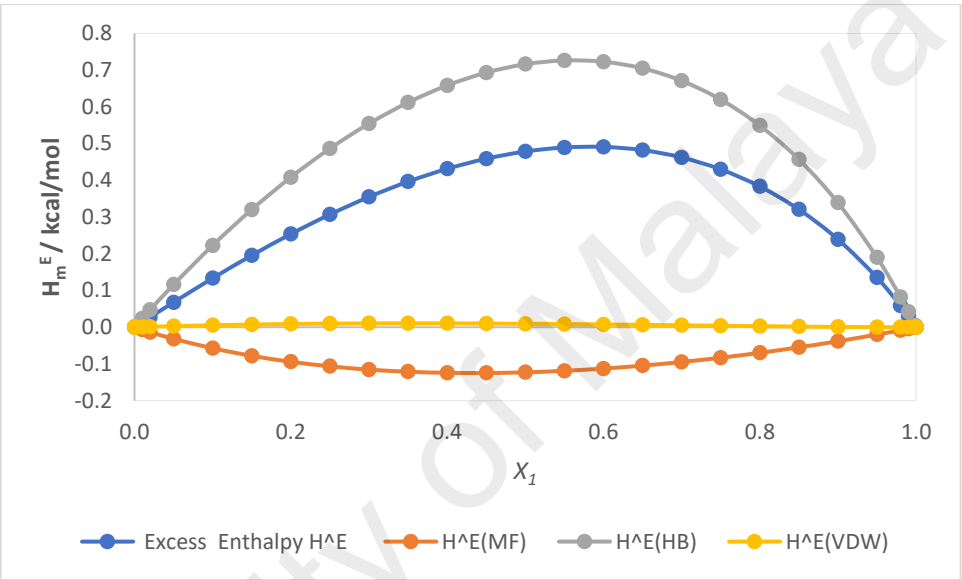

Figure 4.99: Predicted excess enthalpies for [BMIM][NTf_2] (1) + MEA (2) binary mixtures as function of sulfolane mol fraction at T = 298.15 K

4.3.2.4 [BMIM][NTf_2] (1) + MEA (2) + sulfolane (3) ternary mixtures

Figure 4.90 shows the σ-profile of $[BMIM]^+$ cation, $[NTf_2]^-$ anion, MEA and sulfolane molecules. The predominant molecular interaction in the ternary mixtures would likely depend on the major binary mixtures present in the composition. For example, in the ternary mixtures with low MEA composition, strong interaction between [BMIM][NTf_2] and sulfolane is dominant. This is shown by negative excess molar volume of the referred composition. On the contrary, ternary mixtures with high MEA composition exhibit weak

interaction both [BMIM][NTf_2] and sulfolane. This is reflected in the positive excess molar volume, which is caused by the expansion of the volume by the breaking of the MEA intramolecular H-bonding.

Figure 4.100 to Figure 4.102 show the predicted activity coefficient for [BMIM][NTf_2], MEA and sulfolane, respectively, in [BMIM][NTf_2] + MEA + sulfolane ternary mixtures at 298.15 K. Figure 4.100 shows [BMIM][NTf_2] has an activity coefficient value lower than 1 over the majority of composition which indicates a stronger unlike interactions compare to like interaction which leads to dispersion between unlike molecules. However, at lower sulfolane composition, increase in MEA composition led to predicted activity coefficient values higher than 1. Similarly, Figure 4.101 shows MEA has an activity coefficient value higher than 1 over the whole composition which indicates a stronger like interactions compare to unlike interaction which leads to self-association between like molecules. On the other hand, Figure 4.102 shows sulfolane exhibits predicted activity coefficient value higher than 1 in ternary mixture compose of higher MEA composition than [BMIM][NTf_2], reflecting a weak interaction with MEA. However, sulfolane has a predicted activity coefficient value less than 1 in ternary mixture compose of lower MEA composition than [BMIM][NTf_2], reflecting a strong unlike interaction with [BMIM][NTf_2] (Tosun, 2013).

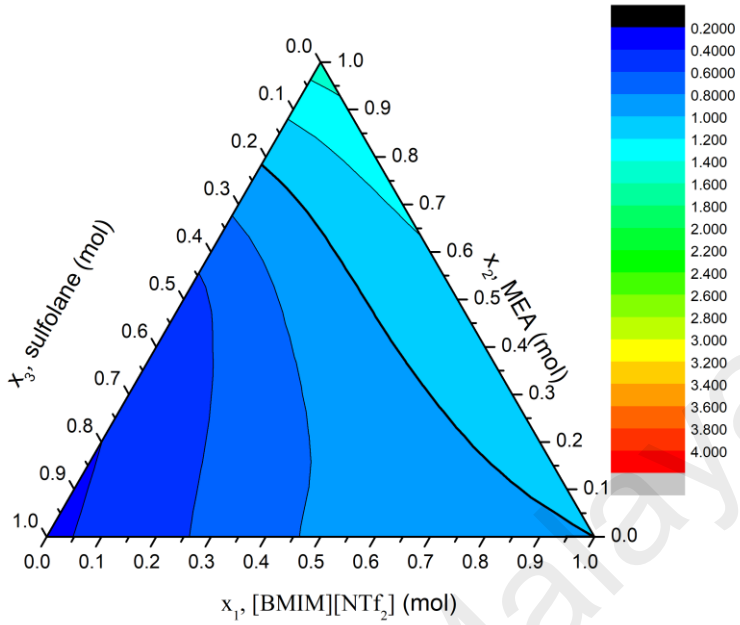

Figure 4.100: Activity coefficient for [BMIM][NTf_2] in [BMIM][NTf_2] (1) + MEA (2) + sulfolane (3) ternary mixtures over whole composition at T = 298.15 K

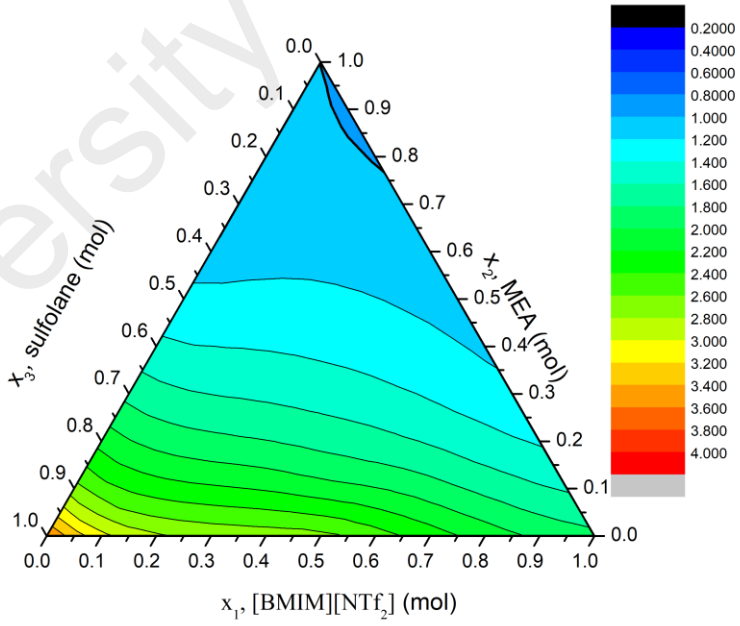

Figure 4.101: Activity coefficient for MEA in [BMIM][NTf_2] (1) + MEA (2) + sulfolane (3) ternary mixtures over whole composition at T = 298.15 K

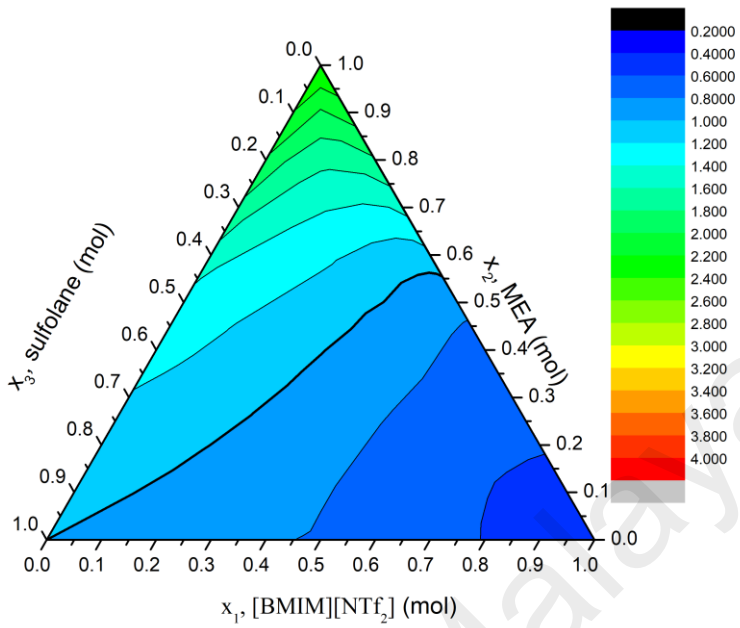

Figure 4.102: Activity coefficient for sulfolane in [BMIM][NTf_2] (1) + MEA (2) + sulfolane (3) ternary mixtures over whole composition at T = 298.15 K

Figure 4.103 shows the predicted total excess enthalpies in the [BMIM][NTf_2] + MEA + sulfolane ternary mixture at 298.15 K. The graph shows that the mixture has a positive excess enthalpy over whole range of composition. This is predominantly attributed to hydrogen bond energy (Figure 4.105) due to the breaking of the intermolecular hydrogen bonding of MEA-MEA molecules by the presence of [BMIM][NTf_2] and sulfolane into the mixture. Figure 4.104 illustrate the predicted excess enthalpy attributed by electrostatic-misfit of the molecules. The graph shows an overall negative value over whole composition. On the other hand, Figure 4.106 illustrate the predicted excess enthalpy attributed by van der Waals interaction of the molecules. The graph shows a negative value for mixture with low [BMIM][NTf_2] – high MEA composition and positive value in mixtures with low MEA - sulfolane composition.

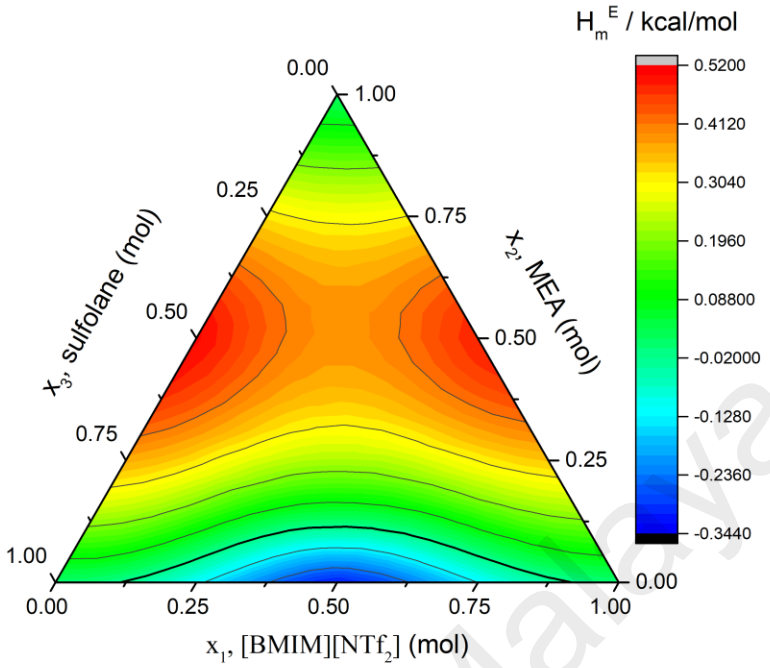

Figure 4.103: Predicted total excess enthalpies in [BMIM][NTf_2] (1) + MEA (2) + sulfolane (3) ternary mixtures over whole composition at T = 298.15 K

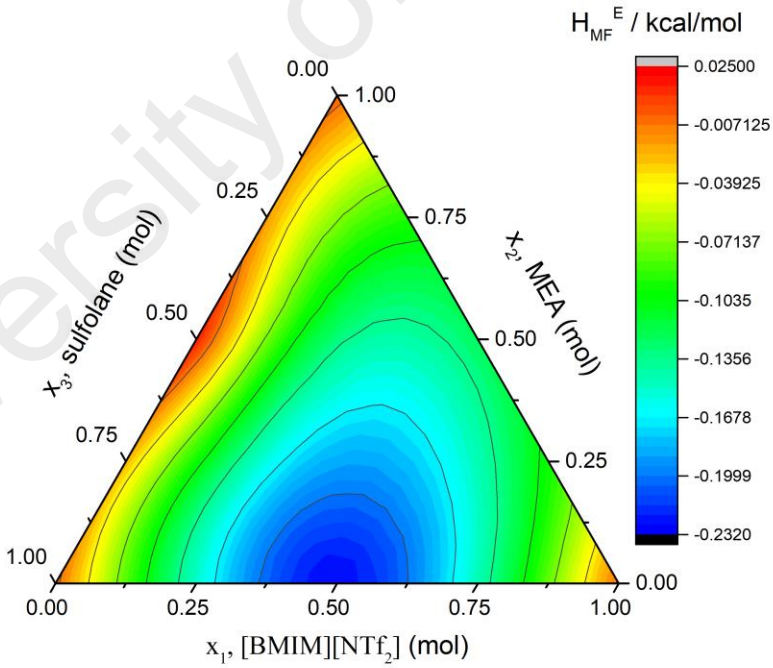

Figure 4.104: Predicted excess enthalpies (electrostatic-misfit, H_{MF}^{E}) in [BMIM][NTf_2] (1) + MEA (2) + sulfolane (3) ternary mixtures over whole composition at T = 298.15 K

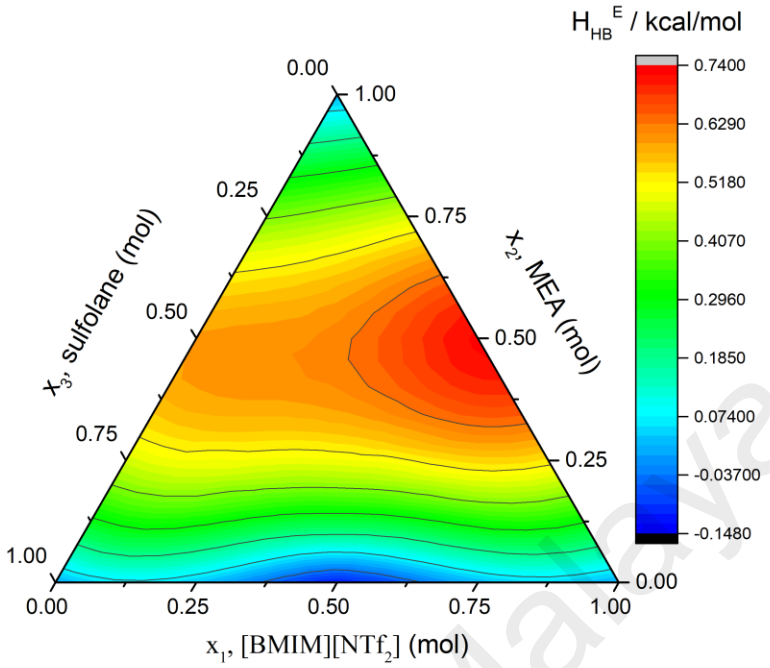

Figure 4.105: Predicted excess enthalpies (hydrogen bond, H_{HB}^{E}) in [BMIM][NTf_2] (1) + MEA (2) + sulfolane (3) ternary mixtures over whole composition at T = 298.15 K

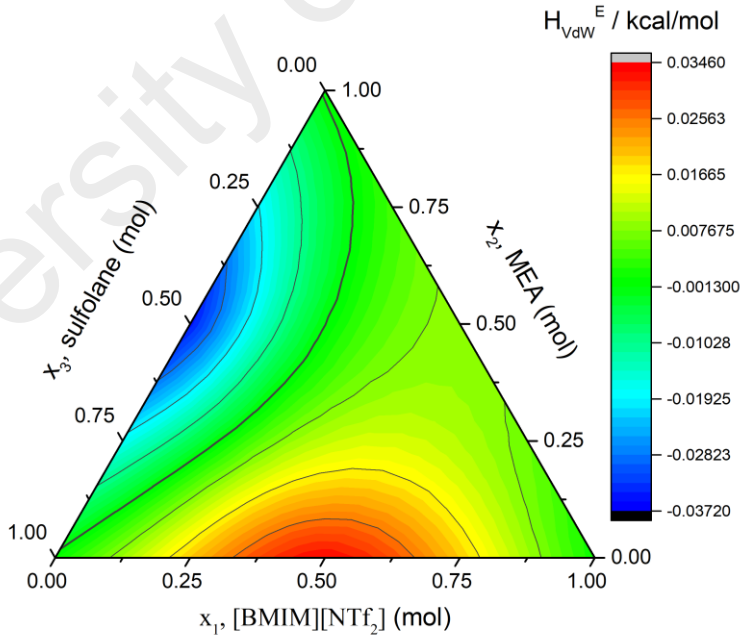

Figure 4.106: Predicted excess enthalpies (van der Waals, H_{VdW}^{E}) in [BMIM][NTf_2] (1) + MEA (2) + sulfolane (3) ternary mixtures over whole composition at T = 298.15 K

CHAPTER 5 : CONCLUSIONS AND RECOMMENDATIONS

5.1 Conclusions

Systematic approach towards evaluation of sulfolane based [BMIM][NTf_2] and MEA non-aqueous ternary mixture for CO_2 absorption application was conducted. Experimental thermophysical and excess properties of the ternary mixtures were performed over the whole range of composition. The calculated results were used to elucidate the molecular interaction between [BMIM][NTf_2], MEA and sulfolane. Furthermore, COSMO-RS model was used to verify the observed molecular interaction. Therefore, the results are concluded in the following three sections: (1) CO_2 solubility, (2) Thermophysical properties, and (3) COSMO-RS modeling

5.1.1 CO_2 solubility

Solubility of CO_2 in sulfolane based ternary mixtures of [BMIM][NTf_2] and MEA was conducted at temperatures ranging from 303.15 to 333.15 K and pressure from 500 to 2000 kPa. The experimental data show that CO_2 loading in the ternary mixtures increases with the increased pressure at constant temperature and composition. On the other hand, the CO_2 loading in the ternary mixtures decreases with the increased of temperature at constant pressure. Furthermore, ternary mixtures with higher composition of MEA has a much higher CO_2 loading in comparison to ternary mixtures with a high composition of [BMIM][NTf_2] due to the higher MEA chemical CO_2 absorption capacity. The experimental data were correlated and calculated data were produced with good consistency to experimental data. Interestingly, formation of a biphasic layer in the solution was observed and identified using

^{13}C NMR. The CO_2-rich layer can be easily separated and transported to the stripper to be regenerated. Furthermore, non-aqueous solvent approaches may overcome limitations faced due to corrosion and degradation in current industrial processes.

5.1.2 Thermophysical properties

Pure [BMIM][NTf_2] has the highest density followed by sulfolane and MEA. In [BMIM][NTf_2] (1) + sulfolane (3), MEA (2) + sulfolane (3), and [BMIM][NTf_2] (1) + MEA (2) binary mixture and [BMIM][NTf_2] (1) + MEA (2) + sulfolane (3) ternary mixture, density of the mixtures increases with an increase in composition of component with higher density. Density of both binary and ternary mixtures decreased linearly with temperature over whole composition. [BMIM][NTf_2] (1) + sulfolane (3) binary mixtures exhibit a negative value of excess molar volume. The negative excess molar volume indicates that attractive interaction and/or efficient packing occurred between [BMIM][NTf_2] and sulfolane. On the other hand, both [BMIM][NTf_2] (1) + MEA (2) and MEA (2) + sulfolane (3) binary mixtures exhibit a positive excess molar. The positive excess molar volume indicates an expansion in volume of the mixture with the possible breakdown of the self-associated molecules. Excess molar volume for [BMIM][NTf_2] + MEA +sulfolane ternary mixtures exhibit both negative and positive value over the whole composition. Negative excess molar volume value is more prominent in the [BMIM][NTf_2]-rich, low MEA and sulfolane composition, (example: 0.8 [BMIM][NTf_2]: 0.1 MEA: 0.1 sulfolane). Positive excess molar volume value is more prominent in the MEA-rich, low [BMIM][NTf_2] and sulfolane composition (example: 0.1 [BMIM][NTf_2]: 0.8 MEA: 0.1 sulfolane). In terms of CO_2 solubility, positive excess molar volume could lead to favorable physical absorption of the solution due to the weak

interactions between each component. Hence, the CO_2 molecules dissolved into the solution will be occupied space between each component easily.

Pure [BMIM][NTf_2] has the highest viscosity followed by pure MEA and pure sulfolane. In [BMIM][NTf_2] (1) + sulfolane (3), MEA (2) + sulfolane (3), [BMIM][NTf_2] (1) + MEA (2) and [BMIM][NTf_2] (1) + MEA (2) + sulfolane (3), viscosity of the mixtures increases with an increased composition of component with higher viscosity. Viscosity of both binary and ternary mixtures decreased with temperature over whole composition. Negative viscosity deviation values were observed in both binary and ternary mixtures over whole compositions and temperatures. In [BMIM][NTf_2] (1) + sulfolane (3) binary mixtures, minimum peak was observed at 0.5 [BMIM][NTf_2] : 0.5 sulfolane binary mixture. For MEA (2) + sulfolane (3) binary mixtures, minimum peak was observed at 0.6 MEA : 0.4 sulfolane binary mixture. In [BMIM][NTf_2] (1) + MEA (2) binary mixtures, minimum peak was observed at 0.8 [BMIM][NTf_2] : 0.2 MEA binary mixture. Similarly, the minimum peak of viscosity deviation for ternary mixtures was observed in ternary mixture with each composition reaching equimolar of each other (example: 0.3 [BMIM][NTf_2]: 0.3 MEA: 0.4 sulfolane). In terms of CO_2 capture processing, negative viscosity deviation could lead to a favorable energy reduction by the solution due to the weak interactions between each component. Hence, the solution requires less energy to be pumped throughout the system.

Pure sulfolane has the highest refractive index followed by MEA and [BMIM][NTf_2]. In [BMIM][NTf_2] (1) + sulfolane (3), MEA (2) + sulfolane (3), [BMIM][NTf_2] (1) + MEA (2) and [BMIM][NTf_2] (1) + MEA (2) + sulfolane (3), refractive index of the mixtures

increases with an increased composition of component with higher refractive index value. Refractive index of both binary and ternary mixtures decreased with temperature over whole composition. [BMIM][NTf_2] (1) + sulfolane (3) binary mixtures exhibit a negative value of refractive index deviation with minimum peak at x_1 = 0.4 mol fraction of [BMIM][NTf_2]. Similarly, negative refractive index deviation was observed for [BMIM][NTf_2] (1) + MEA (2) binary mixtures with minimum peak at x_1 = 0.3 mol fraction of [BMIM][NTf_2]. On the other hand, MEA (2) + sulfolane (3) binary mixtures exhibit a positive refractive index deviation value with maximum peak at x_2 = 0.5 mol fraction of MEA. Refractive index deviation for [BMIM][NTf_2] + MEA +sulfolane ternary mixtures exhibit negative value over the whole composition. The negative refractive index deviation is more prominent in ternary mixtures with composition of 0.4 [BMIM][NTf_2]: 0.5 MEA: 0.1 sulfolane.

5.1.3 COSMO-RS modeling

The structure of the $[BMIM]^+$ cation, $[NTf_2]^-$anion, MEA and sulfolane were drawn and geometry optimized using the TmolX software package at Hartree-Fock theory with 6-31G* basic set. Subsequently, a ***.cosmofile*** was created and imported to the COSMO*therm* software. Using COSMO*therm* software, a 3D polarized charged distribution (σ, sigma) on the molecular surface of the individual components were generated. Subsequently, activity coefficient of [BMIM][NTf_2]-sulfolane, [BMIM][NTf_2]-MEA, MEA-sulfolane binary mixtures and [BMIM][NTf_2]-MEA-sulfolane ternary mixtures were calculated. σ-profile for $[BMIM]^+$ and $[NTf_2]^-$ show an H-bond donor and H-bond acceptor, respectively the complement each of the ion pairs. Both $[BMIM]^+$ cation and $[NTf_2]^-$ anion show a peak in the non-polar region, which reflect the hydrophobicity of the ionic liquid. σ-profile for

sulfolane exhibit a strong non-polar peak and an H-bond acceptor peak and σ-profile for MEA indicate the present of both H-bond donor and H-bond acceptor in the molecule. Strong interaction between [BMIM][NTf_2] and sulfolane was deduced with favorable packing of sulfolane into [BMIM][NTf_2] free volume, which was supported by sulfolane activity coefficient less than 1 (ideality). On the other hand, weak interaction was deduced in both [BMIM][NTf_2]-MEA and sulfolane-MEA binary mixtures due to the breaking of MEA intramolecular H-bonding by [BMIM][NTf_2] and sulfolane molecules, respectively. This was supported by higher than 1 activity coefficient of both MEA and sulfolane in both [BMIM][NTf_2]-MEA and sulfolane-MEA binary mixtures. In case of [BMIM][NTf_2]-MEA-sulfolane ternary mixtures, the predominant molecular interaction in the ternary mixtures would likely depend on the major binary mixtures present in the composition in the ternary mixtures.

5.2 Recommendations

Current study incorporates single alkanolamine, MEA into the ternary mixtures which boosts the total CO_2 loading via chemical absorption. However, this approach is still stochiometric limited of 2 mol of alkanolamine to 1 mol of CO_2 ratio. Application of sterically hinder alkanolamine or diamine has been reported to have higher CO_2 to alkanolamine ratio. Therefore, study of this type of alkanolamine would be beneficial to the overall performance.

This study introduces the application of both ionic liquid and organic solvent as physical absorbent and solvent. The CO_2 loading of ionic liquid and organic solvent are directly proportional to its Henry's Law constant, and CO_2 loading of the solvent mixture is directly proportional to ionic liquid and organic solvent composition in the mixtures. Hence, screening and selection of suitable physical absorbent with higher CO_2 loading are essential to the overall performance.

It has been proposed that substitution of water with thermal stable organic solvent would reduce/eliminate corrosion issues of the operating equipment. However, such study was not conducted for this study. Further corrosion study would validate this claim and provide inside on the corrosion inhibition mechanism and corrosion rate behavior in carbonated solution of [BMIM][NTf_2] + MEA + sulfolane ternary mixtures at different parameters such as temperature, CO_2 loading or exposure time.

This study was conducted using only CO_2 in a pure gas form without any other gases in the mixture. However, for practical industrial application, presence of impurities in the flue gas such as water, H_2S, SO_2 and other gases should be taken into consideration. It will be useful to evaluate the performance of the non-aqueous solvent in term of CO_2 solubility, reusability and stability at various pressure and temperature ranges.

REFERENCES

Aguila-Hernandez, J., Trejo, A., Garcia-Flores, B. E., & Molnar, R. (2008). Viscometric and volumetric behaviour of binary mixtures of sulfolane and N-methylpyrrolidone with monoethanolamine and diethanolamine in the range 303-373 K. *Fluid Phase Equilibria, 267*(2), 172-180.

Aki, S. N. V. K., Mellein, B. R., Saurer, E. M., & Brennecke, J. F. (2004). High-pressure phase behavior of carbon dioxide with imidazolium-based ionic liquids. *The Journal of Physical Chemistry B, 108*(52), 20355-20365.

Albo, J., Luis, P., & Irabien, A. (2010). Carbon dioxide capture from flue gases using a cross-flow membrane contactor and the ionic liquid 1-ethyl-3-methylimidazolium ethylsulfate. *Industrial & Engineering Chemistry Research, 49*(21), 11045-11051.

Alshamrani, A. K., Vanderveen, J. R., & Jessop, P. G. (2016). A guide to the selection of switchable functional groups for CO_2-switchable compounds. *Physical Chemistry Chemical Physics, 18*(28), 19276-19288.

Amundsen, T. G., Øi, L. E., & Eimer, D. A. (2009). Density and viscosity of monoethanolamine + water + carbon dioxide from (25 to 80) °C. *Journal of Chemical & Engineering Data, 54*(11), 3096-3100.

Anderson, C., Harkin, T., Ho, M., Mumford, K., Qader, A., Stevens, G., & Hooper, B. (2013). Developments in the CO_2CRC UNO MK 3 process: a multi-component solvent process for large scale CO_2 capture. *Energy Procedia, 37*, 225-232.

Anderson, J. L., Dixon, J. K., & Brennecke, J. F. (2007). Solubility of CO_2, CH_4, C_2H_6, C_2H_4, O_2, and N_2 in 1-hexyl-3-methylpyridinium *bis*(trifluoromethylsulfonyl)imide: Comparison to other ionic liquids. *Accounts of Chemical Research, 40*(11), 1208-1216.

Appl, M., Fuerst, E., Henrici, H. J., Kuessner, K., Volkamer, K., & Wagner, U. (1982). United States Patent No. US 4336233.

Arshad, M. W., Svendsen, H. F., Fosbøl, P. L., von Solms, N., & Thomsen, K. (2014). Equilibrium Total Pressure and CO_2 Solubility in Binary and Ternary Aqueous Solutions of 2-(Diethylamino)ethanol (DEEA) and 3-(Methylamino)propylamine (MAPA). *Journal of Chemical & Engineering Data, 59*(3), 764-774.

Aschenbrenner, O., & Styring, P. (2010). Comparative study of solvent properties for carbon dioxide absorption. *Energy & Environmental Science, 3*(8), 1106-1113.

Astaria, G., Savage, D. W., & Bisio, A. (1983). *Gas treating with chemical solvents*. John Wiley, New York.

Atilhan, M., Jacquemin, J., Rooney, D., Khraisheh, M., & Aparicio, S. (2013). Viscous behavior of imidazolium-based ionic liquids. *Industrial & Engineering Chemistry Research, 52*(47), 16774-16785.

Ballard, M., Bown, M., James, S., & Yang, Q. (2011). NMR studies of mixed amines. *Energy Procedia*, *4*, 291-298.

Bara, J. E., Camper, D. E., Gin, D. L., & Noble, R. D. (2010). Room-temperature ionic liquids and composite materials: Platform technologies for CO_2 capture. *Accounts of Chemical Research*, *43*(1), 152-159.

Bates, E. D., Mayton, R. D., Ntai, I., & Davis, J. H. (2002). CO_2 capture by a task-specific ionic liquid. *Journal of the American Chemical Society*, *124*(6), 926-927.

Battino, R. (1971). Volume changes on mixing for binary mixtures of liquids. *Chemical Reviews*, *71*(1), 5-45.

Bishnoi, S., & Rochelle, G. T. (2000). Absorption of carbon dioxide into aqueous piperazine: reaction kinetics, mass transfer and solubility. *Chemical Engineering Science*, *55*(22), 5531-5543.

Blanchard, L. A., Gu, Z., & Brennecke, J. F. (2001). High-pressure phase behavior of ionic liquid/CO_2 systems. *The Journal of Physical Chemistry B*, *105*(12), 2437-2444.

Blanchard, L. A., Hancu, D., Beckman, E. J., & Brennecke, J. F. (1999). Green processing using ionic liquids and CO_2. *Nature*, *399*(6731), 28-29.

Böttinger, W., Maiwald, M., & Hasse, H. (2008). Online NMR spectroscopic study of species distribution in MDEA−H_2O−CO_2 and MDEA−PIP−H_2O−CO_2. *Industrial & Engineering Chemistry Research*, *47*(20), 7917-7926.

Brunetti, A., Scura, F., Barbieri, G., & Drioli, E. (2010). Membrane technologies for CO_2 separation. *Journal of Membrane Science*, *359*(1–2), 115-125.

Burdyny, T., & Struchtrup, H. (2010). Hybrid membrane/cryogenic separation of oxygen from air for use in the oxy-fuel process. *Energy*, *35*(5), 1884-1897.

Burr, B., & Lyddon, L. (2008). *A comparison of physical solvents for acid gas removal.* Paper presented at the 87th Annual Gas Processors Association Convention, Grapevine, TX, March.

Cabaço, M. I., Besnard, M., Danten, Y., & Coutinho, J. A. P. (2011). Solubility of CO_2 in 1-butyl-3-methyl-imidazolium-trifluoro acetate ionic liquid studied by Raman spectroscopy and DFT investigations. *The Journal of Physical Chemistry B*, *115*(13), 3538-3550.

Cadena, C., Anthony, J. L., Shah, J. K., Morrow, T. I., Brennecke, J. F., & Maginn, E. J. (2004). Why is CO_2 so soluble in imidazolium-based ionic liquids? *Journal of the American Chemical Society*, *126*(16), 5300-5308.

Camper, D., Bara, J. E., Gin, D. L., & Noble, R. D. (2008). Room-temperature ionic liquid-amine solutions: Tunable solvents for efficient and reversible capture of CO_2. *Industrial & Engineering Chemistry Research*, *47*(21), 8496-8498.

Caplow, M. (1968). Kinetics of carbamate formation and breakdown. *Journal of the American Chemical Society*, *90*(24), 6795-6803.

Chen, C., Kim, J., & Ahn, W.-S. (2014). CO_2 capture by amine-functionalized nanoporous materials: A review. *Korean Journal of Chemical Engineering, 31*(11), 1919-1934.

Clausse, M., Merel, J., & Meunier, F. (2011). Numerical parametric study on CO_2 capture by indirect thermal swing adsorption. *International Journal of Greenhouse Gas Control, 5*(5), 1206-1213.

Darde, V., Thomsen, K., van Well, W. J. M., & Stenby, E. H. (2010). Chilled ammonia process for CO_2 capture. *International Journal of Greenhouse Gas Control, 4*(2), 131-136.

Davison, J. (2007). Performance and costs of power plants with capture and storage of CO_2. *Energy, 32*(7), 1163-1176.

Diedenhofen, M., Eckert, F., & Klamt, A. (2003). Prediction of infinite dilution activity coefficients of organic compounds in ionic liquids using COSMO-RS. *Journal of Chemical & Engineering Data, 48*(3), 475-479.

Dlugokencky, E., & Tans, P. (2017). Trends in atmospheric carbon dioxide. Retrieved from www.esrl.noaa.gov/gmd/ccgg/trends/

Docherty, K. M., & Kulpa Jr, C. F. (2005). Toxicity and antimicrobial activity of imidazolium and pyridinium ionic liquids. *Green Chemistry, 7*(4), 185-189.

Dupont, J., Consorti, C. S., Suarez, P. A., & de Souza, R. F. (2003). Preparation of 1-butyl-3-methyl imidazolium-based room temperature ionic liquids. *Organic Syntheses*, 236-236.

Eckert, F., & Klamt, A. (2001). Validation of the COSMO-RS method: six binary systems. *Industrial & Engineering Chemistry Research, 40*(10), 2371-2378.

Eckert, F., & Klamt, A. (2013). COSMOtherm, Version C3. 0, Release 13.01. *COSMOlogic GmbH & Co. KG,.(Leverkusen, Germany., 2013)*.

Ellis, B., Keim, W., & Wasserscheid, P. (1999). Linear dimerisation of but-1-ene in biphasic mode using buffered chloroaluminate ionic liquid solvents. *Chemical Communications*(4), 337-338.

Fahrenkamp-Uppenbrink, J. (2015). Whither carbon capture and storage? *Science, 349*(6248), 599.

Feng, Z., Cheng-Gang, F., You-Ting, W., Yuan-Tao, W., Ai-Min, L., & Zhi-Bing, Z. (2010). Absorption of CO_2 in the aqueous solutions of functionalized ionic liquids and MDEA. *Chemical Engineering Journal, 160*(2), 691-697.

Figueroa, J. D., Fout, T., Plasynski, S., McIlvried, H., & Srivastava, R. D. (2008). Advances in CO_2 capture technology—the US Department of Energy's Carbon Sequestration Program. *International Journal of Greenhouse Gas Control, 2*(1), 9-20.

Galán Sánchez, L. M., Meindersma, G. W., & de Haan, A. B. (2007). Solvent properties of functionalized ionic liquids for CO_2 absorption. *Chemical Engineering Research and Design, 85*(1), 31-39.

Gao, S., Guo, D., Jin, H., Li, S., Wang, J., & Wang, S. (2015). Potassium carbonate slurry-based CO_2 capture technology. *Energy & Fuels, 29*(10), 6656-6663.

Gao, Y., Zhang, F., Huang, K., Ma, J.-W., Wu, Y.-T., & Zhang, Z.-B. (2013). Absorption of CO_2 in amino acid ionic liquid (AAIL) activated MDEA solutions. *International Journal of Greenhouse Gas Control, 19*, 379-386.

García-Abuín, A., Gomez-Diaz, D., La Rubia, M., & Navaza, J. (2011). Density, speed of sound, viscosity, refractive index, and excess volume of *N*-methyl-2-pyrrolidone + ethanol (or water or ethanolamine) from T=(293.15 to 323.15) K. *Journal of Chemical & Engineering Data, 56*(3), 646-651.

Ge, S., Wu, Z., Zhang, M., Li, W., & Tao, K. (2006). Sulfolene hydrogenation over an amorphous Ni−B alloy catalyst on MgO. *Industrial & Engineering Chemistry Research, 45*(7), 2229-2234.

Geppert-Rybczynska, M., Lehmann, J. K., & Heintz, A. (2014). Physicochemical properties of two 1-alkyl-1-methylpyrrolidinium bis (trifluoromethyl) sulfonyl imide ionic liquids and of binary mixtures of 1-butyl-1-methylpyrrolidinium bis (trifluoromethyl) sulfonyl imide with methanol or acetonitrile. *Journal of Chemical Thermodynamics, 71*, 171-181.

Gonzalez-Miquel, M., Bedia, J., Abrusci, C., Palomar, J., & Rodriguez, F. (2013). Anion effects on kinetics and thermodynamics of CO_2 absorption in ionic liquids. *The Journal of Physical Chemistry B, 117*(12), 3398-3406.

Gonzalez-Miquel, M., Massel, M., DeSilva, A., Palomar, J., Rodriguez, F., & Brennecke, J. F. (2014). Excess enthalpy of monoethanolamine + ionic liquid mixtures: How good are COSMO-RS predictions? *The Journal of Physical Chemistry B, 118*(39), 11512-11522.

Gonzalez, B., & Gonzalez, E. J. (2014). Physical properties of the pure 1-methyl-1-propylpyrrolidinium bis(trifluoromethylsulfonyl) imide ionic liquid and its binary mixtures with alcohols. *Journal of Chemical Thermodynamics, 68*, 109-116.

Gonzalez, E. J., Gonzalez, B., & Macedo, E. A. (2013). Thermophysical properties of the pure ionic liquid 1-butyl-1-methylpyrrolidinium dicyanamide and its binary mixtures with alcohols. *Journal of Chemical and Engineering Data, 58*(6), 1440-1448.

Göttlicher, G., & Pruschek, R. (1997). Comparison of CO_2 removal systems for fossil-fuelled power plant processes. *Energy Conversion and Management, 38, Supplement*, S173-S178.

Gouedard, C., Picq, D., Launay, F., & Carrette, P. L. (2012). Amine degradation in CO_2 capture. I. A review. *International Journal of Greenhouse Gas Control, 10*, 244-270.

Gutowski, K. E., & Maginn, E. J. (2008). Amine-functionalized task-specific ionic liquids: a mechanistic explanation for the dramatic increase in viscosity upon complexation with CO_2 from molecular simulation. *Journal of the American Chemical Society, 130*(44), 14690-14704.

Hamborg, E. S., Derks, P. W., van Elk, E. P., & Versteeg, G. F. (2011). Carbon dioxide removal by alkanolamines in aqueous organic solvents. A method for enhancing the desorption process. *Energy Procedia, 4*, 187-194.

Harris, K. R., Kanakubo, M., & Woolf, L. A. (2007). Temperature and pressure dependence of the viscosity of the ionic liquids 1-hexyl-3-methylimidazolium hexafluorophosphate and 1-butyl-3-methylimidazolium bis(trifluoromethylsulfonyl)imide. *Journal of Chemical & Engineering Data, 52*(3), 1080-1085.

Hart, R., Pollet, P., Hahne, D. J., John, E., Llopis-Mestre, V., Blasucci, V., Liotta, C. L. (2010). Benign coupling of reactions and separations with reversible ionic liquids. *Tetrahedron*, *66*(5), 1082-1090.

Hasib-ur-Rahman, M., Siaj, M., & Larachi, F. (2010). Ionic liquids for CO_2 capture-Development and progress. *Chemical Engineering and Processing, 49*(4), 313-322.

Hasib-ur-Rahman, M., Siaj, M., & Larachi, F. (2012). CO_2 capture in alkanolamine/room-temperature ionic liquid emulsions: A viable approach with carbamate crystallization and curbed corrosion behavior. *International Journal of Greenhouse Gas Control*, *6*, 246-252.

Hatch, L., & Matar, S. (1978). From hydrocarbons to petrochemicals. Part 12. Chemicals from C4′ s. *ChemInform*, *9*(50).

Heldebrant, D. J., Koech, P. K., Ang, M. T. C., Liang, C., Rainbolt, J. E., Yonker, C. R., & Jessop, P. G. (2010). Reversible zwitterionic liquids, the reaction of alkanol guanidines, alkanol amidines, and diamines with CO2. *Green Chemistry, 12*(4), 713-721.

Hiller, H., Reimert, R., Marschner, F., Renner, H.-J., Boll, W., Supp, E., Driesen, H. E. (2000). Gas Production *Ullmann's Encyclopedia of Industrial Chemistry*: Wiley-VCH Verlag GmbH & Co. KGaA.

Hochgesand, G. (1970). Rectisol and Purisol. *Industrial & Engineering Chemistry*, *62*(7), 37-43.

HoiLand, H. (1986). Partial molar volumes of biochemical model compounds in aqueous solution. *Thermodynamic Data for Biochemistry and Biotechnology*, 17-44.

Huang, J., & Rüther, T. (2009). Why are Ionic Liquids Attractive for CO_2 Absorption? An Overview. *Australian Journal of Chemistry, 62*(4), 298-308.

Huang, K., Chen, Y. L., Zhang, X. M., Xia, S., Wu, Y. T., & Hu, X. B. (2014). SO_2 absorption in acid salt ionic liquids/sulfolane binary mixtures: Experimental study and thermodynamic analysis. *Chemical Engineering Journal, 237*, 478-486.

Huang, W., Mi, Y., Li, Y., & Zheng, D. (2015). An aprotic polar solvent, diglyme, combined with monoethanolamine to form CO_2 capture material: Solubility measurement, model correlation, and effect evaluation. *Industrial & Engineering Chemistry Research*, *54*(13), 3430-3437.

Huddleston, J. G., Visser, A. E., Reichert, W. M., Willauer, H. D., Broker, G. A., & Rogers, R. D. (2001). Characterization and comparison of hydrophilic and hydrophobic room temperature ionic liquids incorporating the imidazolium cation. *Green Chemistry, 3*(4), 156-164.

Idem, R., Wilson, M., Tontiwachwuthikul, P., Chakma, A., Veawab, A., Aroonwilas, A., & Gelowitz, D. (2006). Pilot plant studies of the CO_2 capture performance of aqueous MEA and mixed MEA/MDEA solvents at the University of Regina CO_2 capture technology development plant and the boundary dam CO_2 capture demonstration plant. *Industrial & Engineering Chemistry Research, 45*(8), 2414-2420.

Iliuta, I., Hasib-ur-Rahman, M., & Larachi, F. (2014). CO_2 absorption in diethanolamine/ionic liquid emulsions - Chemical kinetics and mass transfer study. *Chemical Engineering Journal, 240*, 16-23.

IPCC. (2013). *Climate Change 2013: The Physical Science Basis. Contribution of Working Group I to the Fifth Assessment Report of the Intergovernmental Panel on Climate Change* (T. F. Stocker, D. Qin, G.-K. Plattner, M. Tignor, S. K. Allen, J. Boschung, A. Nauels, Y. Xia, V. Bex, & P. M. Midgley Eds.). Cambridge, United Kingdom and New York, NY, USA: Cambridge University Press.

J. Javid, R., Nejat, A., & Hayhoe, K. (2014). Selection of CO_2 mitigation strategies for road transportation in the United States using a multi-criteria approach. *Renewable and Sustainable Energy Reviews, 38*, 960-972.

Jalili, A. H., Mehdizadeh, A., Shokouhi, M., Sakhaeinia, H., & Taghikhani, V. (2010). Solubility of CO_2 in 1-(2-hydroxyethyl)-3-methylimidazolium ionic liquids with different anions. *The Journal of Chemical Thermodynamics, 42*(6), 787-791.

Jessop, P. G., Mercer, S. M., & Heldebrant, D. J. (2012). CO_2-triggered switchable solvents, surfactants, and other materials. *Energy & Environmental Science, 5*(6), 7240-7253.

Jing, G., Zhou, L., & Zhou, Z. (2012). Characterization and kinetics of carbon dioxide absorption into aqueous tetramethylammonium glycinate solution. *Chemical Engineering Journal, 181–182*, 85-92.

Jou, F.-Y., Mather, A. E., & Otto, F. D. (1995). The solubility of CO_2 in a 30 mass percent monoethanolamine solution. *The Canadian Journal of Chemical Engineering, 73*(1), 140-147.

Jou, F. Y., & Mather, A. E. (2005). Solubility of carbon dioxide in an aqueous mixture of methyldiethanolamine and N-methylpyrrolidone at elevated pressures. *Fluid Phase Equilibria, 228–229*, 465-469.

Kapetaki, Z., Brandani, P., Brandani, S., & Ahn, H. (2015). Process simulation of a dual-stage Selexol process for 95% carbon capture efficiency at an integrated gasification combined cycle power plant. *International Journal of Greenhouse Gas Control, 39*, 17-26.

Kim, Y. E., Park, J. H., Yun, S. H., Nam, S. C., Jeong, S. K., & Yoon, Y. I. (2014). Carbon dioxide absorption using a phase transitional alkanolamine–alcohol mixture. *Journal of Industrial and Engineering Chemistry, 20*(4), 1486-1492.

Kinart, C. M., & Kinart, W. J. (2000). Physicochemical methods used to study internal structures of liquid binary mixtures. *Physics and Chemistry of Liquids, 38*(2), 155-180.

Kittel, J., & Gonzalez, S. (2014). Corrosion in CO_2 post-combustion capture with alkanolamines - A review. *Oil & Gas Science and Technology-Revue D Ifp Energies Nouvelles, 69*(5), 915-929.

Klamt, A. (1995). Conductor-like screening model for real solvents: A new approach to the quantitative calculation of solvation phenomena. *The Journal of Physical Chemistry, 99*(7), 2224-2235.

Klamt, A., Eckert, F., & Arlt, W. (2010). COSMO-RS: An alternative to simulation for calculating thermodynamic properties of liquid mixtures. *Annual Review of Chemical and Biomolecular Engineering, 1*, 101-122.

Kohl, A. L., & Nielsen, R. B. (1997). Chapter 14 - Physical solvents for acid gas removal *Gas Purification (Fifth Edition)* (pp. 1187-1237). Houston: Gulf Professional Publishing.

Kumar, D. B. K., Reddy, K. R., Rao, G. S., Rao, G. V. R., & Rambabu, C. (2012). Thermodynamic and spectroscopic study of molecular interactions in the binary liquid mixtures of N-methyl-2-pyrrolidone and some substituted benzenes at different temperatures. *Journal of Molecular Liquids, 174*, 100-111.

Kumełan, J., Pérez-Salado Kamps, Á., Tuma, D., & Maurer, G. (2006). Solubility of CO_2 in the ionic liquid [hmim][Tf_2N]. *The Journal of Chemical Thermodynamics, 38*(11), 1396-1401.

Kumełan, J., Tuma, D., Pérez-Salado Kamps, Á., & Maurer, G. (2010). Solubility of the single gases carbon dioxide and hydrogen in the ionic liquid [bmpy][Tf_2N]. *Journal of Chemical & Engineering Data, 55*(1), 165-172.

Kurnia, K. A., & Coutinho, J. A. P. (2013). Overview of the Excess Enthalpies of the Binary Mixtures Composed of Molecular Solvents and Ionic Liquids and Their Modeling Using COSMO-RS. *Industrial & Engineering Chemistry Research, 52*(38), 13862-13874.

Lee, B.-C., & Outcalt, S. L. (2006). Solubilities of gases in the ionic liquid 1-*n*-butyl-3-methylimidazolium bis(trifluoromethylsulfonyl)imide. *Journal of Chemical & Engineering Data, 51*(3), 892-897.

Lepaumier, H., Picq, D., & Carrette, P.-L. (2009). New amines for CO_2 capture. I. Mechanisms of amine degradation in the presence of CO_2. *Industrial & Engineering Chemistry Research, 48*(20), 9061-9067.

Letcher, T. (1975). The excess volumes of some mixtures of saturated and unsaturated C_6 hydrocarbons. *The Journal of Chemical Thermodynamics, 7*(3), 205-209.

Leung, D. Y. C., Caramanna, G., & Maroto-Valer, M. M. (2014). An overview of current status of carbon dioxide capture and storage technologies. *Renewable and Sustainable Energy Reviews, 39*, 426-443.

Li, J., You, C., Chen, L., Ye, Y., Qi, Z., & Sundmacher, K. (2012). Dynamics of CO_2 absorption and desorption processes in alkanolamine with cosolvent polyethylene glycol. *Industrial & Engineering Chemistry Research, 51*(37), 12081-12088.

Liang, Z. H., Rongwong, W., Liu, H., Fu, K., Gao, H., Cao, F., . . . Sumon, K. (2015). Recent progress and new developments in post-combustion carbon-capture technology with amine based solvents. *International Journal of Greenhouse Gas Control, 40*, 26-54.

Ma'mun, S., & Kim, I. (2013). Selection and characterization of phase-change solvent for carbon dioxide capture: precipitating system. *Energy Procedia, 37*, 331-339.

Maham, Y., Liew, C.-N., & Mather, A. (2002). Viscosities and excess properties of aqueous solutions of ethanolamines from 25 to 80 °C. *Journal of Solution Chemistry, 31*(9), 743-756.

Maurer, G., & Tuma, D. (2009). *Gas solubility (and related high-pressure phenomena) in systems with ionic liquids.* Paper presented at the ACS symposium series.

Mchaweh, A., Alsaygh, A., Nasrifar, K., & Moshfeghian, M. (2004). A simplified method for calculating saturated liquid densities. *Fluid Phase Equilibria, 224*(2), 157-167.

Mesquita, F. M. R., Feitosa, F. X., Aznar, M., de Sant'Ana, H. B., & Santiago-Aguiar, R. S. (2014). Density, viscosities, and excess properties for binary mixtures of sulfolane + alcohols and sulfolane + glycols at different temperatures. *Journal of Chemical & Engineering Data*.

Metz, B., Davidson, O., de Coninck, H., Loos, M., Meyer, L., & Change, W. G. I. o. t. I. P. o. C. (2005). IPCC, 2005: IPCC special report on carbon dioxide capture and storage.

Millero, F. J. (1980). *Review of the experimental and analytical methods for the determination of the pressure-volume-temperature properties of electrolytes.* Paper presented at the ACS.

Mondal, M. K., Balsora, H. K., & Varshney, P. (2012). Progress and trends in CO_2 capture/separation technologies: A review. *Energy, 46*(1), 431-441.

Moore, B. J., Headley, J. V., Dupont, R. R., Doucette, W. D., & Armstrong, J. E. (2002). Abatement of gas-condensate hydrocarbon in a natural wetland. *Journal of Environmental Science and Health, Part A, 37*(4), 425-438.

Motin, M. A., Ali, M. A., & Sultana, S. (2007). Density and excess molar volumes of binary mixtures of sulfolane with methanol, n-propanol, n-butanol, and n-pentanol at 298.15-323.15 K and atmospheric pressure. *Physics and Chemistry of Liquids, 45*(2), 221-229.

Muldoon, M. J., Aki, S. N. V. K., Anderson, J. L., Dixon, J. K., & Brennecke, J. F. (2007). Improving carbon dioxide solubility in ionic liquids. *The Journal of Physical Chemistry B, 111*(30), 9001-9009.

Nielsen, P. T., & Rochelle, G. T. (2017). Effects of Catalysts, Inhibitors, and Contaminants on Piperazine Oxidation. *Energy Procedia, 114*, 1919-1929.

Nielsen, R., Lewis, K., McCullough, J., & Hansen, D. (1995). *Corrosion in refinery amine systems*. Retrieved from NACE International, Houston, TX (United States):

Oexmann, J., & Kather, A. (2010). Minimising the regeneration heat duty of post-combustion CO_2 capture by wet chemical absorption: The misguided focus on low heat of absorption solvents. *International Journal of Greenhouse Gas Control, 4*(1), 36-43.

Oh, T. H. (2010). Carbon capture and storage potential in coal-fired plant in Malaysia—A review. *Renewable and Sustainable Energy Reviews, 14*(9), 2697-2709.

Olajire, A. A. (2010). CO_2 capture and separation technologies for end-of-pipe applications – A review. *Energy, 35*(6), 2610-2628.

Pal, A., & Kumar, B. (2011). Volumetric, acoustic and spectroscopic studies for binary mixtures of ionic liquid (1-butyl-3-methylimidazolium hexafluorophosphate) with alkoxyalkanols at T = (288.15 to 318.15) K. *Journal of Molecular Liquids, 163*(3), 128-134.

Park, S.-W., Choi, B.-S., & Lee, J.-W. (2006). Chemical absorption of carbon dioxide with triethanolamine in non-aqueous solutions. *Korean Journal of Chemical Engineering, 23*(1), 138-143.

Park, S.-W., Lee, J.-W., Choi, B.-S., & Lee, J.-W. (2005). Kinetics of absorption of carbon dioxide in monoethanolamine solutions of polar organic solvents. *Journal of Industrial and Engineering Chemistry, 11*(2), 202-209.

Park, S.-W., Lee, J.-W., Choi, B.-S., & Lee, J.-W. (2006). Absorption of carbon dioxide into non-aqueous solutions of N-methyldiethanolamine. *Korean Journal of Chemical Engineering, 23*(5), 806-811.

Patwari, M. K., Bachu, R. K., Boodida, S., & Nallani, S. (2009). Densities, viscosities, and speeds of sound of binary liquid mixtures of sulfolane with ethyl acetate, *n*-propyl acetate, and n-butyl acetate at temperature of (303.15, 308.15, and 313.15) K. *Journal of Chemical and Engineering Data, 54*(3), 1069-1072.

Pfaff, I., & Kather, A. (2009). Comparative thermodynamic analysis and integration issues of CCS steam power plants based on oxy-combustion with cryogenic or membrane based air separation. *Energy Procedia, 1*(1), 495-502.

Pires, J., Timperman, L., Jacquemin, J., Balducci, A., & Anouti, M. (2013). Density, conductivity, viscosity, and excess properties of (pyrrolidinium nitrate-based protic ionic liquid plus propylene carbonate) binary mixture. *Journal of Chemical Thermodynamics, 59*, 10-19.

Qian, W., Xu, Y. J., Zhu, H. Y., & Yu, C. H. (2012). Properties of pure 1-methylimidazolium acetate ionic liquid and its binary mixtures with alcohols. *Journal of Chemical Thermodynamics, 49*, 87-94.

Quadrelli, R., & Peterson, S. (2007). The energy–climate challenge: recent trends in CO_2 emissions from fuel combustion. *Energy Policy, 35*(11), 5938-5952.

Rainbolt, J. E., Koech, P. K., Yonker, C. R., Zheng, F., Main, D., Weaver, M. L., Heldebrant, D. J. (2011). Anhydrous tertiary alkanolamines as hybrid chemical and physical CO_2 capture reagents with pressure-swing regeneration. *Energy & Environmental Science, 4*(2), 480-484.

Raynal, L., Alix, P., Bouillon, P.-A., Gomez, A., de Nailly, M. l. F., Jacquin, M., Trapy, J. (2011). The DMX™ process: An original solution for lowering the cost of post-combustion carbon capture. *Energy Procedia, 4*, 779-786.

Reynolds, A. J., Verheyen, T. V., Adeloju, S. B., Meuleman, E., & Feron, P. (2012). Towards commercial scale postcombustion capture of CO_2 with monoethanolamine solvent: Key considerations for solvent management and environmental impacts. *Environmental Science & Technology, 46*(7), 3643-3654.

Sairi, N. A., Ghani, N. A., Aroua, M. K., Yusoff, R., & Alias, Y. (2015). Low pressure solubilities of CO_2 in guanidinium trifluoromethanesulfonate–MDEA systems. *Fluid Phase Equilibria, 385*, 79-91.

Sánchez, L. G., Meindersma, G., & De Haan, A. (2011). Kinetics of absorption of CO_2 in amino-functionalized ionic liquids. *Chemical Engineering Journal, 166*(3), 1104-1115.

Seki, S., Tsuzuki, S., Hayamizu, K., Umebayashi, Y., Serizawa, N., Takei, K., & Miyashiro, H. (2012). Comprehensive refractive index property for room-temperature ionic liquids. *Journal of Chemical & Engineering Data, 57*(8), 2211-2216.

Shafeeyan, M. S., Wan Daud, W. M. A., & Shamiri, A. (2014). A review of mathematical modeling of fixed-bed columns for carbon dioxide adsorption. *Chemical Engineering Research and Design, 92*(5), 961-988.

Shakerian, F., Kim, K.-H., Szulejko, J. E., & Park, J.-W. (2015). A comparative review between amines and ammonia as sorptive media for post-combustion CO_2 capture. *Applied Energy, 148*, 10-22.

Sharma, P., Park, S. D., Park, K. T., Nam, S. C., Jeong, S. K., Yoon, Y. I., & Baek, I. H. (2012). Solubility of carbon dioxide in amine-functionalized ionic liquids: Role of the anions. *Chemical Engineering Journal, 193–194*, 267-275.

Shin, E.-K., & Lee, B.-C. (2008). High-pressure phase behavior of carbon dioxide with ionic liquids: 1-alkyl-3-methylimidazolium trifluoromethanesulfonate. *Journal of Chemical & Engineering Data, 53*(12), 2728-2734.

Singh, S., Aznar, M., & Deenadayalu, N. (2013). Densities, speeds of sound, and refractive indices for binary mixtures of 1-butyl-3-methylimidazolium methyl sulphate ionic liquid with alcohols at T = (298.15, 303.15, 308.15, and 313.15) K. *Journal of Chemical Thermodynamics, 57*, 238-247.

Smith, K., Lee, A., Mumford, K., Li, S., Indrawan, Thanumurthy, N., Stevens, G. (2015). Pilot plant results for a precipitating potassium carbonate solvent absorption process

promoted with glycine for enhanced CO_2 capture. *Fuel Processing Technology, 135*, 60-65.

Soosaiprakasam, I. R., & Veawab, A. (2008). Corrosion and polarization behavior of carbon steel in MEA-based CO_2 capture process. *International Journal of Greenhouse Gas Control, 2*(4), 553-562.

Stocker, T. F., Qin, D., Plattner, G.-K., Tignor, M., Allen, S. K., Boschung, J., Midgley, P. M. (2014). Climate change 2013: The physical science basis: Cambridge University Press Cambridge, UK, and New York.

Taib, M. M., & Murugesan, T. (2012). Solubilities of CO_2 in aqueous solutions of ionic liquids (ILs) and monoethanolamine (MEA) at pressures from 100 to 1600 kPa. *Chemical Engineering Journal, 181–182*, 56-62.

Takamura, Y., Aoki, J., Uchida, S., & Narita, S. (2001). Application of high-pressure swing adsorption process for improvement of CO_2 recovery system from flue gas. *The Canadian Journal of Chemical Engineering, 79*(5), 812-816.

Tan, J., Shao, H., Xu, J., Du, L., & Luo, G. (2011). Mixture absorption system of monoethanolamine− triethylene glycol for CO_2 capture. *Industrial & Engineering Chemistry Research, 50*(7), 3966-3976.

Tan, L. S., Shariff, A. M., Lau, K. K., & Bustam, M. A. (2012). Factors affecting CO_2 absorption efficiency in packed column: A review. *Journal of Industrial and Engineering Chemistry, 18*(6), 1874-1883.

Tems, R. D., & Al-Zahrani, A. M. (2006). *Cost of corrosion in gas sweetening and fractionation plants*. Paper presented at the CORROSION 2006.

Tilstam, U. (2012). Sulfolane: A Versatile Dipolar Aprotic Solvent. *Organic Process Research & Development, 16*(7), 1273-1278.

Torabi Angaji, M., Ghanbarabadi, H., & Karimi Zad Gohari, F. (2013). Optimizations of Sulfolane concentration in propose Sulfinol-M solvent instead of MDEA solvent in the refineries of Sarakhs. *Journal of Natural Gas Science and Engineering, 15*, 22-26.

Tosun, I. (2013). Chapter 8 - Excess mixture properties and activity coefficients *The Thermodynamics of Phase and Reaction Equilibria* (pp. 271-349). Amsterdam: Elsevier.

Usubharatana, P., & Tontiwachwuthikul, P. (2009). Enhancement factor and kinetics of CO_2 capture by MEA-methanol hybrid solvents. *Energy Procedia, 1*(1), 95-102.

Vahidi, M., & Moshtari, B. (2013). Dielectric data, densities, refractive indices, and their deviations of the binary mixtures of N-methyldiethanolamine with sulfolane at temperatures 293.15–328.15 K and atmospheric pressure. *Thermochimica Acta, 551*, 1-6.

Vranes, M., Zec, N., Tot, A., Papovic, S., Dozic, S., & Gadzuric, S. (2014). Density, electrical conductivity, viscosity and excess properties of 1-butyl-3-methylimidazolium

bis(trifluoromethylsulfonyl) imide plus propylene carbonate binary mixtures. *Journal of Chemical Thermodynamics, 68*, 98-108.

Walden, P. (1914). Molecular weights and electrical conductivity of several fused salts. *Bull. Acad. Imper. Sci.(St. Petersburg), 8*, 405-422.

Wang, M., Lawal, A., Stephenson, P., Sidders, J., & Ramshaw, C. (2011). Post-combustion CO_2 capture with chemical absorption: A state-of-the-art review. *Chemical Engineering Research and Design, 89*(9), 1609-1624.

Wang, Y., Lang, X., & Fan, S. (2013). Hydrate capture CO_2 from shifted synthesis gas, flue gas and sour natural gas or biogas. *Journal of Energy Chemistry, 22*(1), 39-47.

Wilkes, J. S., Levisky, J. A., Wilson, R. A., & Hussey, C. L. (1982). Dialkylimidazolium chloroaluminate melts: a new class of room-temperature ionic liquids for electrochemistry, spectroscopy and synthesis. *Inorganic Chemistry, 21*(3), 1263-1264.

Wilkes, J. S., & Zaworotko, M. J. (1992). Air and water stable 1-ethyl-3-methylimidazolium based ionic liquids. *Journal of the Chemical Society, Chemical Communications*(13), 965-967.

Wolfson, A., Dlugy, C., & Shotland, Y. (2007). Glycerol as a green solvent for high product yields and selectivities. *Environmental Chemistry Letters, 5*(2), 67-71.

Xiao, J., Li, C.-W., & Li, M.-H. (2000). Kinetics of absorption of carbon dioxide into aqueous solutions of 2-amino-2-methyl-1-propanol+ monoethanolamine. *Chemical Engineering Science, 55*(1), 161-175.

Xu, Y., Schutte, R. P., & Hepler, L. G. (1992). Solubilities of carbon dioxide, hydrogen sulfide and sulfur dioxide in physical solvents. *The Canadian Journal of Chemical Engineering, 70*(3), 569-573.

Xu, Y. J., Chen, B., Qian, W., & Li, H. R. (2013). Properties of pure *n*-butylammonium nitrate ionic liquid and its binary mixtures of with alcohols at T = (293.15 to 313.15) K. *Journal of Chemical Thermodynamics, 58*, 449-459.

Xu, Z., Wang, S., & Chen, C. (2013). CO_2 absorption by biphasic solvents: Mixtures of 1,4-Butanediamine and 2-(Diethylamino)-ethanol. *International Journal of Greenhouse Gas Control, 16*, 107-115.

Xue, Z., Zhang, Z., Han, J., Chen, Y., & Mu, T. (2011). Carbon dioxide capture by a dual amino ionic liquid with amino-functionalized imidazolium cation and taurine anion. *International Journal of Greenhouse Gas Control, 5*(4), 628-633.

Yang, C. S., Ma, P. S., & Zhou, Q. (2004). Excess molar volumes and viscosities of binary mixtures of sulfolane with benzene, toluene, ethylbenzene, p-xylene, o-xylene, and m-xylene at 303.15 and 323.15 K and atmospheric pressure. *Journal of Chemical and Engineering Data, 49*(4), 881-885.

Yuan, X., Zhang, S., Chen, Y., Lu, X., Dai, W., & Mori, R. (2006). Solubilities of Gases in 1,1,3,3-Tetramethylguanidium Lactate at Elevated Pressures. *Journal of Chemical & Engineering Data, 51*(2), 645-647.

Zaman, M., & Lee, J. H. (2013). Carbon capture from stationary power generation sources: A review of the current status of the technologies. *Korean Journal of Chemical Engineering, 30*(8), 1497-1526.

Zarei, H., Golroudbari, S. A., & Behroozi, M. (2013). Experimental studies on volumetric and viscometric properties of binary and ternary mixtures of *N*,*N*-dimethylacetamide, *N*-methylformamide and propane-1,2-diol at different temperatures. *Journal of Molecular Liquids, 187*, 260-265.

Zhang, S., Yuan, X., Chen, Y., & Zhang, X. (2005). Solubilities of CO_2 in 1-butyl-3-methylimidazolium hexafluorophosphate and 1,1,3,3-tetramethylguanidium lactate at elevated pressures. *Journal of Chemical & Engineering Data, 50*(5), 1582-1585.

Zhang, X., Liu, Z., & Wang, W. (2008). Screening of ionic liquids to capture CO_2 by COSMO-RS and experiments. *Aiche Journal, 54*(10), 2717-2728.

Zhang, Y., Zhang, S., Lu, X., Zhou, Q., Fan, W., & Zhang, X. (2009). Dual amino-functionalised phosphonium ionic liquids for CO_2 capture. *Chemistry–A European Journal, 15*(12), 3003-3011.

Zhao, M., Minett, A. I., & Harris, A. T. (2013). A review of techno-economic models for the retrofitting of conventional pulverised-coal power plants for post-combustion capture (PCC) of CO_2. *Energy & Environmental Science, 6*(1), 25-40.

Zheng, C., Tan, J., Wang, Y., & Luo, G. (2012). CO_2 solubility in a mixture absorption system of 2-amino-2-methyl-1-propanol with glycol. *Industrial & Engineering Chemistry Research, 51*(34), 11236-11244.

Zheng, C., Tan, J., Wang, Y., & Luo, G. (2013). CO_2 solubility in a mixture absorption system of 2-amino-2-methyl-1-propanol with ethylene glycol. *Industrial & Engineering Chemistry Research, 52*(34), 12247-12252.

Zheng, S., Tao, M., Liu, Q., Ning, L., He, Y., & Shi, Y. (2014). Capturing CO_2 into the precipitate of a phase-changing solvent after absorption. *Environmental Science & Technology, 48*(15), 8905-8910.

SUPPLEMENTARY

LIST OF PUBLICATIONS AND PAPERS PRESENTED

Publications

1. **Kassim, M. A.**, Sairi, N. A., Yusoff, A., Alias, Y., & Aroua, M. K. (2016). Evaluation of 1-butyl-3-methylimidazolium bis(trifluoromethylsulfonyl)imide–alkanolamine sulfolane-based system as solvent for absorption of carbon dioxide. *Industrial & Engineering Chemistry Research*, 2016, *55* (29), 7992–8001.

2. **Kassim, M. A.**, Sairi, N. A., Yusoff, R., Ramalingam, A., Alias, Y., & Aroua, M. K. (2016). Experimental densities and viscosities of binary mixture of 1-butyl-3-methylimidazolium bis(trifluoromethylsulfonyl)imide or glycerol with sulfolane and their molecular interaction by COSMO-RS. *Thermochimica Acta, 639*, 130-147

Papers presented

1. **Mohd Azlan Kassim**, Nor Asrina Sairi, Rozita Yusoff, Yatimah Alias, and Mohamed Kheireddine Aroua. Evaluation of 1-butyl-3-methylimidazolium bis(trifluoromethylsulfonyl)imide–alkanolamine sulfolane-based system as solvent for absorption of carbon dioxide. *2nd Ionic Liquids Symposium 2017, University Malaya Centre For Ionic Liquids & Malaysian Ionic Liquids Society, Universiti Malaya, 2017.*

2. **Mohd Azlan Kassim**, Nor Asrina Sairi, Rozita Yusoff, Yatimah Alias, and Mohamed Kheireddine Aroua. Evaluation of 1-butyl-3-methylimidazolium bis(trifluoromethylsulfonyl)imide–alkanolamine sulfolane-based system as solvent for absorption of carbon dioxide. *Fundamental Science Congress 2016 (FSC2016), Universiti Putra Malaysia, 2016.*

3. **Mohd Azlan Kassim**, Nor Asrina Sairi, Rozita Yusoff, Yatimah Alias, and Mohamed Kheireddine Aroua. Evaluation of ionic liquids–alkanolamine sulfolane based solution as solvent for absorption of carbon dioxide. *13th International Conference On Carbon Dioxide. UM#111-Chemistry Symposium, Universiti Malaya, 2016.*

4. **Mohd Azlan Kassim**, Nor Asrina Sairi, Rozita Yusoff, Yatimah Alias, and Mohamed Kheireddine Aroua. Evaluation of ionic liquids–alkanolamine sulfolane based solution as solvent for absorption of carbon dioxide. *13th International Conference On Carbon Dioxide Utilization, National University of Singapore, Singapore, 2015.*

5. **Mohd Azlan Kassim**, Nor Asrina Sairi, Rozita Yusoff, Anantharaj Ramalingam, Yatimah Alias, Mohamed Kheireddine Aroua. Experimental densities and viscosities of binary mixture of 1-butyl-3-methylimidazolium bis(trifluoromethylsulfonyl)imide or glycerol with sulfolane and their molecular interaction by COSMO-RS, *27th Regional Symposium of Malaysia Analytical Sciences, Universiti Teknologi Malaysia, 2014.*

6. **Mohd Azlan Kassim**, Nor Asrina Sairi, Rozita Yusoff, Anantharaj Ramalingam, Yatimah Alias, Mohamed Kheireddine Aroua. CO_2 capture in ionic liquids: A review on mixed solvent system, *5th UM-NUS-CU Trilateral Mini Symposium and Scientific Meeting, Universiti Malaya, 2014.*

7. **Mohd Azlan Kassim**, Nor Asrina Sairi, Rozita Yusoff, Anantharaj Ramalingam, Yatimah Alias, Mohamed Kheireddine Aroua. CO_2 capture in ionic liquids: A review on mixed solvent system, *International Conference On Ionic Liquids 2013 (ICIL 13), Langkawi, 2013.*